ANNA KIVIAHO

Long QT Syndrome -specific Cardiomyocytes Derived from Induced Pluripotent Stem Cells

From cell lines to disease models

■

ACADEMIC DISSERTATION
To be presented, with the permission of
the Board of the BioMediTech of the University of Tampere,
for public discussion in the Auditorium of Finn-Medi 5,
Biokatu 12, Tampere, on December 13th, 2014, at 12 o'clock.

UNIVERSITY OF TAMPERE

ANNA KIVIAHO

Long QT Syndrome -specific Cardiomyocytes Derived from Induced Pluripotent Stem Cells

From cell lines to disease models

Acta Universitatis Tamperensis 2006
Tampere University Press
Tampere 2014

UNIVERSITY OF TAMPERE

ACADEMIC DISSERTATION
University of Tampere, BioMediTech
Tampere University Hospital, Heart Hospital
Finland

Supervised by
Professor Katriina Aalto-Setälä
University of Tampere
Finland
PhD Mari Pekkanen-Mattila
University of Tampere
Finland

Reviewed by
PhD Steve Oh
Bioprocessing Technology Institute
Singapore
Docent Pasi Tavi
University of Eastern Finland
Finland

The originality of this thesis has been checked using the Turnitin OriginalityCheck service in accordance with the quality management system of the University of Tampere.

Cover design by
Mikko Reinikka

Distributor:
kirjamyynti@juvenes.fi
http://granum.uta.fi

Acta Universitatis Tamperensis 2006
ISBN 978-951-44-9663-9 (print)
ISSN-L 1455-1616
ISSN 1455-1616

Acta Electronica Universitatis Tamperensis 1495
ISBN 978-951-44-9664-6 (pdf)
ISSN 1456-954X
http://tampub.uta.fi

Suomen Yliopistopaino Oy – Juvenes Print
Tampere 2014

To my Mom and Dad

Abstract

Primary human cardiomyocytes are difficult to obtain and maintain *in vitro,* which has been a major obstacle in cardiac research. For this reason, cardiomyocytes differentiated from human embryonic stem cells have been used as a source of cardiac cells in spite of the ethical issues related to the usage of embryos. However, human induced pluripotent stem (iPS) cells have introduced a novel platform for disease modeling, drug testing and diagnostics because human iPS cells can proliferate and self-renew or, alternatively, differentiate into any cell type in the human body, including cardiomyocytes. In addition, iPS cells can be generated from any individual, which enables the establishment of disease- and patient-specific cardiac models, the design of individualized medications and, possibly in the future, the applications to regenerative medicine.

Long QT syndrome (LQTS) is a cardiac disorder that can be either congenital or acquired. The syndrome is characterized by abnormalities in an electrocardiogram (ECG) and an increased risk of developing life-threatening ventricular arrhythmia. The estimated clinical prevalence of LQTS worldwide is between 1:5 000 and 1:10 000, but the increasing identification of asymptomatic mutation carriers indicate that the genetic prevalence may be much higher. In Finland, one out of every 250 people is known to be a carrier of a mutation related to LQTS. Acquired LQTS is the most common severe side effect of medications and one of the most common reasons for the withdrawal of drugs already on the market. Carriers of LQTS-related mutations are thought to be more vulnerable to the adverse effects of different drugs compared to the general population.

In the studies presented in this thesis, iPS cells were generated from skin fibroblasts acquired from patients with LQTS, and these iPS cells were differentiated into cardiomyocytes. The LQTS-specific cardiac myocytes

reproduced the disease phenotype *in vitro* with a prolonged repolarization time. The LQTS phenotype was detected using the patch clamp -technique and Ca^{2+}-imaging and by analyzing the mechanical behavior of the beating cardiomyocytes. In addition, different phenotypes caused by different mutations were distinguished using these three methods. The analysis of the mechanical properties of single cardiomyocytes based on video recordings introduced a novel method for characterizing cardiac myocytes that could be used for cardiac research together with electrophysiological techniques and methods based on detecting the ion concentrations in the cells.

Tiivistelmä

Ihmisen sydänsolujen tutkimus on ollut haastavaa, koska sydänlihassoluja on vaikea sekä saada että kasvattaa soluviljelyolosuhteissa. Alkion kantasoluista erilaistettuja sydänlihassoluja onkin käytetty sydäntutkimuksessa, vaikka alkioiden käyttöön liittyykin eettisiä kysymyksiä. Uudelleen ohjelmoidut, erittäin monikykyiset kantasolut (iPS-solut, engl. induced pluripotent stem cells) ovat kuitenkin luoneet mahdollisuuksia aivan uudenlaiselle sairauksien tutkimiselle ja diagnosoinnille sekä lääketutkimukselle ja -testaukselle. Ihmisen iPS-solut nimittäin lisääntyvät periaatteessa loputtomasti *in vitro* ja niitä voidaan erilaistaa miksi tahansa ihmisen solutyypiksi, myös sydänlihassoluiksi. Lisäksi iPS-soluja voidaan uudelleen ohjelmoida kenen tahansa soluista. Tämä mahdollistaa potilas- ja tautispesifisten sydänsolumallien perustamisen, potilaskohtaisen lääkityksen ja hoidon suunnitelemisen sekä mahdollisesti tulevaisuudessa myös kantasoluihin ja kantasolusovelluksiin perustuvien hoitojen kehittämisen.

Pitkä QT oireyhtymä (LQTS, engl. long QT syndrome) on sydänsairaus, joka voi olla joko perinnöllinen tai hankittu eli jonkin ulkoisen tekijän, kuten lääkkeen aiheuttama. Sairaus havaitaan potilaan sydänsähkökäyrästä (EKG), ja LQTS-potalaalla on kohonnut riski saada kammioperäisiä, hengenvaarallisia rytmihäiriöitä. LQTS:n maailmanlaajuisen kliinisen esiintyvyyden on arvioitu olevan 1:10 000 - 1:5 000, mutta todennäköisesti sairauden geneettinen esiintyvyys on huomattavasti suurempi. Suomessa LQTS:lle altistavan mutaation kantajia tiedetään olevan jopa 1:250. LQTS on yleisin, vakava lääkkeiden aiheuttama sivuvaikutus ja myös yksi yleisimmistä syistä, joiden vuoksi lääkkeitä joudutaan vetämään pois markkinoilta. On myös arveltu, että kyseiset lääkevaikutukset olisivat vakavampia henkilöillä, jokta kantavat LQTS:lle altistavaa mutaatiota.

Tämä väitöskirjatutkimus esittelee iPS-solulinjoja, jotka tehtiin LQTS-potilaiden ihon fibroblasteista ja erilaistettiin sydänlihassoluiksi. LQTS:n fenotyyppi voitiin havaita näissä sydänlihasoluissa pidentyneenä repolarisaatio-aikana. Havaitsemiseen käytetyt menetelmät olivat patch clamp -tekniikka ja Ca^{2+}-kuvantaminen sekä videonauhoituksiin perustuva solujen mekaanisen toiminnan analysointi. Myös eri mutaatioden aiheuttamat erilaiset fenotyypit voitiin erottaa kaikilla näillä kolmella menetelmällä. Yksittäisten sydänlihassolujen sykkeen mekaanisten ominaisuuksien analysointi on täysin uusi tapa määrittää näiden solujen ominaisuuksia ja kyseistä menetelmää voidaan käyttää yhdessä perinteisten elektrofysiologisten- ja ionien pitoisuuksiin perustuvien menetelmien kanssa.

Table of contents

List of abbreviations

AD	arrhythmia with two or more Ca^{2+} peaks
AFP	α-fetoprotein
ALCAM	activated leukocyte cell adhesion molecule
ALP	alkaline phosphatase
AP	action potential
APD_{50}	action potential duration at 50 % of the amplitude
APD_{90}	action potential duration at 90 % of the amplitude
AS	arrhythmia with small Ca^{2+} events in between the stable Ca^{2+} spikes
ATP	adenosine triphosphate
AUC	area under the curve
AV	atrioventricular
A614V	alanine to valine substitution at position 614
A422T	alanine to threonine substitution at position 422
BAF	rg/Brahma-associated factor
bFGF	basic fibroblast growth factor
BMP4	bone morphogenetic protein 4
BR	beating rate
cDNA	complementary DNA
cFPD	beating rate -corrected FPD
Chd1	chromodomain helicase DNA binding protein 1
CHIR99021	specific glycogen synthase kinase 3 (GSK-3) inhibitor
CICR	Ca^{2+}-induced Ca^{2+} release
cMyBP-C	cardiac myosin binding protein C
c-Myc	myelocytomatosis viral oncogene homolog
CRU	Ca^{2+} releasing unit
cTnI	cardiac troponin I
cTnT	cardiac troponin T
Cx-40	connexin 40
Cx-43	connexin 43
Cx-45	connexin 45
DAPI	4’,6-diamidino-2-phenylindole
DIC	digital image correlation
DKK1	dickkopf homolog 1

DMEM	Dulbecco's Modified Eagle -medium
DMSO	dimethyl sulfoxide
DZNep	3-Deazaneplanocin A (an inhibitor of S-adenosylmethionine-dependent methyltransferase)
EAD	early after-depolarization
EB	embryoid body
ECG	electrocardiograph
EMV	electromechanical window
END-2	mouse endodermal-like cell line
ES cell	embryonic stem cell
EtBr	ethidium bromide
E-4031	(N-[4-[[1-[2-(6-Methyl-2-yridinyl)ethyl]4piperidinyl]carbonyl]-phenyl]methanesulfonamide-dihydrochloride
FA	forced aggregation
FBS	fetal bovine serum
FGF4	fibroblast growth factor 4
FP	field potential
FPD	field potential duration
GAPDH	glyceraldehyde 3-phosphate dehydrogenase
GATA4	GATA binding protein 4
GSK-3β	glycogen synthase kinase 3β
G589D	glycine to asparagine substitution at position 589
G1681A	glycine to alanine substitution at position 1681
HDAC	histone deacetylase
hERG	human Ether-à-go-go-Related gene
hESC	human embryonic stem cell
HSA	human serum albumin
H2A	histone 2 A
IBT	Institute of Biomedical Technology
I_{Kr}	rapid delayed rectifying K^+ -current
I_{Ks}	slow delayed rectifying K^+ -current
IN	integrase
iPS cell	induced pluripotent stem cell
Isl-1	Islet-1
ivs7-2A>G	intronic mutation causing alterations in splicing
JLNS	Jervell and Lange-Nielsen

JNJ303	2-(4-Chlorophenoxy)-2-methyl-N-5[(methylsulfonyl)-amino]tricyclo[3.3.1.13,7]dec-2-yl]-propanamide
KCNE1	potassium voltage-gated channel subfamily E, member 1
KCNE2	potassium voltage-gated channel subfamily E, member 2
KCNH2	potassium voltage-gated channel subfamily H, member 2
KCNQ1	potassium voltage-gated channel, KQT-like subfamily, member 1
Klf4	Kruppel-like factor 4
KO	knockout
KSR	knockout serum replacement -medium
KvLQT1	voltage-gated potassium channel, KQT-like subfamily, member 1
LCC	L-type Ca^{2+} channel
Lefty1	left-right determination factor
let-7	miRNA precursor
LIF	leukemia inhibitory factor
Lin28	lineage protein 28
LQTS	long QT syndrome
LQT1	long QT syndrome type 1
LQT2	long QT syndrome type 2
LQT3	long QT syndrome type 3
L552S	leucine to serine substitution at position 552
MAPK	mitogen activated protein kinase
MEA	micro electrode array
MEF	mouse embryonic fibroblast
MESP1	mesoderm posterior 1
MSEP2	mesoderm posterior 2
MHC	myosin heavy chain
miRNA	microRNA
MLC1	myosin light chain 1
MLC2a	atrial myosin light chain 2
MLC2v	ventricular myosin light chain 2
MQD	minimum quadratic difference
mRNA	messenger RNA
MSC	mesenchymal stem cell
MYH7	myosin heavy chain 7
NCX	Na^{+}/Ca^{2+} -exchanger

NEAA	nonessential amino acids
Nkx2.5	NK2 transcription factor related gene, locus 5
N996I	asparagine to isoleucine substitution at position 996
Oct4	octamer-binding transcription factor 4
Pax6	paired box protein 6
PBS	phosphate buffered saline
PFA	paraformaldehyde
PGI_2	prostaglandin I_2
Plat-E	Platinum-E cell line
POU5F1	POU domain, class 5, transcription factor 1
PPI	peak-to-peak interval
PVA	polyvinyl alcohol
qPCR	quantitative polymerase chain reaction
QTc	corrected QT interval
Rex1	RNA exonuclease 1
RNAi	RNA interference
ROCK	rho-associated protein kinase
ROI	region of interest
RT	reverse transcriptase
RT-PCR	reverse transcription polymerase chain reaction
RWS	Romano-Ward
RyR2	ryanodine receptor 2
R176W	arginine to tryptophan substitution at position 176
R190Q	arginine to glutamine substitution at position 190
SCNT	somatic cell nuclear transplantation
SERCA	sarcoplasmic reticulum Ca^{2+} -ATPase
Slc7a1	gene for solute carrier family 7 (cationic amino acid transporter), member 1
SMAD1	an intracellular protein involved in TGF-β signaling
Sox1	sex determining region Y-box 1
Sox2	sex determining region Y-box 2
Sox17	sex determining region Y-box 17
SR	sarcoplasmic reticulum
SSEA3	stage-specific embryonic antigen 3
SSEA4	stage-specific embryonic antigen 4
STAT3	signal transducer and activator of transcription 3
Tbx6	T-box transcription factor 6

TdP	Torsades de Pointes
TGF-β	transforming growth factor β
TNNT2	gene encoding cardiac troponin T (cTnT)
TRA1-60	tumor-related antigen 1-60
TRA1-81	tumor-related antigen 1-81
TSA	trichostatin A
Utf1	undifferentiated embryonic cell transcription factor 1
VCAM1	vascular cell adhesion molecule 1
VEGF	vascular endothelial growth factor
VEGFR2	vascular endothelial growth factor receptor 2
VPA	valproic acid (a histone deacetylase inhibitor)
Wnt	abbreviated combination from *Wingless* and *Integrase-1*
WT	wild type
293FT	cell line derived from 293F cells stably expressing SV40 large antigen
1893delC	deletion of cysteine at position 1893

List of original publications

This study is based on three original publications that are listed bellow. In the text these articles are referred to using Roman numbers (I-III).

I **Lahti AL***, Kujala VJ*, Chapman H, Koivisto AP, Pekkanen-Mattila M, Kerkelä E, Hyttinen J, Kontula K, Swan H, Conklin BR, Yamanaka S, Silvennoinen O, Aalto-Setälä K (2012): *Model for long QT syndrome type 2 using human iPS cells demonstrates arrhythmogenic characteristics in cell culture*. Dis Model Mech 5(2): 220-30. *equal contribution

II Ahola A*, **Kiviaho AL***, Larsson K, Honkanen M, Aalto-Setälä K, Hyttinen J (2014): *Video image-based analysis of single human induced pluripotent stem cell derived cardiomyocyte beating dynamics using digital image correlation*. Biomed Eng Online 7: 13-39. *equal contribution

III **Kiviaho AL**, Ahola A, Larsson K, Kujala K, Pekkanen-Mattila M, Venäläinen H, Paavola K, Hyttinen J, Aalto-Setälä K: *Long QT syndrome type 1 -specific cardiomyocytes carrying different mutations reveal distinct electrophysiological and mechanical phenotypes*. (submitted)

1. Introduction

Human induced pluripotent stem (iPS) cells offer tremendous opportunities for cardiac research. Primary human cardiomyocytes are difficult to both obtain and maintain because obtaining a myocardial biopsy is a high-risk procedure and because primary cardiac myocytes tend to dedifferentiate and stop beating in cell culture conditions relatively quickly (Mitcheson et al, 1996). Human iPS cells, on the other hand, are pluripotent cells; they can be differentiated into any cell type in the human body, including cardiomyocytes (Zhang et al, 2009). The development of iPS cell technology has created many expectations for disease modeling and drug testing in human cardiomyocytes, as well as for new therapeutic possibilities for cardiac diseases. The use of iPS cells in clinical applications still needs to overcome various obstacles, but cardiac disease models using iPS cell technology have been established by various research groups (Bellin et al, 2013; Carvajal-Vergara et al, 2010; Caspi et al, 2013; Davis et al, 2012; Di Pasquale et al, 2013; Egashira et al, 2012; Fatima et al, 2011; Ho et al, 2011; Huang et al, 2011; Itzhaki et al, 2011; Itzhaki et al, 2012; Jung et al, 2012; Kim et al, 2013; Kujala et al, 2012; Lahti et al, 2012; Lan et al, 2013; Ma et al, 2013; Malan et al, 2011; Matsa et al, 2011; Moretti et al, 2010; Novak et al, 2012; Siu et al, 2012; Sun et al, 2012 Terrenoire et al, 2013; Yazawa et al, 2011). In addition, some promising results have been published on pharmacological testing with cardiomyocytes derived from iPS cells (Tanaka et al, 2009; Yokoo et al, 2009). More recently, also iPS cell -derived cardiomyocytes with genetic cardiac disorder have been used for pharmacological testing (Terrenoire et al, 2013).

Traditionally, pharmacological development and preclinical drug testing have utilized animal models and transiently transfected non-cardiac cells expressing cardiac ion channels (ICH, 2005). Unfortunately, these platforms do not provide an appropriate cellular environment that reliably reproduces the

correct responses of human cardiac myocytes. Some regulatory mechanisms in human cardiomyocytes that influence the responses to different internal or external stimuli may exist, and these mechanisms are most likely absent in non-cardiac cells. Also, cardiac regulatory systems may vary among different species, which makes animal models unreliable set-ups for human cardiac research. The usage of cardiac myocytes derived from human iPS cells offers a clear advantage over these traditional systems, although iPS cell -derived cardiomyocytes are not optimal either. Instead, the use of iPS cell -derived cardiomyocytes as reliable models for cardiac diseases or for drug testing still confronts issues related to the fact that these cells are quite different from primary human cardiomyocytes. In addition, the conditions in two dimensional cell culture are very different from those in a complete functional organ, such as the heart. The suitability and limitations of iPS cell -derived cardiomyocytes for cardiac disease modeling and drug testing are extensively reviewed by Šarić and colleagues recently (Šarić et al, 2013). Nevertheless, the cellular milieu in the human iPS cell -derived cardiomyocytes resembles that of primary human cardiac cells which makes them more reliable model for human heart than non-cardiac cells or animal models.

The objective of the present thesis was to evaluate the characteristics of established iPS cell lines and their differentiation into cardiomyocytes. Furthermore, long QT syndrome (LQTS) -specific cardiomyocytes derived from iPS cells were evaluated as *in vitro* models for LQTS by various methods based on the electrophysiology of these cells, the measurement of calcium concentration in these cardiac myocytes and also on the evaluation of the mechanical beating properties of the LQTS-specific cardiomyocytes.

2. Review of the literature

2.1. Stem cells

2.1.1. Hierarchy of stem cells

Stem cells are defined as undifferentiated cells that are able to divide and self-renew indefinitely or, alternatively, to differentiate into specialized cell types. This means that stem cells are capable of both symmetrical cell division that produces two identical copies of the original cell and asymmetrical cell division that results in a cell that resembles the original cell and another cell that begins to differentiate along a certain pathway. (Wolpert et al, 2007.)

Along the process of stem cell development, the cells tend to gradually lose their differentiation capacity. A fertilized egg is considered *totipotent,* which means that it can form all the cell types of a developing organism and the extraembryonic structures, such as the placenta, umbilical cord and fetal membranes. During mammalian embryogenesis, totipotent cells are found in the embryo until it reaches the eight-cell morula stage, after which all the cells are specialized and committed to either constitute the extraembryonic elements or form an entire organism but no extraembryonic tissue. The stem cells that can form all the three germ layers of an embryo, namely the ecto-, endo- and mesoderm, and differentiate into any cell type in an organism are called *pluripotent*. These pluripotent stem cells form the inner cell mass of the embryo (Figure 1). (Wolpert et al, 2007; Yamanaka et al, 2008.)

During the development of an embryo, pluripotent stem cells gradually differentiate toward a special cell type or lineage. At the same time, the cells lose their capacity to differentiate toward an alternative lineage. *Multipotent* stem cells have limited differentiation capacity and can produce only a few different types of cells. Usually, the possible cell types are the ones that can be found in the same tissue where the stem cells reside. Consequently, multipotent

stem cells are also called tissue specific stem cells, and these cells can be found not only in embryos and fetuses but also in adult tissues. Mesenchymal stem cells (MSCs) are an example of a multipotent stem cells. Human MSCs are present in the bone marrow and also in some other tissues, such as the periosteum, trabecular bone, adipose tissue, synovium, skeletal muscle and deciduous teeth, and MSCs can differentiate to form the cells of the connective tissue lineages, including osteoblasts, adipocytes, chondrocytes and myocytes (for a review, see Barry & Murphy, 2004; Kassem 2004).

Finally, the stem cells that are able to differentiate into only one type of cell are called *unipotent* or precursor cells. For example, keratinocytes in the mammalian skin mature from unipotent stem cells that reside in the *stratum basale*, the deepest layer of the epidermis (Wolpert et al, 2007; Yamanaka et al, 2008.). The classification of different stem cells is illustrated in Figure 1.

Traditionally, the development and hierarchy of stem cells are thought to follow a pathway of decreasing differentiation capacity as described above. Also, long it was considered as a fact, that differentiation is a one-way pathway: a cell that has differentiated toward a certain group of cell types has permanently lost the capacity to become a member of another group (Figure 2). However, this theory changed radically in 2006 when induced pluripotent stem (iPS) cells using mouse as a model organism were introduced (Takahashi & Yamanaka, 2006). In 2007, human iPS cells were reported (Takahashi et al 2007; Yu et al, 2007) and provided further evidence that somatic cells can dedifferentiate into stem cells.

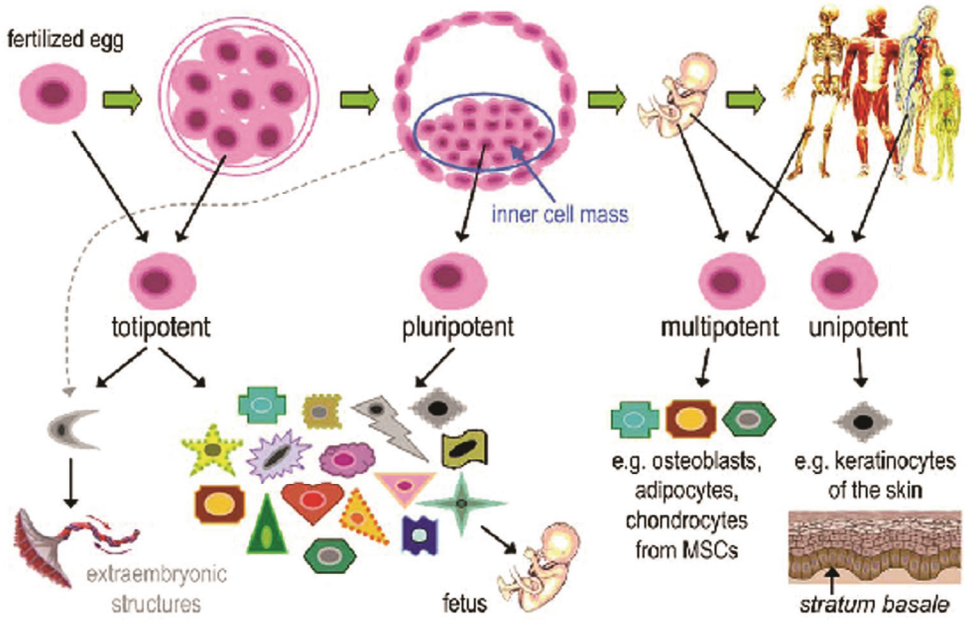

Figure 1. Classification of human stem cells. A fertilized egg and the first eight cells in an embryo are called totipotent; these cells can form the entire human being as well as the extraembryonic structures. Pluripotent stem cells can be isolated from the inner cell mass of an embryo. These cells are able to differentiate into any human cell type, but they are not able to form the extraembryonic structures. Multipotent stem cells have limited differentiation capacity compared to pluripotent stem cells, and unipotent stem cells are able to differentiate into only one type of cell. Multipotent and unipotent stem cells can be found in fetuses as well as in adult tissues. Mesenchymal stem cells (MSCs) are described as an example of multipotent stem cells, which can differentiate into osteoblasts, adipocytes and chondrocytes. Unipotent precursor cells of skin keratinocytes reside in the *stratum basale*.

2.1.2. Human induced pluripotent stem cells

The introduction of induced pluripotent stem (iPS) cells was a revolutionary event for the entire scientific community, although some preceding work had been conducted earlier. For example, cloning techniques that used somatic cell nuclear transplantation (SCNT) (Briggs & King, 1952; Gurdon, 1962; Wilmut et al, 1997), the observation that changes in the gene expression of somatic cells are able to change the entire identity of the cell (Davis et al, 1987) and the first derivations of embryonic stem (ES) cell lines (Evans & Kaufman, 1981;

Notarianni et al, 1991; Moreadith & Graves, 1992; Thomson et al, 1995; Thomson et al, 1998) served as stepping stones for iPS cell production.

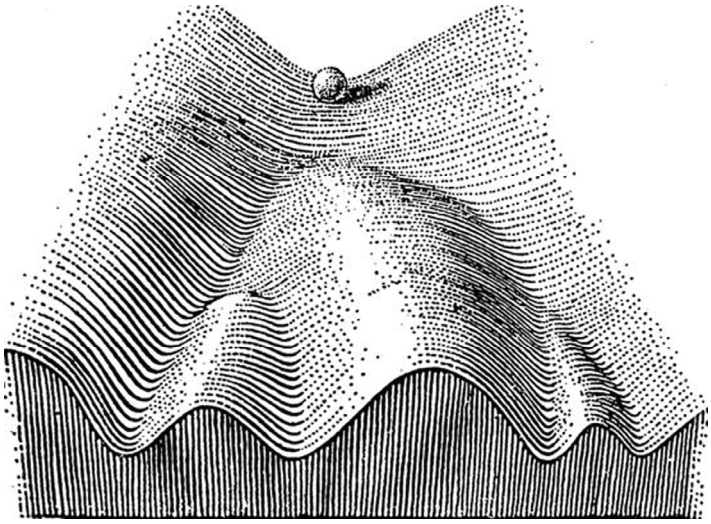

Figure 2. The model for the differentiation of a stem cell presented by Conrad Waddington (1957). Waddington's landscape illustrates how a pluripotent stem cell becomes more determined during development and that the capacity of a cell to differentiate toward an alternative destination decreases during the determination process. The stem cell is demonstrated as a ball that is rolling down the landscape and making its way through different valleys and elevations toward different end points. The end points represent mature differentiated cells. (Waddington, 1957)

2.1.2.1. Generation of induced pluripotent stem cells

In 2006, the generation of iPS cells was first published (Takahashi & Yamanaka, 2006). This study used mouse embryonic fibroblasts where certain pluripotency genes (*Oct4*, *Sox2*, *c-Myc* and *Klf4*) were inserted using retroviral transfections. Oct4 is an abbreviation for octamer-binding transcription factor 4, and this protein is also known as POU5F1 (POU domain, class 5, transcription factor 1). Oct4 is a transcription factor that binds to a certain regulatory region (5'-ATGCAAAT-3') in various genes that are involved in self-renewal and differentiation (Verrijzer et al, 1990). Oct4 is required for the formation of the

inner cell mass in an embryo (Nichols et al, 1998) and maintaining the pluripotency in ES cells (Hay et al, 2004; Wang & Dai, 2010). Sox2 (sex determining region Y-box 2) is also a transcription factor that is essential for the development of an embryo (Avilion et al, 2003), and it co-operates with Oct4 to regulate the expression of other various pluripotency genes (Chew et al, 2005). c-Myc is an abbreviation for the myelocytomatosis viral oncogene homolog that is known to up-regulate the expression of many genes, some of which are involved in cell proliferation. c-Myc promotes the maintenance of ES pluripotency via leukemia inhibitory factor (LIF) and signal transducer and activator of transcription 3 (STAT3) (Cartwright et al, 2005). c-Myc may also induce histone acetylation, allowing Oct4 and Sox2 to bind to their specific loci (Fernandez et al, 2003). Klf4 represents for Kruppel-like factor 4, is an indicator of the pluripotent capacity of stem cells and is required for example for the left-right asymmetry of an embryo (Lai et al, 2011). Klf4 is also known to down-regulate the expression of the p53 tumor suppressor gene, which on the other hand represses the expression of Nanog (Rowland et al, 2005), another important pluripotency factor (addressed later).

In 2007, the first human iPS cells were introduced to the public by two different groups (Takahashi et al, 2007; Yu et al, 2007). One of these studies (Takahashi et al, 2007) utilized the same retroviral transfection method that was used for reprogramming the mouse embryonic fibroblasts (Takahashi & Yamanaka, 2006), while in the other study (Yu et al, 2007), lentiviruses were used for the delivery of the reprogramming factors. In both studies, the starting material was adult skin fibroblasts. The combinations of transgenes were either *OCT4*, *SOX2*, *c-MYC* and *KLF4* (Takahashi et al, 2007) or in the other work *OCT4*, *SOX2*, *NANOG* and *LIN28* (Yu et al, 2007) (Table 1). Nanog is yet another transcription factor that is known to be involved in the self-renewal of ES cells. The expression of Nanog is regulated by Oct4 and Sox2 (Rodda et al,

2005), and Nanog is known to aid the maintenance of the undifferentiated state of ES cells by inhibiting bone morphogenetic protein (BMP) -signaling (Suzuki et al, 2006). *Lin28* encodes a microRNA-binding protein and has been shown to, for example, up-regulate Oct4 expression (Qiu et al, 2010; Thornton & Gregory, 2012). It also has been proposed that Lin28 has an important role in nucleologenesis during early embryonic development (Vogt et al, 2013).

Some variations in these four factor combinations are possible to use for successful reprogramming (Lai et al, 2011), and combining all six factors, *OCT4*, *SOX2*, *c-MYC*, *KLF4*, *NANOG* and *LIN28,* has been shown to increase the reprogramming efficiency (Liao et al, 2008). On the other hand, all the reprogramming factors can be replaced with another factor or even with a chemical or small molecule (for a review, see Walia et al, 2012). Methods to reduce the number of reprogramming factors have taken advantage of endogenously expressed genes, consequently decreasing the need for ectopic expression of pluripotency factors (Lai et al, 2011). The differential gene expression pattern in different cell types results in an unequal need for the exogenous reprogramming factors; therefore, in some cells, one of the factors can be excluded, but in some other cell type, this same factor is essential for reprogramming. For example, *OCT4* alone can convert human neural stem cells into iPS cells (Kim et al, 2009). Also, *c-MYC* can be excluded when human fibroblasts are reprogrammed because these cells endogenously express c-Myc (Nakagawa et al, 2008). Nevertheless, omitting one or more of the factors usually affects the reprogramming efficiency (Lai et al, 2011). Different reprogramming factors are summarized in Table 1.

Table 1. Reprogramming factors (modified from Walia et al, 2012). Abbreviations included in the table: HDAC = histone deacetylase; p53 = protein 53 or tumor protein 53; Lefty1 = left-right determination factor 1; let-7 = miRNA precursor; miRNA = microRNA; Oct4 = octamer binding transcription factor 4; H2A = histone 2 A; BMP = bone morphogenetic protein; SMAD1 = an intracellular protein involved in TGF-β-signaling; TGF-β = transforming growth factor β; Sox2 = sex determining region Y-box 2; FGF4 = fibroblast growth factor 4; and Utf1 = undifferentiated embryonic cell transcription factor 1.

Factor	Interacting domain	Target genes / pathways
c-Myc	E boxes	HDACs, p53
Klf4	Zinc finger	p53, Nanog, Lefty1
Lin28	Cold shock	let-7, miRNA, various mRNAs including Oct4 and H2A
Nanog	Homeobox	BMP pathway via SMAD1, Nanog, Oct4, Sox2
Oct4	POU domain	Oct4, Nanog, FGF4, Utf1, Sox2
Sox2	HMG domain	Oct4, Sox2, Nanog, FGF4, Utf1

2.1.2.2. The cells and delivery methods used for the production of induced pluripotent stem cells

The first human iPS cells were generated from dermal fibroblasts but after that, numerous different cell types have been successfully reprogrammed into human iPS cells. Keratinocytes (Aasen et al, 2008), neural stem or progenitor cells (Kim et al, 2009), astrocytes (Ruiz et al, 2010), amniotic cells (Li et al, 2009a), adipose tissue (Sun et al, 2009), cord blood cells (Takenaka et al, 2010), T lymphocytes (Seki et al, 2011) and skeletal muscle stem cells (Tan et al, 2011) represent examples of other primary human cells that have been reprogrammed thereafter. Also, peripheral blood cells (Staerk et al, 2010, Loh et al, 2010) and human urine -derived cells (Zhou et al, 2011) have been reprogrammed into iPS cells. In addition, cell lines derived from human gastrointestinal cancers have been used as starting material for iPS cell production (Miyoshi et al, 2009).

The increase in the possibilities for iPS cell generation has raised a question about the epigenetic memory of the iPS cells derived from different cell types. The term epigenetic memory refers to the phenomenon of retaining certain features of the epigenomes of the original somatic cell. The mechanisms involved in the development of this memory include enzymatic modifications of the chromatin structure, such as histone modifications and DNA methylation, as well as the regulation of transcription factors, signaling pathways and expression of microRNAs (miRNAs), which are small non-coding RNAs that can modulate mRNA expression (for a review, see Medvedev et al, 2012). It has been shown that iPS cells contain residual epigenetic marks, but also that these marks can be eliminated by continuous cell culturing (Kim et al, 2010). In addition, the residual memory of the iPS cells may be influenced by both the original cell type (Polo et al, 2010) and the reprogramming method (Chin et al, 2009; Kim et al, 2010). The epigenetic memory of iPS cells has been shown to influence the differentiation capacity of the cells, such that an iPS cell favorably differentiates along the lineages related to the original cell type (Kim et al, 2010). Attempts to erase the residual epigenetic marks of iPS cells have included simply growing the iPS cells for several passages (Chin et al, 2009; Polo et al, 2010) or treating the cells with epigenetic modifiers (Kim et al, 2010), such as trichostatin A (TSA), a potent inhibitor of histone deacetylase (Eden et al, 1998), or 5-azacytidine (AZA), a methylation-resistant cytosine analogue (Chiu & Blau, 1985).

Yet another influence on the efficiency of iPS cell generation – and also for the differentiation capacity of the iPS cells (Kim et al, 2010) – is the method that is used for transferring the reprogramming genes into the cells. Retroviral and lentiviral transductions were the first methods that were used to introduce the reprogramming factors into human somatic cells (Takahashi et al, 2007; Yu et al, 2007), and retroviral transduction still remains one of the most widely

used methods. It is also one of the most efficient methods for reprogramming. After the first study (Yu et al, 2007), lentiviral vectors have also been used for gene delivery during human iPS cell production (Hockemeyer et al, 2008; Chang et al, 2009; Hotta et al, 2009; Sommer et al, 2009). Both of these methods involve genomic integration of the viral transgenes, which unfortunately causes a risk of insertional mutagenesis (Figure 3 A). The usage of retroviruses also enables the reactivation of transgenes and tumor formation, which cause this method to be unsuitable for therapeutic purposes.

Adenoviruses can be used for gene delivery without the risk of integration of viral transgenes into the genome of the host cells (Stadtfeld et al, 2008; Zhou & Freed, 2009) (Figure 3 B). Unfortunately, this delivery method produces iPS cells at a lower efficiency and it also requires repeated infections to maintain the expression of the pluripotency factors. One rather encouraging possibility is the use of integrating lentiviral vectors that can be excised from the host cell genome with Cre-recombinase to generate iPS cells that are free of the reprogramming factors (Soldner et al, 2009). Currently, the most promising and rather efficient viral delivery technique utilizes Sendai viruses for transduction (Figure 3 C). Sendai viruses are RNA viruses that accomplish their replication in the host cell cytoplasm without entering the nucleus, and thereby, no integration of the viral transgenes occurs (Fusaki et al, 2009).

Non-viral gene delivery methods have also been introduced, but the efficiency of these methods is notably lower than the viral ones. Nucleofection of a non-viral construct containing reprogramming genes has been used to generate mouse iPS cells (Okita et al, 2008; Gonzalez et al, 2009) with low efficiency. Human iPS cells have been reprogrammed using a non-integrating episomal gene delivery vector, but again the efficiency was quite low (Yu et al, 2009). The *Piggyback* transposon gene delivery system is a non-viral vector that can induce stable genomic integration and persistent gene expression in

mammalian cells (Figure 3 D). The *Piggyback* system seems to be the most efficient among the non-viral systems, and although it involves integration, the transgenes can be removed from the host cell genome after reprogramming (Woltjen et al, 2009; Kaji et al, 2009).

The use of genetic material during iPS cell production may be a problem if the cells are intended for clinical purposes. Therefore, iPS cells have also been generated without any gene delivery into the cells. The delivery of reprogramming proteins attached to cell-penetrating peptides can be used for human iPS cell production (Kim et al, 2009) but with low efficiency. In addition, this method requires repeated delivery of the proteins, which may harm the cells. Delivery of messenger RNAs (mRNA) of pluripotency genes into the cells that are reprogrammed is non-mutagenic and functions with high efficiency, but repeated delivery of the mRNAs is again needed (Warren et al, 2010). Also miRNAs have been used to promote the transcription factor - mediated reprogramming process and also to induce reprogramming in the absence of any additional factors. This method performs with relatively high efficiency, but it also requires repeated transfections of the miRNAs into the cells (Anokye-Danso et al, 2011; Miyoshi et al, 2011).

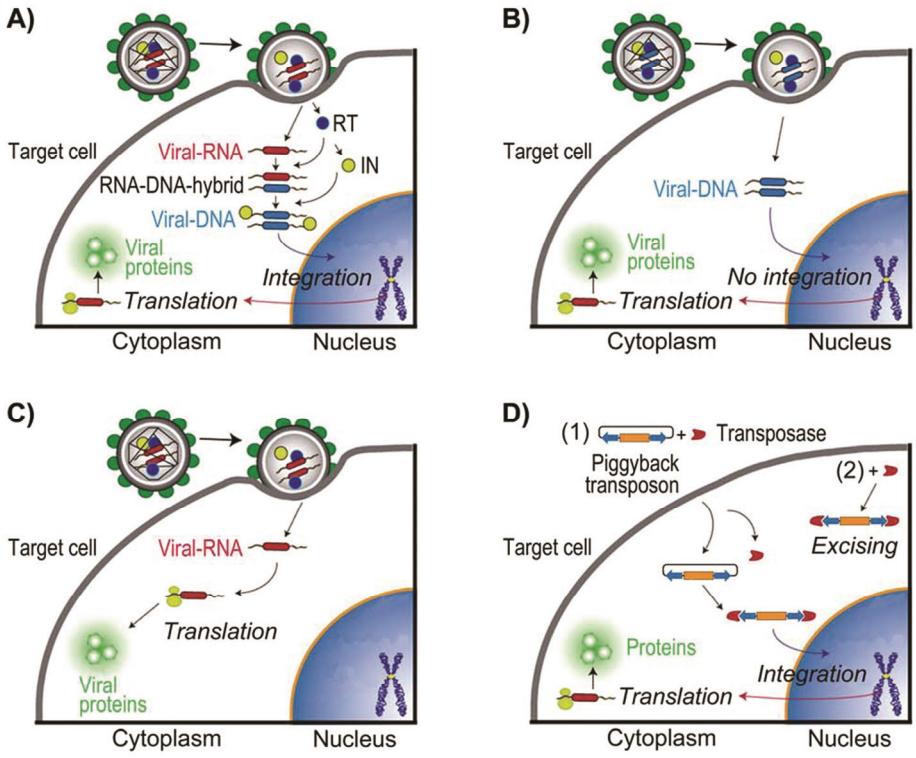

Figure 3. Viral delivery of reprogramming factors into the cells and the *Piggyback* transposon system. **A)** The use of lenti- and retroviral vectors for gene delivery involves conversion of the viral RNA into DNA by reverse transcriptase (RT) and the integration of the viral DNA into the genome of the host cell by integrase (IN). Viral genes are then expressed by the host cell transcription and translation machinery. **B)** Adenoviruses have a DNA genome that enters the nucleus of the host cell but does not integrate into the host cell genome. The expression of the viral genes is achieved using the host cell machinery for transcription and translation. Adenovirus vectors can be used to achieve transient expression of delivered genes, but because no integration occurs, the expression is not permanent. **C)** Sendai viruses are RNA viruses with a negative-strand RNA genome that is directly used as mRNA and translated into proteins by the host cell without entering the nucleus. Sendai virus vectors can be used for efficient gene delivery without the disadvantages caused by integration. **D)** The *Piggyback* transposon system utilizes a transposase enzyme, which is able to detach the delivered genes from the *Piggyback* vector at special cleavage sites and induce the integration of the transgenes into the host cell genome (1). The integrated genes are then expressed as endogenous genes. Subsequently, the transgenes can be excised from the host cell genome by the same transposase enzyme introduced into the cell (2). The figure is modified from a figure regarding lentivirus vectors at the webpage of System Biosciences (SBI), Mountain View, CA, USA (http://www.systembio.com/support/resources/faqs/lenti).

Also, certain chemicals and small molecules can be used to replace some of the reprogramming factors, as mentioned previously, or to improve the efficiency of iPS cell generation (Walia et al, 2012). The enhancement of reprogramming is usually based on chromatin modifications or the inhibition of certain cell signaling pathways. For example, human primary keratinocytes can be reprogrammed to iPS cells using tranylcypromine (an inhibitor of lysine-specific demethylase 1) and CHIR99021 (a specific glycogen synthase kinase 3 (GSK-3) inhibitor) with only Oct4 and Klf4 (Li et al, 2009b). On the other hand, valproic acid (VPA, a histone deacetylase inhibitor) enables reprogramming of primary human fibroblasts to iPS cells with Oct4 and Sox2 alone with a similar efficiency that of Oct4, Sox2 and Klf4 (Huangfu et al, 2008). Murine cells have been successfully reprogrammed using the combination of VPA, tranylcypromine, CHIR99021 and 616452 (a TGF-β kinase inhibitor) in the presence of only transfected Oct4 (Li et al, 2011), and more resently, using only a combination of six chemicals: VPA, tranylcypromine, CHIR99021, 616452, forskolin (cAMP agonist) and DZNep (3-Deazaneplanocin A, an inhibitor of S-adenosylmethionine-dependent methyltransferase) (Hou et al, 2013). In addition to chemicals and small molecules, some cell culture conditions (for example, hypoxia and a high level of basic fibroblast growth factor (bFGF)) are known to induce the expression of pluripotency genes and thereby support reprogramming (For a review, see Walia et al, 2012). A simplified description of the generation and differentiation of iPS cells is illustrated in Figure 4, and the methods currently used for iPS cell production are listed in Table 2.

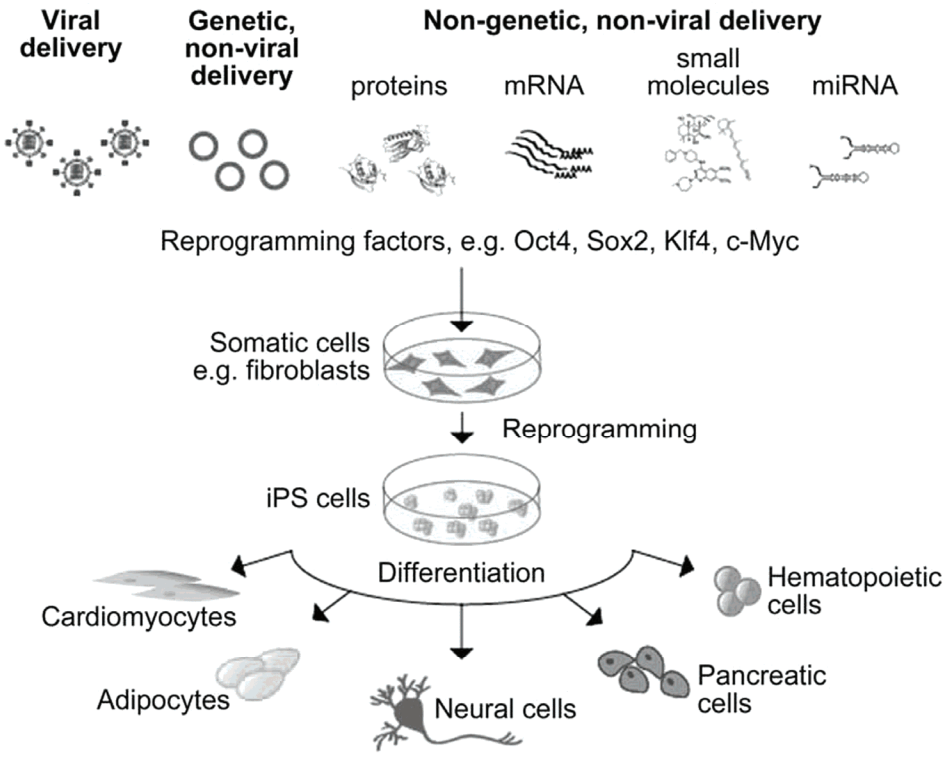

Figure 4. Production and use of iPS cells. The delivery of reprogramming factors into the somatic cells can be achieved by various methods, including the use of different viral vectors, non-viral DNA vectors, complete proteins or mRNA. Small molecules or miRNA can be used to induce and activate the endogenous pluripotency factors inside the cells. Reprogramming of somatic cells into iPS cells occurs gradually as the cells are maintained in ES cell culture conditions. Pluripotent iPS cells can be differentiated into various cell types using specific differentiation protocols. The figure has been modified from the original figure found at the webpage of Mirus Bio LLC, Madison, WI, USA (https://www.mirusbio.com/stem_cell_solutions).

Table 2. Methods for reprogramming induced pluripotent stem cells.

Viral delivery	Non-viral delivery	
	Genetic	*Non-genetic*
Retroviruses (integration of the transgenes)	Nucleofected construct containing reprogramming sequences	Delivery of reprogramming proteins into the cells
Lentiviruses (integration of the transgenes)	Non-integrating episomal vectors	Delivery of mRNAs of the reprogramming factors
Adenoviruses (non-integrating)	*Piggyback* transposon system	Use of miRNA
Sendai viruses (non-integrating)		Use of chemicals and/or small molecules
Cre-recombinase lentiviruses (integrating but excisable)		

2.1.2.3. Characterization of induced pluripotent stem cells

iPS cells are usually first characterized by their morphology, their growth habit and the type of colonies they tend to form (Figure 10 A). Pluripotent human stem cells, including iPS cells, are typically round cells that have a high nucleus to cytoplasm ratio and large nucleoli. Pluripotent human stem cells proliferate in cell culture extensively and form compact colonies with defined edges and distinct cell borders (Thomson et al, 1998). Telomerase and alkaline phosphatase activities are typical for pluripotent stem cells, and the cells retain the normal karyotype during an extended time of cell culturing (Hoffman & Carpenter, 2005). Pluripotency can be verified also by examining the methylation status of certain promoters. For example, *Oct4* and *Nanog* are demethylated during reprogramming, and the unmethylated status of these genes indicates that the genes are actively transcribed as they are in human ES cells (Mikkelsen et al, 2008). Other pluripotency markers that are known to be

expressed in iPS cells as well as in ES cells include Sox2 (see above), RNA exonuclease 1 (Rex1), stage-specific embryonic antigens 3 and 4 (SSEA3 and SSEA4), tumor-related antigens 1-60 and 1-81 (TRA1-60 and TRA1-81) and alkaline phosphatase (ALP) (Adewumi et al, 2007). Transcription profiles of human ES and iPS cells are shown to be very similar, but some differences have been discovered (Marchetto et al, 2009). For characterization of pluripotency, these markers can be detected from iPS cells using the reverse transcriptase polymerase chain reaction (RT-PCR) or by immunocytochemical staining of the cells. RT-PCR reveals the expression of the markers at the mRNA level, while expression at the protein level can be observed by staining the cells.

In addition to DNA methylation, a certain pattern of histone modifications, which includes combinations of activating and repressive histone modifications, occurs in pluripotent stem cells compared to differentiated cells. Bivalent histones typical for ES cells appear also in the chromatin of iPS cells as the cells are completely reprogrammed, which may ensure the transcriptional flexibility of the pluripotent cells (Bernstein et al, 2006; Wernig et al, 2007). During reprogramming, the exogenous (viral) transgenes are silenced, and the expression of endogenous pluripotency genes is up-regulated. In completely reprogrammed cells, silencing of the exogenous factors is complete (Maherali et al, 2007; Okita et al, 2007; Wernig et al, 2007), whereas partially reprogrammed iPS cells show incomplete silencing and persistent expression of the viral factors (Takahashi & Yamanaka, 2006). These data indicate the gradual nature of silencing (Stadtfeld et al, 2008) that is known to involve for example, *de novo* DNA methylation, histone deacetylation and methylation, as well as chromatin remodeling (for a review, see Hotta & Ellis, 2008). Chromodomain helicase DNA binding protein 1 (Chd1) and rg/Brahma-associated factors (BAF) may facilitate the binding between the endogenous reprogramming factors and their target genes and thereby reactivate and maintain the expression of endogenous

pluripotency genes in the absence of exogenous factors (Gaspar-Maia et al, 2009; Singhal et al, 2010). By the end of the reprogramming process, the repressed X-chromosome is also reactivated in female iPS cells (for a review, see Kim et al, 2011).

Usually, the *in vitro* differentiation capacity of iPS cells is verified by an embryoid body (EB) formation -assay to show that the iPS cells can differentiate into cell types of all three germ layers. The ability of iPS cells to form teratomas when injected into immunodeficient mice indicates the pluripotent differentiation capacity of the cells *in vivo*. Tissues that originate from different germ layers are detected from these tumors to confirm pluripotency (Brivanlou et al, 2003; Maherali & Hochedlinger, 2008; Thomson et al, 1998). Finally, the normal karyotype of an iPS cell line is usually verified during the characterization of the cells.

2.2. Cardiomyocytes and the human heart

2.2.1. The structure of the human heart

Heart muscle, *myocardium,* is constructed from elongated and coalesced heart muscle cells called cardiomyocytes that are able to contract (Figure 5 A). Serial cardiomyocytes form cardiac muscle fibers that are surrounded by matrix-containing collagen fibers and other components of the connective tissue, as well as blood vessels and nerves. The human heart is organized to form four separate chambers: left atrium, left ventricle, right atrium and right ventricle. The left and right halves of the heart are separated from each other by a *septum,* and valves are located between the atria and ventricles as well as between the atria and main veins. The inner lining of the heart is covered by endothelial cells and is called the *endocardium.* The external surface of the myocardium is

surrounded by mesothelial cells that form a structure called the *epicardium* (Heikkilä et al, 2000) (Figure 5 A).

2.2.2. Cardiac cells

The atrial and ventricular myocardial cells, also called cardiomyocytes, constitute a major part of the organ and are responsible for the contraction and relaxation of the heart. Nevertheless, approximately half of the cells constituting the heart are fibroblasts (Camelliti et al, 2005). Ventricular cardiomyocytes can still be divided into three different groups according to their position within the myocardium: epicardial, mid-myocardial and endocardial cells (Yan & Antzelevitch, 1998). The different types of ventricular cardiomyocytes differ from each other also by their electrophysiological and functional properties (Antzelevitch et al, 1991; Antzelevitch et al, 1999). The differences can be observed in the depolarization and repolarization characteristics of the cardiomyocytes due to distinct ion current properties of the cells. In addition, electrophysiological differences between the mid-myocardial cells originating from the left or right ventricle have been described (Di Diego et al, 1996; Volders et al, 1999).

A single ventricular cardiomyocyte is typically 50 to 150 μm long and 10 to 20 μm wide, while atrial cardiomyocytes are slightly smaller. The interior of a cardiomyocyte is organized into hundreds of myofibrils that span from one end of the cell to the other (Figure 5 B). Every myofibril is composed of molecular structures called *sarcomeres* that are responsible for the contraction of the cell. The sarcomere is further composed of thick and thin myofilaments and intermediate filaments that are strictly organized to maximize the efficiency of cell contraction. The difference in the length of a sarcomere from complete relaxation to maximum contraction is 0.6 μm (from 2.2 μm to 1.6 μm). Thick myofilaments are comprised of myosin molecules that are connected to each

other by cardiac myosin binding protein C (cMyBP-C), and a myosin molecule contains two identical molecules called myosin heavy chain (MHC) and two pairs of myosin light chains named myosin light chains 1 and 2 (MLC1 and MLC2). Thin myofilaments are composed of actin, a group of troponin molecules and tropomyosin. Certain binding sites for myosin are located along the actin filaments to allow the contraction of the sarcomere (Heikkilä et al, 2000). The structures of a cardiomyocyte and sarcomere are illustrated in Figure 5 B.

In addition to ventricular and atrial cardiomyocytes, two smaller groups of cardiac myocytes can also be found in the heart: the pacemaker cells and the electrical conducting cells. Together these cardiomyocytes are called nodal cells. Pacemaker cells are approximately 5-10 μm long and are able to depolarize spontaneously at a certain rate that is dependent on neural and hormonal actions. Pacemaker cells reside in the *sinus node* (Figure 5 A) and initiate a wave of depolarization through the heart that results in the contraction of the heart. Electrical conducting cells on the other hand are thin and long cells that carry the cardiac current efficiently and rapidly from the sinus node to distant regions of the heart. (Thaler, 1999.)

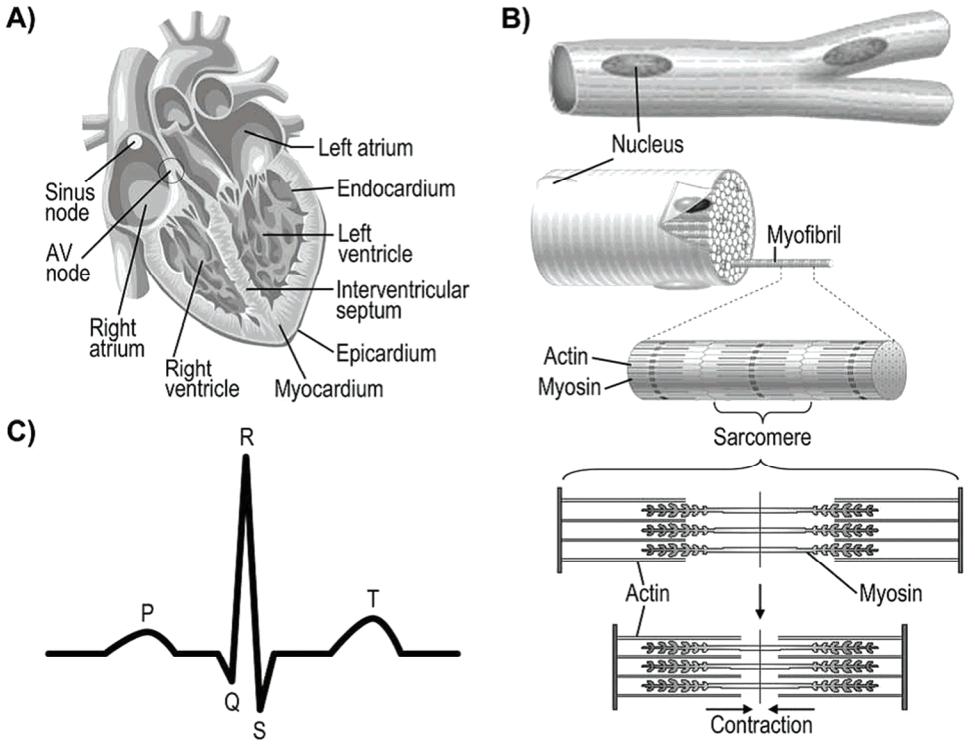

Figure 5. Structure and function of the human heart. **A)** The human heart consists of four separate chambers: the right and left atria and the right and left ventricles, which are separated from each other by the interventricular septum. The endocardium is the innermost layer of the myocardium, or the heart muscle, and the epicardium envelopes the myocardium outside the heart. The sinus node and atrioventricular (AV) node reside as indicated in the figure. **B)** A cardiomyocyte is composed of myofibrils, which are further formed by the highly organized alignment of sarcomeres. The major molecules composing the sarcomere structure are actin and myosin filaments, which are responsible for the contraction of the entire cardiac myocyte. **C)** Here is presented a schematic illustration of an electrocardiogram (ECG). The separate waves of an ECG are named with the letters P, Q, R, S and T (see the following text). The figure collage is composed from original figures and information in the Cardiovascular Medicine Book (http://www.fpnotebook.com/cv/ index.htm), as well as from the original figure of the structure of the cardiac myofibril and sarcomere by Benjamin Cummings, Addison Wesley Longman, Inc. (2001).

2.2.3. Cardiac differentiation in cell culture

Cardiomyocytes are challenging to study in cell culture because obtaining a myocardial biopsy presents a risk for the donor, and primary cardiomyocytes tend to dedifferentiate and stop beating relatively quickly *in vitro* (Mitcheson et al, 1996). However, pluripotent stem cells are able to differentiate into any cell type of an organism; therefore, pluripotent stem cells provide a useful tool also for cardiac research. Human ES cells (Kehat et al, 2001) as well as human iPS cells (Zhang et al, 2009) can differentiate into cardiomyocytes with nodal-, atrial- and ventricular phenotypes, and these cardiac cells also express transcription factors and structural proteins that are specific for cardiomyocytes (Zwi et al, 2009). However, the cardiomyocytes derived from pluripotent stem cells are rather immature based on the morphology and structural organization as well as on their functionality if they are compared to primary adult cardiomyocytes (Lieu et al, 2009; Luna et al, 2011).

Multiple methods are used for cardiac differentiation in cell culture, although all the methods have some limitations and challenges. Usually, pluripotent stem cells differentiate into cardiomyocytes in 20 days, but variations exist between different methods and also between different cell lines (Skottman et al, 2005; Allegrucci & Young, 2007; Moore et al, 2008; Osafune et al, 2008; Pekkanen-Mattila et al, 2009). The epigenetic variation between different iPS cell lines is broad (Kim et al, 2010), which may additionally limit their capacity for cardiac differentiation compared to ES cells and increase the range in differentiation efficiency between the iPS cell lines (Zhang et al, 2009; Toivonen et al, 2013). As evidence of the epigenetic influence on the cardiac differentiation capacity of iPS cells, two studies using mouse cells should be mentioned. One study used murine ventricular myocytes to derive iPS cells, and these cells exhibited a higher tendency to spontaneously differentiate into beating cardiomyocytes compared to ES cells and iPS cells originated from

fibroblasts (Xu et al, 2011). In the other study, neonatal cardiomyocytes were reprogrammed into iPS cells and re-differentiated into cardiac myocytes again at a higher efficiency than ES cells or iPS cells derived from cardiac fibroblasts (Rizzi et al, 2011).

Pluripotent stem cells can be differentiated spontaneously as EBs by dissociating the cell colonies into small cell clusters and allowing the clusters to form aggregates in suspension (Kurosawa, 2007). Cardiomyocytes, as well as other cell types, can be obtained by this EB differentiation method (Itskovitz-Eldor et al, 2000; Kehat et al, 2001; Zhang et al, 2009) that is widely used because it is an easy and inexpensive method for producing cardiac cells. The forced aggregation (FA) -method is another EB-forming technique in which the cells are forced to form aggregates by centrifugation (Ng et al, 2005; Burridge et al, 2007). The advantage of this technique is that the number of cells and thereby the size of the EBs can be standardized, which influences differentiation (Burridge et al, 2007; Bauwens et al, 2008; Mohr et al, 2010).

A more controlled method for cardiac differentiation from pluripotent stem cells utilizes mouse endodermal-like cells (END-2). The stem cells are co-cultured with END-2 cells in the absence of serum or serum replacement and with ascorbic acid (Mummery et al, 2003; Passier et al, 2005). END-2-conditioned medium can also be used instead of co-culturing (Graichen et al, 2008). The mechanisms by which the END-2 method works for cardiac differentiation are still unclear, but the removal of insulin and secretion of prostaglandin I_2 (PGI_2) by END-2 cells are thought to play roles in the process (Xu et al, 2008).

Differentiation of cardiomyocytes can also be driven by defined growth factors and other supplements that influence certain signaling pathways. Ascorbic acid was already mentioned as one supplement that enhances cardiac differentiation (Passier et al, 2005), as well as the removal of insulin and

addition of PGI_2 (Xu et al, 2008). Culturing the cells in serum-free conditions during differentiation also increases the efficiency of cardiac differentiation (Braam et al, 2008). Yet another way to increase the production of cardiomyocytes is the inhibition of p38 mitogen activated protein kinase (MAPK) when END-2-conditioned medium is used (Graichen et al, 2008). A differentiation protocol that is based on the addition of supplements alone utilizes a combination of activin A and bone morphogenetic protein 4 (BMP4) in cardiomyocyte production (Laflamme et al, 2007). Other protocols are based on EB formation, but growth factors are added to the culture medium in a certain order and in certain combinations. For example, the growth factors BMP4, bFGF, activin A, vascular endothelial growth factor (VEGF) and dickkopf homolog 1 (DKK1) can be used in varying combinations to enhance cardiac differentiation (Yang et al, 2008). Also, together with the FA technique, the following supplements added in different phases of the protocol have been used to improve the efficiency of cardiac differentiation: 1-thioglycerol, polyvinyl alcohol (PVA), insulin, BMP4, bFGF, chemically defined lipids, inhibitor of the rho-associated protein kinase (ROCK), human serum albumin (HSA) and ascorbic acid (Burridge et al, 2011). The most recent differentiation method is based on the inhibition of Wnt signaling at certain points during differentiation with different inhibitors that function by slightly different mechanisms (Minami et al, 2012; Lian et al, 2012). During this differentiation method, mesodermal differentiation is first initiated using an aminopyrimidine named CHIR99021, which is a highly selective inhibitor of glycogen synthase kinase 3β (GSK-3β). Inhibition of GSK activates Wnt signaling, thereby causing the differentiation of pluripotent stem cells toward mesoderm. After initiation, Wnt signaling is inhibited by some specific Wnt inhibitor (IWP-4, KY02111 or XAV939), which directs the mesodermal cells toward a cardiac cell lineage (Minami et al, 2012; Lian et al, 2012). (Wnt is an abbreviated combination of

Wingless (the *Drosophila melanogaster* segment-polarity gene) and *Integrase-1* (the vertebrate homolog of *Wingless*).) Recently, Burridge and colleagues published an efficient protocol for chemically defined production of human cardiomyocytes, which also utilizes the inhibition of GSK-3β by CHIR99021 and the inhibition of Wnt signaling by Wnt-C59 (Burridge et al, 2014).

2.2.4. Visual and biochemical characterization of cardiomyocytes

Usually, the first evidence of successful differentiation of stem cells into functional cardiomyocytes *in vitro* is the appearance of spontaneously beating cell aggregates (Kehat et al, 2002; Mummery et al, 2003). The gene expression pattern of these beating cells is known to mimic the pattern during early embryogenesis; thus, the first up-regulated genes are primarily mesodermal, after which the cardiac progenitor genes and the genes that are expressed in fetal cardiomyocytes are activated (Beqqali et al, 2006; Synnergren et al, 2008). The expression of marker genes typical for cardiomyocytes can be detected using RT-PCR or immunocytochemical staining. RT-PCR reveals the mRNAs of the genes, while staining the cells indicates the presence of cardiac-specific proteins.

Cardiomyocytes originate from the mesoderm, one of the three germ layers in an embryo that appears during gastrulation. Brachyury T is traditionally used as a marker for mesoderm and an early marker of the cardiac cell lineage (Kispert & Herrmann, 1994). During the development of the mammalian heart, several cardiac regulatory transcription factor genes are expressed in myocardial progenitors and immature cardiomyocytes. Islet-1 (*Isl-1*), mesoderm posterior 1 and 2 (*MESP1* and *MESP2*), NK2 transcription factor -related gene, locus 5 (*Nkx 2.5*), GATA binding protein 4 (*GATA4*) and T-box transcription factor 6 (*Tbx6*) are all activated during the process of cardiomyocyte development (Brand, 2003; Graichen et al, 2008; Yang et al,

2008). Cardiac-specific structural proteins, such as cardiac troponin T (cTnT, encoded by the gene named *TNNT2*) (Thierfelder et al, 1994), cardiac troponin I (cTnI), different myosin proteins and cardiac α-actinin, can be used as markers for a more mature cardiac phenotype (Kehat et al, 2001; Mummery et al, 2003). The cardiac specific connexin (Cx) proteins of gap junctions (Cx43, Cx40 and Cx45) (Gaborit et al, 2007) and ion channels, such as hERG or KCNQ1 (see later), are also used as cardiomyocyte markers. Gap junctions are channels in the cell membrane that participate in the electrical coupling of the cells, the transfer of ions and molecules between cells and the control of differentiation, proliferation, migration and metabolism. In cardiomyocytes, gap junctions play a crucial role in the electrical activation of the cells (reviewed by Maizels & Gepstein, 2012).

During cardiac differentiation in cell culture, the expression of certain ion channels is up-regulated, indicating further maturation of the cardiomyocytes with time (Sartiani et al, 2007). Nevertheless, human iPS cell -derived, as well as ES cell -derived, cardiac myocytes are quite immature when compared to primary adult cardiomyocytes. Morphologically, these cells are usually approximately ten times smaller than adult cells, and the intracellular structures are deficiently organized (Luna et al, 2011). In addition, the absence of transverse (t-) tubules in cardiomyocytes derived from pluripotent stem cells (Lieu et al, 2009) may reflect a certain immaturity of these cells. At least the lack of t-tubules can be assumed to affect the proper calcium (Ca^{2+}) handling in the cardiomyocytes differentiated from iPS or ES cells because the t-tubules are transverse invaginations of the sarcolemma that facilitate the fast spread of an electrical signal inside the cardiomyocytes, trigger homogenous calcium release into the cytoplasm and thereby enable the rapid and simultaneous contraction of the cell (Ferrantini et al, 2013). The network of t-tubules is highly developed

within the ventricles of the human heart, but absent or poorly developed in atrial cardiomyocytes (Heikkilä et al, 2000).

2.2.5. Electrocardiogram

Depolarization and repolarization are the fundamental functions of the heart. These processes are the electrophysiological events occurring in cardiomyocytes that produce an electrical current through the entire organ. This electrical activity can be measured by electrodes placed on the surface of the body and result in an electrocardiogram (ECG) (Figure 5 C). During one cycle of a cardiac contraction and relaxation, the first event is atrial depolarization that is initiated from the sinus node. The wave of depolarization spreads outward into the atrial myocardium and results in atrial contraction. Atrial depolarization is observed on an ECG as the P wave. The first part of the P wave corresponds to the right atrial depolarization, while the latter part reflects the left atrial depolarization. The *atrioventricular* (AV) *node* is the structure that is responsible for the conduction delay that is essential for the proper function of the heart. The delay is followed by ventricular depolarization that is observed on the ECG as the QRS complex. This complex consists of several distinct waves: the first downward wave is the Q wave, the first upward deflection is called the R wave and the second downward deflection is called the S wave. The earliest part of the QRS complex reflects the depolarization of the interventricular septum. The latter part represents primarily the depolarization of the left ventricle because the signal from the right ventricle is weaker and thereby covered by the simultaneously depolarizing left ventricle. The cycle of one contraction and relaxation is completed as the ventricular repolarization occurs and can be observed on an ECG as the T wave. (Thaler, 1999.) A schematic illustration of an ECG is presented in Figure 5 C.

2.2.6. Electrophysiology of cardiomyocytes

2.2.6.1. Patch clamp -method and cardiac action potential

The electrophysiology of beating cardiomyocytes can be studied using a variety of methods. For single cell investigation, the patch clamp -technique has traditionally been the gold standard (Hamill et al, 1981; Sakmann & Neher, 1984; Zilberter et al, 1982; Kornreich, 2007). The patch clamp -method utilizes glass micropipettes filled with ionic solution as electrodes. The micropipette forms a high resistance seal with the cell membrane, enabling the observations of changes in membrane potential or ion channel currents at the level of single cells or even single channels (Molleman, 2002). With the patch clamp -technique, a cardiac action potential (AP), an electrical event that eventually leads to the contraction of the cell, can be recorded from a single cardiomyocyte. A cardiac AP reflects the changes in ion currents across the cell membrane through different ion channels (Figure 6 A). The main ions that are involved in the cardiac AP are sodium (Na^+), calcium (Ca^{2+}) and potassium (K^+). Na^+ ions have the most important role in initiating the depolarization of a cardiomyocyte, while Ca^{2+} ions play a role during the mechanical contraction of the cell. The repolarization of the cardiac myocyte is primarily mediated by K^+ ions (Pollard et al, 2010). The AP measured from a ventricular cardiomyocyte is different from the one captured from an atrial cardiomyocyte or from a nodal cell (He et al, 2003; Zhang et al, 2009). Schematics of different APs as well as the main ion currents during one ventricular AP are illustrated in Figure 6. According to their AP, the cardiac myocytes differentiated from pluripotent stem cells in cell culture resemble fetal cardiomyocytes more than adult cardiac cells (He et al, 2003), although some maturation occurs if the cells are maintained for longer (Sartiani et al, 2007).

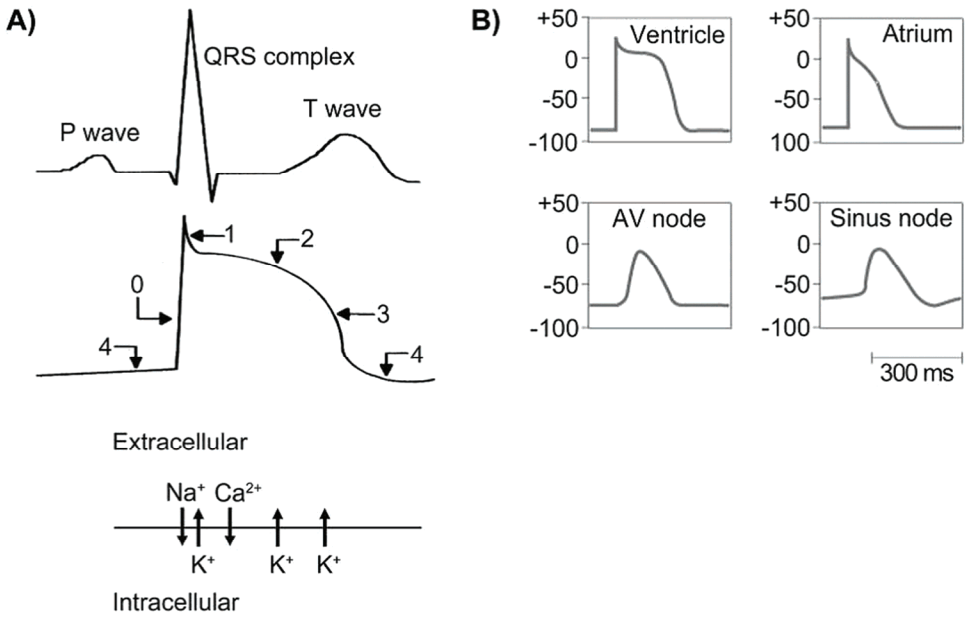

Figure 6. Cardiac action potentials and ECG waves. **A)** The ventricular cardiac action potential (AP) involves four different phases. The resting phase (4) is disrupted by the upstroke (0) that is achieved mainly by the inward current of Na^+ ions. The upstroke is followed by transient repolarization (1) that is induced by a small outward K^+ current and the plateau phase (2) during which the intracellular Ca^{2+} concentration arises. The final repolarization (3) is achieved by the K^+ current through I_{Kr} and I_{Ks} (see the text above). The timing during a cardiac AP can be compared to one cycle of depolarization and repolarization in an ECG as shown in the figure. **B)** Cardiac APs measured from different subtypes of cardiomyocytes are different from each other as illustrated here. The differences are due to distinct functions of the ion channels in different subtypes of cardiac myocytes. The figure is a merged rendition of the information gathered from an article by Hanno and colleagues (Hanno et al, 1995) and the webpage: http://rezidentiat.3x.ro/eng/ tulbritmeng.htm.

The depolarization of a cardiomyocyte means that the membrane potential (the voltage between the intracellular and extracellular space) changes to values that are more positive. The initiation of a cardiac AP is due to the opening of voltage-gated Na^{2+} channels in the cell membrane. This voltage change then influences L-type Ca^{2+} channels (LCCs) in the cell membrane through which the Ca^{2+} ions flow into the cardiomyocyte from the extracellular space (Figure 7). The influx of calcium then triggers the release of Ca^{2+} ions

from intracellular stores via ryanodine receptors (RyRs) in a process called Ca^{2+}-induced Ca^{2+} release (CICR) (Bers, 2002). This process elevates the cytoplasmic Ca^{2+} concentration one hundred-fold, and Ca^{2+} ions bind to troponin C molecules in the actin filaments. The interaction of Ca^{2+} ions and troponin C receptors allows the binding between actin and myosin filaments and thereby the contraction of the entire sarcomere. (Heikkilä et al, 2000; Poon et al, 2011.) T-tubules play an important role in enabling the fast spread of the electrical signal inside the cardiomyocytes as well as in triggering the homogenous increase in Ca^{2+} concentration in the cytoplasm by CICR (Ferrantini et al, 2013).

The relaxation of the cardiomyocyte results from the release of the Ca^{2+} ions from the troponin C molecules. This process can occur when the cytoplasmic Ca^{2+} concentration is reduced by the sarcoplasmic reticulum Ca^{2+} ATPase (SERCA) that pumps the Ca^{2+} back into the sarcoplasmic reticulum and by the Na^{+}/Ca^{2+} exchanger (NCX) that extrudes the Ca^{2+} ions out of the cell (Poon et al, 2011) (Figure 7). The rapidity of the cell relaxation depends on the rate of the discharge between the actin and myosin filaments. This process on the other hand is dependent on the affinity of Ca^{2+} ions to the troponin C molecules and the efficiency of Ca^{2+} removal from the cytoplasm into the endoplasmic reticulum and out of the cell (Heikkilä et al, 2000). The proper and fast escalation of Ca^{2+} concentration during depolarization and efficient Ca^{2+} removal from the cytoplasm during repolarization are crucial for the mechanical function of the cardiac myocyte (Poon et al, 2011).

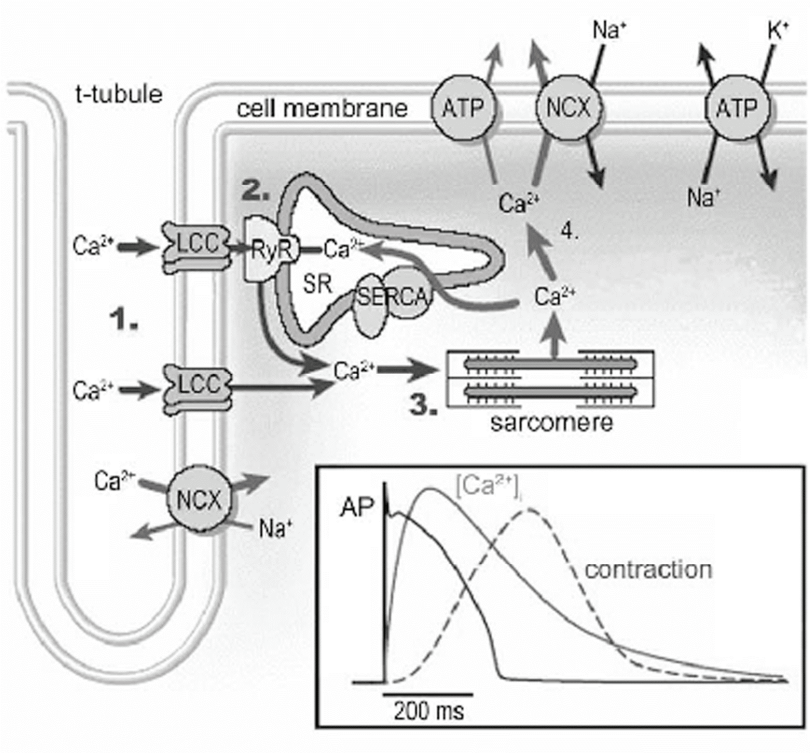

Figure 7. Elevation of the cytoplasmic Ca^{2+} concentration [Ca^{2+}] in cardiomyocytes. The depolarization of the cardiomyocyte and thereby the voltage change of the cell membrane influences the L-type Ca^{2+} channels (LCCs) through which the Ca^{2+} ions flow into the cardiomyocyte. This influx triggers the release of Ca^{2+} from sarcoplasmic reticulum (SR) via ryanodine receptors (RyRs). The increase in [Ca^{2+}] enables the binding of Ca^{2+} ions to sarcomere (troponin C) and the contraction of the cardiomyocyte. As [Ca^{2+}] is reduced by the sarcoplasmic reticulum Ca^{2+} ATPase (SERCA) and by the Na^{+}/Ca^{2+} exchanger (NCX), the Ca^{2+} ions are released from the sarcomere, and the cell relaxes. This figure is modified from the original illustration published in a review article by Bers in Nature (2002).

The repolarization of the cardiac cell membrane is accomplished by the efflux of K^+ ions through a variety of K^+ channels and inward currents of Na^+ and Ca^{2+} ions (Charpentier et al, 2010). One important channel in cardiomyocytes mediates the repolarizing rapid delayed rectifying K^+ (I_{Kr}) - current. This channel is often called the hERG channel because of its α-subunit encoded by the human Ether-à-go-go-Related gene (*hERG*, also called *KCNH2*), and the hERG current is one of the most important currents that determines

cardiac repolarization (Sanguinetti et al, 1995; Trudeau et al, 1995). The hERG channel is formed from four α-units (hERG) and four β-subunits called potassium voltage-gated channel subfamily E member 2 (KCNE2). Another K^+ current that contributes to the repolarization and termination of the cardiac AP is the slow delayed rectifying K^+ (I_{Ks}) -current. The channel responsible for the I_{Ks} current is a tetramer composed of four identical subunits expressed by the *KCNQ1* gene. KCNQ1 is an abbreviation for potassium voltage-gated channel, KQT-like subfamily, member 1 (Wang et al, 1996; Barhanin et al, 1996; Sanguinetti et al, 1996) and is alternatively called KvLQT1. There are also two β-subunits called KCNE1 forming the channel together with the KCNQ1 subunits. The delayed rectifying K^+ currents and cardiac repolarization have been extensively reviewed by Charpentier and colleagues (Charpentier et al, 2010).

2.2.6.2. Microelectrode array

A microelectrode array (MEA) can be used to measure the electrical activity of beating cell aggregates. MEA provides an additional platform for electrophysiological studies of cardiomyocytes. This method is rather easy and straightforward to use but has some limitations due to the dimensions of the instrumentation (Kehat et al, 2001; Hescheler et al, 2004; Reppel et al, 2004). In MEA, the beating cell aggregates are plated onto microelectrodes at the bottom of a chamber that is suitable for cell culturing, allowing cells to be maintained and measured for long periods of time. In addition, the MEA platform is suitable for pharmacological testing of cardiac effects (Braam et al, 2010), and large-scale testing is easier to accomplish than with the patch clamp -technique. However, the scale and structure of the MEA chamber allows cell aggregates but not single cardiomyocytes to be measured. For this reason, the results are unequal and not comparable to those gathered using the methods suitable for

single cells, such as the patch clamp -technique. On the other hand, MEA introduces an additional method and reveals additional data regarding the cardiomyocytes. MEA can be used as a complement to the patch clamp -method and for example Ca^{2+}-imaging, rather than a replacement for these methods.

The MEA system allows the recording of the field potential (FP) that resembles an ECG measurement (Reppel et al, 2004) although FP reflects the electrophysiology of a 2-dimensional structure while ECG is recorded from the 3-dimensional organ. Human iPS cell -derived cardiomyocytes have been successfully measured using MEA (Itzhaki et al, 2011; Mehta et al, 2011). From the cardiac FP, at least three parameters are usually defined. These parameters are the peak-to-peak interval (PPI), from which the beating rate can be calculated; the field potential duration (FPD) that can be used as a surrogate for the QT interval of an ECG; and the amplitude, shape and area under the curve (AUC) of the signal (Caspi et al, 2009).

2.2.6.3. Calcium imaging and calcium handling in human cardiomyocytes

Elevation of the intracellular Ca^{2+} through the CICR mechanism is closely associated with the contraction of a cardiomyocyte in the adult mammalian heart (Bers 2002) (Figure 7). Therefore, exploring the elevating calcium levels in cardiomyocytes during contraction and relaxation is one way to study the functionality of cardiac myocytes. Discrete Ca^{2+} signaling events related to the beating of a cardiomyocyte are termed Ca^{2+} trancients. Ca^{2+} trancients are Ca^{2+} events triggered by APs that can be detected using fluorescent tracers for Ca^{2+} ions (Cheng et al, 1993).

Sustained 10^4-fold gradients of calcium concentration exist across the cell membrane, which partitions the extracellular space from the cytoplasm, and also between the sarcoplasmic reticulum (SR) and the cytoplasm. The cytoplasmic Ca^{2+} concentration is actively maintained at a very low level by

NCXs, SERCAs and Ca^{2+} ATPases. During the cardiac excitation/contraction coupling, a Ca^{2+} influx through L-type Ca^{2+} channels (LCCs) that is induced by depolarization serves as the trigger of evoked Ca^{2+} trancients in cardiomyocytes, and the trancients are generated via the CICR mechanism. Thus, the extracellular calcium is first released into the cytoplasm via LCCs, and this initial increase in intracellular Ca^{2+} concentration induces a further Ca^{2+} release from the SR storage via ryanodine receptors (RyRs) (Figure 7) (Cheng & Lederer, 2008). RyRs are organized as clusters of channels in the SR and form individual Ca^{2+} releasing units (CRUs). How many RyRs within a CRU contribute to the AP-induced Ca^{2+} trancient remains unclear, but the activation of single RyR is thought to cause a Ca^{2+} releasing event with smaller magnitude than a Ca^{2+} trancient (for a review, see Shkryl & Blatter, 2013). As previously mentioned, the t-tubules play an important role during Ca^{2+} release in cardiomyocytes (Ferrantini et al, 2013). The organization of t-tubules is highly developed in ventricular cardiomyocytes, and the AP-induced Ca^{2+} release in these cells is indeed exactly synchronized and spatially homogenous. On the other hand, in atrial cardiomyocytes, the t-tubules are poorly developed or even entirely absent, which causes the AP-induced Ca^{2+} releases to be spatially non-homogenous (Shkryl & Blatter, 2013).

Calcium imaging is a method that quantitatively measures the intracellular free calcium levels using a fluorescent tracer that binds to Ca^{2+} ions. Chemical indicators allow for Ca^{2+} detection over a large range because high affinity tracers can be used to quantify the cytosolic Ca^{2+} levels, and low affinity indicators are suitable for measuring the higher Ca^{2+} concentrations located in subcellular compartments (Paredes et al, 2008). Chemical Ca^{2+} indicators can be either non-ratiometric or ratiometric. Non-ratiometric tracers utilize only one wavelength and are usually very bright. The use of non-ratiometric tracers is optimal for detecting more than one fluorophore.

Ratiometric indicators on the other hand, can be calibrated precisely and minimize the problems associated with uneven loading, leakage of the dye, photobleaching and variability in cell volume (Paredes et al, 2008). The emission properties of the tracer change upon binding to Ca^{2+} ions. As the cells are loaded with the ratiometric tracer and excited with two different wavelengths, the amount of intracellular calcium can be determined by the ratio between the two emission amplitudes (Grynkiewicz et al, 1985).

2.2.6.4. Calcium handling in cardiomyocytes derived from pluripotent stem cells

As described previously, human ES and iPS cells are able to differentiate into cardiac myocytes with all nodal, atrial and ventricular phenotypes (Kehat et al, 2001; Zhang et al, 2009). Though these stem cell -derived cardiac cells have been shown to express markers that are specific for cardiomyocytes (Zwi et al, 2009), they seem to be immature compared to adult and even fetal cardiac myocytes in their morphology and structural organization, as well as in their electrophysiological properties (for a review, see Poon et al, 2011) and Ca^{2+} handling (Liu et al, 2007; Liu et al, 2009; Fu et al, 2010; Lee et al, 2011). For the most part, the immature nature of the Ca^{2+} handling in stem cell -derived cardiomyocytes most likely results from the lack of t-tubules in these cells (Lieu et al, 2009). However, Ca^{2+} trancients in cardiomyocytes derived from human iPS cells share similar properties when compared to adult cardiomyocytes, and also, the RyR receptors have been shown to function in iPS cell -derived cardiomyocytes. However, the Ca^{2+} trancients in these cells appear to have some properties that may indicate incomplete arrangement of RyR receptors into CRUs and an immature t-tubule system (Zhang et al, 2013).

In cardiomyocytes generated from human iPS cells, the Ca^{2+} transients are known to be dependent on the CICR mechanism, and the most important calcium handling proteins are RyR2, SERCA2a and L-type Ca^{2+} channels (Lee

et al, 2011; Itzhaki et al, 2011). The developmental stage of a cardiomyocyte may be related to its ability to trigger Ca^{2+} trancients, and the trancients may have different properties depending on the extent of differentiation (Sauer et al, 2001). Thus, the maturity of iPS cell -derived cardiac myocytes is at least partially dependent on the length of culturing after differentiation.

2.3. Long QT syndrome

Long QT syndrome (LQTS) is a group of monogenic or acquired cardiac disorders that are characterized by a prolonged QT interval and T wave abnormalities in the patient's ECG (Hedley et al, 2009). The QT interval designates the time from the beginning of ventricular depolarization to the end of ventricular repolarization. In an ECG, this interval is the time measured from the beginning of the Q wave to the end of the T wave (Thaler, 1999). The patients with LQTS have an increased risk of developing arrhythmias called Torsades de Pointes (TdP), which are life threatening polymorphic ventricular tachycardias (Crotti et al, 2008). A prolonged QT interval and an example of a TdP arrhythmia as observed in an ECG are presented in Figure 8.

Prolongation of QT interval is not straightforward to estimate because the normal QT intervals vary inversely with the beating frequency. For this reason, the absolute measurements need to be corrected. Bazett's formula (Indik et al, 2006) is generally used for this correction, although it has some limitations and should be used only within the normal range of beating rates (Dogan et al, 2005). According Bazett's formula, a corrected QT interval (QTc) results from dividing the QT time by the square root of the beating rate ($QTc = QT/\sqrt{BR}$). In addition to beating rate dependence, the QT interval varies during the 24 hours in a day due to a number of factors, including circadian rhythms and impulses from the autonomic nervous system (Dogan et al, 2005). In addition, the threshold values of a normal and prolonged QTc interval are slightly different

depending on the gender. This variability has resulted in separate defined limits for males and females, as well as grouping certain values of QT times as borderline values (Viskin, 2009). According to this grouping, the normal value for males in less than 440 ms; the borderline long value is 440-460 ms; and long QT interval is defined as longer than 460 ms. For females, the same values are: less than 450 ms, 450-470 ms and longer than 470 ms. Arrhythmias occur usually when the QT interval is longer than 500 ms (for a review, see Kaye et al, 2013).

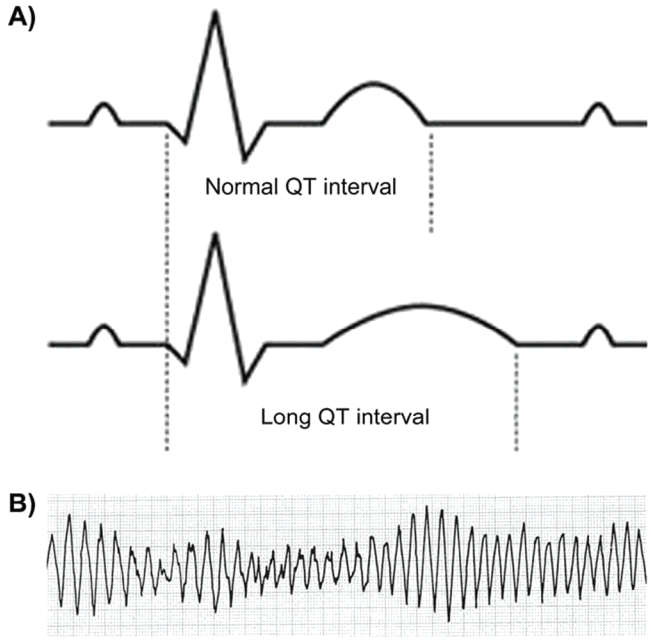

Figure 8. Manifestation of LQTS. **A)** Here is an illustration of a prolonged QT interval that can be observed in an ECG as the lengthening of the time from the beginning of the Q wave to the end of the T wave. **B)** Torsades de Pointes (TdP) is the type of arrhythmia that is typical for LQTS patients.

A prolonged QT interval on an ECG can be seen at the single cell level as a prolonged AP duration, which results from a delay during the repolarization of the cardiomyocyte. The delay is usually due to a reduction in the outward current of K^+, but a delay can also be caused by the increased inward current of

Na^+ and Ca^{2+} or by any combination of these ionic movements that limit the efflux of K^+ (Roden, 2004). A prolonged AP duration is more prominent in mid-myocardial cells compared to epicardial or endocardial cells due to the weaker repolarizing capacity of mid-myocardial myocytes. In mid-myocardial cells, the I_{Ks} current is smaller, while the Na^+ and Ca^{2+} currents are larger compared to epi- and endocardial myocytes, which explains the difference in the prolongation of the AP duration (Antzelevitch et al, 1999; Anyukhovsky et al, 1999; Sicouri & Antzelevitch, 1991).

TdPs are triggered by early after-depolarizations (EADs) occurring in cardiomyocytes at phase 2 of the AP (see Figure 6 A) when the APD, and thereby the QT interval, are prolonged and transmural dispersion occurs. EADs are primarily due to the reactivation of LLCs, and this reactivation is dependent on the repolarization time, any alterations in the kinetics of activation and inactivation of LLCs and changes in the membrane potentials during phases 2 or 3 of the AP (Lankipalli et al, 2005). An increase in transmural dispersion is thought to play an important role in the development of TdPs because it facilitates the propagation of EADs by triggering a subsequent AP in the cell with a longer APD from the adjacent cardiomyocyte with a shorter APD. Transmural dispersion is also responsible for maintaining a TdP once it has been initiated (Lankipalli et al, 2005).

2.3.1. Diversity and prevalence of long QT syndrome

LQTS can be either genetic or acquired. Inherited LQTS can be either autosomal dominant (Romano-Ward, RWS) or recessive (Jervell and Lange-Nielsen, JLNS) by nature (Romano, 1965; Ward, 1964; Jervell & Lange-Nielsen, 1957). Congenital LQTS can be caused by a variety of mutations in several different genes encoding proteins that are directly or indirectly involved in the development of APs in cardiomyocytes. In addition, several different

drugs are known to cause abnormalities to the AP duration and QT interval and thereby induce the acquired form of LQTS (Kaye et al, 2013).

Several different subtypes of congenital LQTS are known. The most common subtypes are LQTS type 1 (LQT1) and type 2 (LQT2). LQT1 accounts for 40-55 % of the patients, while 35-45 % of all LQTS patients suffer from LQT2 (Hedley et al, 2009). LQT1 and LQT2 result from loss-of-function mutations in K^+ channels that are supposed to function during the repolarization of cardiomyocytes (Hedley et al, 2009). LQT1 patients typically have symptoms when the beating rate is high, while patients suffering from LQT2 usually develop symptoms when the beating frequency is low (Schwartz et al, 2001). With low beating rates, the QT interval is prolonged, which provides an elongated time window for Ca^{2+} current reactivation and thereby for the EADs to occur (Lankipalli et al, 2005). In the case of LQT1, the I_{Ks} reduction is responsible for the prolonged APDs and QT intervals. The reason the arrhythmia occurs at high beating rates resulting from exercise or emotional stress in LQT1 patients can be explained as a lack of sufficient increase in the mutant I_{Ks} current during β-adrenergic stimulation (Amin et al, 2010).

LQTS type 3 (LQT3) on the other hand, is due to gain-of-function mutations in depolarizing voltage-activated Na^+ channels (Hedley et al, 2009). Due to the mutations, these Na^+ channels show a persistent inward current of Na^+ ions during a cardiac AP and seem to fluctuate between normal and non-inactivating gating modes (Bennett et al, 1995), which cause the prolongation of cardiac AP. The prolonged AP is dependent on the heart rate, and the effect is stronger at lower heart rates, which means that the life-threatening arrhythmias in LQT3 patients usually occur at rest or during sleep (Schwartz et al, 2001). The LQT3 subtype accounts for 2-8 % of the LQTS patients (Hedley et al, 2009). Even less abundant congenital LQTS subtypes result from mutations in the genes that encode β-subunits of the K^+ channels or parts of Ca^{2+} channels. In

addition, mutated cardiac structural proteins, as well as defects in cytoskeletal proteins, can lead to LQTS. In total, 12 different subtypes of congenital LQTS are known, and all are caused by mutations in different genes (Hedley et al, 2009) (Table 3).

The estimated prevalence of LQTS worldwide is between 1:5,000 and 1:10,000, although the increasing identification of asymptomatic mutation carriers with normal QT intervals may indicate that this estimation is low (Ackerman, 1998; Piippo et al, 2001). Due to the Finnish national history with hundreds of years of isolation, certain mutations have been enriched in the Finnish population (Norio et al, 1973; Norio, 2003). In the case of LQTS, this means that only four founder mutations account for 73 % of the genetic spectrum of LQTS patients in Finland; thus, this situation is quite unique among population-specific studies (Fodstad et al, 2004). Because the spectrum of different mutations in Finland is so narrow, genetic studies have been extended to evaluate the asymptomatic population. In Finland, one individual out of every 250 people is a carrier of a founder mutation related to LQTS, and this value is the highest known genetic prevalence for this disease (Marjamaa et al, 2009).

2.3.1.1. Long QT syndrome type 1 (LQT1)

LQT1, the most common subtype of LQTS, is caused by mutations in the *KCNQ1* gene, which result in a reduced I_{Ks} current. The mechanism of reduction can be an alteration in the gating properties of the KCNQ1 channels (Park et al, 2005) or a failure in the trafficking of the channel to the cell membrane (Gouas et al, 2004; Moretti et al, 2010; Egashira et al, 2012). Nevertheless, the decrease in I_{Ks} current results in the reduced repolarization capacity of a cardiomyocyte and thereby a prolonged cardiac AP. LQT1 patients typically experience symptoms during exercise or emotional stress when the heart rate is high (Schwartz et al, 2001). This effect is most likely because the dysfunctional I_{Ks}

current is not able to react accurately to the β-adrenergic stimulation (Amin et al, 2010).

Table 3. The subtypes of LQTS. The table lists the different types of LQTS as well as the genes involved and the products of these genes. In addition, the functions of these LQTS-related proteins in cardiomyocytes and the types of mutations involved in each type of the disease are listed. Finally, the characteristics and typical triggers of symptoms and the percentage of the subtype among LQTS patients are described. The table is condensed from one published by Hedley and colleagues (Hedley et al, 2009).

Type	Gene	Protein	Function	Mech.	Characteristics and triggers	(%)
LQT1	KCNQ1	Kv7.1	α-subunit I_{Ks}	Loss-of-function	Arrhythmia triggered by exercise, swimming and emotion	40–55
LQT2	KCNH2	Kv11.1	α-subunit I_{Kr}	Loss-of-function	Arrhythmia triggered by sound or emotion	35–45
LQT3	SCN5A	Nav1.5	α-subunit I_{Na}	Gain-of-function	Arrhythmia triggered by sleep, rest and emotion	2–8
LQT4	ANK2	Ankyrin B	Adaptor (I_{Na-K}, I_{Na-Ca}, I_{Na})	Loss-of-function	Arrhythmia triggered by exercise	< 1
LQT5	KCNE1	minK	β-subunit I_{Ks}	Loss-of-function	Arrhythmia triggered by exercise and emotion	< 1
LQT6	KCNE2	MiRP1	β-subunit I_{Kr}	Loss-of-function	Arrhythmia triggered by rest and exercise	< 1
LQT7	KCNJ2	Kir2.1	α-subunit I_{K1}	Loss-of-function	Syndromic, arrhythmia triggered by rest and exercise, frequent ectopy	< 1
LQT8	CACNA 1C	Cav1.2	α-subunit I_{Ca}	Gain-of-function	Syndromic, early onset and death from arrhythmia	< 1
LQT9	CAV3	M-Caveolin	Adaptor (I_{Na})	Loss-of-function	Rest and sleep triggers arrhythmia	< 1
LQT10	SCN4B	Navb4	β-subunit I_{Na}	Loss-of-function	Exercise triggers arrhythmia	< 0.1
LQT11	AKAP9	Yotiao	Adaptor (I_{Ks})	Loss-of-function	Exercise triggers arrhythmia	< 0.1
LQT12	SNTA1	a1-Syntrophin	Scaffolding protein (I_{Na})	Loss-of-function	Rest triggers arrhythmia	< 0.1

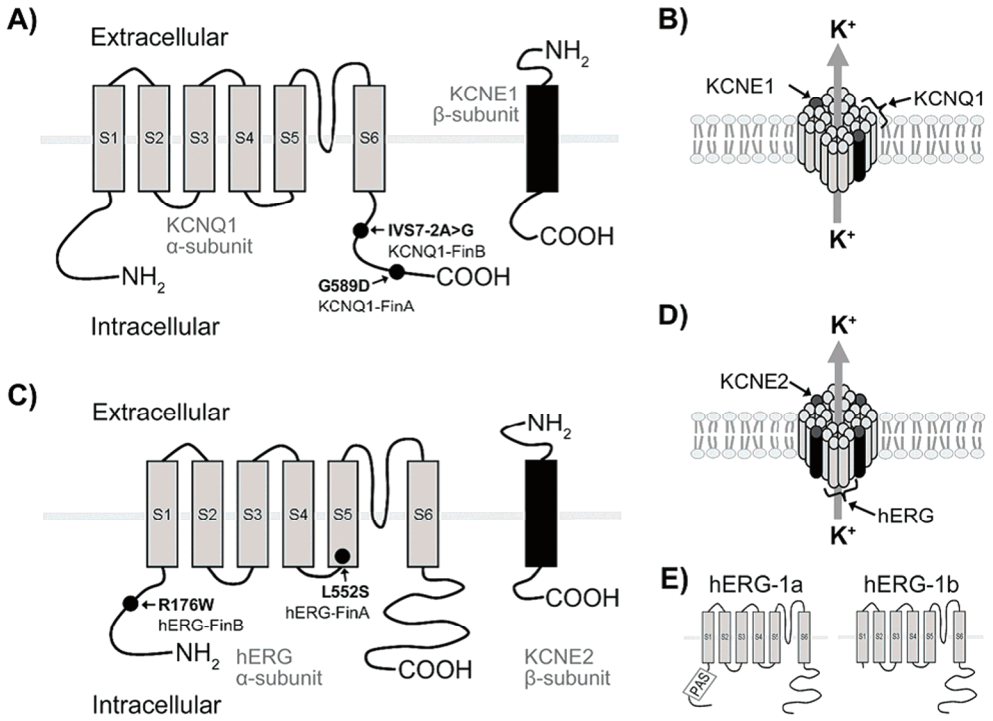

Figure 9. K^+ channels involved in I_{Ks} and I_{Kr} currents in cardiomyocytes. **A)** KCNQ1, the α-subunit of the channel responsible for the I_{Ks} current, is composed of six transmembrane domains, while the β-subunit of the same channel, KCNE1, has only one transmembrane domain. Together these subunits form the functional K^+ channel (**B**) that includes four α-subunits and two β-subunits. **C)** Similarly, the α-subunit of the hERG channel (I_{Kr} current) has six transmembrane motifs and KCNE2, the β-subunit, penetrates the cell membrane only once. **D)** The functional hERG channel is a homotetramer composed of four α-subunits and four β-subunits. The positions of Finnish founder mutations (KCNQ1-FinA and -FinB, and hERG-FinA and -FinB) are also marked in the figure (**A** and **C**). **E)** Two alternative isoforms of hERG differ from each other only at the N-terminus; the hERG-1a isoform has an N-terminal regulatory domain (PAS), while the hERG-1b does not. This figure was assembled using information from three different review articles (Bokil et al, 2010; Chiang & Roden, 2000; Friedrichs et al, 2013) and a research article by Sale and colleagues (Sale et al, 2008).

The channel that is responsible for the I_{Ks} current is composed of four pore-forming KCNQ1 α-subunits and two auxiliary β-subunits named KCNE1 (potassium voltage-gated channel subfamily E member 1) (Barhanin et al, 1996; Sanguinetti et al, 1996) (Figure 9). Each α-subunit contains six transmembrane domains and intracellular N-terminal and C-terminal domains, while the β-

subunits are smaller and consist of only one transmembrane domain, extracellular N-terminal domain and intracellular C-terminal domain (Bokil et al, 2010). See Figure 9 A and B for the structure of the KCNQ1/KCNE1 channel.

2.3.1.2. Long QT syndrome type 2 (LQT2)

LQT2 is the second most common subtype of LQTS. LQT2 is caused by a mutated *hERG* gene, resulting in a reduced of I_{Kr} current. Trafficking alterations in hERG channels to the cell membrane (Anderson et al, 2006), formation of dysfunctional channels and alterations in the gating properties of the channels have been suggested to be the mechanisms behind the reduction in K^+ efflux (Zhou et al, 1998; Hedley et al, 2009). As in the case of LQT1, the defect in the K^+ current leads to an impairment in repolarization and a prolonged AP. The I_{Kr} current is largely responsible for the repolarization phase of an AP in most cardiomyocytes (Amin et al, 2010). The role of the I_{Kr} current may be even more pronounced in mid-myocardial cells compared to other ventricular cardiomyocytes because the I_{Ks} current is smaller in these cells (Antzelevitch et al, 1999). Mid-myocardial cells are indeed thought to play an important role in the development of LQTS (Lankipalli et al, 2005). Patients suffering from LQT2 usually experience symptoms, namely cardiac arrhythmias, if they are emotionally stressed or if auditory stimuli with a low beating frequency are present (Schwartz et al, 2001). Because the prolonged QT interval is more prominent with low beating rates, the possibility of provoking an EAD is also higher as the beating rate decreases (Lankipalli et al, 2005).

The hERG channel is a tetramer, and each α-subunit consists of six transmembrane domains (Trudeau et al, 1995) and intracellular N-terminal and C-terminal domains (Morais Cabral et al, 1998). Four accessory β-subunits are also associated with the hERG units to form a complete channel, and these β-

subunits are called KCNE2 (potassium voltage-gated channel subfamily E member 2) (Figure 9 C and D). It has been suggested that the four α-subunits are not identical, but that the hERG channels are heteromers that arise from the co-assembly of two different isoforms of hERG, hERG-1a and hERG-1b (Lees-Miller et al, 1997). The different isoforms result from alternative splicing of the transcript, and the two transcripts are identical except for alternate 5′ exons encoding a cytoplasmic N-terminus. The 1a-isoform has an N-terminal PAS regulatory domain, while the hERG-1b does not (Lees-Miller et al, 1997; London et al, 1997; Morais Cabral et al, 1998). The PAS domain functions as an intracellular signal sensor (for a review see Taylor & Zhulin, 1999) and was named after the three proteins in which it occurs: Per, which is period circadian protein; Arnt or aryl hydrocarbon receptor nuclear translocator protein; and Sim, which is abbreviated from single-minded protein. The two isoforms of hERG, hERG-1a with the N-terminal PAS domain and hERG-1b without it, are illustrated in Figure 9 E.

2.3.1.3. Acquired long QT syndrome

LQTS may also be triggered by extrinsic factors, such as drugs or hypokalemia (Vincent et al, 1992). The drugs that are currently known to be able to induce acquired LQTS are listed in a recently published review article (Kaye et al, 2013). The drugs include antiarrhythmics and other cardiac drugs, antipsychotics, antidepressants, antibacterials, antifungals, antivirals, anti-cancer agents, anesthetic agents, muscle relaxants, opiates, antimigraine agents, antihistamines, diuretics and other drugs that can cause hypokalemia.

Most drugs that are known to induce the QT interval prolongation function by blocking the I_{Kr} current in cardiomyocytes by binding to hERG (Roden et al, 1996; De Bruin et al, 2005) or by interrupting hERG trafficking to the cell membrane (Dennis et al, 2007). However, some drugs are exceptions;

for example, Alfuzosin results in a prolonged QT interval without affecting hERG but enhances the Na^+ current (Lacerda et al, 2008). The structure of hERG allows it to bind a wide variety of different drugs. Two aromatic amino acid residues are located on each of the subunits, and all eight residues line the central cavity of the channel pore. These aromatic amino acids dictate the high affinity and binding of hERG to most drugs (Mitcheson et al, 2000).

Mid-myocardial cells are more susceptible to the effects of I_{Kr} blockage than epicardial or endocardial cells because the I_{Ks} current is smaller in these cells (Antzelevitch et al, 1999), which results in a more severe, prolonged action potential in the cell residing in the middle of the myocardial wall (Antzelevitch & Sicouri, 1994). This result potentially induces the spatial dispersion of repolarization and amplifies the risk of TdP arrhythmias in patients suffering from an acquired, prolonged QT interval by enhancing the electrical vulnerability of the ventricles (Antzelevitzh & Sicouri, 1994; Antzelevitzh, 2005). On the other hand, the drugs blocking I_{Kr} channels may induce the prolonged QT interval only in individuals who are already sensitive for to a prolonged interval (Roden, 2005).

2.3.2. Genetic defects behind long QT syndrome types 1 and 2 in Finland

Four founder mutations account for 73 % of the LQTS cases in Finland. Two of the mutations are located in the *KCNQ1* gene and are called KCNQ1-FinA and KCNQ1-FinB. The other two mutations reside in *hERG* and have been named hERG-FinA and hERG-FinB (Figure 9). KCNQ1-FinA is a missense mutation located at amino acid residue 589 and changes a glycine into an asparagine acid (G589D). KCNQ1-FinB is an intronic mutation (ivs7-2A>G) causing alterations in splicing. Both of these mutations are located at the C-terminal domain of KCNQ1. hERG-FinA and -B are both missense mutations; hERG-FinA changes the leucine into a serine at position 552 (L552S), which is in the fifth

transmembrane domain. hERG-FinB changes an arginine into a tryptophan at amino acid residue 176 (R176W), which is located in the N-terminal domain of the protein (Fostad et al, 2004).

2.4. Modeling long QT syndrome

In previous years, drug-induced LQTS has primarily been studied using experimental animals, such as dogs or monkeys (Sugiyama 2008). More recently, a small species of mini-pig has been used as an animal model for acquired LQTS (Sugiyama et al, 2011). The studies on congenital LQTS on the other hand, have relied on the usage of non-cardiac cells, such as fibroblasts that were transfected either with the wild type or mutated gene encoding the ion channel of interest (Paavonen et al, 2003). Neither of these approaches is optimal for studying the function of the human heart or human cardiac cells.

Human iPS cell technology (Takahashi et al, 2007) enabled a novel mode for modeling LQTS as well as other human diseases. With this approach, LQTS can be studied in human cardiac myocytes, which are the only type of cells that have the appropriate cellular environment for LQTS studies. An even better option would be to use primary cardiomyocytes, but these cells are very difficult to obtain and maintain functional in cell culture (Mitcheson et al, 1996). Thus, human iPS cells have been used for LQTS modeling by several research groups (Bellin et al, 2013; Moretti et al, 2010; Itzhaki et al, 2011; Ma et al, 2013; Malan et al, 2011; Matsa et al, 2011; Davis et al, 2012; Egashira et al, 2012; Terrenoire et al, 2013; Yazawa et al, 2011). The current models of LQTS based on iPS cell technology have been extensively reviewed by Friedrichs, Malan and Sasse (Friedrichs et al, 2013), as well as by Egashira and colleagues (Egashira et al, 2013). More recently also Savla and colleagues reviewed various cardiovascular diseases that have been modeled using iPS cell

-derived cardiomyocytes, as weel as the utilization of these models for drug discovery and toxicity studies (Savla et al, 2014).

2.4.1. Characterization of the disease phenotype in long QT syndrome -specific cardiomyocytes cardiomyocytes

The approximation of gene expression, structural characterization and evaluation of beating activity are traditionally used as criteria for cardiac differentiation and the characterization of cardiomyocytes (Gai et al, 2009). Functional parameters, such as electrophysiological measurements and calcium imaging, are crucial characterization methods when the disease cardiac phenotype is to be distinguished from the normal one (Yokoo et al, 2009; Zhang et al, 2009; Zwi et al, 2009). An important consideration is the comparison of wild type and disease phenotypes because of the possible immature characteristics of iPS cell-derived cardiomyocytes (see section 2.2.6.4. Calcium handling in cardiomyocytes derived from pluripotent stem cells).

The first human iPS cell -based model for LQTS regarded subtype 1 (Moretti et al, 2010). This model showed a 75 % reduction in the I_{Ks} amplitude compared to control cells, altered activation and kinetics of the I_{Ks} current and prolonged AP duration as measured by the patch clamp -technique. In addition, pacing induced shortening of the AP duration in control cells quite efficiently, while in LQT1-specific cardiomyocytes, the effect was rather poor (Moretti et al, 2010). This result is consistent with the fact that the mutated I_{Ks} current is not able to increase properly in response to β-adrenergic signals (Amin et al, 2010). In addition, the LQT1-specific cardiomyocytes showed catecholamine-induced EADs, which were attenuated using a β-blocker (Moretti et al, 2010). Indeed, β-adrenergic-blocking drugs are known to suppress arrhythmia events in LQT1 patients (Amin et al, 2010). Later, LQT1 was modeled by another group, and this model was evaluated using the patch clamp -method as well as a MEA

setup. Again, an approximately 75 % reduction in I_{Ks} current densities were identified, and the LQT1-specific AP durations, as well as FPDs, were prolonged compared to control cells (Egashira et al, 2012).

iPS cell -derived LQT2 cell models have been introduced by our group (I) and three other research groups (Bellin et al, 2013; Itzhaki et al, 2011; Matsa et al, 2011). The first LQT2 model based on iPS cell technology was tested using the patch clamp -technique and MEA. The LQT2-specific cardiomyocytes showed an approximately 60 % reduction in I_{Kr} current and prolonged AP and FP durations compared to control cells (Itzhaki et al, 2011). In addition, the LQT2 cells exhibited marked arrhythmic activity, which were observed as the development of EADs in 66 % of the cardiomyocytes and premature beats in 36 % of the cardiac cells. A Ca^{2+} blocker and ATP-sensitive potassium (K_{ATP}) channel opener were able to abolish the EADs and reduce the AP duration in the LQT2-specific cells (Itzhaki et al, 2011). Another model for LQT2 exhibited prolonged APs and FPDs as measured by patch clamp and MEA (Matsa et al, 2011). The application of a β-adrenergic agonist reduced the AP duration but also induced EADs, which then abolished by β-blockers. K^+ channel activators were able to reduce the AP duration in LQT2-specific cardiomyocytes, and no EADs occurred (Matza et al, 2011). More recently, Bellin and colleagues published an improved iPS cell -based model for LQT2 (Bellin et al, 2013): iPS cells were derived from a patient with congenital LQT2, differentiated into cardiomyocutes and used as a disease model, but also the mutation in the iPS cells was corrected to create genetically defined control cells for the LQT2 model. The correction of the mutation normalized the I_{Kr} current and the AP duration (Bellin et al, 2013).

LQT3 has been modeled using iPS cells generated from a mouse model carrying a human mutation in the cardiac Na^+ channel (Malan et al, 2011), and more recently also from patients with LQT3 (Ma et al, 2013; Spencer et al,

2014; Terrenoire et al, 2013). The first model revealed similar Na^+ current densities and steady state activation and inactivation properties in LQT3-specific and control cardiomyocytes. However, the recovery from inactivation was faster in LQT3-specific cells, and the late Na^+ currents were larger compared to control cells. In addition, the AP duration was minimally affected by pacing rates in the control cardiomyocytes, but in LQT3-specific cells, the AP was quite prolonged at lower pacing rates, which is consistent with the fact that LQT3 patients suffer from symptoms usually when the beating frequency is low. In addition, EADs were found in 50 % of the LQT3-specific cardiac myocytes at low pacing rates but not in control cells (Malan et al, 2011). Another study used LQT3-specific iPS cells derived from a patient and differentiated them to cardiomyocytes. In that study very pronounced rate dependence of Na^+ current was also found in LQT3-specific cardiomyocytes (Terrenoire et al, 2013) Ma and colleagues published yet another iPS cell -based model for LQT3 which demonstrated that a dominant mutation of the gene coding for Na^+ channel -subunit, significantly prolonged AP duration (Ma et al, 2013). Also, Spencer and colleagues demonstrated that in LQT3 specific cardiomyocytes the AP duration was markedly prolonged. In addition, that study showed that also intracellular Ca^{2+} transients were prolonged. LQT3 specific cardiomyocytes often incorporated long trains of EADs, and oscillating contractions were observed but this oscillation was not further analysed (Spencer et al, 2014). iPS cells have also been generated from cells of a patient carrying a complex mutation in the Na^+ channel. This mutation results in both gain- and loss-of-function effects and leads to a mixed phenotype of both LQT3 and Brugada syndrome, another cardiac disorder (Davis et al, 2012).

2.4.2. Challenges with the development of long QT syndrome -specific induced pluripotent stem cells and their differentiation into cardiomyocytes

The general challenges concerning all disease models utilizing iPS cell technology are safety, efficiency and speed, and these challenges become even more important if clinical aspects are considered. Low efficiency and kinetics of induction of iPS cells with non-viral and non-genetic methods, risk of mutagenesis and tumors when the methods based on genetic alterations are used, and re-activation of silenced transgenes if the gene transfer is implemented using retroviruses are some examples of the challenges related to iPS cell production. If the iPS cells are to be used clinically, the optimal xeno-free production of the cells and culture conditions are required (for a review, see Lai et al, 2011 and Walia et al, 2012).

The differentiation of cardiomyocytes from iPS cells also involves challenges that are related to the efficiency of differentiation, as well as the high costs of growth factors and complex differentiation protocols. Pure populations of cardiomyocytes cannot be produced, and the sorting and enrichment of cardiac cells have been challenging because cardiac-specific surface markers are not known (Mummery, 2010). However, activated leukocyte cell adhesion molecule (ALCAM) (Rust et al, 2009) and vascular cell adhesion molecule 1 (VCAM1) (Uosaki et al, 2011) have been used for the purification and enrichment of cardiomyocytes. In addition, a fluorescent dye that labels mitochondria has been shown to mark cardiomyocytes derived from human pluripotent stem cells (Hattori et al, 2010). Nevertheless, different subtypes of cardiomyocytes cannot be produced in a controlled manner, and instead, the differentiated cardiomyocytes are a mixed population of ventricular-, atrial- and nodal-like cardiac myocytes, as well as non-cardiac cells. In addition, the maturity of differentiated cardiomyocytes should be considered. iPS cell -

derived cardiomyocytes appear to be immature in their Ca^{2+} handling (Liu et al, 2007; Liu et al, 2009; Fu et al, 2010), and this immaturity may result in an inadequate phenotype that must not be confused with the disease characteristics.

With respect to the models of LQTS, an important question is the sufficiency of the phenotype, and the methods that are appropriate for the detection of the phenotype need to be considered. The clinical phenotypes of the disease vary among the patients, and the different mutations seem to result in different severities and manifestations (Shimizu, 2003). In addition, a large variation in phenotype can occur among family members carrying the same mutation (Moss & Kass, 2005). For the criterion of a sufficient phenotype for LQTS models, this heterogeneity of the disease causes additional challenges.

2.4.3. Possibilities for induced pluripotent stem cell technology in cardiac research

In spite of the variety of challenges described above and the immature nature of iPS cell -derived cardiomyocytes, pluripotent stem cells have enabled cardiac research in a novel way. The first revolutionary event was the differentiation of human ES cells into cardiomyocytes (Kehat et al, 2001). Before that study, the options to study cardiac function and dysfunction had been the usage of either quite large animal models (Sugiyama 2008; Sugiyama et al, 2011) or alternatively non-cardiac human cells expressing only the cardiac ion channel of interest (Paavonen et al, 2003). Obtaining primary human cardiomyocytes involves certain obstacles related to cardiac biopsy as well as maintaining the cardiac myocytes *in vitro* (Mitcheson et al, 1996). Because human iPS cells have been differentiated into cardiomyocytes (Zhang et al, 2009), cardiomyocytes with a defined genotype can be studied. The possibility to generate disease- and patient-specific iPS cells and differentiate those cells into cardiomyocytes has opened new possibilities for cardiac research. These cells

can be used for *in vitro* disease modeling, studying the basic pathology of cardiac diseases, drug screening, designing personalized medications for patients, and developing and screening new drugs not only for cardiac diseases but also to reveal possible cardiac side effects of other drugs. Studies have already demonstrated that cardiomyocytes originating from different patients with distinct clinical phenotypes also reproduce different phenotypes in cell culture (Davis et al, 2012; Egashira et al, 2012; Itzhaki et al, 2011; Malan et al, 2011; Matsa et al, 2011; Moretti et al, 2010) even if the cells have the same LQTS-related mutation (Matsa et al, 2011). These phenomena need more detailed study before iPS cell -derived cardiomyocytes can be utilized for example, for designing personalized treatments for the patients. Genetic background variation between different patients may be overcome by targeted gene correction (Bellin et al, 2013) or by allele-specific RNA interference (Matsa et al, 2014). Both of these techniques have been shown to normalize the AP duration and the defected K^+ current in the cells, and that allows the use of these corrected or RNA-treated cells as controls for the original cell population with the disease. In the future, cardiomyocytes derived from pluripotent stem cells may also be used for regenerative medicine, although clinical applications face even more challenges than other uses of iPS cells.

3. Aims of the study

The aim of the first study (I) was to develop a cell model for long QT syndrome type 2 (LQT2) utilizing patient-specific induced pluripotent stem cells. With this model, the objective was to recapitulate the disease phenotype of LQT2 using electrophysiological measurements and to validate the model with regards to its capacity for subsequent studies.

In the second study (II), we aimed to develop a novel method that could be used together with traditional methods to characterize cardiomyocytes. The new method was intended to be informative and reliable but still easy to use and gentle on the cells. The study was conducted together with experts at Tampere University of Technology.

The aims of the third study (III) were firstly to prove that the method introduced in the second work (II) can distinguish LQTS-specific cardiomyocytes from control cells. Second, we aimed to explore the phenotype of LQT1 that is caused by different mutations more closely using variety of methods and comparing the results gathered by different means.

4. Materials and methods

The following paragraphs concerning materials and methods apply to studies I-III if not mentioned otherwise.

4.1. Ethical approval

The iPS cell lines used in studies I-III were generated in BioMediTech (BMT), University of Tampere with permission from the ethical committee of Pirkanmaa Hospital District (R08070). Written consent for the research was also obtained from all the skin biopsy donors.

4.2. Patient characteristics and derived pluripotent cell lines

In the present studies, two LQT1 patients were investigated. From skin fibroblasts of a 46-year-old female who carried a G589D mutation in *KCNQ1* (KCNQ1-FinA), two iPS cell lines were generated: UTA.00208.LQT1 and UTA.00211.LQT1. This patient was having episodes of unconsciousness and syncope, although her QTc was 456 ms, which is normal for a female. Another LQT1 patient was a 51-year-old female carrying an ivs7-2A>G mutation in *KCNQ1* (KCNQ1-FinB). Two iPS cell lines, namely UTA.00102.LQT1 and UTA.00118.LQT1, were derived and characterized from this patient. This patient has suffered from dizziness, darkening of vision and more recently episodes of unconsciousness. Her QTc was abnormally long at 492 ms.

The LQT2 patient was a 61-year-old male with a R176W-mutation in *hERG* (hERG-FinB). His QTc interval observed in an ECG was 437 ms, and he was asymptomatic except for occasional palpitations. Nevertheless, his sister died suddenly at the age of 32 with diagnosed LQTS, a QTc of 550 ms and

previous palpitations. Two iPS cell lines were established from skin fibroblasts from this patient: UTA.00514.LQT2 and UTA.00525.LQT2.

The control iPS cell lines were generated from a healthy individual, a 55-year-old female. Similar to the LQTS-specific lines, two iPS cell lines were used as controls for the studies (UTA.04602.WT and UTA.04607.WT). As a control, the pluripotent stem cells of human ES cell line H7 (WiCell Research Institute, Madison, WI, USA) and one iPS cell line (UTA.00112.hFF) derived from a cell line of human foreskin fibroblasts were used.

4.3. Cell culture

4.3.1. Primary fibroblasts, commercial cell lines and END-2 cells

Skin biopsies (∅ 4 mm) obtained from the lower back of the donors were cultured in 0.2 % gelatin (Sigma-Aldrich, St. Louis, MO, USA) -coated flasks under fibroblast culturing conditions: Dulbecco's Modified Eagle Medium (DMEM, Lonza, Basel, Switzerland) supplemented with 10 % fetal bovine serum (FBS, Lonza), 2 mM GlutaMAX (Life Technologies Ltd., Paisley, UK), 50 U/ml of penicillin / streptomycin (Lonza) and 0.25 µl/ml of amphotericin B (Merck Millipore, Billerica, MA, USA). After the first passaging, the primary fibroblasts were further cultured without amphotericin B.

293FT cells (Life Technologies Ltd) were also cultured in fibroblast culturing conditions with the addition of 1 % nonessential amino acids (NEAA, Cambrex, East Rutherford, NJ, USA). Plat-E cells (Cell Biolabs, San Diego, CA, USA) and irradiated or mitomycin C (Sigma-Aldrich) -treated mouse embryonic fibroblasts (MEF, Merck Millipore) were maintained in the same conditions but without antibiotics.

END-2 cells were grown in a 1:1 mixture of DMEM and Ham's F12 medium (Lonza) containing 7.5 % FBS, 50 U/ml of penicillin / streptomycin, 1

% NEAA and 2 mM GlutaMAX. To arrest the cells from dividing, the cells were treated with 0.02 mg/ml of mitomycin C for 3 hours and used as feeder cells for cardiac differentiation (Mummery et al, 1991). All cells were grown at 37 °C with 5 % CO_2.

4.3.2. Induced pluripotent stem cell culture

iPS cells were maintained in human ES cell (hESC) medium: knockout (KO) - DMEM containing 20 % knockout serum replacement (KSR, Life Technologies Ltd), 2 mM GlutaMAX, 1 % NEAA, 0.2 % β-mercaptoethanol (Life Technologies Ltd) and 50 U/ml of penicillin and streptomycin. Immediately prior to use, basic fibroblast growth factor (bFGF, R&D Systems, Minneapolis, MN, USA) was added into the medium at a final concentration of 4 ng/ml. Fresh medium was applied to the iPS cells every other day, and the culture conditions were 37 °C and 5 % CO_2. The cell lines were passaged once a week; the feeder cells were mechanically removed, and then the iPS cells were treated with collagenase type IV (Life Technologies Ltd) for approximately five minutes and plated onto fresh feeder cells in hESC medium.

4.4. Generation and characterization of induced pluripotent stem cells

4.4.1. Establishment of induced pluripotent stem cell lines

iPS cells were generated using the original protocol (Takahashi et al, 2007) that utilizes lentivirus infection to transfer the receptor for murine viruses into human fibroblasts followed by retrovirus infection to transfer the pluripotency genes (Oct4, Sox2, Klf4 and c-Myc) into the cells.

293FT cells were used for lentivirus production. ViraPower packaging mix (pLP1, pLP2 and pLP/VSVG mixture, Life Technologies Ltd) and 3 μg of

pLenti6/UbC (Addgene, Cambridge, MA, USA) encoding the mouse *Slc7a1* gene were transfected into 293FT cells using Lipofectamine 2000 (Life Technologies Ltd). Twenty-four hours after transfection, the medium was changed, and after 48 hours, the viral supernatant was collected for infection and filtrated through a 0.45 μm pore size filter.

Primary human fibroblasts were seeded at 8 x 10^5 cells per 100 mm dish and incubated overnight at 37 °C and 5 % CO_2 prior to infection. To infect the cells, the medium was replaced with 10 ml per dish of the virus-containing supernatant supplemented with 4 μg/ml polybrene (Sigma-Aldrich) and incubated overnight. Twenty-four hours after transduction, the virus-containing medium was replaced with fresh medium.

One week after the lentivirus infection, the fibroblasts were infected with retroviruses that were produced in Plat-E cells using FuGENE 6 (Roche Diagnostics, Mannheim, Germany) to transfect 9 μg of pMXs plasmid DNAs (encoding human OCT4, SOX2, KLF4 and c-MYC, Addgene) into the cells. Human fibroblasts expressing the mouse *Slc7a1* gene were counted and plated onto 100 mm dishes (8 x 10^5 cells / dish) one day before the first retrovirus infection. Fibroblasts were infected two times; the viral supernatant was collected and transferred onto fibroblasts 24 and 48 hours after the transfection of Plat-E cells. Before infection, the viral supernatant was filtered through a 0.45 μm pore size filter, and polybrene was added to the filtrated virus-containing medium at a final concentration of 4 μg/ml. Fibroblasts were incubated with the polybrene/virus-containing medium overnight at 37 °C and 5 % CO_2, then fresh medium was applied to the cells two times per week.

One week after infection, the fibroblasts were plated onto MEF feeder cells at three different densities: 2.5 x 10^4, 5 x 10^4, and 1 to 5 x 10^5 cells per dish. The cells were incubated overnight in DMEM, and then they were

maintained in hESC medium that was changed every other day until the colonies were large enough for iPS cell line derivation.

iPS cell colonies were isolated around day 30 under the microscope, transferred onto 24-well plates with MEF feeder cells in hESC medium and incubated at 37 °C and 5 % CO_2. Usually after approximately seven days, the cells reached 80-90 % confluence, and they were passaged onto 6-well plates and maintained as described previously. From one donor of fibroblasts, two iPS cell lines were selected for further culturing, and for those cell lines, the following characterizations were performed.

4.4.2. Karyotype analysis of the cells

Normal karyotypes of the iPS cell lines were verified using standard G-banding chromosome analysis. This analysis was performed according the standard procedure (Schreck & Distèche, 2001) by a commercial company (Medix Laboratories, Espoo, Finland).

4.4.3. Expression of pluripotency markers

4.4.3.1. Reverse transcription polymerase chain reactions

RNA was isolated from the iPS cells using a RNA II kit (Macherey-Nagel GmbH & Co, Düren, Germany), and the RNA concentrations were measured with a NanoDrop (ND-1000, Thermo Scientific, Wilmington, DE, USA). For reverse transcription (RT) reactions, 200 ng of RNA were used in the high-capacity cDNA reverse transcriptase kit (Life Technologies Ltd). The RT reactions were executed as follows: 10 minutes at 25 °C, 120 minutes at 37 °C, and 5 seconds at 85 °C. The samples were stored at 4 °C or for longer periods at -20 °C. PCR was conducted with Dynazyme II (Thermo Scientific) using 1 µl of cDNA and primers at a final concentration of 2 µM. The primer sequences are

listed in Table 4. As a positive control for the expression of exogenous transgenes, PCR was also conducted using the transfected plasmids (*hOCT3/4*, *hSOX2*, *hKLF4* and *hc-MYC*) as templates. *β-actin* and *GAPDH* were used as housekeeping control genes. The PCR reaction conditions were: 2 minutes at 94 °C, followed by 35 cycles of 30 seconds at 94 °C, 30 seconds at X °C and 1 minute at 72 °C, and finally the reactions were terminated with 5 minutes at 72 °C. X designates the annealing temperatures, which were 60 °C for endogenous Oct4, Sox2 and c-Myc; 55 °C for Rex1, β-actin and all exogenous genes; and 45 °C for Nanog (Table 4). The samples were stored at 4 °C or -20 °C if longer storage was needed.

4.4.3.2. Agarose gel electrophoresis

The products from the PCR reactions were run on 2 % agarose (PeqGold Universals, PEQLAB Biotechnologie GMBH, Erlangen, Germany) gels containing 0.5 μg/ml of ethidium bromide (EtBr, Fisher Scientific Oy, Vantaa, Finland). Electrophoresis was conducted with 80 V for one hour with a 50 bp ladder (Thermo Fisher Scientific, Inc., Waltham, MA, USA), and the samples were prepared using 6 x loading buffer (Thermo Fisher Scientific, Inc.). The gels were studied and photographed using UVIdoc gel documentation machinery (UVItec Limited, Cambridge, UK).

Table 4. Sequences of the primers used for reverse transcriptase polymerase chain reactions (RT-PCR). All the primers used to detect pluripotency markers as well as markers of cardiomyocytes and different germ layers in embryoid bodies are listed here. In addition, the sizes of the PCR products in base pairs (bp) and the annealing temperatures (Ann. °C) are stated in the table below.

GENE	Forward primer	Reverse primer	Size (bp)	Ann. (°C)
exo-Oct4	gct ctc cca tgc att caa act ga	ccc ttt ttc tgg aga cta aat aaa	250	55
exo-Sox2	ttc aca tgt ccc agc act acc aga	gac atg gcc tgc ccg gtt att att	225	55
exo-Klf4	cca cct cgc ctt aca cat gaa ga	ccc ttt ttc tgg aga cta aat aaa	275	55
exo-cMyc	ata cat cct gtc cgt cca agc aga	ccc ttt ttc tgg aga cta aat aaa	350	55
endo-Nanog	cca aca tcc tga acc tca gc	att gtt cca ggt ctg gtt gc	287	45
endo-Oct4	gac agg ggg agg gga gga gct agg	ctt ccc tcc aac cag ttg ccc caa ac	144	60
endo-Sox2	ggg aaa tgg gag ggg tgc aaa aga gg	ttg cgt gag tgt gga tgg gat tgg tg	151	60
endo-Rex1	cag atc cta aac agc tcg cag aat	gcg tac gca aat taa agt cca ga	306	55
endo-c-Myc	gcg tcc tgg gaa ggg aga tcc gga gc	ttg agg ggc atc gtc gcg gga ggc tg	328	60
AFP	aga acc tgt cac aag ctg tg	gac agc aag ctg agg atg tc	672	55
AFP	gct gga ttg tct gca gga tgg gga a	tcc cct gaa gaa aat tgg tta aaa t	216	60
PAX6	aac aga cac agc cct cac aaa ca	cgg gaa ctt gaa ctg gaa ctg ac	274	60
α-cardiactin	gga gtt atg gtg ggt atg ggt c	agt ggt gac aaa gga gta gcc a	486	55
SOX17	cgc acg gaa ttt gaa cag ta	cac acg tca gga tag ttg cag	166	55
SOX1	aaa gtc aaa acg agg cga ga	aag tgc ttg gac ctg cct ta	158	55
VEGFR2	gtg acc aac atg gag tcg tg	tgc ttc aca gaa gac cat gc	218	60
TNNT2	atc ccc gat gga gag aga gt	tct tct tct ttt ccc gct ca	385	55
MLC2v	ggt gct gaa ggc tga tta cgt t	tat tgg aac atg gcc tct gga t	382	55
MLC2a	gtc ttc ctc acg ctc ttt gg	gcc cct cat tcc tct ttc tc	269	55
Cx-34	tac cat gcg acc agt ggt gcg ct	gaa ttc tgg tta tca tcg ggg aa	270	55
MYH7	agc tgg ccc agc ggc tgc agg	ctc cat ctt ctc ggc ctc cag ct	443	55
GATA4	gac ggg tca cta tct gtg caa c	aga cat cgc act gac tga gaa c	474	55
HERG	gaa cgc ggt gct gaa ggg ct	aac ttg cgc ttg cgt tgc cg	527	55
β-actin	gtc ttc ccc tcc atc gtg	ggg gtg ttg aag gtc tca aa	302	60
GAPDH	agc cac atc gct cag aca cc	gta ctc agc gcc agc atc g	302	55
KCNQ1-FinA	ttg act ctc agc tac ctc cc	tgc agg agc ttc acg ttc ac	267	60
KCNQ1-FinB	ggg gag ctg tag ctt cca ta	agc caa atg cat ggt gag at	300	60
hERG-FinB	acc acg tgc ctc tcc tct c	gtc ggg gtt gag gct gtg	330	62

4.4.3.3. Immunocytochemical staining of pluripotency markers

iPS cell colonies were fixed with 4 % paraformaldehyde (PFA, Sigma-Aldrich) for 20 minutes and washed three times before and after fixation using phosphate buffered saline (PBS). For the detection of pluripotency markers by immunocytochemistry, the following antibodies were used: anti-Oct4 (1:400, R&D Systems), anti-tumor related antigen 1-60 (TRA1-60, 1:200, Merck Millipore), anti-Sox2, anti-Nanog, anti-stage specific embryonic antigen 4 (SSEA4) and anti-TRA1-81 (all 1:200, and from Santa Cruz Biotechnology, Santa Cruz, CA, USA). The secondary antibodies were Alexa fluor 568 donkey anti-goat IgG, Alexa fluor 568 goat anti-mouse IgM or Alexa fluor 568 donkey anti-mouse IgG (all from Life Technologies Ltd). Blocking was performed with 10 % NDS, 0.1 % Triton X-100 and 1 % BSA in PBS for 45 minutes at room temperature. The samples were incubated with the primary antibodies at 4 °C overnight (1 % NDS, 0.1 % TritonX-100, 1 % BSA in PBS) and with the secondary antibodies for one hour at room temperature protected from the light (1 % BSA in PBS). After the secondary antibody incubation, the samples were mounted with Vectashield containing DAPI (Vector Laboratories, Inc., Burlingame, CA, USA) and stored protected from the light at 4 °C. The stained cells were monitored and photographed using an Olympus IX51 phase-contrast microscope containing fluorescent optics (Olympus Corporation, Tokyo, Japan) and an Olympus DP30BW camera (Olympus Corporation).

4.4.4. Differentiation capacity of the cells

4.4.4.1. Embryoid body formation -assay

For embryoid body (EB) formation, the MEF feeder cells were mechanically removed, and iPS cell colonies were detached from the bottom of the cell culture plate. The colonies were retained as whole as possible and moved onto

low attachment plates in EB medium containing KO-DMEM supplemented with 20 % FBS, 2 mM GlutaMAX, 50 U/ml of penicillin/streptomycin and 1 % NEAA. The medium was changed once per week, and EBs were grown for 5-6 weeks before the cells were lysed. RNA was isolated and purified from the cell lysates using a RNA II kit and converted into cDNA similarly as described for undifferentiated colonies (see above). PCR reactions were conducted as follows: 2 minutes at 94 °C followed by 40 cycles involving 30 seconds at 94 °C, 30 seconds at 55 or 60 °C, and 1 minute at 72 °C, and the final step was 5 minutes at 72 °C. The samples were stored at 4 °C or -20 °C if electrophoresis was not performed during the next 24 hours. The PCR reactions were run on 2 % agarose gels in the same manner as the products from the PCR reactions for pluripotency markers (see above).

4.4.4.2. Teratoma formation and analysis

The teratoma formation assay was performed by injecting iPS cells into the testis capsules of immunodeficient mice. Eight weeks after injection, the mice were sacrificed, and tumor samples were collected. For microscopy, the samples were fixed in 4 % PFA and stained with hematoxylin and eosin. Teratoma assays were conducted in Helsinki by professors Timo Otonkoski and Hannu Sariola (University of Helsinki, Helsinki, Finland).

4.4.5. Mutation analysis of the cell lines

The generated iPS cell lines were assayed by PCR and restriction enzyme reactions to detect the correct mutations in *KCNQ1* and *hERG* in the genomic DNA. DNA was isolated using a DNA Tissue XS kit (Macherey-Nagel GmbH & Co) and multiplied with AmpliTaq 360 Polymerase (Life Technologies Ltd). In total reaction volume of 40 µl, 100 ng of template, 2 mM $MgCl_2$, 200 µM

NTPs, 0.5 µM primers (see Table 4, Biomers.net GmbH, Ulm, Germany) and 1 U / µl of enzyme were used. The reactions were conducted as follows: 96 °C for 10 minutes, 35 cycles of 96 °C for 30 seconds, 60 °C for 30 seconds, and 72 °C for 2 minutes, and then 72 °C for 5 minutes. For the hERG-R176Wmutation, the annealing temperature was 62 °C instead of 60 °C.

The digestion for KCNQ1-G589D was performed with HIN6I (Thermo Fisher Scientific, Inc.) in Tango Buffer (Thermo Fisher Scientific, Inc.) and the digestion for KCNQ1-ivs7-2A>G was performed with Dde1 (Thermo Fisher Scientific, Inc.). The hERG-R176W mutation was detected using SmaI (Thermo Fisher Scientific, Inc.) in Tango Buffer. All reactions were performed with 10 µl of PCR reaction in a total volume of 20 µl at 37 °C overnight.

The products from the digestion reactions were run on a 4 % agarose gel (EuroClone S.p.A., Milano, Italy) with 80 V for two and a half hours. The following results were expected: KCNQ1: G589D-WT generates product sizes of 146, 82 and 39 bp; G589D-Hez results in 185, 146, 82 and 39 bp; ivs7-2A>G-WT produces product sizes of 228, 39 and 33 bp; and ivs7-2A>G-Hez produces sizes of 261, 228, 39 and 33 bp. The homozygous results are as follows: G589D-Hoz: 185 and 82; ivs7-2A>G-Hoz: 261 and 39. For hERG, the R176W-WT mutation results in digestion products with sizes of 182, 79, 46 and 23 bp, and the R176W-Hez should produce sizes of 182, 125, 79, 46 and 23 bp. The homozygous results for R176W-Hoz should be 182, 125 and 23 bp.

4.5. Cardiac differentiation and biochemical analysis of cardiomyocytes

4.5.1. Differentiation

To initiate cardiac differentiation, the iPS cell colonies were dissected mechanically into small aggregates containing a few hundred cells. These

aggregates were plated on mitomycin C -treated END-2 cells and co-cultured in hESC medium with no serum, serum replacement or bFGF (Mummery et al, 2003). The medium was supplemented with 2.92 mg/ml of ascorbic acid (Sigma-Aldrich, Takahashi et al, 2003) and changed on days 5, 8 and 12. On day 14, serum (10 %) was added to the medium, and ascorbic acid was no longer used. Colonies were monitored daily with phase-contrast microscopy (Nikon Eclipse TS100, Nikon Corporation, Tokyo, Japan) to detect spontaneously beating aggregates.

4.5.2. Reverse transcriptase polymerase chain reactions

Total RNA was isolated from the beating aggregates using a RNA XS kit (Macherey-Nagel GmbH & Co), and the concentrations of RNA were measured with a NanoDrop. RNA (50 - 200 ng) was used for RT reactions that were implemented with the high-capacity cDNA reverse transcriptase kit in a similar manner as for pluripotency markers (described above). PCR was conducted using Dynazyme II, 1 µl of cDNA as a template and 2 µM primers (listed in Table 4). PCR reactions were conducted similarly as described in the EB formation assay section. The storage temperature for PCR reactions was 4 °C or -20 °C for longer storage.

4.5.3. Immunocytochemical characterization

4.5.3.1. Dissociation of the cardiomyocytes

The beating aggregates were isolated using a micro scalpel, collected into culture medium and washed for 30 minutes at room temperature with buffer containing 1 M each NaCl, KCl, $MgSO_4$, Na-pyruvate, glucose and HEPES and 0.1 M taurine pH-corrected to 6.9 using NaOH. The aggregates were then incubated in enzyme buffer (previous buffer supplemented with 1 M $CaCl_2$ and

1 mg/ml of collagenase A (Life Technologies Ltd)) at 37 °C for 45 minutes and then at room temperature for one hour in a buffer consisting of 1 M each K_2HPO_4, $MgSO_4$, EGTA, Na-pyruvate and glucose, 0.1 M creatine and taurine, and 2 mmol/l of Na_2ATP pH-corrected to 7.2 using NaOH. After the incubations, the aggregates were re-suspended in EB medium by pipetting up and down to break up the cell clusters (approximately 2 - 5 times), and the dissociated cells were allowed to attach onto gelatin-coated (0.1 % for one hour) wells of a 24-well plate at 37 °C in EB culture medium.

4.5.3.2. Fixation and staining of the cells

Approximately seven days after dissociation, the cardiomyocytes were fixed in a similar manner as the iPS cells (see above) and stained with anti-cardiac troponin T (1:2000, Abcam, Cambridge, MA, USA), anti-α-actinin (1:1500, Sigma-Aldrich), anti-connexin 43 (1:1500, Merck Millipore), anti-MHC (1:100, Merck Millipore), anti-MLC2v (1:150, Synaptic Systems, Goettingen, Germany) and anti-MLC2a (1:300, Synaptic Systems). The secondary antibodies (Life Technologies Ltd) used were Alexa fluor 568 donkey anti-goat IgG, Alexa fluor 568 goat anti-mouse IgG, Alexa fluor 488 goat anti-mouse IgG or Alexa fluor 488 donkey anti-rabbit IgG. The stained cardiomyocytes were monitored and photographed using the same microscope and camera used for the stained pluripotent cells.

4.6. Cardiac field potential recordings and analysis

Spontaneously beating cell aggregates were mechanically excised and plated in EB medium onto MEA chambers that were previously coated with FBS for 30 minutes and 0.1 % gelatin for one hour. The medium was changed every other day.

The FP recordings were performed with the MEA platform (Multi Channel Systems MCS GmbH, Reutlingen, Germany) at 37 °C. For data acquisition, the MC_rack software (Multi Channel Systems MCS GmbH) was used, and FPDs and beating frequencies were designated manually using AxoScope software (Molecular Devices, Sunnyvale, CA, USA). Recordings were two minutes long and were implemented after 2 minutes of stabilization. The beating rate corrected FPDs (cFPD) were counted using Bazett's formula (Indik et al, 2006).

For testing the pharmacological responses of the iPS cell -derived cardiomyocytes, D,L-sotalol (Sigma-Aldrich) was dissolved in dimethyl sulphoxide (DMSO, Sigma-Aldrich) at a concentration of 10 mM. E-4031 (Alomone labs, Jerusalem, Israel) was dissolved in sterile H_2O at a concentration of 1 mg/ml. Isoprenaline (Isuprel, Hospira, Lake Forest, IL, USA) was ready to use as supplied. The dilutions for drug tests were performed using EB medium containing 5 % FBS. All the MEA recordings (both baseline and drug tests) were two minutes long and were performed after a 2 minute stabilization phase.

4.7. Video recording and analysis (II, III)

4.7.1. Video microscopy

The beating clusters were dissociated similarly as for immunocytochemical staining (see above, 4.5.3.1.). Videos of dissociated cardiomyocytes were recorded using phase-contrast microscopy (Nikon Eclipse TS100, Nikon Corporation) and a digital video camera (Optika DIGI-12, Optica Microscopes, Ponteranica, Italy or IGV-B1620, IMPERX, Boca Raton, FL, USA). During the recordings, the cells were maintained under sterile conditions at 37 °C in EB

medium, and the recordings for one plate lasted for a maximum of one hour. One recording was 30 - 60 seconds long with 30 frames per second.

4.7.2. Beating analysis of cardiomyocytes

The LQT1-specific cardiomyocytes were first monitored visually. The cells that were beating abnormally and those that were beating normally were counted, and the relative portions of the beating types were calculated. For the beating analysis, the abnormally and normally beating LQT1-specific cells were classified into different groups and analyzed separately.

The digital image correlation (DIC) method acquires images, stores them in a digital form and performs an image analysis (Sutton et al, 2009). To remove the disadvantage of DIC due to its emphasis on bright pixels in a standard cross-correlation analysis, the minimum quadratic difference (MQD) method was used. The DIC method uses a least-square principle for obtaining the velocity vector field across the image based on two consecutive video frames (Gui & Merzkirch, 1996).

From the recorded videos, the cardiomyocytes to be analyzed were manually selected and cropped so that only the moving parts of the cells were inside the region of interest (ROI). The focus points of the beating inside the cells were approximated by eye, and the ROIs were divided into 8 sectors, leaving the beating focus in the middle of the sectors. From every sector, two sum vectors for velocity were calculated: the approximate radial component and the approximate tangential component (see Figure 12 G-I). These vectors resulted in 16 different signals: 8 radial and 8 tangential signals from every cell analyzed. The beating analysis defined several measurements from the videos: the time required for contraction, the time the cell remained contracted, the time needed for relaxation, possible incomplete relaxation phase and the time the cell remained relaxed. The beating frequency was also measured.

The beating analysis was verified using artificial displacement images, and the noise resistance of the method was tested by adding speckle noise to each frame of the generated artificial video data.

4.8. Patch clamp -measurements and analysis (I, II, III)

The cardiomyocytes were dissociated for patch clamp -analysis as described for immunocytochemistry (see above) except that the cells were plated onto coverslips (sterilized with 70 % ethanol). Action potentials (APs) were recorded from spontaneously beating dissociated cells in whole-cell configuration using a perforated patch technique either at room temperature (II, III) or at 36±1 °C (I). Amphotericin B (Sigma-Aldrich) dissolved in DMSO (Sigma-Aldrich) was used for membrane perforation at a final concentration of 0.24 mg/ml. The cells in the recording chamber were perfused with an extracellular solution consisting of (in mmol/l): 143 NaCl, 4 (I) or 5 (II, III) KCl, 1.8 $CaCl_2$, 1.2 $MgCl_2$, 5 glucose, and 10 HEPES. The pH was adjusted to 7.4 with NaOH, and the osmolarity was adjusted to 301±3 mOsm (Gonotec, Osmomat 030, Labo Line Oy, Helsinki, Finland). The intracellular solution consisted of (in mmol/l): 122 $KMeSO_4$, 30 KCl, 1 $MgCl_2$ and 5 (I) or 10 (II, III) HEPES. KOH was used to set the pH to 7.2 (I) or 7.15 (II, III), and the osmolarity was adjusted to 290±3 mOsm (I) or 295±2 mOsm (II, III).

Patch clamp -recordings were digitally sampled at 10 kHz (I) or 20 kHz (II, III) and filtered at 2 kHz (I) or 5 kHz (II, III). The data were acquired and analyzed with pClamp 9.2 (I) or pClamp 10.2 software (II, III) (Molecular Devices).

Potassium channel blockers were used to investigate the function of the channels. The I_{Kr} current blocker, E-4031 (Sigma-Aldrich), (N-[4-[[1-[2-(6-Methyl-2-pyridinyl)ethyl]-4-piperidinyl]carbonyl]phenyl]methanesulfonamide dihydrochloride (Wettwer et al, 1991) was used at a final concentration of 100

nM in HEPES-based perfusate (2.11 mM stock dissolved in H_2O and stored at -20 °C). The I_{Ks} blocker, 2-(4-Chlorophenoxy)-2-methyl-N-[5 [(methylsulfonyl)-amino]tricyclo[3.3.1.13,7]dec-2-yl]-propanamide, JNJ303 (Tocris Bioscience, Bristol, United Kingdom) (Towart et al, 2009) was used at a final concentration of 300 nM in the same HEPES-based solution (the stock was 25 mM dissolved in DMSO and stored at -20 °C). The perfusate with JNJ303 contained 0.03 % DMSO from the stock solution; therefore, the baseline properties of five cardiomyocytes were tested and found to be unaffected by 0.03 % DMSO alone.

4.9. Combining the patch clamp -method and video analysis (II)

Dissociated cardiomyocytes were recorded, and their concurrent action potentials were acquired with patch clamp -measurements using a high resolution 12 bit Andor XION 885 camera (Andor Technology plc., Belfast, UK) mounted to an Olympus IX71 microscope (Olympus Corporation). Images were acquired for 60 s with 50 frames per second using TILLvisION software. The video data obtained simultaneously with patch clamp -measurements were analyzed using the method described in the section "4.7.2. Beating analysis of cardiomyocytes". The data from this beating analysis were then integrated with respect to time and compared with the patch clamp -data. The time between the peaks of electrical activity and mechanical activity was calculated.

4.10. Calcium imaging (III)

For Ca^{2+}-imaging, the cardiomyocytes were dissociated (see the description in paragraph 4.5.3.1.) and plated onto coverslips. Approximately one week after dissociation, the cells were loaded with 4 µmol/l Fura-2 AM (Life Technologies Ltd) in HEPES-based medium at 37 ºC for 30 minutes. Then, the coverslips

were transferred to a recording chamber (RC-25, Warner Instruments Inc., CT, USA) and perfused with 37 ºC HEPES-based solution: 137 mmol/l NaCl, 5 mmol/l KCl, 0.44 mmol/l KH_2PO_4, 20 mmol/l HEPES, 4.2 mmol/l $NaHCO_3$, 5 mmol/l D-glucose, 2 mmol/l $CaCl_2$, 1.2 mmol/l $MgCl_2$ and 1 mmol/l Na-pyruvate with the pH adjusted to 7.4 with NaOH. Ca^{2+}-imaging was performed using an inverted IX70 microscope and UApo/340 x20 air objective (Olympus Corporation). Images (8-10 frames / second) were acquired using an ANDOR iXon 885 CCD camera (Andor Technology, Belfast, Northern Ireland). Synchronization was performed with a Polychrome V light source using a real-time digital signal processing control unit and TILLvisION software (TILL photonics GmbH, Munich, Germany). Fura-2 was exited at 340 nm and 380 nm, and emission was detected at 505 nm. The baseline recordings were performed from spontaneously beating cardiomyocytes, and the cells were analyzed in three different rhythm categories.

4.11. Allelic imbalance (III)

The differential allelic expression of *KCNQ1* was determined from the iPS cell-derived cardiac myocytes heterozygous for either the G589D (KCNQ1-FinA) mutation or ivs7-2A>G (KCNQ1-FinB) mutation in the *KCNQ1* gene. The relative expression levels of the mutant and wild type (WT) *KCNQ1* were defined based on plasmid-derived standard curves, which were produced by quantitative PCR (qPCR) using plasmids carrying WT and mutant genes at different ratios (1:0, 8:1, 4:1, 2:1, 1:1, 1:2, 1:4, 1:8 and 0:1). For plasmid preparation, the WT cDNA and the cDNA heterozygous for one of the two mutations in KCNQ1 (G589D or ivs7-2A>G) were amplified using primers with the BamHI restriction site in the forward primer (for G589D: 5'-gcg gga tcc gaa att cca gca agc gcg ga-3', for ivs7-2A>G: 5'-gcg gga tcc ttt gcc atc tcc ttc ttt gc-3') and the NotI restriction site in the reverse primer (for G589D: 5'-gcc gcg gcc

gcc agg aag agc tca ggg tcg a-3', for ivs7-2A>G: 5'-gcg gcg gcc gcg tct ccc ctt cca ggt cc-3'). After amplification, the product from the PCR reaction with heterozygous cDNA was treated with the KasI enzyme (New England Biolabs, Ipswich, MA, USA) to digest the WT allele while retaining the mutant alleles, which were then purified using agarose gel electrophoresis. The different alleles of *KCNQ1* were inserted into the pBluescript SK+ plasmid using BamHI and NotI restriction enzymes (Thermo Scientific). The constructs were verified by sequencing to ensure proper insertion of the WT and mutant alleles (3130-16 Genetic Analyzer, Life Technologies).

To determine the allelic imbalance in the iPS cell lines (UTA.00208.LQT1, UTA.00211.LQT1, and UTA.00118.LQT1) heterozygous for the mutations in *KCNQ1*, the beating areas from patient-specific cardiomyocytes were cut by scalpel, and total RNA was isolated using the NucleoSpin® RNA II Kit (Macherey-Nagel). The mRNA was converted into cDNA using the High Capacity cDNA Reverse Transcription Kit (Life Technologies Ltd) according to the manufacturer's protocol. RT reactions were performed with 10 minutes at 25 °C, 120 minutes at 37 °C and 5 minutes at 85 °C, and the cDNA samples were stored at -20 °C before qPCR analysis.

Allelic discrimination was performed by qPCR using custom-made primers and probes (Table 5) and a TaqMan® SNP Genotyping Assay (Life Technologies Ltd). Two specific probes were used to detect both the WT and mutated sequence of *KCNQ1*. The two probes carried different fluorochromes and emitted different fluorescence signals, which were detected during the amplification state of the qPCR analysis. The difference between the expression levels of the two alleles was determined based on these fluorescence intensities. The 7300 Real-Time PCR system (Life Technologies Ltd) was used to generate the standard curves and to analyze the cDNA samples of the mutated cardiomyocytes. The reactions contained 7.5 µl of TaqMan® Universal PCR

Master Mix, 0.375 µl of Custom TaqMan® SNP Genotyping Assay solution, 2.125 µl of sterile H_2O and 3 µl of cDNA or plasmid DNA. The qPCR program was initiated with 2 minutes at 50 °C and 10 minutes at 95 °C, followed by 40 cycles of 15 seconds at 95 °C and 1 minute at 60 °C. All the reactions were performed in triplicate, and the averages from these reactions were used to generate a standard curve and to analyze the samples.

Table 5. Custom-made primers and probes for allelic discrimination of the *KCNQ1* gene (Custom TaqMan® SNP Genotyping Assay service).

Gene	Primer/probe	Sequence 5' > 3'
G589D *KCNQ1*-FinA	Forward primer	ccc cca tag aaa aga gca agg at
	Reverse primer	cta cct tgt ctt cta ctc ggt tca g
	Probe (WT)_VIC	cga tcg **G**cg ccc gc
	Probe (G589D)_FAM	acg atc g**A**c gcc cgc
ivs7-2A>G *KCNQ1*-FinB	Forward primer	gct cgg ggt ttg ccc tga agg
	Reverse primer	ggc agc ata gca cct cca
	Probe (WT)_VIC	ctc att cag acc gc
	Probe (ivs7-2A>G)_FAM	cga cct cgg acc gc

The standard curves were plotted with the expression ratio of the WT and mutant alleles as $\log_2$ on the y-axis and the corresponding ΔCt (Ct = cycle threshold) values on the x-axis. The ΔCt values were defined by subtracting the Ct value of the WT allele from the Ct value of the mutant allele. The Ct values were defined as the number of cycles required for the fluorescent signal to cross the threshold; i.e., it exceeded the background level. In standard curves, the ΔCt values for the plasmid ratios are represented in the statistical form of the mean ±

standard deviation (n=3). The ΔCt values defined for different mutation-specific samples were also placed on the standard curves, and these locations were used to define the allelic imbalance of *KCNQ1*.

4.12. Statistical analysis (I, III)

In study I, Student's *t*-test and one-way analysis of variance followed by a Tukey test were used to compare the patch clamp data from LQT2-specific and control cardiomyocytes (SPSS software, IBM Corporation, Armonk, NY, USA). The differences in FPDs between control cells and LQT2-specific cardiomyocytes were determined by nonlinear regression analysis using R software (Bell Labs, New Providence, NJ, USA) and by *t*-test using SPSS. In study III, the variance between two different experiments was calculated in Microcal Origin™ 9.0 using the two sample t-test. A one-way ANOVA test followed by Scheffe's test was used when more than two experiments were compared.

5. Overview of the results

The results section of the text refers to all the three original articles (I-III) if not indicated otherwise.

5.1. Characterization of induced pluripotent stem cells

5.1.1. Pluripotency of the cells

All the iPS cell lines that were used in the present studies (I-III) were characterized for their pluripotent properties. iPS cells were found to form colonies typical of human pluripotent stem cells (Figure 10 A), and the individual cells were round and compact with a high nucleus to cytoplasm ratio, which is also typical for pluripotent cells. The generated iPS cells were also shown to express multiple markers of the pluripotent state. Using RT-PCR, the expression of Nanog, Oct4, Sox2 and Rex1 was confirmed, and by immunocytochemistry, the cells were shown to express Nanog, Oct4, Sox2, SSEA4, TRA1-60 and TRA1-81 (Figure 10 B-D). RT-PCR was also used to verify the silencing of the exogenous transgenes that indeed were found to be silenced.

The *in vitro* pluripotent capacity of the iPS cells was shown by EB formation and by detecting the expression of certain markers for each of the three germ layers in the EBs. Sox1, paired box protein 6 (Pax-6), Nestin and Mushashi 1 were used as ectodermal markers. Markers for the mesoderm were kinase insert domain receptor (KDR), also known as vascular endothelial growth factor receptor 2 (VEGFR-2), and α-cardiac actin. α-fetoprotein (AFP) was used as an endodermal marker. The pluripotency of the iPS cells was further confirmed *in vivo* by a teratoma forming assay, and tissues originating from all germ layers were found in histological sections of the teratomas.

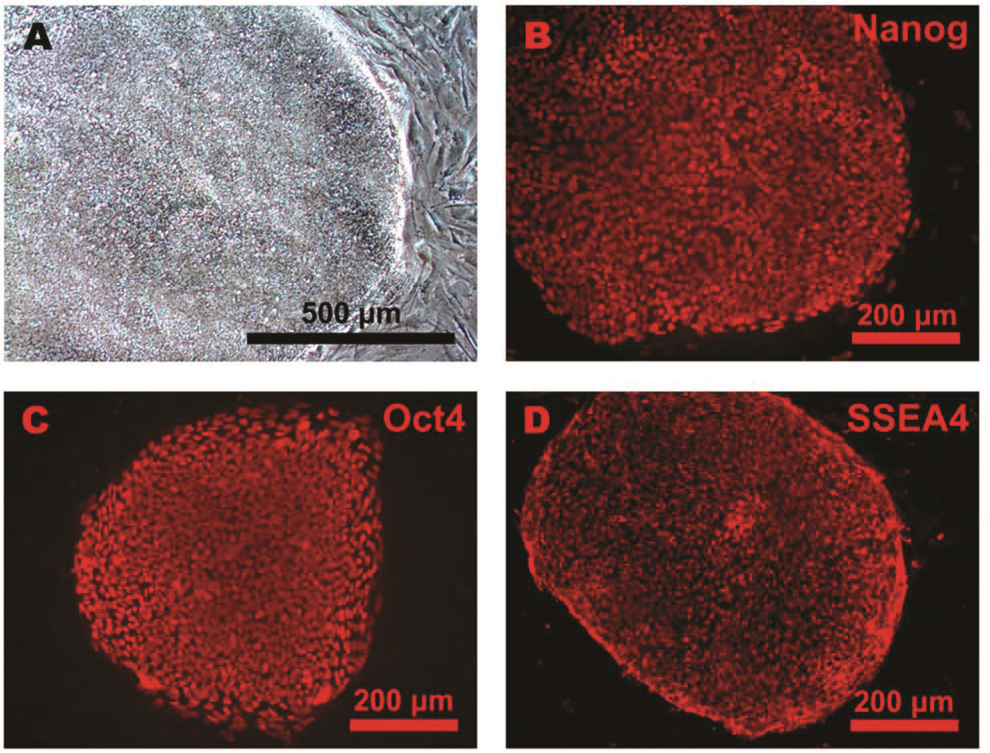

Figure 10. Colonies formed by induced pluripotent stem cells. **A)** iPS cells form colonies with a compact, round shape and defined edges. This type of growth is typical of pluripotent stem cells. **B-D:** iPS cells expressed several markers of pluripotency, as shown by immunocytochemistry. Three examples are shown here: Nanog (**B**), Oct4 (**C**) and SSEA4 (**D**).

5.1.2. Normal karyotypes and correct mutations

All the iPS cell lines that were generated and used in these studies were verified for a normal karyotype. If any alterations in chromosomes were found, the cell line was not used for further studies, but instead another line from the particular donor was thawed and characterized. In addition, the correct mutations, namely KCNQ1-G589D (KCNQ1-FinA), KCNQ1-ivs7-2A>G (KCNQ1-FinB), or hERG-R176W (hERG-FinB), were detected from the LQTS-specific cells. The

control iPS cells were also explored for these mutations to verify that the control individuals were not carriers of these LQTS-related mutations.

5.2. Cardiac differentiation and biochemical features of the cardiomyocytes

5.2.1. Expression of cardiac markers

Cardiac differentiation of the iPS cells was accomplished by co-culturing stem cells with END-2 cells. Spontaneously beating cells were detected usually in two weeks after the initiation of differentiation. As these beating cells were further characterized, they were found to express different markers that are typical of cardiomyocytes. By immunocytochemistry, the cells were found to express cardiac troponin T (cTnT, encoded by *TNNT2*), α-actinin, myosin heavy chain (MHC), ventricular-specific myosin light chain (MLC2v), atrial-specific myosin light chain (MLC2a) and connexin 43 (Cx-43) (Figure 11). RT-PCR was used to detect a more comprehensive spectrum of cardiac-specific genes expressed in the iPS cell-derived cardiomyocytes. At the mRNA level, the cells were found to express *TNNT2*, *MLC2v*, *MLC2a*, *Cx-43*, *hERG*, *MYH7* (which encodes the β-isoform of myosin heavy chain) and the transcription factor *GATA4*.

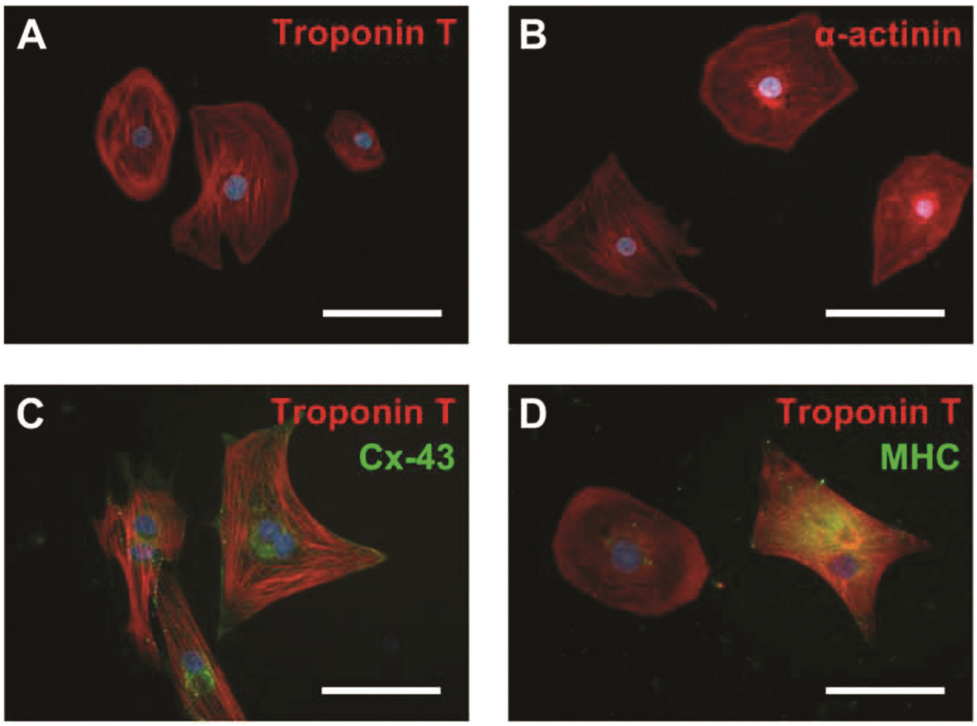

Figure 11. Cardiomyocytes derived from iPS cells expressing cardiac markers as shown by immunocytochemistry. iPS cell -derived cardiomyocytes were shown to express a variety of cardiac markers, including cardiac troponin T (**A**), cardiac α-actinin (**B**), connexin 43 (Cx-43) (**C**), and myosin heavy chain (MHC) (**D**). Scale bar represents 100 µm.

5.2.2. Allelic imbalance of heterozygous mutations (III)

To determine the allelic discrimination between the WT and mutated *KCNQ1* alleles in cardiomyocytes derived from different iPS cell lines, the ΔCt values were calculated for the different samples, and these values were compared with the standard curves. The expression ratio between the WT version of *KCNQ1* and the G589D (FinA) -mutated *KCNQ1* was found to be closest to 4:1 (WT:mutated). This result indicates that approximately 80 % of the expressed *KCNQ1* in these cells is the normal form of the gene at least at the mRNA level, and only approximately 20 % is the mutated version. This result indicates the

ratio in the cell population, not in single cells. For the KCNQ1-ivs7-2A>G (FinB) mutation, the discovered ratio was 3:1 (WT:mutated) because the ΔCt values of these samples were located on the standard curve between the values of 2:1 and 4:1. The 3:1 ratio signifies that 75 % of *KCNQ1* expressed in these cells is transcribed from the WT allele, while 25 % is transcribed using the mutated allele. This ratio represents the allelic discrimination at the mRNA level and is viewed for the entire cell population.

5.3. Mechanical analysis of the cardiomyocytes derived from induced pluripotent stem cells (II, III)

5.3.1. Beating of long QT syndrome -specific cardiomyocytes (III)

Variation in the beating of LQTS-specific cardiomyocytes was identified from cell to cell. First, the cardiomyocytes originating from the two separate iPS cell lines carrying different mutations (G589D or ivs7-2A>G) in *KCNQ1* showed distinct abnormalities in their mechanical beating behavior: G589D-specific cells seemed to become stuck after contraction, while the cardiomyocytes carrying the ivs7-2A>G mutation vibrated or vacillated during relaxation. The second observation was that within the same cell line, some cardiomyocytes beat in a clearly abnormal manner while others seemed to beat normally. The numbers of cells with normal and abnormal beating were counted, and the relative portions of the beating types were calculated. Approximately 71 % (n=17/24) of the cells carrying the G589D mutation (FinA) were beating abnormally. From the cardiomyocytes specific for the ivs7-2A>G mutation in *KCNQ1* (FinB), approximately 68 % (n=17/25) showed abnormal beating.

5.3.2. Analysis of the beating attributes from control cardiomyocytes (II)

The sum displacement signals were obtained from the video recordings, and several time parameters for different phases of beating were measured from these signals: (1) the time of contraction, (2) the time the cell stayed contracted, (3) the time of relaxation, (4) incomplete relaxation, and (5) the time the cell was relaxed (Figure 12 G). For each analyzed cell, the average values from three separate signals were calculated and used for further inspection of the beating characteristics. The beating rates (BRs) for each video recorded cell were also determined from the signals. All these parameters were successfully obtained from the cardiomyocytes derived from iPS cells using the DIC method for video analysis, and control cardiomyocytes were typically found to contract rather rapidly, after which they immediately relaxed as rapidly as they contracted (phases 1, 3 and 5). The BRs varied from 12 to 67, but a majority of the cells beat with a frequency of around approximately 25 beats per minute.

5.3.3. Long QT syndrome type 1 -phenotype in video analysis (III)

In addition to the parameters described above for the control cardiomyocytes, the LQT1-specific beating typically exhibited the phases 2 (cell staying contracted) and 4 (incomplete relaxation) during the contraction/relaxation cycle (Figure 12 G). As the control cells typically contracted and relaxed consecutively and had rather constant BRs, approximately 70 % of the LQT1-specific cardiomyocytes showed abnormal beating characteristics (Figure 12 A-F). LQT1-specific cells carrying the KCNQ1-FinA (G589D) mutation typically were stuck after contraction and thereby stayed contracted for a longer time than the control cells (Figure 12 C and D). LQT1-specific cells with a KCNQ1-FinB (ivs7-2A>G) mutation exhibited the tendency to vibrate and vacillate before or during relaxation or tremble after relaxation (Figure 12 E and F). Both types of abnormalities were found among both LQT1-specific (G589D and ivs7-2A>G)

cells, but the most prevalent for each subtype of LQTS was that described previously. The abnormal beating behavior of LQT1-specific cardiomyocytes was considered a sufficient disease phenotype.

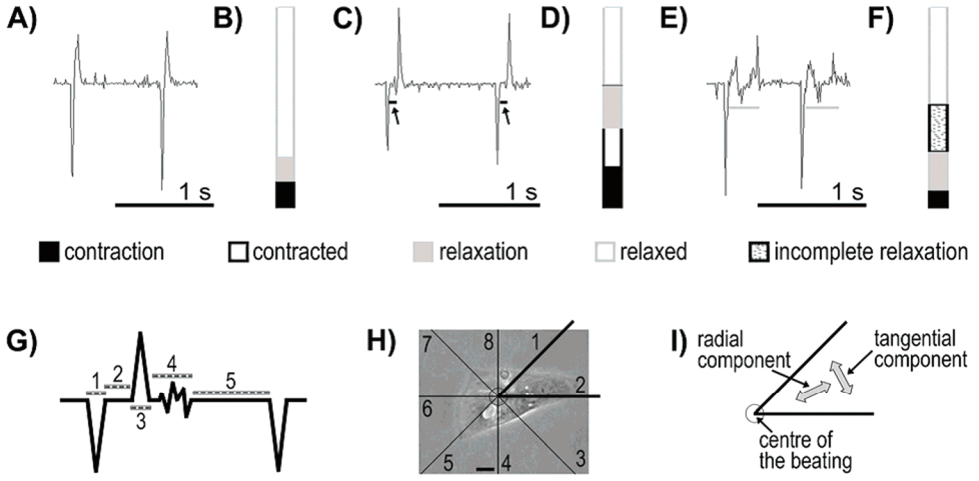

Figure 12. The beating analysis of single cardiomyocytes based on video recordings. Examples of the signals received from the video analysis are presented in **A**, **C** and **E**. Panel **A** shows an example from control cardiomyocytes, which show that the relaxation of the cell starts immediately after contraction. In other words, the upward peak (relaxation) follows the downward peak (contraction) without delay. **C)** Here is an example signal measured from a cardiomyocyte carrying the G589D (KCNQ1-FinA) mutation and showing a pause between the contraction and relaxation, as designated with arrows. **E)** This figure presents an example from an ivs7-2A>G (KCNQ1-FinB) -specific cardiomyocyte. The vibration or vacillation appears in the signal as a relaxation that does not occur unbroken and efficiently. In other words, the proper upward peak is missing. **B**, **D** and **F)** Histograms present the portions of different phases of cardiac contraction/relaxation cycle: (1) contraction, (2) the time that a cell stays contracted, (3) relaxation, (4) the time of vibration or vacillation, also called incomplete relaxation, and (5) the time that a cell stays relaxed. The definitions for each phase are also illustrated in an artificial signal presented in figure **G**. **H)** The focus point of beating was approximated by eye, and the beating cardiomyocyte was divided into 8 sectors with the focus in the middle (scale bar represents 10 µm). **I)** From each sector, two sum vectors for velocity were calculated: the radial component and the tangential component. This analysis resulted in 16 different signals from every cell analyzed. Three of these signals were used to analyze each cardiomyocyte.

5.3.4. Applicability of the mechanical analysis for cardiomyocyte research (II, III)

The mechanical analysis method was verified using artificial displacement images and with noise-resistant testing. In addition, the method was tested by combining the mechanical analysis method with the patch clamp -technique. The time difference between the electrical activity of the cells measured by patch clamp and the mechanical activity determined by DIC from the videos was calculated using synchronized data. The electrical and mechanical signals occurred at the same time, but the electrical activity declined earlier than the mechanical activity.

The results from the mechanical analysis method were also compared with the results obtained separately from patch clamp and Ca^{2+}-imaging. Using video recordings and DIC, abnormal signals were obtained from LQT1-specific cells, while control cardiomyocytes resulted in signals with consecutive contraction/relaxation phases and constant BRs. In addition, the abnormalities obtained from LQT1-specific cells carrying different mutations in *KCNQ*1 were different from each other. Using Ca^{2+}-imaging, similar differences were found, which supported the relevance of mechanical analysis. However, some differences in the portions of the types of abnormalities were identified. While the video analysis clearly showed that the KCNQ1-G589D (FinA) mutation typically caused the cells to become stuck after contraction and the KCNQ1-ivs7-2A>G (FinB) mutation resulted in some vibration or vacillation in the cells, the Ca^{2+}-imaging results indicated that in KCNQ1-G589D-specific cardiomyocytes, two different types of abnormalities were equally common. The Ca^{2+}-imaging results also indicated that in KCNQ1-ivs7-2A>G-specific cardiomyocytes, the other type of abnormality was observed two times more often than the other.

The results from the patch clamp -measurements were more similar between the two cell lines carrying the different mutations (G589D or ivs7-2A>G). Nevertheless, also with the patch clamp -method, differences between the effects of these two mutations could be identified. Only the G589D mutation caused EADs in the baseline measurements. The APDs were more prolonged in the same cells with a G589D mutation compared to the cells carrying the other mutation (ivs7-2A>G) when they were exposed to E-4031, a specific hERG channel blocker.

5.4. Electrophysiology and calcium handling of the cardiomyocytes

5.4.1. Patch clamp -measurements (I, II, III)

In study I, the spontaneous APs were measured from iPS cell-derived LQT2-specific cardiomyocytes as well as from control cardiomyocytes, and two types of AP morphology were found among the cells. The majority of the cardiac myocytes exhibited ventricular-like APs, which displayed a distinct plateau phase. Some of the cells had atrial-like APs that were triangularly shaped. At 50 % repolarization (APD_{50}) and 90 % repolarization (APD_{90}), the APDs of LQT2-specific cardiomyocytes were prolonged compared to control cells, and this difference was significant in ventricular-like cells. In atrial-like cardiomyocytes, a difference was identified in APD_{50} and APD_{90}, but the difference was not statistically significant. This prolonged AP indicated that the cardiomyocytes derived from LQT2-specific iPS cells exhibited the disease phenotype, although EADs were observed only in one LQT2-specific cell (n=20). In control cells, no EADs were present. Using E-4031 (hERG channel blocker), the I_{Kr} current was further investigated, and the magnitude of this current was notably reduced in LQT2-specific cells compared to control cardiomyocytes.

In study III, the baseline properties of spontaneously beating cardiomyocytes (both control and LQT1-specific) were obtained from patch clamp -recordings using the perforated patch technique. According to the properties of the APs, the cells were categorized as nodal, atrial and ventricular cardiomyocytes. The majority of the cardiomyocytes were ventricular-like, and only a marginal proportion was nodal-like. The examples of ventricular APs from control cells as well as from two LQT1-specific lines are presented in Figure 13 A-C. The APDs were significantly prolonged in all subtypes of LQT1-specific cells compared to the control cardiomyocytes. Spontaneous EADs were found in cardiomyocytes specific for the G589D (FinA) mutation in *KCNQ1* but not in control cells or cardiomyocytes carrying the ivs7-2A>G mutation in *KCNQ1* (FinB).

To investigate the role of the I_{Ks} current in the extension of the baseline APs in LQT1-specific cells, ventricular cardiomyocytes were exposed to the I_{Ks} blocker JNJ303 (300 nM). In control cardiomyocytes, JNJ303 significantly prolonged APD_{50} and APD_{90}, but the I_{Ks} block did not significantly affect the AP characteristics in the LQT1-specific cardiac myocytes. To evaluate the findings concerning I_{Ks} blockage, a specific hERG (I_{Kr}) blocker, E-4031 (100 nM), was used to expose ventricular cardiomyocytes. In control cells, the APD_{50} and APD_{90} were prolonged, but no EADs were provoked. Nevertheless, all ventricular cardiomyocytes carrying either the G589D or ivs7-2A>G mutation in *KCNQ1* exhibited EADs when exposed to E-4031, and both lines had significantly prolonged APD_{50} and APD_{90}.

5.4.2. Calcium imaging (III)

Ca^{2+} handling of LQT1-specific and control cardiomyocytes was measured during spontaneous baseline beating. Based on the Ca^{2+} measurements, the cells were categorized into three different groups according to the rhythm and

arrhythmias. The first group included cells with a normal beating rhythm and stable amplitude. The second group included cells with arrhythmias with two or more Ca^{2+} peaks (AD). The third group consisted of cells with arrhythmias in small amplitude Ca^{2+} events in between the stable amplitude Ca^{2+} spikes (AS) (Figure 13).

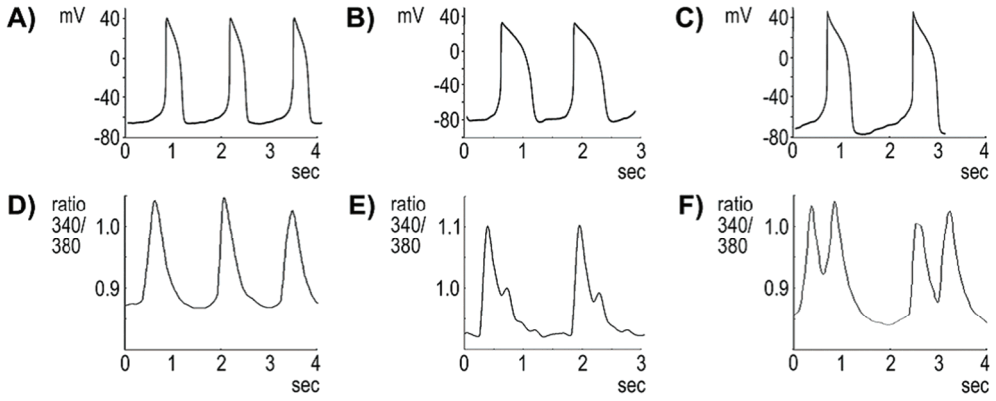

Figure 13. Ventricular action potentials (APs) and signals indicating Ca^{2+} handling in iPS cell-derived cardiomyocytes. **A-C:** APs measured using the patch clamp technique are presented here. The AP durations (APDs) in LQT1-specific cardiomyocytes (**B** and **C**) are prolonged compared to the APD of a control cardiomyocyte (**A**). An AP from a cell carrying the G589D mutation (FinA) is shown in **B,** and an example of an AP measured from a cardiomyocyte with ivs7-2A>G in *KCNQ1* (FinB) is presented in figure **C**. **D-F:** Here are the examples of Ca^{2+} signals from two LQT1-specific and control cardiomyocytes. Control cells typically showed a normal beating rhythm and stable amplitude (**D**), while two different types of arrhythmia were observed in LQT1-specific cardiomyocytes. **E:** The measurement from a G589D-specific cell having an arrhythmia with two or more Ca^{2+} peaks (AD) is presented here. **F:** An example of an arrhythmia with small amplitude Ca^{2+} events in between the stable amplitude Ca^{2+} spikes (AS) shown here was measured from a cardiomyocyte carrying the ivs7-2A>G (FinB) mutation in *KCNQ1*.

Ca^{2+} handling abnormalities were more dominant in LQT1-specific cells than in control cardiomyocytes and were more prevalent in G589D-carrying cells than in the cells with ivs7-2A>G. No significant difference was identified between the LQT1-specific cells with different mutations when the two types of abnormalities were compared. Nevertheless, the AS type of arrhythmia was

more common than ADs in the cells carrying the ivs7-2A>G mutation in *KCNQ1,* while no difference between the two types of arrhythmia in the G589D-specific cells was identified. The cardiomyocytes carrying the G589D mutation in *KCNQ1* (FinA) showed abnormalities in 47 % of the cells. From these cells, 22 % were of the type AD (Figure 13 E) and 25 % were the AS type of arrhythmia. In KCNQ1-ivs7-2A>G (FinB)-specific cardiomyocytes, the abnormalities were observed in 30 % of the cells, and 11 % of these showed the AD type of abnormality. In 19 %, the arrhythmias were the AS type (Figure 13 F). In control cardiomyocytes, abnormal Ca^{2+} handling was observed in 7 % of the cells (2 % with AD and 4 % with AS).

5.4.3. Cardiac field potential analysis (I, II, III)

The electrophysiological properties of the beating cell aggregates were measured using MEA. From the MEA measurements, the BRs and FPDs were determined. As the control cardiomyocytes and LQT2-specific cells were compared, LQT2-specific cardiac myocytes had more significantly prolonged FPDs than the control cells. This difference was more remarkable at low BRs compared to average BRs, and at high BRs, no differences between the control and LQT2-specific cells were identified. Nevertheless, a negative correlation was found between FPDs and BRs in both control and LQTS-specific cells (I). Although variation existed between the measurements, the estimated average of FPDs for LQT1-specific cardiomyocytes was also longer than the FPDs generally measured from control cells (III).

In the first study (I), LQT2-specific cardiomyocytes were studied for their drug responses using MEA. Sotalol (19 μmol/l) and E-4031 (500 nmol/l for LQT2-specific cells and 700 nmol/l for control cells) were applied to the cardiomyocyte aggregates differentiated from both control iPS cells and LQT2-specific iPS cells. Both baseline and drug conditions for sotalol and E-4031

were measured. Sotalol induced premature beats only in LQT2-specific cardiomyocytes and not in control cells. Using E-4031, premature beats were induced in both cell lines, but the induction required a higher concentration (700 nmol/l) in control cells compared to LQT2-specific cardiomyocytes (500 nmol/l).

6. Discussion

The aim of this thesis was to introduce iPS cell lines established from both control individuals and patients carrying certain mutations related to different subtypes of LQTS. The iPS cells were differentiated into cardiomyocytes, and these cells were evaluated as possible *in vitro* models for LQTS types 1 and 2.

This thesis also introduces a novel method for analyzing cardiomyocytes. This analysis is based on video recording and the characterization of the mechanical properties of single beating cardiac cells. The video analysis method is easier to use compared to the patch clamp -technique, which is considered the gold standard method for the characterization of the electrical properties of cardiomyocytes. Video analysis is a non-invasive, non-toxic and label-free method, which makes it gentler for the cells and enables research on the cardiomyocytes that are stressed as slightly as possible. Moreover, studying the mechanical properties of cardiac myocytes may reveal additional information compared to purely electrophysiological studies. This novel method could be considered an adjacent technique for cardiomyocyte characterization. Notably, the analysis of the mechanical properties of beating exposes different aspects of the beating characteristics than the electrophysiological measurements or techniques based on quantifying the ion concentrations inside the cardiomyocytes.

6.1. Production of induced pluripotent stem cells and their cardiac differentiation (I-III)

In the studies presented in this thesis, several iPS cell lines were successfully established. The method that was used for iPS cell production utilizes lenti- and retroviruses (Takahashi et al, 2007), which is a clear obstacle for the use of these iPS cells for clinical purposes. The present studies were not aimed at

clinical application but for establishment of *in vitro* disease models for different subtypes of LQTS. For this purpose, the iPS cell lines produced using viruses can be considered as good as lines produced by some other techniques. In addition, the method based on viral delivery of reprogramming factors was efficient for iPS cell production, which was an obvious advantage of this particular method. The produced iPS cells were pluripotent as indicated by the expression of certain pluripotency markers both at the mRNA and protein levels. The pluripotent nature of the cells was further confirmed using both *in vitro* EB and *in vivo* teratoma forming -assays, and most importantly, the iPS cells differentiated into functional cardiomyocytes.

Cardiac myocytes differentiated from pluripotent stem cells are thought to be rather immature because of their Ca^{2+} handling (Liu et al, 2007; Liu et al, 2009; Fu et al, 2010) and electrical properties (Moore et al, 2005; Cao et al, 2008). The immaturity of iPS cell-derived cardiomyocytes may result in an inadequate phenotype that is not comparable to the phenotype observed in primary cardiomyocytes. For this reason, comparisons should only be made between cardiomyocytes with a similar history. In practice, this consideration means that *in vitro* models for different cardiac diseases based on iPS cell technology always need control cells that are derived from similarly produced iPS cells. In addition, the disease phenotype, as well as all the responses to different stimuli that are observed in disease-specific cardiomyocytes, need to be evaluated with respect to the phenotype and responses observed in these control cells. Nevertheless, the human cardiomyocytes derived from pluripotent stem cells are still a more optimal environment to study human cardiac diseases compared to animal models (Sugiyama 2008; Sugiyama et al, 2011) or transiently transfected non-cardiac cells (Paavonen et al, 2003), which were used as cardiac disease models before the possibilities that were introduced by the invention of iPS cells. Primary human cardiomyocytes would obviously

offer the most optimal platform to study the phenomena that occur in the human heart, but as mentioned previously, these cells are difficult to obtain and maintain *in vitro* (Mitcheson et al, 1996).

6.2. Mechanical analysis of the beating cardiomyocytes (II, III)

6.2.1. A novel method based on video recordings (II)

The second study of this thesis (II) introduced a novel method for the mechanical analysis of the beating motion in cardiac myocytes. This method is based on video recordings and introduces an additional tool for the characterization of single cardiomyocytes. This method is considerably easier to use and is gentler on cells than the patch clamp technique or Ca^{2+}-imaging because it is non-invasive, non-toxic and label-free. Thus, the cells can be studied in normal cell culture conditions without any additional stress for the cells from fluorescent tracers or invasive detectors. A patent application is pending concerning this novel manner to analyze the mechanical functionality of cardiomyocytes based on video recordings (application number: fi20126384).

The method was tested using artificial displacement images and by the addition of supplemental noise. The patch clamp -technique was used as a reference method to verify the correlation between the timing of the AP and the initiation of contraction. The timing of the mechanical behavior of the beating cardiomyocytes corresponded to the electrical activity measured from the same cells by the patch clamp -method, meaning that the starting point of the APs were nicely followed by the initiation of the cardiomyocyte contraction. This result indicated that the video analysis is able to detect the mechanical features of beating with good accuracy.

The method described in study II has clear advantages over the traditional methods used for the characterization of cardiomyocytes. This

method does not require highly trained personnel or expensive equipment, is easier and faster to use, and is gentler the cells. In addition, the analysis of the mechanical properties of beating cardiomyocytes may reveal additional information about the cells compared to electrophysiological analysis only. As the patch clamp -method reveals purely electrophysiological phenomena in the cells and Ca^{2+}-imaging exposes the events of Ca^{2+} handling in the cardiomyocytes, the video analysis is based on uncovering the mechanical properties of the cardiomyocytes, which can be visualized as the contraction and relaxation of the cells. Possibly, parts of the disease phenotype can be clearly observed as abnormalities of the electrophysiology of the cells. However, some other features may be considered a mechanical abnormality, while the AP properties appear to be normal.

6.2.2. Disease phenotype observed by video analysis (III)

The third study (III) it was clearly demonstrated that the LQTS phenotype can be detected from single cardiomyocytes using video analysis, which was based on determining purely the mechanical features of the beating cells. The results from this mechanical analysis were consistent with the results obtained by patch clamp and Ca^{2+}-imaging -methods, although the video analysis revealed some additional information from the cells. According to the patch clamp -recordings, the cells carrying different mutations in *KCNQ1* seemed to behave more similarly with each other compared to the results from the mechanical analysis. Indeed, the video recordings showed phenotypic differences between the two genotypes, and this difference was partially confirmed by Ca^{2+}-imaging.

With the video analysis method, two separate groups of cardiomyocytes could be distinguished. Approximately 70 % of the disease-specific cardiomyocytes beat abnormally, while the rest of the cells resembled control cells with normal beating behavior. The same grouping could be performed for

the measurements done by Ca^{2+}-imaging, although the sizes of the groups were slightly different. By patch clamp -measurements, it was observed that all ventricular LQTS-specific cardiomyocytes had prolonged APDs. The differences in the sizes of the group of abnormally beating cells may be explained by the variability in the sensitivity between the different methods as well as by differences in the selection of cells for the measurements. Also, it again needs to be remembered that the different methods used in the study measure different functions of the cells and thereby reveal different aspects of the phenotype.

Ventricular-, atrial- and nodal-like cardiomyocytes are known to differ in their electrophysiological properties. The APs measured from these different types of cardiac myocytes have their own characteristics (Figure 6), which indicate differences in the ion channel function in the cells (He et al, 2003; Zhang et al, 2009). The variation observed in the mechanical functionality of the LQTS-specific cardiomyocytes may reflect the differences between the various subtypes of cardiac myocytes. Using video analysis or Ca^{2+}-imaging, the different cardiomyocyte subtypes cannot be distinguished; however, by the patch clamp -method, the diversity of APs can be detected. Based on the patch clamp -measurements, the majority of the cardiomyocytes were ventricular-like, and only marginal portions of the other subtypes of cardiomyocytes were found. On the other hand, the portions of normally and abnormally beating cells detected from the videos were approximately 30 % and 70 %, respectively. This difference compared to the patch clamp -data may also advocate the hypothesis that the variation could be explained by cells being either ventricular or other types of cardiomyocytes. If the mechanical abnormalities are observed only in ventricular-like cardiomyocytes, it is in accordance to the clinical manifestation of LQTS with the tendency to ventricular arrhythmia.

It is also known that there are differences in APDs measured from cardiomyocytes residing at different sections of the myocardium. The longest APDs in LQTS models have been reported in endocardial electrical conducting cells as well as in endocardial and mid-myocardial myocytes compared to epicardial myocytes (Dun & Boyden, 2008; Yan & Antzelevitch, 1998). Also, the mechanical contraction duration has been shown to be longer in cardiomyocytes residing under the endocardium (sub-endocardium) compared to cells in the mid-myocardium in symptomatic LQTS patients (Haugaa et al, 2011). This mechanical dispersion was not present in the hearts of asymptomatic mutation carriers or healthy individuals (Haugaa et al, 2011). Indeed, the transmural dispersion of APDs in LQTS patients has been considered a major cause of arrhythmias (Conrath & Opthof, 2006), and the mid-myocardial cells are thought to play an important role in the development of the severe symptoms of LQTS (Lankipalli et al, 2005). The differential beating observed in LQT1-specific cardiomyocytes *in vitro* may reflect this difference detected in the entire heart. More subtypes among the ventricular cardiomyocytes than those that are currently known may exist, and the differences in the APDs may not be solely dependent on the position of the cells in the myocardium, but some other differences in the phenotype of the cardiomyocytes. Some differences exist between the mid-myocardial cells and the other ventricular cardiomyocytes at the level of ion currents. In mid-myocardial cells, the I_{Ks} current is smaller, and the late Na^+ current is larger compared to the other types of ventricular cardiac myocytes (Antzelevitch et al, 1999; Zygmunt et al, 2001). This result and the possible other differences between the cells make the other types of cardiomyocytes more vulnerable for the symptoms of LQTS than the others, and this phenomenon may be detected *in vitro* as differences in the severity of the disease phenotype among the cells studied.

Mechanical phenotype of LQTS has been studied on the level of an entire heart (ter Bekke et al, 2014; De Ferrari et al, 1994; Gallacher et al, 2007; van der Linde et al, 2010; Nador et al, 1991), but the study III in this thesis demonstrates for the first time that the mechanical abnormalities can be detected also from single cardiomyocytes. It has been reported that approximately half of the LQTS patients exhibit extended thickening of left ventricular wall during the contraction of the heart, and in some symptomatic patients also a double-peak pattern of this thickening has been observed which may represent the mechanical correlate of EADs (Nador et al, 1991). These LQTS-related mechanical abnormalities have been normalized by Ca^{2+} channel blockers (De Ferrari et al, 1994) which is in agreement with the current knowledge on the mechanism of EADs; EADs are primarily due to the reactivation of L-type Ca^{2+} channels during the late phases of the cardiac AP (Lankipalli et al, 2005). In a canine model it has been demonstrated that under baseline conditions the left ventricular -pressure duration is longer than QT interval creating a positive "electro-mechanical window" (EMW) (van der Linde et al, 2010). In this model EMW turned negative during pharmacological I_{Ks} block prior to the induction of TdP-arrhythmia (Gallacher et al, 2007; van der Linde et al, 2010). In a recent study by ter Bekke and colleagues it was also demonstrated that EMW is positive in control individuals but negative in LQTS patients, and the negativity is more significant in symptomatic patients compared to asymptomatic (event-free) patients (ter Bekke et al, 2014). In addition to the studies on the entire heart, mechanical characteristics of iPS cell -derived cardiomyocyte monolayer have been evaluated using simultaneous video analysis and MEA-measurements (Hayakawa et al, 2014), but the study II in this thesis is the first published work on the mechanical features of single cadiomyocytes, and the study III is the first work that introduces the mechanical abnormalities detected in LQTS specific iPS cell -derived cardiomyocytes.

The mechanical abnormalities observed in LQTS-specific cardiomyocytes most likely are reflections of the electrophysiological dysfunction of the cells. The impaired function of K^+ currents results in prolongation of APD but it also may affect the function of other ion channels, including L-type Ca^{2+} channels, in the cells. And this may cause the occurrence of EADs in patch clamp -recordings and additional Ca^{2+} spikes observed by Ca^{2+}-imaging but also, the re-elevation of intracellular Ca^{2+} concentration may alter the function of saecomeres leading to impaired lengthening of the sarcomere stuctures and problems in the relaxation of the cardiomyocytes.

6.3. Modeling of long QT syndrome (I, III)

6.3.1. Long QT syndrome type 1 (III)

The most widespread type of LQTS is subtype 1. The genetic basis of LQT1 is a defective *KCNQ1* gene, but several different mutations in *KCNQ1* are known to cause the disease (Splawski et al, 2000). In the iPS cell studies that introduced *in vitro* cell models for LQT1, several different mutations have been presented. The first published model for LQT1 used patient-specific cells that carried a loss-of-function substitution of arginine to glutamine (R190Q) (Moretti et al, 2010). In these cells, the APD_{90} was increased by half, although the ECG of the patient showed a QT prolonged by 15 %. The other study presented iPS cell-derived cardiomyocytes with a dominant-negative mutation, namely the deletion of a cysteine at position 1893 (1893delC) in *KCNQ1* (Egashira et al, 2012). This mutation was shown to result in a trafficking deficiency of the KCNQ1 channel onto the cell membrane, and the MEA system revealed a significantly prolonged field potential duration (FPD) in cardiomyocytes carrying 1893delC compared to control cells (Egashira et al, 2012).

In the third study presented in this thesis (III), the cell lines carrying two different mutations of *KCNQ1* were used. The G589D mutation lies in the C-terminal domain of the protein encoded by *KCNQ1* and likely results in a difficulty of assembling the tetramers that form the functional K^+ channels (Piippo et al, 2001). It has also been proposed that the G589D mutation results in hindered transportation of the channel to the plasma membrane (unpublished data). The other mutation is an intronic mutation (ivs7-2A>G) that causes splicing alterations. In addition, ivs7-2A>G is located at the C-terminal domain of KCNQ1 and causes the complete loss-of-function of the particular K^+ channel (Fodstad et al, 2006). From the results in study III, these two different mutations of *KCNQ1* resulted in different phenotypes. This result was confirmed by various methods including the patch clamp -technique, Ca^{2+}-imaging and mechanical analysis based on video recordings. According to the video analysis, the cells carrying the G589D mutation had a prolonged contraction period, while the cells carrying ivs7-2A>G in *KCNQ1* vibrated, vacillated before or during relaxation or trembled afterwards. Both of the patients studied here suffer from symptoms related to LQTS, but the symptoms are not very severe. The patient with the G589D mutation has a QTc of only 456 ms but has still been suffering from episodes of unconsciousness and syncope. The other patient carrying ivs7-2A>G in *KCNQ1* had suffered from dizziness, darkening of vision and episodes of unconsciousness, and her QTc is clearly prolonged (492 ms).

The APDs measured from the LQT1-specific cardiomyocytes, both G589D and ivs7-2A>G carrying cells, were significantly prolonged compared to the control cardiomyocytes; thus, the LQTS phenotype can be considered to be reproduced (III). Spontaneous EADs were observed in ventricular cardiomyocytes specific for the G589D mutation but not in control cells or in cardiomyocytes carrying the ivs7-2A>G mutation. This difference was the only

difference between the two mutations observed by the patch clamp technique, while the effects of the two different mutations were more obvious from the results gathered by video analysis or Ca^{2+}-imaging. JNJ303, an I_{Ks} current inhibitor, prolonged APDs significantly in control cardiomyocytes (ventricular), while it did not have a significant effect on the AP characteristics in either of the LQT1-specific cells. This result is in agreement with the fact that the I_{Ks} current is already affected in LQT1-specific cardiomyocytes, and further blockage of that particular current does not alter the situation in the cells that much, while the effect in control cardiomyocytes was rather dramatic. On the other hand, the blockage of the I_{Kr} current by E-4031 triggered EADs in ventricular cardiomyocytes carrying either the G589D or ivs7-2A>G mutation in *KCNQ1* but not in control cells, although the APD was prolonged in all ventricular cardiac myocytes including control cells. This difference may be explained by the more severe effect of I_{Kr} blockage in the cardiac myocytes where the I_{Ks} current is also affected by mutations in *KCNQ1*. In addition, mid-myocardial cells exhibited a smaller I_{Ks} current compared to the other types of ventricular cardiomyocytes; therefore, the blockage of the I_{Kr} channel may have a more dramatic effect in these cells. And still it is possible that there are other differences in the current densities between the different types of ventricular cardiac cells may predispose other cells to the symptoms more extensively than others. However, the difference between the control cardiomyocytes and LQT10specific cardiomyocytes was clear and most likely cannot be explained by a coincidence of different subtypes of cardiac myocytes.

As indicated by the results from the third study (III) of this thesis as well as by comparing the results from different research groups (Egashira et al, 2012; Kiviaho et al, submitted; Moretti et al, 2010), the different mutations in *KCNQ1* result in different phenotypes of LQT1 in the patient, and these differences can be detected from the *in vitro* models established from the patients utilizing iPS

technology (Table 6). This observation emphasizes the need for a variety of cell models for LQTS with different mutations and the importance of the usage of the correct model for studies of a certain mutation. For example, if the medication is designed for a patient individually, the drug tests should be performed using the cells from that particular patient. When the phenotypes observed in different iPS cell-based models for LQTS are compared (Table 6), the baseline APDs measured from spontaneously beating cardiomyocytes are different. In some cases, the APDs reflect the clinical phenotypes of the original donors (Matsa et al, 2011), but this conclusion cannot be drawn between the different studies and different mutations (Kiviaho et al, submitted; Moretti et al, 2010). All in all, it is impossible to compare the results from different studies because the cells and methods used in these studies vary from each other and because the measurement set-ups are different. If the results from studies introducing models for LQT1 are compared with each other, no correlation can be observed between the clinical phenotypes and the phenotypes observed in the cell culture models. Instead, the asymptomatic R190Q mutation carrier (Moretti et al, 2010) had an APD as long as 745 (±91) ms, while the APDs measured from the cells of symptomatic patients carrying the G589D or ivs7-2A>G mutation (Kiviaho et al, submitted) were only 536 (±34) and 526 (±54) ms, respectively. In these two studies, the difference between the APDs measured from control cardiomyocytes was not very substantial (381 vs. 308 ms), which allows a tentative comparison between the results from the LQT1-specific cells.

Table 6. Comparison between the iPS cell -based models for LQTS. The table compares the APD_{90} (action potential duration at 90 % of the amplitude) values (ms) detected from a variety of LQTS-specific cardiomyocytes and from control cells used in each study. The baseline measurements from spontaneously beating cardiomyocytes are presented here. The individual mutations that the cells were carrying are also indicated as well as the references (Egashira et al, 2012; Itzhaki et al, 2011; Kiviaho et al, submitted; Lahti et al, 2012; Matsa et al, 2011; Moretti et al, 2010). In the work of Moretti and colleagues, two individuals had the same mutation, but the results were reported for only one of them. Instead, the results were described to be similar for both individuals (Moretti et al, 2010). In addition, the data regarding the APDs were completely missing in the article published by Egashira and colleagues (Egashira et al, 2012) as well as in the article by Bellin and colleagues (Bellin et al, 2013). Matsa and colleagues only published the APD for LQT2-cells and there were no information about the symptoms of the patient (Matsa et al, 2014). S = symptomatic, AS = asymptomatic.

LQT1 (*KCNQ1*)							
R190Q		*1893delC*		*G589D*		*ivs7-2A>G*	
Moretti et al, 2010		Egashira et al, 2012		Kiviaho et al, submitted		Kiviaho et al, submitted	
WT	LQT1	WT	LQT1	WT	LQT1	WT	LQT1
381 ± 35	745 ± 91 (AS)	n / a	n / a (S)	308 ± 30	536 ± 34 (S)	308 ± 30	526 ± 54 (S)
n / a	n / a (AS)						

LQT2 (*hERG*)											
A614V		*G1681A*		*R176W*		*N996I*		*G1681A*		*A422T*	
Itzhaki et al, 2011		Matsa et al, 2011		Lahti et al, 2012		Bellin et al, 2013		Matsa et al, 2014		Spencer et al, 2014	
WT	LQT2	WT	LQT2	WT	LQT2	WT	LQT2	WT	LQT2	WT	LQT2
495 ± 36	1280 ± 81 (S)	386 ± 139	881 ± 205 (S)	314 ± 18	538 ± 29 (AS)	n / a	n / a	n / a	929 ± 167 n / a	550 ± 50	5800 ± 900 (S)
			705 ± 57 (AS)					n / a			

One possible explanation for the contradictions in genotype-phenotype relations in cell models for LQT1 and in phenotypes observed in the cell models versus patients is the repolarization reserve in cardiac cells, which is used during stress or pharmacological challenge. It is thought, that some auxiliary mechanisms are available to cause normal repolarization, indicating that multiple occurrences might be required to induce the LQTS phenotype (Roden, 2006). These occurrences might be the presence of compound mutations, polymorphisms, drug exposure, female gender, hypokalemia or other risk factors (Roden, 2006; Lehtonen et al, 2007).

6.3.2. Subtype 2 of long QT syndrome (I)

The first study (I) aimed to reproduce the phenotype of LQT2 in a cell culture model (Lahti et al, 2012). Patient-specific iPS cells carrying a R176W mutation (Fodstad et al, 2004) in the *hERG* gene were generated and successfully differentiated into functional cardiac myocytes. These LQT2-specific cardiomyocytes reproduced the disease phenotype, including prolonged AP duration and increased arrhythmogenicity. Also, at low beating frequencies, the FPDs were significantly more prolonged in LQT2-specific cells compared to control cardiomyocytes, which is consistent with the clinical observation that the QT interval is more prolonged in LQT2 patients than in healthy individuals precisely at low beating rates (Swan et al, 1999). Although the patient studied here was rather asymptomatic, the cells derived from his fibroblasts exhibited an approximately 40 % decreased I_{Kr} current as shown by voltage clamp recordings and a prolonged cardiac repolarization time, which was demonstrated by both patch clamp -measurements and MEA. On the other hand, EADs were detected only in 5 % of the patient-specific cardiomyocytes, and this result correlates nicely with the fact that the original patient has not suffered from severe arrhythmias (Lahti et al, 2012).

Sotalol is an antiarrhythmic drug due to its property to block K^+ channels, and it functions as a β-adrenergic antagonist (Edvardsson et al, 1980). Sotalol was used in MEA measurements and induced premature beats only in LQT2-specific cardiomyocytes not in control cells. E-4031, a specific hERG (I_{Kr}) channel blocker, induced premature beats in both LQT2-specific and control cardiomyocytes, but the induction required a higher concentration (700 nmol/l) in control cells compared to LQT2-specific cardiomyocytes (500 nmol/l). The sensitivity of the LQT2-specific cells for sotalol may be explained by the already defective efflux of K^+ in these cells compared to control cardiomyocytes; therefore, the LQT2-specific cardiomyocytes are more vulnerable to further blockage of the K^+ channels by sotalol. E-4031 is a specific blocker of hERG channels, and it may have a more pronounced effect on LQT2-specific cells compared to control cardiomyocytes because only a portion of the hERG channels are fully functional in LQT2-specific cells. In addition, it is possible that the actual number of the hERG channels on the cell membrane is lower in the cardiac myocytes with LQT2. According to the results included in study I, the density of the I_{Kr} current in LQT2-specific cardiomyocytes is approximately half of the I_{Kr} density in the control cells. This finding possibly explains the reason that the lower concentration of E-4031 is enough to induce EADs in LQT2-specific cardiomyocytes compared to control cells. EADs are mostly due to the reactivation of LLCs during the plateau phase (2) of an AP. If a further prolonged AP is induced by E-4031 in LQT2-specific cardiomyocytes, this effect extends the time window even longer for LLC reactivation and the occurrence of EADs (Lankipalli et al, 2005).

The majority of the individuals carrying a R176W mutation in *hERG* are asymptomatic and unaware of their genetic burden. However, this particular mutation has been identified in cases of sudden death (Tester and Ackerman, 2007; Tu et al, 2011), and among the close relatives of the individual studied

here were two cases of sudden cardiac death at a young age, although the person himself was asymptomatic. The mechanism why the R176W mutation impairs the function of hERG is presently unknown, but when the mutation is heterologously expressed, it reduces the hERG tail current density by 75 % compared to the expression of wild type *hERG*. On the other hand, if the WT *hERG* is coexpressed with the R176W-mutated, the difference in current densities is abolished (Fodstad et al, 2006). In cardiomyocytes derived from patient-specific iPS cells, the decrease in I_{Kr} density was 43 %, although the cells were heterozygous for the R176W mutation. The ambivalent results may reflect the difference in the cellular milieu in cardiac versus non-cardiac cells. hERG is the major component of the I_{Kr} channel, which is composed of four α-subunits (hERG) and four β-subunits called KCNE2. Two different isoforms of hERG result from alternative splicing: hERG-1a has an N-terminal PAS regulatory domain, and hERG-1b has a truncated N-terminus (Lees-Miller et al, 1997; London et al, 1997; Morais Cabral et al, 1998). The R176W mutation is located in the N-terminal end of hERG and may not be present in the hERG-1b isoform. The two isoforms are thought to co-assemble to form the functional tetrameric K^+ channel (Lees-Miller et al, 1997), and how the position of the mutation affects the functionality of the channel is unclear. It is possible that the hERG-1b isoforms may be unaffected by the R176W mutation. This could explain why the co-expression of the WT allele together with the R176W allele abolished the difference in current densities observed between the cells expressing only the mutant allele or only the WT allele (Fodstad et al, 2006). If hERG-1b is less frequently present in the channel than hERG-1a, the expression of the WT allele might be sufficient to cover the need for hERG-1b in assembling functional channels. On the other hand, in cardiomyocytes, the expression of both alleles could not rescue the cells from the disease phenotype, and this difference may be explained by differences in the cellular milieus in

cardiac and non-cardiac cells. One possible difference could be related to alternative splicing. Possibly the portions of hERG-1a and -1b are different in cardiomyocytes compared to the scenario where the *hERG* gene is transiently transfected into non-cardiac cells. Nevertheless, both model systems, the iPS cell-based cardiac model and transiently transfected non-cardiac cell model, have shown that the R176W mutation is recessive by nature and not dominant negative.

An example of a *hERG* mutation with a dominant negative effect was introduced by another research group who presented a cell model for LQT2 based on iPS cell technology (Itzhaki et al, 2011). In that study, iPS cell lines with an alanine to valine substitution (A614V) in *hERG* at position 614 (Nakajima et al, 1998) were derived from a severely symptomatic LQT2 patient with documented episodes of TdP arrhythmias (Itzhaki et al, 2011). The A614V mutation caused a more severe decrease in I_{Kr} current density than observed in the studies with the R176W mutation included in this thesis (I). Cardiomyocytes carrying the A614V mutation also had a more prolonged APD_{90} compared to the R176W mutation carriers. EADs were present in 66 % of the cells containing the A614V mutation, while only 5 % of the cells carrying R176W in *hERG* showed EADs. These results most likely reflect the difference in severity of the two mutations, R176W vs. A614V. This difference is at least partially explained by the different effects of the mutations; A614V is known to have a dominant negative effect (Nakajima et al, 1998), while R176W is recessive by nature (Fodstad et al, 2006). On the other hand, in the first study (I) presented in this thesis (Lahti et al, 2012), the cardiomyocytes that were heterozygous for R176W still presented the disease phenotype (see the comparison between the phenotypes observed in *in vitro* models carrying different LQT2-related mutations in Table 6).

Another example of an *in vitro* model for LQT2 also introduced a patient with episodes of syncope, seizures and TdP (Matsa et al, 2011). That study demonstrated that the APDs of both atrial-like and ventricular-like iPS cell-derived cardiomyocytes were significantly prolonged. These cells carried a glycine to alanine substitution in *hERG* at position 1681 (G1681A); the cells did not demonstrate any spontaneous EADs, but EADs were triggered by β-adrenergic stimulation. The APDs were prolonged, but other AP properties were comparable to those reported for wild type cardiomyocytes (Gai et al, 2009; Yokoo et al, 2009; Zwi et al, 2009). In that study, iPS cells were generated from symptomatic and asymptomatic individuals, both carrying the same mutation (G1681A). The cardiac myocytes originated from the symptomatic daughter had a more pronounced, prolonged AP duration than the cells generated from the asymptomatic mother (Matsa et al, 2011). This fact indicates that even the same mutation does not guarantee a similar phenotype of LQTS in the cardiomyocytes, but instead the cell model derived from the patient's own cells is needed, for example, for designing individualized medications.

Recently, Bellin and colleagues published an iPS cell -based model for LQT2 which utilized patient's own cells as control cells after targeted gene correction (Bellin et al, 2013). In this LQT2-model, the mutation that caused LQT2 was a substitution of an asparagine to isoleucine at position 996 in *hERG* (N996I). The same mutation was also introduced in human embryonic stem cells (hESCs) to create another isogenic pair of LQT2-specific- and control cardiomyocytes to be compared. The correction of the mutation in iPS cells normalized the I_{Kr} current and the AP duration, and the introduction of the mutation reduced I_{Kr} and prolonged the AP duration in hESCs. This study also revealed a trafficking defect caused by N996I on hERG (Bellin et al, 2013). Matsa and colleagues also published a work were LQT2-phenotype was rescued (Matsa et al, 2014). In this study the iPS cell -derived cardiomyocytes carried

the same mutation as was published in the previous work from the same group, G1681A (Matsa et al, 2011), and allele-specific RNA interference (RNAi) toward the mutated hERG was used to normalize the AP duration and I_{Kr} current. The study also revealed that G1681A mutation causes a dominant-negative trafficking defect on hERG (Matsa et al, 2014). Yet another iPS cell -based model for LQT2 was published by Spencer and colleagues very recently (Spencer et al, 2014). In this study the LQT2 specific cells carried alanine to threonine substitution at position 422 (A422T) which produces trafficking-defective hERG channels and decreased I_{Kr} current. The A422T specific cardiomyocytes exhibited prolonged APs as well as prolonged intracellular Ca^{2+} transients. Also, EADs were present in LQT2 specific cardiomyocytes, and correlates of EADs were detected with Ca^{2+}-imaging (Spencer et al, 2014).

In the case of LQT2, it seems that there is a correlation between the severity of the clinical manifestation of the disease and the phenotype observed in the *in vitro* model but because the results are from separate works, and there are only four models that can be compared, this conclusion may be incorrect (Table 6). The information included in the two recent articles (Bellin et al, 2013; Matsa et al, 2014) was not enough to make any comparisons.

Almost all the drugs that are known to induce a prolonged QT interval and thereby the acquired form of LQTS, function by blocking the I_{Kr} current in cardiomyocytes by binding to hERG (Roden et al, 1996; De Bruin et al, 2005) or by interrupting hERG trafficking to the cell membrane (Dennis et al, 2007). In addition, it has been suggested that the drugs blocking I_{Kr} channels may induce the prolonged QT interval only in individuals who are already sensitive for a prolonged interval (Roden, 2005). Whether this sensitivity is due to a latent mutation in *hERG* or another possibility that reduces the repolarization reserve of the cardiomyocyte is unknown. These other sensitizing factors may include the presence of mutations in other genes, simultaneous exposure to other

drugs, female gender or hypokalemia (Roden, 2006; Lehtonen et al, 2007). Notably, the estimated prevalence of LQTS worldwide is between 1:5,000 and 1:10,000; however, in Finland, one individual out of 250 is a carrier of a LQTS-related mutation (Marjamaa et al, 2009). In addition, the increasing identification of asymptomatic mutation carriers throughout the world may indicate that the worldwide approximation is also an underestimation (Schwartz, 1985; Ackerman, 1998; Piippo et al, 2001). This finding indicates that quite a large human population may be predisposed to an increased risk of prolonged QT by a variety of drugs (Kaye et al, 2013).

6.3.3. Comparison of the disease phenotype revealed by different methods (I, II, III)

An interesting observation of the LQTS-specific cardiomyocytes is that the disease phenotype is more clearly observed in single cells compared to cell clusters or the entire heart. This result is obvious if the results from patch clamp -recordings, Ca^{2+}-imaging and video analysis are compared to the results obtained by MEA measurements and clinical ECG recordings from the same patient. However, all the methods mentioned above measure different matters. The patch clamp -recordings reveal electrophysiological phenomena of the cells; Ca^{2+}-imaging measures the fluctuation of Ca^{2+} concentrations in the cytoplasm; and the video analysis describes purely the mechanical characteristics of the contraction and relaxation of the cardiomyocytes. On the other hand, the MEA measures the FPs from the clusters of cardiomyocytes, and an ECG reveals the electrical activity of the whole heart. All of these methods are able to expose the disease phenotype, even though the approach is different if different methods are used. In the first study presented in this thesis (I), the single cell recordings by the patch clamp -method showed a prolonged difference of 66 % in the APD_{90} in LQT2-specific cells compared to control

cardiomyocytes, while the FPDs measured from cell aggregates using MEA differed by only 20 % between the LQT2-specific and control cells. The results from MEA measurements more resembled the differences observed in the ECG of the patient and healthy individuals (Fodstad et al, 2006) than the results gathered by patch clamp. The iPS cell-based models for LQT2 generated by other research groups have also demonstrated the same: a better correlation between the clinical ECG and MEA data than between clinical measurements and measurements from single cells, as well as a more prolonged repolarization observed in single cells than in cell aggregates (Itzhaki et al, 2011; Matsa et al, 2011; Moretti et al, 2010). Again, it needs to be remembered that these methods are not comparable with each other, although they all measure electrical properties of the cell, cell aggregate or an organ. As the measurements from single cells or from cell aggregates are two-dimensional, the ECG draws a three-dimensional picture of the electrical activity of the heart. Nevertheless, this difference in the intensity of the disease phenotype observed by different methods raises the question whether some compensatory mechanisms are involved that are unable to function without the connections between the cells. This hypothesis might explain the stronger manifestation of LQTS in single cells compared to cell clusters or the whole heart.

On the other and, it was observed that part of the LQT1-specific cells beat normally, and their beating behavior was not distinct from the beating observed in control cardiomyocytes (III). One possible explanation for this observation could be that the expression ratio of wild type to mutated allele varied from cell to cell. The patients studied here (III) were both heterozygous for the LQT1-related mutation, so both alleles are present in the cells. Nevertheless, the fact that the disease phenotype was observed in some cardiomyocytes more clearly than in others underscores the importance of studying the LQTS specific-cardiomyocytes on a single cell level. As mentioned

previously, the defects that can be detected from single cells may be compensated when cardiomyocytes are beating in aggregates. Normally beating cardiomyocytes may synchronize the cells that beat abnormally, resulting in a more or less normally beating cell cluster. Also it is possible that the atrial and conducting type of cardiomyocytes are present in the cell clusters, and they may pace the beating and synchronize the beating behavior. The compensatory mechanisms may explain why the patients experience arrhythmias only in certain circumstances; e.g., LQT1 patients during exercise when the beating rate is high and LQT2 patients typically if they are awakened by an auditory stimulus (Table 3).

Yet another way to approach the issue of difference in the intensity of the disease phenotype observed by different methods, is through the EMV (Gallacher et al, 2007; van der Linde et al, 2010; ter Bekke et al, 2014). It is possible, that the abnormalities are partially manifested as differences in timing between electrophysiological and mechanical behavior and thereby not observed when only one method is used, but instead, simultaneous measurement of electrical activity and mechanical features is needed.

Using the patch clamp -technique, one obvious difference between the LQT1-specific cardiomyocytes carrying either of the two different mutations (G589D or ivs7-2A>G) was observed. Spontaneous EADs occurred in cardiomyocytes specific for the G589D mutation, but no spontaneous EADs were observed in control cells or in cardiomyocytes carrying the ivs7-2A>G mutation in *KCNQ1*. Both mutations prolonged APD, but G589D may have an additional function to promote EADs in the cells carrying the particular mutation. EADs are primarily due to the reactivation of L-type Ca^{2+} channels during phases 2 and 3 of the cardiac AP. This reactivation is dependent on voltage and changes in the membrane potential during phase 2 or 3 (Lankipalli et al, 2005). In deed, LQTS-related EADs have been abolished by blocking of

L-type Ca^{2+} channels using nifedipine (Spencer et al, 2014). Similarly to the patch clamp -data, the cardiomyocytes carrying these different mutations behaved in a mechanically distinct manner, as observed by video analysis. In the G589D-specific cardiac myocytes, the most prevalent abnormality detected was prolonged contraction, while the most commonly observed abnormal behavior in ivs7-2A>G-specific cardiomyocytes was the vacillation before or during relaxation. The differential effects of the two mutations on Ca^{2+} handling in these cells was exposed by Ca^{2+}-imaging, which also resulted in the distinction of two different types of arrhythmic behavior: arrhythmias with two or more Ca^{2+} peaks (AD) and arrhythmias of small amplitude Ca^{2+} events in between the stable amplitude Ca^{2+} spikes (AS). The portions of these different abnormalities were slightly variable as different methods were used, but the distinction between the effects of the two mutations could be observed with multiple techniques.

LQT2 phenotype detected using Ca^{2+}-imaging was demonstrated very recently in iPS cell -derived cardiomyocytes also by another research group (Spencer et al, 2014). This study showed that intracellular Ca^{2+} transients were markedly prolonged in LQT2 specific cardiomyocytes compared to controls, and also correlates of EADs were observed in Ca^{2+} signals. In the same study it was reported that LQT3 specific cardiomyocytes exhibited abnormal mechanical beating behavior with oscillating contraction phase but the phenomenon was not further analysed, and such observation was not reported for LQT2 specific cells (Spencer et al, 2014).

6.3.4. Allelic imbalance and beating behavior of long QT syndrome -specific cardiomyocytes (III)

Approximately 70 % of the LQT1-specific cardiomyocytes beat abnormally, and approximately 30 % were normally beating cells and resembled control cardiomyocytes with regard to their mechanical properties. A similar variation was observed in Ca^{2+} handling as observed by Ca^{2+}-imaging, although the proportions were slightly different. To uncover the reason for this phenomenon, allelic imbalance qPCR was performed. With this method, the expression levels of the wild type and mutated versions of *KCNQ1* in heterozygous cells can be identified. In the cells carrying the G589D mutation in *KCNQ1,* the expression ratio was 4:1; the WT allele was responsible for 80 % of the expression, while 20 % of the expressed *KCNQ1* was of the mutated form. This ratio reflects the situation at the mRNA level, which does not report the portions of the two alleles at the protein level. The transcripts may be alternatively processed before translation into proteins. Nevertheless, the expression ratio of 4:1 nicely agrees with the fact that 71 % of the G589D-specific cardiomyocytes beat abnormally, and 29 % of the cells carrying the mutation beat normally. If the mathematic probability of one tetrameric ion channel to contain only WT subunits is counted, the result is 41 %. On the other hand, the probability for the same channel to contain one or more subunits carrying the mutation is 59 %. These probabilities are counted in the situation where the expression ratio is exactly 4:1. In short, with a probability of 59 %, the I_{Ks} channel contains one or more mutated subunits, which may cause impaired function of the channel. Approximately 71 % of G589D-carrying cardiomyocytes beat abnormally. However, unpublished data from another research group suggest that G589D mutation is a trafficking mutation with normal functioning but with hindered transportation to the plasma membrane (personal communication with Professors William R. Kobertz and Henry M. Colecraft). This comportment

would mean that all the subunits in the cell membrane are WT ones, but the number of functioning I_{Ks} channels may be reduced.

For the KCNQ1-ivs7-2A>G mutation, the allelic discrimination resulted in an expression ratio of 3:1, which indicates 75 % of the mRNA is WT and 25 % of the mRNA is mutated mRNA. The observed portion of normally beating cardiomyocytes among these cells was 32 %, and the abnormally beating portion was 68 %. The calculated probabilities for the WT and mutated subunits to form the tetrameric K^+ channel using the ratio of 3:1 are exactly 32 % for the channel with only WT subunits and 68 % for the situation that at least one of the subunits is mutated. These mathematical calculations support the results from the allelic discrimination studies, although the allelic imbalance qPCR does not reveal the expression ratio at the protein level. The mechanism of ivs7-2A>G mutation is unknown but it does have a complete loss-of-function effect on the I_{Ks} channel, and the effect is dominant negative (Fodstad et al, 2006). This suggests that the ivs7-2A>G-mutated KCNQ1 is transported to the plasma membrane where the mutation affects the functioning of the I_{Ks} channel. When the results from allelic discrimination analysis are evaluated, this technique shows the expression ratios in the whole population of cells. This analysis does not detect differences between the expression ratios in single cells that form the population, indicating that variation may exist in the allelic discrimination from one cardiomyocyte to another.

6.3.5. Limitations in the use of cardiomyocytes derived from pluripotent stem cells (I, II, III)

Although iPS cell technology has provided a clear improvement over previous ways to model human cardiac diseases, the iPS cell-based models are far from perfect. One of the most distracting disadvantages of these cardiomyocytes derived from pluripotent stem cells is their immaturity. When compared to

primary cardiomyocytes, the stem cell-derived cardiac cells have an immature morphology because they are usually not as elongated as primary cells, and their shape can vary from round to triangular, square or polygon. In addition, the organization of the sarcomeric structure is incomplete. In primary cardiomyocytes, the sarcomeres are parallel, and the chains of sarcomeres stretch from one end of the cell to another. In contrast, the sarcomeres in iPS cell-derived cardiomyocytes are usually in disarray instead of arranged in a sequence (Lieu et al, 2009; Luna et al, 2011). The immaturity can also be observed as the lack of t-tubule structures in cardiomyocytes derived from pluripotent stem cells, although the cells were ventricular-like (Lieu et al, 2009). The lack of t-tubules causes deficiencies in Ca^{2+} handling in these cardiomyocytes because the spread of electrical signals in the cells may not be rapid enough to induce a homogenous Ca^{2+} release from the SR. The non-homogenous release of Ca^{2+} finally leads to a non-synchronous contraction of the cardiomyocyte (Ferrantini et al, 2013).

The immature nature of the cardiomyocytes derived from iPS cells may cause some errors when the phenotypes of these cells are evaluated. This fact is important to remember if iPS-derived cardiomyocytes are used as a disease model or for drug testing because part of the abnormalities observed in these cells may result from the immature state of the cells instead of the disease phenotype. Indeed, an abnormal beating behavior and anomalies in Ca^{2+} signaling were observed in control cardiomyocytes in study III included in this thesis. However, the occurrence of anomalies was not as common in control cells as in LQT1-specific cardiomyocytes, which may indicate that at least a portion of the abnormalities was due to the disease. However, the “disease phenotype” may actually be a consequence of the immaturity of the cardiomyocytes.

In addition to the general immaturity of the iPS cell-derived cardiomyocytes, the rate and uniformity of differentiation is a matter of concern. How can one verify that all the cardiomyocytes studied are equally mature? It is possible for exampe, that a certain mutation related to cardiac disease may affect the function of the cardiomyocyte in a manner that the differentiation and maturation of that cell is slower compared to the differentiation and maturation of a control cardiomyocyte. If this difference occurs and the functionality of the cardiomyocytes with a disease are compared to control cells that have been differentiated similarly, it is possible that the two groups of cells will not be at the same phase of differentiation and maturation at the same time. The rate of differentiation may also vary for other reasons that are not related to the genotype of the cells, but may be related to for exampe, the variability in the cell culture conditions or the original iPS cell lines. AP characteristics are known to vary among cardiomyocytes derived from different iPS cell lines (Doss et al, 2012). Nevertheless, the time of culturing after differentiation has an effect on the maturity of the cardiomyocytes, which can be seen as changes in the expression of ion channels related to the cardiac AP (Sartiani et al, 2007). As a general observation concerning cardiomyocytes derived from a large group of iPS cell lines, it seems that the I_{Kr} current has a pronounced role at the expense of other K^+ currents (Doss et al, 2012), which may make iPS cell-derived cardiomyocytes oversensitive to disturbances in the I_{Kr} current. To evaluate the iPS cell-derived cardiomyocytes as a reliable model for the human cardiac system, the state of their maturity should be tested; however, this procedure is not straightforward. Using the patch clamp -technique, maturity could be measured by analyzing the properties of an AP; however, if other methods are used, the evaluation may be impossible.

6.4. Future perspectives

An important goal of iPS cell technology and its cardiac applications is in regenerative medicine. However, reaching this goal is restrained by a variety of obstacles related to safety issues as well as the efficiency and rapidity of the methods involved. First, the efficient production of iPS cells still utilizes viruses for the delivery of reprogramming factors. The usage of retroviruses involves problems with genomic integration of the viral transgenes, reactivation of these genes even if the genes are silenced after reprogramming and the risk of tumor formation. For these reasons, iPS cells produced using integrating viruses are obviously unsuitable for therapeutic purposes. On the other hand, novel, non-viral and non-genetic methods for reprogramming have been developed and are improving quickly, and these methods may resolve the problem. Second, the differentiation of iPS cells into cardiomyocytes still needs to be refined because the current methods are not able to efficiently produce homogenous populations of cardiomyocytes with a high enough quality and in large quantities. Instead, the differentiated cardiomyocytes form cell aggregates or cell sheets that are usually composed of a mixed population of different subtypes of cardiac cells as well as non-cardiac cells. In addition, the maturation state of the cardiomyocytes may vary among the cell aggregates and between different instances of differentiation. Third, defined, xeno-free culture conditions are needed for reprogramming, for maintenance of the iPS cells, and for the differentiation of iPS cells into cardiomyocytes if these cells are to be used for clinical purposes. Finally, the time that is needed for iPS cell production and their differentiation into functional cardiomyocytes might be too long for the treatment of some acute conditions, such as myocardial infarction. However, this problem may be circumvented by directly reprogramming fibroblasts into cardiac myocytes, which has been performed previously (Jayawardena et al, 2012; Nam et al, 2013).

While the usage of iPS cell applications for regenerative medicine in cardiology will most likely not become a reality in the near future, the iPS cell technology most likely can be utilized earlier for cardiac disease modeling, preclinical drug testing and designing personalized medications for patients. Multiple iPS cell lines specific for a variety of cardiac diseases have already been introduced: The LEOPARD syndrome (Carvajal-Vergara et al, 2010), an overlap syndrome of cardiac Na^+ channel disease (Davis et al, 2012), hypertrophic cardiomyopathy (Lan et al, 2013), familial dilated cardiomyopathy (Ho et al, 2011; Siu et al, 2012; Sun et al, 2012), arrhythmogenic right ventricular cardiomyopathy (Caspi et al, 2013; Kim et al, 2013; Ma et al, 2013), catecholaminergic polymorphic ventricular tachycardia (Di Pasquale et al, 2013; Fatima et al, 2011; Itzhaki et al, 2012; Jung et al, 2012; Kujala et al, 2012; Novak et al, 2012), Pompe disease (Huang et al, 2011) and LQTS (Bellin et al, 2013; Egashira et al, 2012; Itzhaki et al, 2011; Lahti et al, 2012; Ma et al, 2013; Malan et al, 2011; Matsa et al, 2011; Moretti et al, 2010; Terrenoire et al, 2013; Yazawa et al, 2011), and the functionality of the cardiomyocytes derived from these cells has been evaluated. The disease phenotypes have been reproduced in these *in vitro* models, and some drug testing has been conducted using models generated using patient-specific iPS cells (Liang et al, 2013). However, for reliable studies on the pathogenesis of certain cardiac diseases or for pharmacological testing with sufficient accuracy and reproducibility, the cardiomyocyte population should be homogenous and contain only one subtype of cardiac myocytes. Furthermore, these cells should be mature and adult-like in their phenotype. To fulfill this requirement, the differentiation methods need to be improved as mentioned previously. In addition, three-dimensional model systems may be required to mimic the physiological condition more reliably and to regulate the differentiation of cardiomyocytes toward a more mature state.

A prolonged QT interval is the most common severe side effect of pharmaceuticals and the most common reason for the withdrawal of drugs already on the market (Roden, 2004). Because the individuals carrying a mutation related to LQTS may be more sensitive for this prolonged interval, preclinical drug testing should be implemented in cell models that have LQTS-related mutations as well as in models of wild type cardiomyocytes. For this reason, these *in vitro* models for LQTS need to be developed, although the quality of the methods involved in the production and characterization of the models still needs further polishing.

Although many obstacles need to be overcome before iPS cell-derived cardiomyocytes can be used for clinical applications or for drug discovery, these cardiomyocytes already supply unprecedented opportunities for disease modeling. In the near future, the cardiomyocytes derived from patient- and disease-specific iPS cells can most likely be utilized for designing individualized medications and for the diagnostics of a variety of genetic cardiac diseases. In spite of the fact that cardiomyocytes derived from pluripotent stem cells are rather immature by their nature, the models based on iPS cell technology provide a huge improvement compared to previous models using animals or transfected non-cardiac cells (Paavonen et al, 2003; Sugiyama 2008; Sugiyama et al, 2011). Besides, problems are there to be solved, and iPS cell derived cardiomyocytes may offer tremendous opportunities for pharmacological industry and even for the regenerative medicine in the future.

7. Conclusions

The aim of this work was to establish iPS cell lines from both control individuals and patients suffering from different subtypes of LQTS, differentiate the iPS cells into cardiac myocytes and evaluate the characteristics and function of these cardiomyocytes. Based on the three studies presented in this thesis, the following can be concluded.

- Several iPS cell lines were established from dermal fibroblasts of healthy individuals as well as patients with LQT1 or LQT2. These iPS cells differentiated into functional cardiomyocytes expressing cardiac markers and exhibiting electrophysiological properties that are typical of cardiac myocytes.
- LQT1-specific iPS cells differentiated into cardiac myocytes and reproduced the disease phenotype, which was observed as prolonged APDs of the LQT1-specific cardiomyocytes compared to the APDs measured from control cells.
- LQT2-specific cardiomyocytes displayed the disease phenotype *in vitro,* although the fibroblast donor had a relatively mild clinical phenotype. The abnormal electrophysiology of the cardiac myocytes was observed as a prolonged repolarization time, which was shown by both the patch clamp method and MEA.
- A novel method for the characterization of mechanical properties of cardiomyocytes was developed. This method is based on video recordings and is an easy, fast and relatively inexpensive method to use. This method is non-invasive, non-toxic and label-free and may result in additional information compared to the results obtained purely by electrophysiological analysis of cardiomyocytes.

- The LQTS phenotype can be detected by analyzing only the mechanical behavior of single cardiomyocytes, and for the first time, the abnormal mechanical properties of beating in the LQTS-specific cardiomyocytes derived from iPS cells were reported.
- Two different mutations (G589D and ivs7-2A>G) in *KCNQ1* caused distinct phenotypes of LQT1 *in vitro,* which could be detected using the patch clamp -technique and Ca^{2+}-imaging, as well as by analyzing the mechanical behavior of the beating cardiomyocytes.

Acknowledgements

With all my heart, I thank my accomplished, kind and sympathetic supervisor, Professor Katriina Aalto-Setälä, MD, PhD. These thanks are for the scientific guidance as well as the help and support in personal issues. Katriina, I consider You both an excellent supervisor and a precious friend. I also thank my other skilled supervisor, Mari Pekkanen-Mattila, PhD, whose help was indispensable in guiding me through both the theoretical background information and practicalities in the lab. Mari, You are also considered more that just a colleague and supervisor.

These studies were performed in the Institute of Biomedical Technology (IBT) at the University of Tampere during the years 2009-2014 and funded by the Finnish Cultural Foundation, the Finnish Funding Agency for Technology and Innovation (TEKES), Orion R&D and the Tampere Graduate Program in Biomedicine and Biotechnology (TGPBB). I am grateful to Professor Riitta Suuronen and the Head of IBT, Hannu Hanhijärvi, for providing excellent research facilities for my studies and to TGPBB for the scientific education and personal salary.

Next, I wish to acknowledge all the members of my thesis committee, Docent Heli Skottman, PhD; Professor Timo Otonkoski, MD, PhD; and Professor Olli Silvennoinen, MD, PhD. I am also grateful to Steve Oh, PhD and Pasi Tavi, PhD for the critical review of my thesis and for the suggestions and guidance concerning the improvement of the quality of the work.

All my co-authors deserve my gratitude for their work included in the studies of my thesis. Therefore, I thank Ville Kujala, MSc; Hugh Chapman, MSc; Ari-Pekka Koivisto, PhD; Erja Kerkelä, PhD; Jari Hyttinen, PhD (Tech.); Kimmo Kontula, MD, PhD; Heikki Swan, MD, PhD; Bruce Conklin, MD, PhD; Shinya Yamanaka, MD, PhD; Olli Silvennoinen, MD, PhD; Antti Ahola, MSc (Tech.); Kim Larsson, PhD; Markus Honkanen, PhD (Tech.); Kirsi Kujala, MSc

(Tech.); Henna Venäläinen; and Kiti Paavola, BSc for their efforts. I also express special thanks to Antti for sharing the exciting moments in studies II and III described in this thesis.

The Heart Group has been a warm and enjoyable society in which to work, and the entire group, including former and present members, is thanked here. Special thanks are reserved for the Bachelors of Laboratory Services Merja Lehtinen, Henna Venäläinen and Markus Haponen for their technical help. Henna is also thanked for the precious friendship we have shared. In addition, I wish to express my gratitude for the friendship I have shared with Liisa Ikonen, MSc (Tech.); Marisa Ojala, MSc; and Kirsi Kujala, MSc (Tech.).

I also thank Soile Nymark, PhD (Tech.) for sharing her electrophysiological expertise with me and helping with this challenging field of science to improve the manuscript of my thesis.

I thank my dearest friend, Hanna, for being there for so many years and for sharing all the joys and challenges along the way. You truly are like a sister to me.

The support from my parents, Outi and Matti Lahti, has been indescribably valuable. My loving parents, you are most warmly thanked for all your encouragement, faith and trust in my work. In particular, I thank my mom for taking care of my son during the process of writing the thesis, and my dad for the financial support concerning the party held after my doctoral defense. You both also deserve my gratitude for being the most wonderful parents.

Finally, I am SO grateful to Sami, who has tolerated me during my times of stress and tiredness. You are the love of my life and because of You, I have finally become myself and have been able to make all my dreams come true. I also thank the “love and light of the world” for giving me two beautiful and beloved children, Toivo Kipinä and Lahja Illusia, who have helped me to put everything into perspective.

References

Aasen T, Raya A, Barrero MJ, Garreta E, Consiglio A, Gonzalez F, Vassena R, Bilić J, Pekarik V, Tiscornia G, Edel M, Boué S, Izpisúa Belmonte JC (2008): Efficient and rapid generation of induced pluripotent stem cells from human keratinocytes. Nature Biotechnology 26(11): 1276-1284.

Ackerman MJ (1998): The long QT syndrome: ion channel diseases of the heart. Mayo Clinic Proceedings 73(3): 250-269.

Adewumi O, Aflatoonian B, Ahrlund-Richter L, Amit M, Andrews PW, Beighton G, Bello PA, Benvenisty N, Berry LS, Bevan S, Blum B, Brooking J, Chen KG, Choo AB, Churchill GA, Corbel M, Damjanov I, Draper JS, Dvorak P, Emanuelsson K, Fleck RA, Ford A, Gertow K, Gertsenstein M, Gokhale PJ, Hamilton RS, Hampl A, Healy LE, Hovatta O, Hyllner J, Imreh MP, Itskovitz-Eldor J, Jackson J, Johnson JL, Jones M, Kee K, King BL, Knowles BB, Lako M, Lebrin F, Mallon BS, Manning D, Mayshar Y, McKay RD, Michalska AE, Mikkola M, Mileikovsky M, Minger SL, Moore HD, Mummery CL, Nagy A, Nakatsuji N, O'Brien CM, Oh SK, Olsson C, Otonkoski T, Park KY, Passier R, Patel H, Patel M, Pedersen R, Pera MF, Piekarczyk MS, Pera RA, Reubinoff BE, Robins AJ, Rossant J, Rugg-Gunn P, Schulz TC, Semb H, Sherrer ES, Siemen H, Stacey GN, Stojkovic M, Suemori H, Szatkiewicz J, Turetsky T, Tuuri T, van den Brink S, Vintersten K, Vuoristo S, Ward D, Weaver TA, Young LA, Zhang W (2007): Characterization of human embryonic stem cell lines by the International Stem Cell Initiative. Nature Biotechnology 25(7): 803-816.

Allegrucci C, Young LE (2007): Differences between human embryonic stem cell lines. Human Reproduction Update 13: 103-120.

Amin AS, Tan HL, Wilde AA (2010): Cardiac ion channels in health and disease. Heart Rhythm 7(1): 117-126.

Anderson CL, Delisle BP, Anson BD, Kilby JA, Will ML, Tester DJ, Gong Q, Zhou Z, Ackerman MJ, January CT (2006): Most LQT2 mutations reduce Kv11.1 (hERG) current by a class 2 (trafficking-deficient) mechanism. Circulation 113: 365-373.

Anokye-Danso F, Trivedi CM, Juhr D, Gupta M, Cui Z, Tian Y, Zhang Y, Yang W, Gruber PJ, Epstein JA, Morrisey EE (2011): Highly efficient miRNA-mediated reprogramming of mouse and human somatic cells to pluripotency. Cell Stem Cell 8(4): 376-388.

Antzelevitch C, Sicouri S, Litovsky SH, Lukas A, Krishnan SC, Di Diego JM, Gintant GA, Liu DW (1991): Heterogeneity within the ventricular wall. Electrophysiology and pharmacology of epicardial, endocardial, and M cells. Circulation Research 69(6): 1427-1449.

Antzelevitch C, Sicouri S (1994): Clinical relevance of cardiac arrhythmias generated by afterdepolarizations. Role of M cells in the generation of U waves, triggered activity and torsade de pointes. Journal of American College of Cardiology 23(1): 259-277.

Antzelevitch C, Shimizu W, Yan GX, Sicouri S, Weissenburger J, Nesterenko VV, Burashnikov A, Di Diego J, Saffitz J, Thomas GP (1999): The M cell: its contribution to the ECG and to normal and abnormal electrical function of the heart. Journal of Cardiovascular Electrophysiology 10(8): 1124-1152.

Antzelevitch C (2005): Modulation of transmural repolarization. Annals of the New York Academy of Sciences 047: 314-323.

Anyukhovsky EP, Sosunov EA, Gainullin RZ, Rosen MR (1999): The controversial M cell. Journal of Cardiovascular Electrophysiology 10(2): 244-260.

Avilion AA, Nicolis SK, Pevny LH, Perez L, Vivian N, Lovell-Badge R (2003): Multipotent cell lineages in early mouse development depend on SOX2 function. Genes & Development 17(1): 126-140.

Barhanin J, Lesage F, Guillemare E, Fink M, Lazdunski M, Romey G (1996): KvLQT1 and lsK (minK) proteins associate to form the I_{Ks} cardiac potassium current. Nature 384(6604): 78-80.

Barry FP, Murphy JM (2004): Mesenchymal stem cells: clinical applications and biological characterization. The International Journal of Biochemistry & Cell Biology 36(4): 568-584.

Bauwens CL, Peerani R, Niebruegge S, Woodhouse KA, Kumacheva E, Husain M, Zandstra PW (2008): Control of human embryonic stem cell colony and aggregate size heterogeneity influences differentiation trajectories. Stem Cells 26(9): 2300-2310.

ter Bekke RM, Haugaa KH, van den Wijngaard A, Bos JM, Ackerman MJ, Edvardsen T, Volders PG (2014): Electromechanical window negativity in genotyped long-QT syndrome patients: relation to arrhythmia risk. European Heart Journal (ehu370. Epub ahead of print).

Bellin M, Casini S, Davis RP, D'Aniello C, Haas J, Ward-van Oostwaard D, Tertoolen LGJ, Jung CB, Elliott DA, Welling A, Laugwitz K-L, Moretti A, Mummery CL (2013): Isogenic human pluripotent stem cell pairs reveal the role of a KCNH2 mutation in long-QT syndrome. EMBO 11;32(24): 3161–3175.

Bennett PB, Yazawa K, Makita N, George AL Jr (1995): Molecular mechanism for an inherited cardiac arrhythmia. Nature 376(6542): 683-685.

Beqqali A, Kloots J, Ward-van Oostwaard D, Mummery C, Passier R (2006): Genome-wide transcriptional profiling of human embryonic stem cells differentiating to cardiomyocytes. Stem Cells 24(8): 1956-1967.

Bernstein BE, Mikkelsen TS, Xie X, Kamal M, Huebert DJ, Cuff J, Fry B, Meissner A, Wernig M, Plath K, Jaenisch R, Wagschal A, Feil R, Schreiber SL, Lander ES (2006): A bivalent chromatin structure marks key developmental genes in embryonic stem cells. Cell 125(2): 315-326.

Bers DM (2002): Cardiac excitation-contraction coupling. Nature 415: 198-205.

Bokil NJ, Baisden JM, Radford DJ, Summers KM (2010): Molecular genetics of long QT syndrome. Molecular Genetics and Metabolism 101(1): 1-8.

Braam SR, Denning C, Matsa E, Young LE, Passier R, Mummery CL (2008): Feeder-free culture of human embryonic stem cells in conditioned medium for efficient genetic modification. Nature Protocols 3(9): 1435-1443.

Braam SR, Tertoolen L, van de Stolpe A, Meyer T, Passier R, Mummery CL (2009): Prediction of drug-induced cardiotoxicity using human embryonic stem cell-derived cardiomyocytes. Stem Cell Research 4(2): 107-116.

Brand T (2003): Heart development: molecular insights into cardiac specification and early morphogenesis. Developmental Biology 258(1): 1-19.

Briggs R, King TJ (1952): Transplantation of Living Nuclei From Blastula Cells into Enucleated Frogs' Eggs. Proceedings of the National Academy of Sciences of the United States of America 38(5): 455-463.

Brivanlou AH, Gage FH, Jaenisch R, Jessell T, Melton D, Rossant J (2003): Stem cells. Setting standards for human embryonic stem cells. Science 300: 913-916.

Burridge PW, Anderson D, Priddle H, Barbadillo Muñoz MD, Chamberlain S, Allegrucci C, Young LE, Denning C (2007): Improved human embryonic stem cell embryoid body homogeneity and cardiomyocyte differentiation from a novel V-96 plate aggregation system highlights interline variability. Stem Cells 25(4): 929-938.

Burridge PW, Thompson S, Millrod MA, Weinberg S, Yuan X, Peters A, Mahairaki V, Koliatsos VE, Tung L, Zambidis ET (2011): A universal system for highly efficient cardiac differentiation of human induced pluripotent stem cells that eliminates interline variability. PLoS One 6(4): 18293.

Burridge PW, Matsa E, Shukla P, Lin ZC, Churko JM, Ebert AD, Lan F, Diecke S, Huber B, Mordwinkin NM, Plews JR, Abilez OJ, Cui B, Gold JD, Wu JC (2014): Chemically defined generation of human cardiomyocytes. Nature Methods 11(8):855-860.

Camelliti P, Borg TK, Kohl P (2005): Structural and functional characterisation of cardiac fibroblasts. Cardiovascular Research 65: 40-51.

Cao F, Wagner RA, Wilson KD, Xie X, Fu JD, Drukker M, Lee A, Li RA, Gambhir SS, Weissman IL, Robbins RC, Wu JC (2008): Transcriptional and functional profiling of human embryonic stem cell-derived cardiomyocytes. PLoS One 3(10): 3474.

Cartwright P, McLean C, Sheppard A, Rivett D, Jones K, Dalton S (2005): LIF/STAT3 controls ES cell self-renewal and pluripotency by a Myc-dependent mechanism. Development 132(5): 885-896.

Carvajal-Vergara X, Sevilla A, D'Souza SL, Ang YS, Schaniel C, Lee DF, Yang L, Kaplan AD, Adler ED, Rozov R, Ge Y, Cohen N, Edelmann LJ, Chang B, Waghray A, Su J, Pardo S, Lichtenbelt KD, Tartaglia M, Gelb BD, Lemischka IR (2010): Patient-specific induced pluripotent stem-cell-derived models of LEOPARD syndrome. Nature 465: 808-812.

Caspi O, Itzhaki I, Kehat I, Gepstein A, Arbel G, Huber I, Satin J, Gepstein L (2009): In vitro electrophysiological drug testing using human embryonic stem cell derived cardiomyocytes. Stem Cells Development 18(1): 161-172.

Caspi O, Huber I, Gepstein A, Arbel G, Maizels L, Boulos M, Gepstein L (2013): Modeling of arrhythmogenic right ventricular cardiomyopathy with human induced pluripotent stem cells. Circulation: Cardiovascular Genetics 6: 557-568.

Chang CW, Lai YS, Pawlik KM, Liu K, Sun CW, Li C, Schoeb TR, Townes TM (2009): Polycistronic lentiviral vector for "hit and run" reprogramming of adult skin fibroblasts to induced pluripotent stem cells. Stem Cells 27(5): 1042-1049.

Charpentier F, Mérot J, Loussouarn G, Baró I (2010): Delayed rectifier K^+ currents and cardiac repolarization. Journal of Molecular and Cellular Cardiology 48(1): 37-44.

Cheng H, Lederer WJ, Cannell MB (1993): Calcium sparks: elementary events underlying excitation contraction coupling in heart muscle. Science 262: 740-744. Cheng H, Lederer WJ (2008): Calcium sparks. Physiological Reviews 88(4): 1491-1545.

Chew JL, Loh YH, Zhang W, Chen X, Tam WL, Yeap LS, Li P, Ang YS, Lim B, Robson P, Ng HH (2005): Reciprocal transcriptional regulation of Pou5f1 and Sox2 via the Oct4/Sox2 complex in embryonic stem cells. Molecular and Cellular Biology 25(14): 6031-6046.

Chiang CE, Roden DM (2000): The long QT syndromes: genetic basis and clinical implications. Journal of American College of Cardiology 36(1): 1-12.

Chin MH, Mason MJ, Xie W, Volinia S, Singer M, Peterson C, Ambartsumyan G, Aimiuwu O, Richter L, Zhang J, Khvorostov I, Ott V, Grunstein M, Lavon N, Benvenisty N, Croce CM, Clark AT, Baxter T, Pyle AD, Teitell MA, Pelegrini M, Plath K, Lowry WE (2009): Induced pluripotent stem cells and embryonic stem cells are distinguished by gene expression signatures. Cell Stem Cell 5(1): 111-123.

Chiu CP, Blau HM (1985): 5-Azacytidine permits gene activation in a previously noninducible cell type. Cell 40: 417-424.

Conrath CE, Opthof T (2006): Ventricular repolarization: an overview of (patho)physiology, sympathetic effects and genetic aspects. Progress in Biophysics and Molecular Biology 92(3): 269-307.

Crotti L, Celano G, Dagradi F, Schwartz PJ (2008): Congenital long QT syndrome. Orphanet Journal of Rare Diseases 3:18.

Davis RL, Weintraub H, Lassar AB (1987): Expression of a single transfected cDNA converts fibroblasts to myoblasts. Cell 51(6): 987-1000.

Davis RP, Casini S, van den Berg CW, Hoekstra M, Remme CA, Dambrot C, Salvatori D, Oostwaard DW, Wilde AA, Bezzina CR, Verkerk AO, Freund C, Mummery CL (2012): Cardiomyocytes derived from pluripotent stem cells recapitulate electrophysiological characteristics of an overlap syndrome of cardiac sodium channel disease. Circulation 125(25): 3079-3091.

De Bruin ML, Pettersson M, Meyboom RH, Hoes AW, Leufkens HG (2005): Anti-HERG activity and the risk of drug-induced arrhythmias and sudden death. European Heart Journal 26(6): 590-597.

De Ferrari GM, Nador F, Beria G, Sala S, Lotto A, Schwartz PJ (1994): Effect of calcium channel block on the wall motion abnormality of the idiopathic long QT syndrome. Circulation 89(5): 2126-2132.

Dennis A, Wang L, Wan X, Ficker E (2007): hERG channel trafficking: novel targets in drug-induced long QT syndrome. Biochemical Society Transactions 35(5): 1060-1063.

Di Diego JM, Sun ZQ, Antzelevitch C (1996): I_{to} and action potential notch are smaller in left vs. right canine ventricular epicardium. American Journal of Physiology 271: 548-561.

Di Pasquale E, Lodola F, Miragoli M, Denegri M, Avelino-Cruz JE, Buonocore M, Nakahama H, Portararo P, Bloise R, Napolitano C, Condorelli G, Priori SG (2013): CaMKII inhibition rectifies arrhythmic phenotype in a patient-specific model of catecholaminergic polymorphic ventricular tachycardia. Cell Death & Disease 4(10): e843.

Dogan A, Tunc E, Varol E, Ozaydin M, Ozturk M (2005): Comparison of the four formulas of adjusting QT interval for the heart rate in the middle-aged healthy Turkish men. Annals of Noninvasive Electrocardiology 10(2): 134-141.

Doss MX, Di Diego JM, Goodrow RJ, Wu Y, Cordeiro JM, Nesterenko VV, Barajas-Martínez H, Hu D, Urrutia J, Desai M, Treat JA, Sachinidis A, Antzelevitch C (2012): Maximum diastolic potential of human induced pluripotent stem cell-derived cardiomyocytes depends critically on I_{Kr}. PLoS One 7(7): 40288.

Dun W, Boyden PA (2008): The Purkinje cell; 2008 style. Journal of Molecular and Cellular Cardiology 45(5): 617-624.

Eden S, Hashimshony T, Keshet I, Cedar H, Thorne AW (1998): DNA methylation models histone acetylation. Nature 394: 842.

Edvardsson N, Hirsch I, Emanuelsson H, Pontén J, Olsson SB (1980): Sotalol-induced delayed ventricular repolarization in man. European Heart Journal 1(5): 335-343.

Egashira T, Yuasa S, Suzuki T, Aizawa Y, Yamakawa H, Matsuhashi T, Ohno Y, Tohyama S, Okata S, Seki T, Kuroda Y, Yae K, Hashimoto H, Tanaka T, Hattori F, Sato T, Miyoshi S, Takatsuki S, Murata M, Kurokawa J, Furukawa T, Makita N, Aiba T, Shimizu W, Horie M, Kamiya K, Kodama I, Ogawa S, Fukuda K (2012): Disease characterization using LQTS-specific induced pluripotent stem cells. Cardiovascular Research 95(4): 419-429.

Egashira T, Yuasa S, Fukuda K (2013): Novel insights into disease modeling using induced pluripotent stem cells. Biological & Pharmaceutical Bulletin 36(2): 182-188.

Evans MJ, Kaufman MH (1981): Establishment in culture of pluripotential cells from mouse embryos. Nature 292(5819): 154-156.

Fatima A, Xu G, Shao K, Papadopoulos S, Lehmann M, Arnáiz-Cot JJ, Rosa AO, Nguemo F, Matzkies M, Dittmann S, Stone SL, Linke M, Zechner U, Beyer V, Hennies HC, Rosenkranz S, Klauke B, Parwani AS, Haverkamp W, Pfitzer G, Farr M, Cleemann L, Morad M, Milting H, Hescheler J, Šaric T (2011): *In vitro* Modeling of Ryanodine Receptor 2 Dysfunction Using Human Induced Pluripotent Stem Cells. Cellular Physiology and Biochemistry 28(4): 579-592.

Fernandez PC, Frank SR, Wang L, Schroeder M, Liu S, Greene J, Cocito A, Amati B (2003): Genomic targets of the human c-Myc protein. Genes & Development 17(9): 1115-1129.

Ferrantini C, Crocini C, Coppini R, Vanzi F, Tesi C, Cerbai E, Poggesi C, Pavone FS, Sacconi L (2013): The transverse-axial tubular system of cardiomyocytes. Cellular and Molecular Life Sciences 70(24): 4695-4710.

Fodstad H, Swan H, Laitinen P, Piippo K, Paavonen K, Viitasalo M, Toivonen L, Kontula K (2004): Four potassium channel mutations account for 73% of the genetic spectrum underlying long-QT syndrome (LQTS) and provide evidence for a strong founder effect in Finland. Annals of Medicine 36 Suppl 1: 53-63.

Fodstad H, Bendahhou S, Rougier JS, Laitinen-Forsblom PJ, Barhanin J, Abriel H, Schild L, Kontula K, Swan H (2006): Molecular characterization of two founder mutations causing long QT syndrome and identification of compound heterozygous patients. Annals of Medicine 38(4): 294-304.

Friedrichs S, Malan D, Sasse P (2013): Modeling long QT syndromes using induced pluripotent stem cells: current progress and future challenges. Trends in Cardiovascular Medicine 23(4): 91-98.

Fu JD, Jiang P, Rushing S, Liu J, Chiamvimonvat N, Li RA (2010): Na^+/Ca^{2+} exchanger is a determinant of excitation-contraction coupling in human embryonic stem cell-derived ventricular cardiomyocytes. Stem Cells Development 19(6): 773-782.

Fusaki N, Ban H, Nishiyama A, Saeki K, Hasegawa M (2009): Efficient induction of transgene-free human pluripotent stem cells using a vector based on Sendai virus, an RNA virus that does not integrate into the host genome. Proceedings of the Japan Academy. Series B, Physical and Biological Sciences 85(8): 348-362.

Gaborit N, Le Bouter S, Szuts V, Varro A, Escande D, Nattel S, Demolombe S (2007): Regional and tissue specific transcript signatures of ion channel genes in the non-diseased human heart. Journal of Physiology 582(2): 675-693.

Gai H, Leung EL, Costantino PD, Aguila JR, Nguyen DM, Fink LM, Ward DC, Ma Y (2009): Generation and characterization of functional cardiomyocytes using induced pluripotent stem cells derived from human fibroblasts. Cell Biology International 33(11): 1184-1193.

Gallacher DJ, Van de Water A, van der Linde H, Hermans AN, Lu HR, Towart R, Volders PG (2007): In vivo mechanisms precipitating torsades de pointes in a canine model of drug-induced long-QT1 syndrome. Cardiovascular Research 76(2): 247-256.

Gaspar-Maia A, Alajem A, Polesso F, Sridharan R, Mason MJ, Heidersbach A, Ramalho-Santos J, McManus MT, Plath K, Meshorer E, Ramalho-Santos M (2009): Chd1 regulates open chromatin and pluripotency of embryonic stem cells. Nature 460(7257): 863-868.

Gonzalez F, Barragan Monasterio M, Tiscornia G, Montserrat Pulido N, Vassena R, Batlle Morera L, Rodriguez Piza I, Izpisua Belmonte JC (2009): Generation of mouse-induced pluripotent stem cells by transient expression of a single nonviral polycistronic vector. Proceedings of the National Academy of Sciences of the United States of America 106(22): 8918-8922.

Gouas L, Bellocq C, Berthet M, Potet F, Demolombe S, Forhan A, Lescasse R, Simon F, Balkau B, Denjoy I, Hainque B, Baró I, Guicheney P (2004): New KCNQ1 mutations leading to haploinsufficiency in a general population; Defective trafficking of a KvLQT1 mutant. Cardiovascular Research 63(1): 60-68.

Graichen R, Xu X, Braam SR, Balakrishnan T, Norfiza S, Sieh S, Soo SY, Tham SC, Mummery C, Colman A, Zweigerdt R, Davidson BP (2008): Enhanced cardiomyogenesis of human embryonic stem cells by a small molecular inhibitor of p38 MAPK. Differentiation 76(4): 357-370.

Grynkiewicz G, Poenie M, Tsien RY (1985): A new generation of Ca^{2+} indicators with greatly improved fluorescence properties. Journal of Biological Chemistry 260(6): 3440-3450.

Gui L, Merzkirch W (1996): A method of tracking ensembles of particle images. Experiments in Fluids 21: 465-468.

Gurdon JB (1962): Adult frogs derived from the nuclei of single somatic cells. Developmental Biology 4: 256-273.

Hamill OP, Marty A, Neher E, Sakmann B, Sigworth FJ (1981): Improved patch-clamp techniques for high-resolution current recording from cells and cell-free membrane patches. Pflügers Archiv 391(2): 85-100.

Hattori F, Chen H, Yamashita H, Tohyama S, Satoh YS, Yuasa S, Li W, Yamakawa H, Tanaka T, Onitsuka T, Shimoji K, Ohno Y, Egashira T, Kaneda R, Murata M, Hidaka K, Morisaki T, Sasaki E, Suzuki T, Sano M, Makino S, Oikawa S, Fukuda K (2010): Nongenetic method for purifying stem cell-derived cardiomyocytes. Nature Methods 7(1): 61-66.

Haugaa KH, Amlie JP, Berge KE, Leren TP, Smiseth OA, Edvardsen T (2010): Transmural differences in myocardial contraction in long-QT syndrome: mechanical consequences of ion channel dysfunction. Circulation 122(14): 1355-1363.

Hay DC, Sutherland L, Clark J, Burdon T (2004): Oct-4 knockdown induces similar patterns of endoderm and trophoblast differentiation markers in human and mouse embryonic stem cells. Stem Cells 22(2): 225-235.

Hayakawa T, Kunihiro T, Ando T, Kobayashi S, Matsui E, Yada H, Kanda Y, Kurokawa J, Furukawa T (2014): Image-based evaluation of contraction–relaxation kinetics of human-induced pluripotent stem cell-derived cardiomyocytes: Correlation and complementarity with extracellular electrophysiology. Journal of Molecular and Cellular Cardiology (in press).

He JQ, Ma Y, Lee Y, Thomson JA, Kamp TJ (2003): Human embryonic stem cells develop into multiple types of cardiac myocytes: action potential characterization. Circulation Research 93(1): 32-39.

Hedley PL, Jørgensen P, Schlamowitz S, Wangari R, Moolman-Smook J, Brink PA, Kanters JK, orfield VA, Christiansen M (2009): The genetic basis of long QT and short QT syndromes: a mutation update. Human Mutation 30(11): 1486-1511.

Heikkilä J, Huikuri H, Luomanmäki K, Nieminen MS, Peuhkurinen K: Kardiologia. Helsinki: Kustannus Oy Duodecim, 2000, pp. 31-37.

Hescheler J, Halbach M, Egert U, Lu ZJ, Bohlen H, Fleischmann BK, Reppel M (2004): Determination of electrical properties of ES cell-derived cardiomyocytes using MEAs. Journal of Electrocardiology 37 Suppl: 110-116.

Ho JCY, Zhou T, Lai W-H, Huang Y, Chan Y-C, Li X, Wong NLY, Li Y, Au K-W, Guo D, Xu J, Siu C W, Pei D, Tse H-F, Esteban MA (2011): Generation of induced pluripotent stem cell lines from 3 distinct laminopathies bearing heterogeneous mutations in lamin A/C. Aging (Albany NY) 3(4): 380-390.

Hockemeyer D, Soldner F, Cook EG, Gao Q, Mitalipova M, Jaenisch R (2008): A drug-inducible system for direct reprogramming of human somatic cells to pluripotency. Cell Stem Cell 3(3): 346-353.

Hoffman LM, Carpenter MK (2005): Characterization and culture of human embryonic stem cells. Nature Biotechnology 23(6): 699-708.

Hotta & Ellis (2008): Retroviral vector silencing during iPS cell induction: An epigenetic beacon that signals distinct pluripotent states. Journal of Cellular Biochemistry 105: 940-948.

Hotta A, Cheung AY, Farra N, Vijayaragavan K, Séguin CA, Draper JS, Pasceri P, Maksakova IA, Mager DL, Rossant J, Bhatia M, Ellis J (2009): Isolation of human iPS cells using EOS lentiviral vectors to select for pluripotency. Nature Methods 6(5): 370-376.

Hou P, Li Y, Zhang X, Liu C, Guan J, Li H, Zhao T, Ye J, Yang W, Liu K, Ge J, Xu J, Zhang Q, Zhao Y, Deng H (2013): Pluripotent Stem Cells Induced from Mouse Somatic Cells by Small-Molecule Compounds. Science 341(6146): 651-654.

Huang HP, Chen PH, Hwu WL, Chuang CY, Chien YH, Stone L, Chien CL, Li LT, Chiang SC, Chen HF, Ho HN, Chen CH, Kuo HC (2011): Human Pompe disease-induced pluripotent stem cells for pathogenesis modeling, drug testing and disease marker identification. Human Molecular Genetics 15;20(24): 4851-4864.

Huangfu D, Osafune K, Maehr R, Guo W, Eijkelenboom A, Chen S, Muhlestein W, Melton DA (2008): Induction of pluripotent stem cells from primary human fibroblasts with only Oct4 and Sox2. Nature Biotechnology 26: 1269-1275.

ICH (2005). S7B: The nonclinical evaluation of the potential for delayed ventricular repolarization (qt interval prolongation) by human pharmaceuticals. In: International Conference on Harmonisation editor.

Indik JH, Pearson EC, Fried K, Woosley RL (2006): Bazett and Fridericia QT correction formulas interfere with measurement of drug-induced changes in QT interval. Heart Rhythm 3(9): 1003-1007.

Itskovitz-Eldor J, Schuldiner M, Karsenti D, Eden A, Yanuka O, Amit M, Soreq H, Benvenisty N (2000): Differentiation of human embryonic stem cells into embryoid bodies compromising the three embryonic germ layers. Molecular Medicine 6(2): 88-95.

Itzhaki I, Maizels L, Huber I, Zwi-Dantsis L, Caspi O, Winterstern A, Feldman O, Gepstein A, Arbel G, Hammerman H, Boulos M, Gepstein L (2011): Modelling the long QT syndrome with induced pluripotent stem cells. Nature 471(7337): 225-229.

Itzhaki I, Maizels L, Huber I, Gepstein A, Arbel G, Caspi O, Miller L, Belhassen B, Nof E, Glikson M, Gepstein L (2012): Modeling of catecholaminergic polymorphic ventricular tachycardia with patient specific human-induced pluripotent stem cells. Journal of the American College of Cardiology 11;60(11):990-1000.

Jayawardena TM, Egemnazarov B, Finch EA, Zhang L, Payne JA, Pandya K, Zhang Z, Rosenberg P, Mirotsou M, Dzau VJ (2012): MicroRNA-mediated in vitro and in vivo direct reprogramming of cardiac fibroblasts to cardiomyocytes. Circulation Research 110(11): 1465-1473.

Jervell A, Lange-Nielsen F (1957): Congenital deaf-mutism, functional heart disease with prolongation of the Q-T interval and sudden death. American Heart Journal 54(1): 59-68.

Jung CB, Moretti A, Mederos y Schnitzler M, Iop L, Storch U, Bellin M, Dorn T, Ruppenthal S, Pfeiffer S, Goedel A, Dirschinger RJ, Seyfarth M, Lam JT, Sinnecker D, Gudermann T, Lipp P, Laugwitz KL (2012): Dantrolene rescues arrhythmogenic RYR2 defect in a patient-specific stem cell model of catecholaminergic polymorphic ventricular tachycardia. EMBO Molecular Medicine 4(3): 180-191.

Kaji K, Norrby K, Paca A, Mileikovsky M, Mohseni P, Woltjen K (2009): Virus-free induction of pluripotency and subsequent excision of reprogramming factors. Nature 458(7239): 771-775.

Kassem M (2004): Mesenchymal stem cells: biological characteristics and potential clinical applications. Cloning Stem Cells 6(4): 369-374.

Kaye AD, Volpi-Abadie J, Bensler JM, Kaye AM, Diaz JH (2013): QT interval abnormalities: risk factors and perioperative management in long QT syndromes and Torsades de Pointes. Journal of anesthesia 27/4: 575-587.

Kehat I, Kenyagin-Karsenti D, Snir M, Segev H, Amit M, Gepstein A, Livne E, Binah O, Itskovitz Eldor J, Gepstein L (2001): Human embryonic stem cells can differentiate into myocytes with structural and functional properties of cardiomyocytes. Journal of Clinical Investigation 108(3): 407-414.

Kehat I, Gepstein A, Spira A, Itskovitz-Eldor J, Gepstein L (2002): High-resolution electrophysiological assessment of human embryonic stem cell-derived cardiomyocytes: a novel in vitro model for the study of conduction. Circulation Research 91(8): 659-661.

Kim JB, Greber B, Araúzo-Bravo M, Meyer J, Park K, Zaehres H (2009): Direct reprogramming of human neural stem cells by OCT4. Nature 461: 649-653.

Kim K, Doi A, Wen B, Ng K, Zhao R, Cahan P, Kim J, Aryee MJ, Ji H, Ehrlich LI, Yabuuchi A, Takeuchi A, Cunniff KC, Hongguang H, McKinney-Freeman S, Naveiras O, Yoon TJ, Irizarry RA, Jung N, Seita J, Hanna J, Murakami P, Jaenisch R, Weissleder R, Orkin SH, Weissman IL, Feinberg AP, Daley GQ (2010): Epigenetic memory in induced pluripotent stem cells. Nature 467: 285-290.

Kim DH, Jeon Y, Anguera MC, Lee JT (2011): X-chromosome epigenetic reprogramming in pluripotent stem cells via noncoding genes. Seminars in Cell and Developmental Biology 22(4): 336-342.

Kim C, Wong J, Wen J, Wang S, Wang C, Spiering S, Kan NG, Forcales S, Puri PL, Leone TC, Marine JE, Calkins H, Kelly DP, Judge DP, Chen HS (2013): Studying arrhythmogenic right ventricular dysplasia with patient-specific iPSCs. Nature 7;494(7435): 105-110.

Kispert A, Herrmann BG (1994): Immunohistochemical analysis of the Brachyury protein in wild-type and mutant mouse embryos. Developmental Biology 161(1): 179-193.

Kornreich BG (2007): The patch clamp technique: principles and technical considerations. Journal of Veterinary Cardiology 9(1): 25-37.

Kujala K, Paavola J, Lahti A, Larsson K, Pekkanen-Mattila M, Viitasalo M, Lahtinen AM, Toivonen L, Kontula K, Swan H, Laine M, Silvennoinen O, Aalto-Setälä K (2012): Cell model of catecholaminergic polymorphic ventricular tachycardia reveals early and delayed afterdepolarizations. PLoS One 7(9): 44660.

Kurosawa H (2007): Methods for inducing embryoid body formation: in vitro differentiation system of embryonic stem cells. Journal of Bioscience and Bioengineering 103(5): 389-398.

Lacerda AE, Kuryshev YA, Chen Y, Renganathan M, Eng H, Danthi SJ, Kramer JW, Yang T, Brown AM (2007): Alfuzosin delays cardiac repolarization by a novel mechanism. Journal of Pharmacology and Experimental Therapeutics 324(2): 427-433.

Laflamme MA, Chen KY, Naumova AV, Muskheli V, Fugate JA, Dupras SK, Reinecke H, Xu C, Hassanipour M, Police S, O'Sullivan C, Collins L, Chen Y, Minami E, Gill EA, Ueno S, Yuan C, Gold J, Murry CE (2007): Cardiomyocytes derived from human embryonic stem cells in pro-survival factors enhance function of infarcted rat hearts. Nature Biotechnology 25(9): 1015-1024.

Lahti AL, Kujala VJ, Chapman H, Koivisto AP, Pekkanen-Mattila M, Kerkelä E, Hyttinen J, Kontula K, Swan H, Conklin BR, Yamanaka S, Silvennoinen O, Aalto-Setälä K (2012): Model for long QT syndrome type 2 using human iPS cells demonstrates arrhythmogenic characteristics in cell culture. Disease Models and Mechanisms 5(2): 220-230.

Lai MI, Wendy-Yeo WY, Ramasamy R, Nordin N, Rosli R, Veerakumarasivam A, Abdullah S (2011): Advancements in reprogramming strategies for the generation of induced pluripotent stem cells. Journal of Assisted Reproduction and Genetics 28(4): 291-301.

Lan F, Lee AS, Liang P, Sanchez-Freire V, Nguyen PK, Wang L, Han L, Yen M, Wang Y, Sun N, Abilez OJ, Hu S, Ebert AD, Navarrete EG, Simmons CS, Wheeler M, Pruitt B, Lewis R, Yamaguchi Y, Ashley EA, Bers DM, Robbins RC, Longaker MT, Wu JC (2013): Abnormal Calcium Handling Properties Underlie Familial Hypertrophic Cardiomyopathy Pathology in Patient-Specific Induced Pluripotent Stem Cells. Cell Stem Cell 12(1): 101-113.

Lankipalli RS, Zhu T, Guo D, Yan GX (2005): Mechanisms underlying arrhythmogenesis in long QT syndrome. Journal of Electrocardiology 38(4): 69-73.

Lee YK, Ng KM, Lai WH, Chan YC, Lau YM, Lian Q, Tse HF, Siu CW (2011): Calcium Homeostasis in Human Induced Pluripotent Stem Cell-Derived Cardiomyocytes. Stem Cell Reviews 7: 976-986.

Lehtonen A, Fodstad H, Laitinen-Forsblom P, Toivonen L, Kontula K, Swan H (2007): Further evidence of inherited long QT syndrome gene mutations in antiarrhythmic drug-associated torsades de pointes. Heart Rhythm 4(5): 603-607.

Li C, Zhou J, Shi G, Ma Y, Yang Y, Gu J, Yu H, Jin S, Wei Z, Chen F, Jin Y (2009a): Pluripotency can be rapidly and efficiently induced in human amniotic fluid-derived cells. Human Molecular Genetics 18(22): 4340-4349.

Li W, Zhou HY, Abujarour R, Zhu S, Joo JY, Lin T, Hao E, Schöler HR, Hayek A, Ding S (2009b): Generation of Human Induced Pluripotent Stem Cells in the Absence of Exogenous *Sox2*. Stem Cells 27(12): 2992-3000.

Li Y, Zhang Q, Yin X, Yang W, Du Y, Hou P, Ge J, Liu C, Zhang W, Zhang X, Wu Y, Li H, Liu K, Wu C, Song Z, Zhao Y, Shi Y, Deng H (2011): Generation of iPSCs from mouse fibroblasts with a single gene, *Oct4*, and small molecules. Cell Research 21: 196-204.

Lian X, Hsiao C, Wilson G, Zhu K, Hazeltine LB, Azarin SM, Raval KK, Zhang J, Kamp TJ, Palecek SP (2012): Robust cardiomyocyte differentiation from human pluripotent stem cells via temporal modulation of canonical Wnt signaling. Proceedings of the National Academy of Sciences of the United States of America 109(27): 1848-1857.

Liang P, Lan F, Lee AS, Gong T, Sanchez-Freire V, Wang Y, Diecke S, Sallam K, Knowles JW, Nguyen PK, Wang PJ, Bers DM, Robbins RC, Wu JC (2013): Drug Screening Using a Library of Human Induced Pluripotent Stem Cell-Derived Cardiomyocytes Reveals Disease Specific Patterns of Cardiotoxicity. Circulation (published online before print March 21 2013).

Liao J, Wu Z, Wang Y, Cheng L, Cui C, Gao Y (2008): Enhanced efficiency of generating induced pluripotent stem (iPS) cells from human somatic cells by a combination of six transcription factors. Cell Research 18: 600-603.

Lieu DK, Liu J, Siu CW, McNerney GP, Tse HF, Abu-Khalil A, Huser T, Li RA (2009): Absence of transverse tubules contributes to non-uniform Ca^{2+} wavefronts in mouse and human embryonic stem cell-derived cardiomyocytes. Stem Cells Development 18(10): 1493-1500.

van der Linde HJ, Van Deuren B, Somers Y, Loenders B, Towart R, Gallacher DJ (2010): The Electro Mechanical window: a risk marker for Torsade de Pointes in a canine model of drug induced arrhythmias. British Journal of Pharmacology 161(7): 1444-1454.

Liu J, Fu JD, Siu CW, Li RA (2007): Functional sarcoplasmic reticulum for calcium handling of human embryonic stem cell-derived cardiomyocytes: insights for driven maturation. Stem Cells 25(12): 3038-3044.

Liu J, Lieu DK, Siu CW, Fu JD, Tse HF, Li RA (2009): Facilitated maturation of Ca^{2+} handling properties of human embryonic stem cell-derived cardiomyocytes by calsequestrin expression. Cell Physiology: American Journal of Physiology 297(1): 152-159.

Loh Y-H, Hartung O, Li H, Guo C, Sahalie JM, Manos PD, Urbach A, Heffner GC, Grskovic M, Vigneault F, Lensch MW, Park I-H, Agarwal S, Church GM, Collins JJ, Irion S, Daley GQ (2010): Reprogramming of T Cells from Human Peripheral Blood. Cell Stem Cell 7(1): 15-19.

Luna JI, Ciriza J, Garcia-Ojeda ME, Kong M, Herren A, Lieu DK, Li RA, Fowlkes CC, Khine M, McCloskey KE (2011): Multiscale biomimetic topography for the alignment of neonatal and embryonic stem cell-derived heart cells. Tissue Engineering Part C Methods 17(5): 579-588.

Ma D, Wei H, Zhao Y, Lu J, Li G, Sahib NB, Tan TH, Wong KY, Shim W, Wong P, Cook SA, Liew R (2013): Modeling type 3 long QT syndrome with cardiomyocytes derived from patient-specific induced pluripotent stem cells. International Journal of Cardiology 168(6): 5277-5286.

Maherali N, Sridharan R, Xie W, Utikal J, Eminli S, Arnold K, Stadtfeld M, Yachechko R, Tchieu J, Jaenisch R, Plath K, Hochedlinger K (2007): Directly reprogrammed fibroblasts show global epigenetic remodeling and widespread tissue contribution. Cell Stem Cell 1(1): 55-70.

Maherali N, Hochedlinger K (2008): Guidelines and techniques for the generation of induced pluripotent stem cells. Cell Stem Cell 3: 595-605.

Maizels L, Gepstein L (2012): Gap junctions, stem cells, and cell therapy: rhythmic/arrhythmic implications. Heart Rhythm 9(9): 1512-1516.

Malan D, Friedrichs S, Fleischmann BK, Sasse P (2011): Cardiomyocytes obtained from induced pluripotent stem cells with long-QT syndrome 3 recapitulate typical disease-specific features in vitro. Circulation Research 109(8): 841-847.

Marchetto MC, Yeo GW, Kainohana O, Marsala M, Gage FH, Muotri AR (2009): Transcriptional signature and memory retention of human-induced pluripotent stem cells. PLoS One 4(9): 7076.

Marjamaa A, Salomaa V, Newton-Cheh C, Porthan K, Reunanen A, Karanko H, Jula A, Lahermo P, Väänänen H, Toivonen L, Swan H, Viitasalo M, Nieminen MS, Peltonen L, Oikarinen L, Palotie A, Kontula K (2009): High prevalence of four long QT syndrome founder mutations in the Finnish population. Annals of Medicine 41(3): 234-240.

Matsa E, Rajamohan D, Dick E, Young L, Mellor I, Staniforth A, Denning C (2011): Drug evaluation in cardiomyocytes derived from human induced pluripotent stem cells carrying a long QT syndrome type 2 mutation. European Heart Journal 32(8): 952-962.

Matsa E, Dixon JE, Medway C, Georgiou O, Patel MJ, Morgan K, Kemp PJ, Staniforth A, Mellor I, Denning C (2014): Allele-specific RNA interference rescues the long-QT syndrome phenotype in human induced pluripotency stem cell cardiomyocytes. European Heart Journal 35(16): 1078-1087.

Medvedev SP, Pokushalov EA, Zakian SM (2012): Epigenetics of pluripotent cells. Acta Naturae 4(4): 28-46.

Mehta A, Chung YY, Ng A, Iskandar F, Atan S, Wei H, Dusting G, Sun W, Wong P, Shim W (2011): Pharmacological response of human cardiomyocytes derived from virus-free induced pluripotent stem cells. Cardiovascular Research 91(4): 577-586.

Mikkelsen TS, Hanna J, Zhang X, Ku M, Wernig M, Schorderet P, Bernstein BE, Jaenisch R, Lander ES, Meissner A (2008): Dissecting direct reprogramming through integrative genomic analysis. Nature 454(7200): 49-55.

Minami I, Yamada K, Otsuji TG, Yamamoto T, Shen Y, Otsuka S, Kadota S, Morone N, Barve M, Asai Y, Tenkova-Heuser T, Heuser JE, Uesugi M, Aiba K, Nakatsuji N (2012): A small molecule that promotes cardiac differentiation of human pluripotent stem cells under defined, cytokine- and xeno-free conditions. Cell Reports 2(5): 1448-1460.

Mitcheson JS, Hancox JC, Levi AJ (1996): Action potentials, ion channel currents and transverse tubule density in adult rabbit ventricular myocytes maintained for 6 days in cell culture. Pflugers Archiv 431: 814-827.

Mitcheson JS, Chen J, Lin M, Culberson C, Sanguinetti MC (2000): A structural basis for drug induced long QT syndrome. Proceedings of the National Academy of Sciences of the United States of America 97(22): 12329-12333.

Miyoshi N, Ishii H, Nagai K, Hoshino H, Mimori K, Tanaka F, Nagano H, Sekimoto M, Doki Y, Mori M (2009): Defined factors induce reprogramming of gastrointestinal cancer cells. Proceedings of the National Academy of Sciences of the United States of America 107(1): 40-45.

Miyoshi N, Ishii H, Nagano H, Haraguchi N, Dewi DL, Kano Y, Nishikawa S, Tanemura M, Mimori K, Tanaka F, Saito T, Nishimura J, Takemasa I, Mizushima T, Ikeda M, Yamamoto H, Sekimoto M, Doki Y, Mori M (2011): Reprogramming of mouse and human cells to pluripotency using mature microRNAs. Cell Stem Cell 8(6): 633-638.

Mohr JC, Zhang J, Azarin SM, Soerens AG, de Pablo JJ, Thomson JA, Lyons GE, Palecek SP, Kamp TJ (2010): The microwell control of embryoid body size in order to regulate cardiac differentiation of human embryonic stem cells. Biomaterials 31(7): 1885-1893.

Molleman A: Patch Clamping. An Introductory Guide to Patch Clamp Electrophysiology. Chichester: John Wiley & Sons Ltd, 2002, pp. 5-41.

Moore JC, van Laake LW, Braam SR, Xue T, Tsang SY, Ward D, Passier R, Tertoolen LL, Li RA, Mummery CL (2005): Human embryonic stem cells: genetic manipulation on the way to cardiac cell therapies. Reproductive Toxicology 20(3): 377-391.

Moore JC, Fu J, Chan YC, Lin D, Tran H, Tse HF, Li RA (2008): Distinct cardiogenic preferences of two human embryonic stem cell (hESC) lines are imprinted in their proteomes in the pluripotent state. Biochemical and Biophysical Research Communications 372: 553-558.

Morais Cabral JH, Lee A, Cohen SL, Chait BT, Li M, Mackinnon R (1998): Crystal structure and functional analysis of the HERG potassium channel N terminus: a eukaryotic PAS domain. Cell 95(5): 649-655.

Moreadith RW, Graves KH (1992): Derivation of pluripotential embryonic stem cells from the rabbit. Transactions of the Association of American Physicians 105: 197-203.

Moretti A, Bellin M, Welling A, Jung CB, Lam JT, Bott-Flügel L, Dorn T, Goedel A, Höhnke C, Hofmann F, Seyfarth M, Sinnecker D, Schömig A, Laugwitz KL (2010): Patient-specific induced pluripotent stem-cell models for long-QT syndrome. New England Journal of Medicine 363(15): 1397-1409.

Moss AJ, Kass RS (2005): Long QT syndrome: from channels to cardiac arrhythmias. Journal of Clinical Investigation 115(8): 2018-2024.

Mummery CL, van Achterberg TA, van den Eijnden-van Raaij AJ, van Haaster L, Willemse A, de Laat SW, Piersma AH (1991): Visceral-endoderm-like cell lines induce differentiation of murine P19 embryonal carcinoma cells. Differentiation 46(1): 51-60.

Mummery C, Ward-van Oostwaard D, Doevendans P, Spijker R, van den Brink S, Hassink R, van der Heyden M, Opthof T, Pera M, de la Riviere AB, Passier R, Tertoolen L (2003): Differentiation of human embryonic stem cells to cardiomyocytes: role of coculture with visceral endoderm-like cells. Circulation 107(21): 2733-2740.

Mummery C (2010): Sorting cardiomyocytes: a simple solution after all? Nature Methods 7(1): 40-42.

Nador F, Beria G, De Ferrari GM, Stramba-Badiale M, Locati EH, Lotto A, Schwartz PJ (1991): Unsuspected echocardiographic abnormality in the long QT syndrome. Diagnostic, prognostic, and pathogenetic implications. Circulation 84(4): 1530-1542.

Nakagawa M, KoyanagiM, Tanabe K, Takahashi K, Ichisaka T, Aoi T (2008): Generation of induced pluripotent stem cells without Myc from mouse and human fibroblasts. Nature Biotechnology 26: 101-106.

Nakajima T, Furukawa T, Tanaka T, Katayama Y, Nagai R, Nakamura Y, Hiraoka M (1998): Novel mechanism of HERG current suppression in LQT2: shift in voltage dependence of HERG inactivation. Circulation Research 83(4): 415-422.

Nam YJ, Song K, Luo X, Daniel E, Lambeth K, West K, Hill JA, DiMaio JM, Baker LA, Bassel-Duby R, Olson EN (2013): Reprogramming of human fibroblasts toward a cardiac fate. Proceedings of the National Academy of Sciences of the United States of America 110(14): 5588-5593.

Ng ES, Davis RP, Azzola L, Stanley EG, Elefanty AG (2005): Forced aggregation of defined numbers of human embryonic stem cells into embryoid bodies fosters robust, reproducible hematopoietic differentiation. Blood 106(5): 1601-1603.

Nichols J, Zevnik B, Anastassiadis K, Niwa H, Klewe-Nebenius D, Chambers I, Schöler H, Smith A (1998): Formation of pluripotent stem cells in the mammalian embryo depends on the POU transcription factor Oct4. Cell 95(3): 379-391.

Norio R, Nevanlinna HR, Perheentupa J (1973): Hereditary diseases in Finland; rare flora in rare soul. Annals of Clinical Research 5(3): 109-141.

Norio R (2003a): Finnish Disease Heritage I: characteristics, causes, background. Human Genetics 112(56): 441-456.

Norio R (2003b): Finnish Disease Heritage II: population prehistory and genetic roots of Finns. Human Genetics 112(5-6): 457-469.

Norio R (2003c): The Finnish Disease Heritage III: the individual diseases. Human Genetics 112(5-6): 470-526.

Notarianni E, Galli C, Laurie S, Moor RM, Evans MJ (1991): Derivation of pluripotent, embryonic cell lines from the pig and sheep. Journal of reproduction and fertility 43: 255-260.

Novak A, Barad L, Zeevi-Levin N, Shick R, Shtrichman R, Lorber A, Itskovitz-Eldor J, Binah O (2012): Cardiomyocytes generated from CPVTD307H patients are arrhythmogenic in response to β adrenergic stimulation. Cellular and Molecular Medicine 16(3): 468-482.

Okita K, Ichisaka T, Yamanaka S (2007): Generation of germline-competent induced pluripotent stem cells. Nature 448(7151): 313-317.

Okita K, Nakagawa M, Hyenjong H, Ichisaka T, Yamanaka S (2008): Generation of mouse induced pluripotent stem cells without viral vectors. Science 322(5903): 949-953.

Osafune K, Caron L, Borowiak M, Martinez RJ, Fitz-Gerald CS, Sato Y, Cowan CA, Chien KR, Melton DA (2008): Marked differences in differentiation propensity among human embryonic stem cell lines. Nature Biotechnology 26(3): 313-315.

Paavonen KJ, Chapman H, Laitinen PJ, Fodstad H, Piippo K, Swan H, Toivonen L, Viitasalo M, Kontula K, Pasternack M (2003): Functional characterization of the common amino acid 897 polymorphism of the cardiac potassium channel KCNH2 (HERG). Cardiovascular Research 59(3): 603-611.

Paredes RM, Etzler JC, Watts LT, Zheng W, Lechleiter JD (2008): Chemical calcium indicators. Methods 46(3): 143-151.

Park KH, Piron J, Dahimene S, Mérot J, Baró I, Escande D, Loussouarn G (2005): Impaired KCNQ1 KCNE1 and phosphatidylinositol-4,5-bisphosphate interaction underlies the long QT syndrome. Circulation Research 96(7): 730-739.

Passier R, Oostwaard DW, Snapper J, Kloots J, Hassink RJ, Kuijk E, Roelen B, de la Riviere AB, Mummery C (2005): Increased cardiomyocyte differentiation from human embryonic stem cells in serum-free cultures. Stem Cells 23(6): 772-780.

Pekkanen-Mattila M, Kerkelä E, Tanskanen JM, Pietilä M, Pelto-Huikko M, Hyttinen J, Skottman H, Suuronen R, Aalto-Setälä K (2009): Substantial variation in the cardiac differentiation of human embryonic stem cell lines derived and propagated under the same conditions--a comparison of multiple cell lines. Annals of Medicine 41(5): 360-370.

Piippo K, Swan H, Pasternack M, Chapman H, Paavonen K, Viitasalo M, Toivonen L, Kontula K (2001): A founder mutation of the potassium channel KCNQ1 in long QT syndrome: implications for estimation of disease prevalence and molecular diagnostics. Journal of American College of Cardiology 37(2): 562-568.

Pollard CE, Abi Gerges N, Bridgland-Taylor MH, Easter A, Hammond TG, Valentin JP (2010): An introduction to QT interval prolongation and non-clinical approaches to assessing and reducing risk. British Journal of Pharmacology 159(1): 12-21.

Polo JM, Liu S, Figueroa ME, Kulalert W, Eminli S, Tan KY, Apostolou E, Stadtfeld M, Li Y, Shioda T, Natesan S, Wagers AJ, Melnick A, Evans T, Hochedlinger K (2010): Cell type of origin influences the molecular and functional properties of mouse induced pluripotent stem cells. Nature Biotechnology 28(8): 848-855.

Poon E, Kong CW, Li RA (2011): Human pluripotent stem cell-based approaches for myocardial repair: from the electrophysiological perspective. Molecular Pharmacology 8(5): 1495-1504.

Qiu C, Ma Y, Wang J, Peng S, Huang Y (2010): Lin28-mediated post-transcriptional regulation of Oct4 expression in human embryonic stem cells. Nucleic Acids Research 38(4): 1240-1248.

Reppel M, Pillekamp F, Lu ZJ, Halbach M, Brockmeier K, Fleischmann BK, Hescheler J (2004): Microelectrode arrays: a new tool to measure embryonic heart activity. Journal of Electrocardiology 37 Suppl: 104-109.

Rizzi R, Di Pasquale E, Portararo P, Papait R, Cattaneo P, Latronico MV, Altomare C, Sala L, Zaza A, Hirsch E, Naldini L, Condorelli G, Bearzi C (2012): Post-natal cardiomyocytes can generate iPS cells with an enhanced capacity toward cardiomyogenic re-differentation. Cell Death & Differentiation 19(7): 1162-1174.

Rodda DJ, Chew JL, Lim LH, Loh YH, Wang B, Ng HH, Robson P (2005): Transcriptional regulation of nanog by OCT4 and SOX2. Journal of Biological Chemistry 280(26): 24731-24737.

Roden DM, Lazzara R, Rosen M, Schwartz PJ, Towbin J, Vincent GM (1996): Multiple mechanisms in the long-QT syndrome. Current knowledge, gaps, and future directions. The SADS Foundation Task Force on LQTS. Circulation 94(8): 1996-2012.

Roden DM (2004): Drug-induced prolongation of the QT interval. New England Journal of Medicine 350(10): 1013-1022.

Roden DM (2005): Proarrhythmia as a pharmacogenomic entity: A critical review and formulation of a unifying hypothesis. Cardiovascular Research 67: 419-425.

Roden DM, Viswanathan PC (2005): Genetics of acquired long QT syndrome. Journal of Clinical Investigation 115: 2025-2032.

Roden DM (2006): Long QT syndrome: reduced repolarization reserve and the genetic link. Journal of Internal Medicine 259(1): 59-69.

Romano C (1965): Congenital cardiac arrhythmia. Lancet 1(7386): 658-659.

Rowland BD, Bernards R, Peeper DS (2005): The KLF4 tumour suppressor is a transcriptional repressor of p53 that acts as a context-dependent oncogene. Nature Cell Biology 7(11): 1074-1082.

Ruiz S, Brennand K, Panopoulos AD, Herrerías A, Gage FH, Izpisua-Belmonte JC (2010): High efficient generation of induced pluripotent stem cells from human astrocytes. PLoS One 5(12): 15526.

Rust W, Balakrishnan T, Zweigerdt R (2009): Cardiomyocyte enrichment from human embryonic stem cell cultures by selection of ALCAM surface expression. Regenerative Medicine 4(2): 225-237.

Sakmann B, Neher E (1984): Patch clamp techniques for studying ionic channels in excitable membranes. Annual Review of Physiology 46: 455-472.

Sale H, Wang J, O'Hara TJ, Tester DJ, Phartiyal P, He JQ, Rudy Y, Ackerman MJ, Robertson GA (2008): Physiological properties of hERG 1a/1b heteromeric currents and a hERG 1b-specific mutation associated with Long-QT syndrome. Circulation Research 103(7): 81-95.

Sanguinetti MC, Jiang C, Curran ME, Keating MT (1995): A mechanistic link between an inherited and an acquired cardiac arrhythmia: HERG encodes the I_{Kr} potassium channel. Cell 81(2): 299-307.

Sanguinetti MC, Curran ME, Zou A, Shen J, Spector PS, Atkinson DL, Keating MT (1996): Coassembly of KvLQT1 and minK (IsK) proteins to form cardiac I_{Ks} potassium channel. Nature 384(6604): 80-83.

Sarić T, Halbach M, Khalil M, Er F (2014): Induced pluripotent stem cells as cardiac arrhythmic in vitro models and the impact for drug discovery. Expert Opinion on Drug Discovery 9(1): 55-76.

Sartiani L, Bettiol E, Stillitano F, Mugelli A, Cerbai E, Jaconi ME (2007): Developmental changes in cardiomyocytes differentiated from human embryonic stem cells: a molecular and electrophysiological approach. Stem Cells 25(5): 1136-1144.

Sauer H, Theben T, Hescheler J, Lindner M, Brandt MC, Wartenberg M (2001): Characteristics of calcium sparks in cardiomyocytes derived from embryonic stem cells. Heart and Circulatory Physiology: American Journal of Physiology 281: 411-421.

Savla JJ, Nelson BC, Perry CN, Adler ED (2014): Induced Pluripotent Stem Cells for the Study of Cardiovascular Disease. Journal of the American College of Cardiology 64(5): 512-519.

Schreck RR, Distèche C (2001): Karyotyping. Current Protocols in Human Genetics Appendix 4A.

Schwartz PJ, Priori SG, Spazzolini C, Moss AJ, Vincent GM, Napolitano C, Denjoy I, Guicheney P, Breithardt G, Keating MT, Towbin JA, Beggs AH, Brink P, Wilde AA, Toivonen L, Zareba W, Robinson JL, Timothy KW, Corfield V, Wattanasirichaigoon D, Corbett C, Haverkamp W, Schulze-Bahr E, Lehmann MH, Schwartz K, Coumel P, Bloise R (2001): Genotype-phenotype correlation in the long-QT syndrome: gene-specific triggers for life-threatening arrhythmias. Circulation 103: 89-95.

Seki T, Yuasa S, Fukuda K (2011): Derivation of induced pluripotent stem cells from human peripheral circulating T cells. Current Protocols in Stem Cell Biology Chapter 4:Unit4A.3.

Shimizu W (2003): Genotype-specific clinical manifestation in long QT syndrome. Expert Review of Cardiovascular Therapy 1(3): 401-409.

Shkryl VM, Blatter LA (2013): Ca^{2+} release events in cardiac myocytes up close: insights from fast confocal imaging. PLoS One 8(4): 61525.

Sicouri S, Antzelevitch C (1991): A subpopulation of cells with unique electrophysiological properties in the deep subepicardium of the canine ventricle. The M cell. Circulation Research 68(6): 1729-1741.

Singhal N, Graumann J, Wu G, Araúzo-Bravo MJ, Han DW, Greber B, Gentile L, Mann M, Schöler HR (2010): Chromatin-Remodeling Components of the BAF Complex Facilitate Reprogramming. Cell 141(6): 943-955.

Siu CW, Lee YK, Ho JC, Lai WH, Chan YC, Ng KM, Wong LY, Au KW, Lau YM, Zhang J, Lay KW, Colman A, Tse HF (2012): Modeling of lamin A/C mutation premature cardiac aging using patient-specific induced pluripotent stem cells. Aging (Albany NY) 4(11): 803-822.

Skottman H, Mikkola M, Lundin K, Olsson C, Strömberg AM, Tuuri T, Otonkoski T, Hovatta O, Lahesmaa R (2005): Gene expression signatures of seven individual human embryonic stem cell lines. Stem Cells 23: 1343-1356.

Soldner F, Hockemeyer D, Beard C, Gao Q, Bell GW, Cook EG, Hargus G, Blak A, Cooper O, Mitalipova M, Isacson O, Jaenisch R (2009): Parkinson's disease patient-derived induced pluripotent stem cells free of viral reprogramming factors. Cell 136: 964-977.

Sommer CA, Stadtfeld M, Murphy GJ, Hochedlinger K, Kotton DN, Mostoslavsky G (2009): Induced pluripotent stem cell generation using a single lentiviral stem cell cassette. Stem Cells 27(3): 543-549.

Spencer CI, Baba S, Nakamura K, Hua EA, Sears MA, Fu CC, Zhang J, Balijepalli S, Tomoda K, Hayashi Y, Lizarraga P, Wojciak J, Scheinman MM, Aalto-Setälä K, Makielski JC, January CT, Healy KE, Kamp TJ, Yamanaka S, Conklin BR (2014): Calcium Transients Closely Reflect Prolonged Action Potentials in iPSC Models of Inherited Cardiac Arrhythmia. Stem Cell Reports 3(2): 269-281.

Splawski I, Shen J, Timothy KW, Lehmann MH, Priori S, Robinson JL, Moss AJ, Schwartz PJ, Towbin JA, Vincent GM, Keating MT (2000): Spectrum of Mutations in Long-QT Syndrome Genes KvLQT1, HERG, SCN5A, KCNE1, and KCNE2. Circulation 102: 1178-1185.

Stadtfeld M, Nagaya M, Utikal J, Weir G, Hochedlinger K (2008): Induced pluripotent stem cells generated without viral integration. Science 322(5903): 945-949.

Staerk J, Dawlaty MM, Gao Q, Maetzel D, Hanna J, Sommer CA, Mostoslavsky G, Jaenisch R (2010): Reprogramming of human peripheral blood cells to induced pluripotent stem cells. Cell Stem Cell 7(1): 20-24.

Sugiyama A (2008): Sensitive and reliable proarrhythmia in vivo animal models for predicting drug induced torsades de pointes in patients with remodelled hearts. British Journal of Pharmacology 154: 1528-1537.

Sugiyama A, Nakamura Y, Akie Y, Saito H, Izumi Y, Yamazaki H, Kaneko N, Itoh K (2011): Microminipig, a non-rodent experimental animal optimized for life science research: in vivo proarrhythmia models of drug-induced long QT syndrome: development of chronic atrioventricular block model of microminipig. Journal of Pharmacological Sciences 115(2): 122-126.

Sun N, Panetta NJ, Gupta DM, Wilson KD, Lee A, Jia F, Hu S, Cherry AM, Robbins RC, Longaker MT, Wu JC (2009): Feeder-free derivation of induced pluripotent stem cells from adult human adipose stem cells. Proceedings of the National Academy of Sciences of the United States of America 106(37): 15720-15725.

Sun N, Yazawa M, Liu J, Han L, Sanchez-Freire V, Abilez OJ, Navarrete EG, Hu S, Wang L, Lee A, Pavlovic A, Lin S, Chen R, Hajjar RJ, Snyder MP, Dolmetsch RE, Butte MJ, Ashley EA, Longaker MT, Robbins RC, Wu JC (2012): Patient-specific induced pluripotent stem cells as a model for familial dilated cardiomyopathy. Science Translational Medicine 4(130): 130ra47.

Sutton MA, Orteu J-J, Schreier HW. Image Correlation for Shape, Motion and Deformation Measurements. New York: Springer-Verlag, 2009, pp. 1, 81-82, 95-96.

Suzuki A, Raya A, Kawakami Y, Morita M, Matsui T, Nakashima K, Gage FH, Rodríguez-Esteban C, Izpisúa Belmonte JC (2006). Nanog binds to Smad1 and blocks bone morphogenetic protein-induced differentiation of embryonic stem cells. Proceedings of the National Academy of Sciences of the United States of America 103(27): 10294-10299.

Swan H, Viitasalo M, Piippo K, Laitinen P, Kontula K, Toivonen L (1999): Sinus node function and ventricular repolarization during exercise stress test in long QT syndrome patients with KvLQT1 and HERG potassium channel defects. Journal of American College of Cardiology 34(3): 823-829.

Synnergren J, Adak S, Englund MC, Giesler TL, Noaksson K, Lindahl A, Nilsson P, Nelson D, Abbot S, Olsson B, Sartipy P (2008): Cardiomyogenic gene expression profiling of differentiating human embryonic stem cells. Journal of Biotechnology 134(1-2): 162-170.

Synnergren J, Akesson K, Dahlenborg K, Vidarsson H, Améen C, Steel D, Lindahl A, Olsson B, Sartipy P (2008): Molecular signature of cardiomyocyte clusters derived from human embryonic stem cells. Stem Cells 26(7): 1831-1840.

Takahashi T, Lord B, Schulze PC, Fryer RM, Sarang SS, Gullans SR, Lee RT (2003): Ascorbic acid enhances differentiation of embryonic stem cells into cardiac myocytes. Circulation 107(14): 1912-1916.

Takahashi K, Yamanaka S (2006): Induction of pluripotent stem cells from mouse embryonic and adult fibroblast cultures by defined factors. Cell 126(4): 663-676.

Takahashi K, Tanabe K, Ohnuki M, Narita M, Ichisaka T, Tomoda K, Yamanaka S (2007): Induction of pluripotent stem cells from adult human fibroblasts by defined factors. Cell 131(5): 861-872.

Takenaka C, Nishishita N, Takada N, Jakt LM, Kawamata S (2009): Effective generation of iPS cells from CD34+ cord blood cells by inhibition of p53. Experimental Hematology 38(2): 154-162.

Tan HL, Hou CJY, Lauer MR, Sung RJ (1995): Electrophysiologic Mechanisms of the Long QT Interval Syndromes and Torsade de Pointes. Annals of Internal Medicide 122(9): 701-714.

Tan KY, Eminli S, Hettmer S, Hochedlinger K, Wagers AJ (2011): Efficient generation of iPS cells from skeletal muscle stem cells. PLoS One 6(10): 26406.

Tanaka T, Tohyama S, Murata M, Nomura F, Kaneko T, Chen H, Hattori F, Egashira T, Seki T, Ohno Y, Koshimizu U, Yuasa S, Ogawa S, Yamanaka S, Yasuda K, Fukuda K (2009): In vitro pharmacologic testing using human induced pluripotent stem cell-derived cardiomyocytes. Biochemical and Biophysical Research Communications 385(4): 497-502.

Taylor BL & Zhulin IB (1999): PAS domains: Internal sensors of oxygen, redox potential, and light. Microbiology and Molecular Biology Reviews 63(2): 479-506.

Terrenoire C, Wang K, Tung KW, Chung WK, Pass RH, Lu JT, Jean JC, Omari A, Sampson KJ, Kotton DN, Keller G, Kass RS (2013): Induced pluripotent stem cells used to reveal drug actions in a long QT syndrome family with complex genetics. Journal of General Physiology 141(1): 61-72.

Tester DJ, Ackerman MJ (2007): Postmortem long QT syndrome genetic testing for sudden unexplained death in the young. Journal of American College of Cardiology 49(2): 240-246.

Thaler MS: The Only EKG Book You'll Ever Need. Philadelphia: Lippincott Williams & Wilkins, 1999, pp. 10-30.

Thierfelder L, Watkins H, MacRae C, Lamas R, McKenna W, Vosberg HP, Seidman JG, Seidman CE (1994): Alpha-tropomyosin and cardiac troponin T mutations cause familial hypertrophic cardiomyopathy: a disease of the sarcomere. Cell 77(5): 701-712.

Thomson JA, Kalishman J, Golos TG, Durning M, Harris CP, Becker RA, Hearn JP (1995): Isolation of a primate embryonic stem cell line. Proceedings of the National Academy of Sciences of the United States of America 92(17): 7844-7848.

Thomson JA, Itskovitz-Eldor J, Shapiro SS, Waknitz MA, Swiergiel JJ, Marshall VS, Jones JM (1998): Embryonic stem cell lines derived from human blastocysts. Science 282(5391): 1145-1147.

Thornton JE, Gregory RI (2012): How does Lin28 let-7 control development and disease? Trends in Cell Biology 22(9): 474-482.

Toivonen S, Ojala M, Hyysalo A, Ilmarinen T, Rajala K, Pekkanen-Mattila M, Äänismaa R, Lundin K, Palgi J, Weltner J, Trokovic R, Silvennoinen O, Skottman H, Narkilahti S, Aalto-Setälä K, Otonkoski T (2013): Comparative analysis of targeted differentiation of human induced pluripotent stem cells (hiPSCs) and human embryonic stem cells reveals variability associated with incomplete transgene silencing in retrovirally derived hiPSC lines. Stem Cells Translational Medicine 2(2):83-93.

Towart R, Linders JT, Hermans AN, Rohrbacher J, van der Linde HJ, Ercken M, Cik M, Roevens P, Teisman A, Gallacher DJ (2009): Blockade of the I_{Ks} potassium channel: an overlooked cardiovascular liability in drug safety screening? Journal of Pharmacological and Toxicological Methods 60(1): 1-10.

Trudeau MC, Warmke JW, Ganetzky B, Robertson GA (1995): HERG, a human inward rectifier in the voltage-gated potassium channel family. Science 269(5220): 92-95.

Tu E, Bagnall RD, Duflou J, Semsarian C (2011): Post-mortem review and genetic analysis of sudden unexpected death in epilepsy (SUDEP) cases. Brain Pathology 21(2): 201-208.

Uosaki H, Fukushima H, Takeuchi A, Matsuoka S, Nakatsuji N, Yamanaka S, Yamashita JK (2011): Efficient and scalable purification of cardiomyocytes from human embryonic and induced pluripotent stem cells by VCAM1 surface expression. PLoS One 6(8): 23657.

Verrijzer CP, Kal AJ, van der Vliet PC (1990): The oct-1 homeo domain contacts only part of the octamer sequence and full oct-1 DNA-binding activity requires the POU-specific domain. Genes & Development 4(11): 1964-1974.

Vincent GM (1992): Hypothesis for the molecular physiology of the Romano-Ward long QT syndrome. Journal of American College of Cardiology 20(2): 500-503.

Viskin S (2009): The QT interval: too long, too short or just right. Heart Rhythm 6(5): 711-715.

Vogt EJ, Meglicki M, Hartung KI, Borsuk E, Behr R (2012): Importance of the pluripotency factor LIN28 in the mammalian nucleolus during early embryonic development. Development 139(24): 4514-4523.

Volders PG, Sipido KR, Carmeliet E, Spätjens RL, Wellens HJ, Vos MA (1999): Repolarizing K^+ currents I_{TO1} and I_{Ks} are larger in right than left canine ventricular midmyocardium. Circulation 99(2): 206-210.

Waddington CH: The Strategy of the Genes: A Discussion of Some Aspects of TheoreticalBiology. London: Ruskin House/George Allen and Unwin Ltd, 1957.

Walia B, Satija N, Tripathi RP, Gangenahalli GU (2012): Induced pluripotent stem cells: fundamentals and applications of the reprogramming process and its ramifications on regenerative medicine. Stem Cell Reviews 8(1): 100-115.

Wang Q, Curran ME, Splawski I, Burn TC, Millholland JM, VanRaay TJ, Shen J, Timothy KW, Vincent GM, de Jager T, Schwartz PJ, Toubin JA, Moss AJ, Atkinson DL, Landes GM, Connors TD, Keating MT (1996): Positional cloning of a novel potassium channel gene: KvLQT1 mutations cause cardiac arrhythmias. Nature Genetics 12(1): 17-23.

Wang X, Dai J (2010): Concise review: isoforms of OCT4 contribute to the confusing diversity in stem cell biology. Stem Cells 28(5): 885-893.

Ward OC (1964): A new familial cardiac syndrome in children. Journal of the Irish Medical Association 54: 103-106.

Warren L, Manos PD, Ahfeldt T, Loh YH, Li H, Lau F, Ebina W, Mandal PK, Smith ZD, Meissner A, Daley GQ, Brack AS, Collins JJ, Cowan C, Schlaeger TM, Rossi DJ (2010): Highly efficient reprogramming to pluripotency and directed differentiation of human cells with synthetic modified mRNA. Cell Stem Cell 7(5): 618-630.

Wernig M, Meissner A, Foreman R, Brambrink T, Ku M, Hochedlinger K, Bernstein BE, Jaenisch R (2007): In vitro reprogramming of fibroblasts into a pluripotent ES-cell-like state. Nature 448(7151): 318-324.

Wettwer E, Scholtysik G, Schaad A, Himmel H, Ravens U (1991): Effects of the new class III antiarrhythmic drug E-4031 on myocardial contractility and electrophysiological parameters. Journal of Cardiovascular Pharmacology 17(3): 480-487.

Wilmut I, Schnieke AE, McWhir J, Kind AJ, Campbell KH (1997): Viable offspring derived from fetal and adult mammalian cells. Nature 385(6619): 810-813.

Wolpert L, Jessell T, Lawrence P, Meyerowitz E, Robertson E, Smith J: Principles of Development. New York: Oxford University Press, 2007, pp. 26, 300, 310-312, 332-334.

Woltjen K, Michael IP, Mohseni P, Desai R, Mileikovsky M, Hämäläinen R, Cowling R, Wang W, Liu P, Gertsenstein M, Kaji K, Sung HK, Nagy A (2009): piggyBac transposition reprograms fibroblasts to induced pluripotent stem cells. Nature 458(7239): 766-770.

Xu XQ, Zweigerdt R, Soo SY, Ngoh ZX, Tham SC, Wang ST, Graichen R, Davidson B, Colman A, Sun W (2008): Highly enriched cardiomyocytes from human embryonic stem cells. Cytotherapy 10(4): 376-389.

Xu XQ, Graichen R, Soo SY, Balakrishnan T, Rahmat SN, Sieh S, Tham SC, Freund C, Moore J, Mummery C, Colman A, Zweigerdt R, Davidson BP (2008): Chemically defined medium supporting cardiomyocyte differentiation of human embryonic stem cells. Differentiation 76(9): 958-970.

Xu H, Yi BA, Wu H, Bock C, Gu H, Lui KO, Park JH, Shao Y, Riley AK, Domian IJ, Hu E, Willette R, Lepore J, Meissner A, Wang Z, Chien KR (2012): Highly efficient derivation of ventricular cardiomyocytes from induced pluripotent stem cells with a distinct epigenetic signature. Cell Research 22(1): 142-154.

Yamanaka S, Li J, Kania G, Elliott S, Wersto RP, Van Eyk J, Wobus AM, Boheler KR (2008): Pluripotency of embryonic stem cells. Cell and Tissue Research 331(1): 5-22.

Yan GX, Antzelevitch C (1998): Cellular basis for the normal T wave and the electrocardiographic manifestations of the long-QT syndrome. Circulation 98(18): 1928-1936.

Yang L, Soonpaa MH, Adler ED, Roepke TK, Kattman SJ, Kennedy M, Henckaerts E, Bonham K, Abbott GW, Linden RM, Field LJ, Keller GM (2008): Human cardiovascular progenitor cells develop from a KDR+ embryonic-stem-cell-derived population. Nature 453(7194): 524-528.

Yazawa M, Hsueh B, Jia X, Pasca AM, Bernstein JA, Hallmayer J, Dolmetsch RE (2011): Using induced pluripotent stem cells to investigate cardiac phenotypes in Timothy syndrome. Nature 471: 230-234.

Yokoo N, Baba S, Kaichi S, Niwa A, Mima T, Doi H, Yamanaka S, Nakahata T, Heike T (2009): The effects of cardioactive drugs on cardiomyocytes derived from human induced pluripotent stem cells. Biochemical and Biophysical Research Communications 387(3): 482-488.

Yu J, Vodyanik MA, Smuga-Otto K, Antosiewicz-Bourget J, Frane JL, Tian S, Nie J, Jonsdottir GA, Ruotti V, Stewart R, Slukvin II, Thomson JA (2007): Induced pluripotent stem cell lines derived from human somatic cells. Science 318(5858): 1917-1920.

Yu J, Hu K, Smuga-Otto K, Tian S, Stewart R, Slukvin II, Thomson JA (2009): Human induced pluripotent stem cells free of vector and transgene sequences. Science 324(5928): 797-801.

Zhang J, Wilson GF, Soerens AG, Koonce CH, Yu J, Palecek SP, Thomson JA, Kamp TJ (2009): Functional cardiomyocytes derived from human induced pluripotent stem cells. Circulation Research 104: 30-41.

Zhang HB, Li RC, Xu M, Xu SM, Lai YS, Wu HD, Xie XJ, Gao W, Ye H, Zhang YY, Meng X, Wang SQ (2013): Ultrastructural uncoupling between T-tubules and sarcoplasmic reticulum in human heart failure. Cardiovasc Research 98(2): 269-276.

Zhou Z, Gong Q, Epstein ML, January CT (1998): HERG channel dysfunction in human long QT syndrome. Intracellular transport and functional defects. Journal of Biological Chemistry 273(33): 21061-21066.

Zhou W, Freed CR (2009): Adenoviral gene delivery can reprogram human fibroblasts to induced pluripotent stem cells. Stem Cells 27(11): 2667-2674.

Zhou T, Benda C, Duzinger S, Huang Y, Li X, Li Y, Guo X, Cao G, Chen S, Hao L, Chan YC, Ng KM, Ho JC, Wieser M, Wu J, Redl H, Tse HF, Grillari J, Grillari-Voglauer R, Pei D, Esteban MA (2011): Generation of induced pluripotent stem cells from urine. Journal of the American Society of Nephrology 22(7): 1221-1228.

Zhu X, Altschafl BA, Hajjar RJ, Valdivia HH, Schmidt U (2005): Altered Ca^{2+} sparks and gating properties of ryanodine receptors in aging cardiomyocytes. Cell Calcium 37: 583-591.

Zilberter YI, Timin EN, Bendukidze ZA, Burnashev NA (1982): Patch-voltage-clamp method for measuring fast inward current in single rat heart muscle cells. Pflugers Archiv 394(2): 150-155.

Zwi L, Caspi O, Arbel G, Huber I, Gepstein A, Park IH, Gepstein L (2009): Cardiomyocyte differentiation of human induced pluripotent stem cells. Circulation 120(15): 1513-1523.

Zygmunt AC, Eddlestone GT, Thomas GP, Nesterenko VV, Antzelevitch C (2001): Larger late sodium conductance in M cells contributes to electrical heterogeneity in canine ventricle. American Journal of Physiology Heart and Circulatory Physiology 281(2): 689-697.

Original publications

RESEARCH ARTICLE

Disease Models & Mechanisms 5, 220-230 (2012) doi:10.1242/dmm.008409

Model for long QT syndrome type 2 using human iPS cells demonstrates arrhythmogenic characteristics in cell culture

Anna L. Lahti[1,2,*], Ville J. Kujala[1,2,*], Hugh Chapman[3], Ari-Pekka Koivisto[3], Mari Pekkanen-Mattila[1,2], Erja Kerkelä[1,‡], Jari Hyttinen[2,4], Kimmo Kontula[5], Heikki Swan[5], Bruce R. Conklin[6], Shinya Yamanaka[6,7], Olli Silvennoinen[1,2,8] and Katriina Aalto-Setälä[1,2,9,§]

SUMMARY

Long QT syndrome (LQTS) is caused by functional alterations in cardiac ion channels and is associated with prolonged cardiac repolarization time and increased risk of ventricular arrhythmias. Inherited type 2 LQTS (LQT2) and drug-induced LQTS both result from altered function of the hERG channel. We investigated whether the electrophysiological characteristics of LQT2 can be recapitulated in vitro using induced pluripotent stem cell (iPSC) technology. Spontaneously beating cardiomyocytes were differentiated from two iPSC lines derived from an individual with LQT2 carrying the R176W mutation in the *KCNH2* (*HERG*) gene. The individual had been asymptomatic except for occasional palpitations, but his sister and father had died suddenly at an early age. Electrophysiological properties of LQT2-specific cardiomyocytes were studied using microelectrode array and patch-clamp, and were compared with those of cardiomyocytes derived from control cells. The action potential duration of LQT2-specific cardiomyocytes was significantly longer than that of control cardiomyocytes, and the rapid delayed potassium channel (I_{Kr}) density of the LQT2 cardiomyocytes was significantly reduced. Additionally, LQT2-derived cardiac cells were more sensitive than controls to potentially arrhythmogenic drugs, including sotalol, and demonstrated arrhythmogenic electrical activity. Consistent with clinical observations, the LQT2 cardiomyocytes demonstrated a more pronounced inverse correlation between the beating rate and repolarization time compared with control cells. Prolonged action potential is present in LQT2-specific cardiomyocytes derived from a mutation carrier and arrhythmias can be triggered by a commonly used drug. Thus, the iPSC-derived, disease-specific cardiomyocytes could serve as an important platform to study pathophysiological mechanisms and drug sensitivity in LQT2.

INTRODUCTION

Signal propagation between cardiomyocytes is a very tightly regulated system. Mutations in ion channels involved in this system can cause electrical alterations that, in certain circumstances, such as during exercise or emotional stress, could trigger arrhythmias. Sudden death in a young healthy person can be the first devastating presentation of an underlying genetic disease. Long QT syndrome (LQTS) can either be genetic or acquired (e.g. drug-induced) in nature and is due to defective functioning of cardiac ion channels. LQTS is characterized by a prolonged cardiac repolarization phase resulting in a long QT interval in the surface electrocardiogram (ECG). The clinical symptoms of LQTS include palpitations, syncope, seizures and even sudden cardiac death. A special type of polymorphic ventricular tachycardia [torsade de pointes (TdP)] is associated with LQTS. Intriguingly, many mutation carriers are without any symptoms. A total of 12 congenital LQTS subtypes are presently known (Hedley et al., 2009). Two of these subtypes account for more than 90% of all genetically identified LQTS cases and both are due to defective functioning of potassium channels. LQTS type 1 (LQT1) is the most common subtype, resulting from mutations in the *KCNQ1* gene, which encodes the α-subunit of the slow component of the delayed rectifier potassium current (I_{Ks}) channel (Chiang and Roden, 2000). Individuals with LQT1 typically have symptoms during exercise (Schwartz, 2001; Roden, 2008). LQTS type 2 (LQT2) is due to defective functioning of the α-subunit of the rapid delayed potassium channel (I_{Kr}), encoded by the *KCNH2* [also known as human ether-a-go-go-related gene (*HERG*)] gene (Curran et al., 1995). Typically, individuals with LQT2 have clinical symptoms after abrupt auditory stimuli, often during sleep when the heart rate is slow (Schwartz, 2001; Roden, 2008). The acquired form of LQTS is also due to altered functioning of the same *KCNH2* ion channel.

Induced pluripotent stem cell (iPSC) technology (Takahashi et al., 2007; Yu et al., 2007) has revolutionized research on genetic

[1]Institute of Biomedical Technology, and [2]BioMediTech, University of Tampere, Biokatu 6-12, 33520 Tampere, Finland
[3]Department of In Vitro Pharmacology, Orion Pharma, Orion Corporation, Turku, Finland
[4]Department of Biomedical Engineering, Tampere University of Technology, Tampere, Finland
[5]Department of Medicine, University of Helsinki, Tukholmankatu 8 B, 5th and 6th floors, P.O. Box 20, 00014 Helsinki, Finland
[6]Gladstone Institute of Cardiovascular Disease and Department of Medicine, University of California, 1650 Owens Street, San Francisco, CA 94158, USA
[7]Center for iPS Cell Research and Application (CiRA), Kyoto University, 53 Kawahara-cho, Shogoin Yoshida, Sakyo-ku, Kyoto 606-8507, Japan
[8]Tampere University Hospital, Tampere, Finland
[9]Heart Center, Tampere University Hospital, Tampere, Finland
*These authors contributed equally to this work
‡Current address: Finnish Red Cross, Blood Service, Helsinki, Finland
§Author for correspondence (katriina.aalto-setala@uta.fi)

Received 30 June 2011; Accepted 20 October 2011

diseases. iPSCs can be generated from somatic cells of any individual and these pluripotent cells can be differentiated into the desired cell type. Accordingly, it is possible to create genotype-specific cell models with a correct functional intracellular environment. However, a major challenge in the iPSC approach is to reproduce the phenotype of the disease or the individual in iPSC-derived cells. An appropriate disease phenotype has been reproduced with iPSC technology from individuals with LQT1 (Moretti et al., 2010), LQT2 (Itzhaki et al., 2011; Matsa et al., 2011) and with Timothy syndrome (Yazawa et al., 2011). Considering non-cardiac disorders, a disease phenotype or pathogenesis in iPSC-derived models has been demonstrated only for a few neurological diseases (Lee and Studer, 2010) and for the LEOPARD syndrome (Carvajal-Vergara et al., 2010).

The penetrance of the clinical symptoms of LQTS is low and there is considerable variation in phenotypic expression even within families carrying the same mutation (Priori et al., 1999). In addition, it has been proposed that the population prevalence of milder LQTS mutations might be high, suggesting that the prevalence of latent or concealed LQTS, i.e. relatively asymptomatic individuals, is higher than currently anticipated (Marjamaa et al., 2009). For these reasons, LQTS is clinically very challenging. The previous LQT2 iPSC reports used individuals with severe symptoms and the severity of their symptoms was translated to the cardiomyocytes derived from the patient-specific iPSCs. However, a cell model for asymptomatic LQT2 mutation carriers would be valuable to help with clinical decisions about medical treatments and lifestyle restrictions for relatively asymptomatic patients.

A more thorough understanding of the molecular mechanisms underlying LQTS would be very helpful for the pharmaceutical industry. Drug-induced forms of LQTS often arise as a result of inhibition of the hERG channel gating, and is thus analogous to LQT2 (Hancox et al., 2008). These adverse cardiac effects have led to labeling restrictions on both cardiac and non-cardiac drugs as well as to withdrawal from the market (Roden, 2004). Currently, preclinical testing of new chemical entities (NCEs) for proarrhythmic potential relies on animal experiments and ectopic expression of individual ion channels in non-cardiac cells (Pollard et al., 2008). However, current models lack the relevant human physiological environment that might regulate or modify cellular responses (Pollard et al., 2008). Thus, some NCEs could be unnecessarily discarded in the preclinical phase, and others already in clinical use might in fact elicit adverse cardiac side effects. Functional cardiomyocytes derived from both symptomatic and, possibly even more importantly, asymptomatic LQTS individuals would add to and complement presently used models. These cell models would provide the relevant cellular milieu to study genetic and non-genetic interactions influencing the phenotype.

In the present study, we developed an in vitro cell model of LQT2. In contrast to the previous reports (Itzhaki et al., 2011; Matsa et al., 2011), we aimed at generating a model from cells of an individual with LQT2 without severe symptoms. To that end, iPSC lines were derived from a patient's fibroblasts carrying a mutation for LQT2. Although there is a family history of overt LQTS, this individual was asymptomatic except for occasional palpitations and his 12-lead ECG exhibited a heart-rate-corrected QT time (QTc) of 437 ms. This model for LQT2 provides an important platform to study the pathophysiology of LQT2 and to evaluate adverse cardiac effects of drugs with the potential to prolong the QT interval.

RESULTS

Patient characteristics

A skin biopsy was obtained from a 61-year-old man with a missense mutation in *KCNH2* causing an arginine-to-tryptophan substitution at position 176 (R176W, hERG-FinB; Fig. 1A). Although there is a family history of overt LQTS, this individual was asymptomatic except for occasional palpitations. His 12-lead ECG exhibited a QTc of 437 ms (Fig. 1B). His sister was diagnosed with LQTS having a QT(U)c interval of 550 ms (Fig. 1C), presence of palpitations and sudden death at the age of 32.

Characterization of iPSCs

Fibroblasts from an individual with LQT2 were infected with retroviruses encoding for *OCT4*, *SOX2*, *KLF4* and *MYC* to generate iPSCs. Morphologically, iPSC colonies exhibited characteristics similar to those of human embryonic stem cells (hESCs), with rounded shape and clear defined edges (Fig. 2A). Both LQT2-specific iPSC lines (UTA.00514.LQT2 and UTA.00525.LQT2) and control iPSC lines expressed endogenous pluripotent markers at the mRNA level, as shown by reverse transcriptase PCR (RT-PCR) (Fig. 2B). The protein expression of pluripotency genes was also demonstrated by immunocytochemical stainings (Fig. 2C) for further confirmation. By contrast, exogenous gene expression was turned off in all iPSC lines by passage six (Fig. 2B). Exogenous gene expression was not detected after cardiac differentiation, demonstrating that these genes were not reactivated in the process (data not shown). The generated iPSC lines were also analyzed for their karyotypes, which were all normal (Fig. 2D).

To confirm the pluripotency of our iPSC lines, an embryoid body (EB) formation assay was performed. The EB-derived cells from LQT2 iPSC and control iPSC lines all expressed markers from the three different embryonic lineages: endoderm, ectoderm and mesoderm (Fig. 2F). Pluripotency of the lines was further confirmed by teratoma formation. Teratomas were made from one LQT2-specific line (UTA.00525.LQT2) and two control lines (UTA.00112.hFF and UTA.01006.WT). In every case, tissues from all three germ layers were found in the teratomas (Fig. 2E).

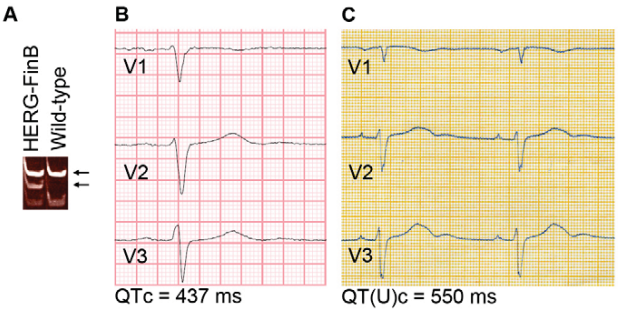

Fig. 1. Mutation and ECG analysis. (A) Mutation analysis confirmed the hERG-FinB mutation in the LQT2 iPSC line, which gave altered DNA cleavage by the *Sma*I restriction enzyme (lower arrow). (B,C) ECG from leads V1-V3 of the index patient, with a QTc of 437 ms (B), and from the patient's sister, with the presence of a U-wave following the T-wave; QT(U)c=550 ms.

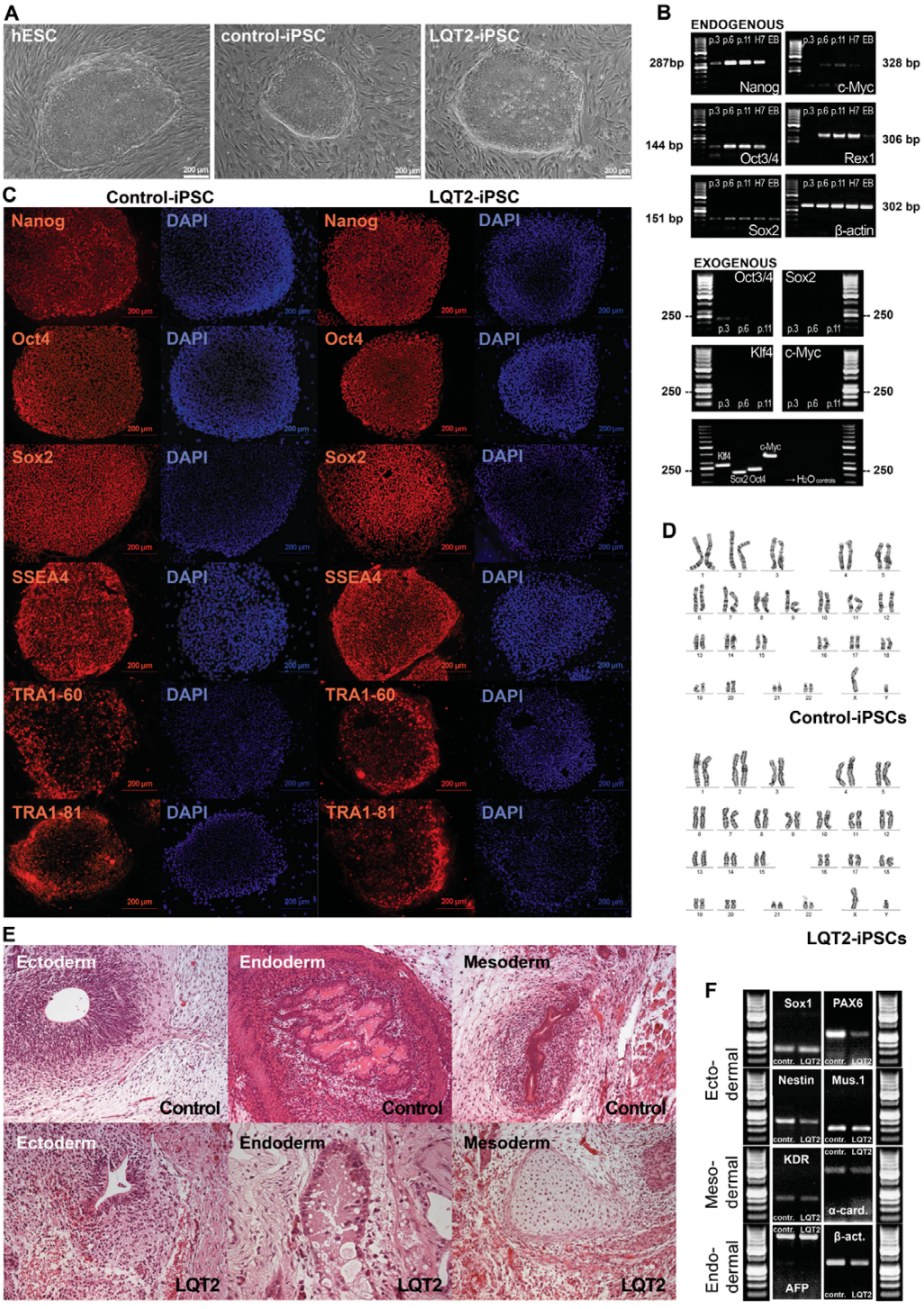

Fig. 2. Characterization of iPSCs. (A) Morphology of the iPSC colonies is similar to those of hESCs. The colonies are rather roundish and the edges are well defined and sharp, which is typical for a stem cell colony. (B) Expression of pluripotency markers in LQT2-specific iPSCs is shown by RT-PCR. All the endogenous pluripotency genes studied were turned on in iPSCs by passage 6 (top panel). As a positive control, they were also expressed in hESCs (H7). Expression of *Sox2* and very modest expression of *Rex1* and *Myc* was found also in EBs, which were used as a negative control. β-actin served as a loading control. None of the exogenous genes were expressed in iPSCs at passage 11. As a positive control, PCR was also done using the transfected plasmids as templates (bottom panel). RT-PCR results were similar for all the iPSC lines. (C) Immunocytochemical staining of the cells shows that pluripotency markers are expressed also at the protein level. The expression of Nanog, Oct3/4, Sox2, SSEA-4, TRA1-60 and TRA1-81 was similar in all iPSC lines and there were no differences between LQT2-specific and control lines. (D) Karyotypes of all the iPSC lines were analyzed and proved to be normal. (E) Teratomas were made from one LQT2-specific line and two control lines to further confirm the pluripotency of the lines. Tissues from all three germ layers were found in teratomas from every line. (F) EBs were also formed from all the lines to show the pluripotent differentiation capacity. The EB-derived cells from both LQT2-iPSC and all control iPSC lines expressed markers from the three embryonic germ layers.

Cardiomyocyte differentiation and characterization

LQT2-specific iPSCs, control iPSCs and hESCs differentiated into spontaneously beating cells. As shown by RT-PCR, these differentiated control and LQT2 cardiomyocytes expressed cardiac markers: troponin T (TNTT2), ventricular myosin light chain (MLC2V), atrial myosin light chain (MLC2A), connexin-43 (Cx-43), myosin heavy chain β (MHC-β; MYH7), HERG and GATA4 (Fig. 3B). The expression of cardiac troponin T, α-actinin and Cx-43 was also seen at the protein level as evidenced in Fig. 3A. The electrical properties of iPSC- and hESC-derived cardiomyocytes were also studied using microelectrode array (MEA; Fig. 3C,D). There were differences between control and LQT2-specific cells

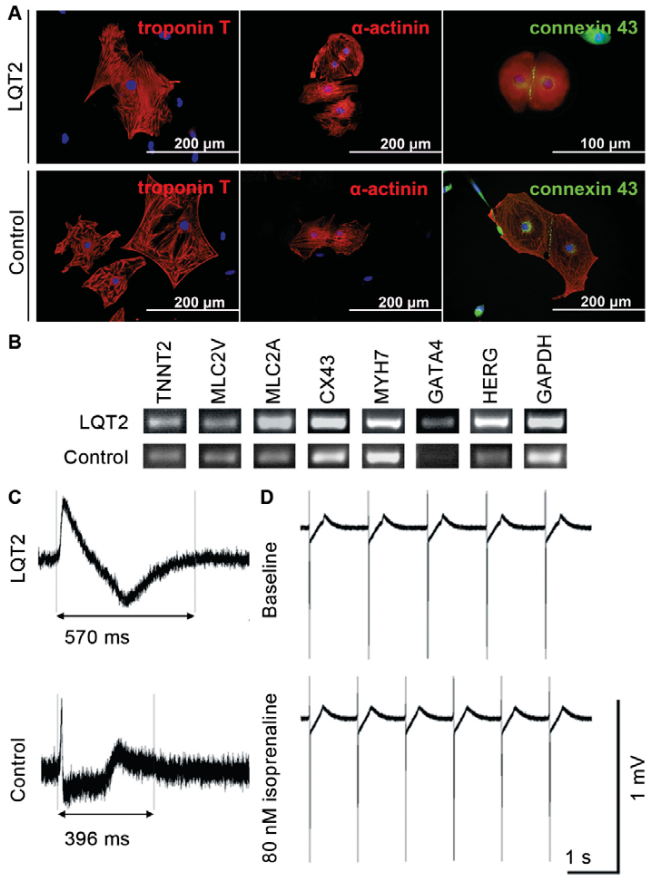

Fig. 3. The expression of cardiac markers in iPSC-derived cardiomyocytes and the electrical properties of the cells. (A) Immunocytochemical staining of different cardiac markers: troponin T and α-actinin are shown in red; green indicates connexin-43 and blue represents DAPI-staining for nuclei. The expression was similar in LQT2-specific and control cells, and there were no line-specific differences in the expression of cardiac proteins. (B) The expression of a larger repertoire of cardiac markers was also studied, with RT-PCR showing that the iPSC-derived cardiac cells manifest cardiac properties. *TNTT2*, *MLC2V*, *MLC2A*, *Cx-43*, *MYH7*, *GATA4* and *HERG* were present in the cells at the mRNA level. (C) Electrical properties of the cells were studied with MEA, which revealed the differences between LQT2-specific and control cells. FPD was significantly longer in LQT2-specific cardiomyocytes than in control cardiac cells. However, all lines evince the typical electrical properties of cardiomyocytes. (D) LQT2-specific cardiomyocytes showed increased chronotrophy when challenged with isoprenaline, a β-adrenergic agonist.

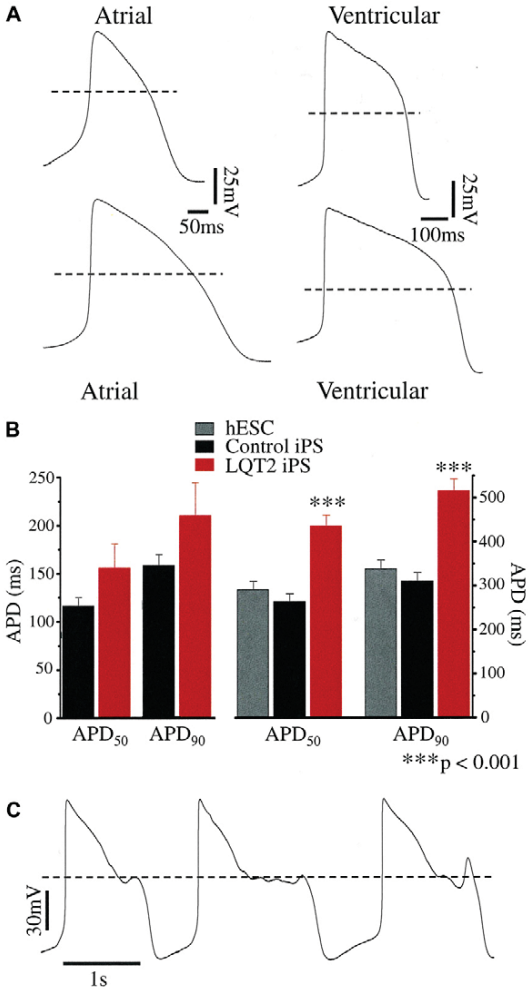

Fig. 4. Current-clamp recordings from human iPSC-derived cardiomyocytes. (A) Spontaneous APs from healthy control iPSC-derived (upper APs) and LQT2 patient-derived (lower APs) cardiomyocytes. The dashed line denotes 0 mV. (B) The action potential duration (APD) measured at 50% and 90% repolarization from the AP peak (APD_{50} and APD_{90}) of spontaneous atrial-like (n=5-6) and ventricular-like APs. For the latter, both the APD_{50} and APD_{90} of LQT2 patient-derived cardiomyocytes (n=13) were significantly prolonged compared with those of hESCs (n=7) or control-iPSC origin (n=11). (C) Spontaneous arrhythmogenic activity of an LQT2-iPSC-derived cardiomyocyte.

in their field potential durations (FPDs) (Fig. 3C), but both types showed increased chronotrophy when treated with isoprenaline, a β-adrenergic agonist (Fig. 3D), which is the anticipated response and indicates intact β-adrenergic signaling.

Electrophysiological properties of differentiated cardiomyocytes

The differentiation of both control and LQT2-specific iPSCs into cardiomyocyte subtypes was evident from the morphology of the spontaneous action potentials (APs) recorded with the patch-clamp technique. Two types of AP morphology were observed: ventricular-like, which displayed a distinct plateau phase; and atrial-like, which were triangular shaped (Fig. 4A). The AP properties of control-iPSC-derived cardiomyocytes were similar to those of other human ESC and iPSC studies (Table 1) (Gai et al., 2009; Yokoo et al., 2009; Zwi et al., 2009). For most AP parameters there was no significant difference between control and LQT2-iPSC-derived cardiomyocytes (P>0.05; Table 1). However, ventricular-like LQT2-iPSC-derived cardiomyocytes had significantly prolonged AP durations at 50% and 90% repolarization (APD_{50} and APD_{90}, respectively). The APD_{50} and APD_{90} of atrial-like LQT2-iPSC-derived cardiomyocytes, although prolonged, did not reach statistical significance. On the borderline of statistical significance was the slower AP frequency of ventricular-

Table 1. AP properties of atrial- and ventricular-like cardiomyocytes

	No. cells	Frequency (Hz)	APD_{50} (ms)	APD_{90} (ms)	dV/dt_{max} (V/second)	APA (mV)	MDP (mV)
Atrial-like							
Control	6	1.8±0.1	116.7±8.4	157.7±11.0	9.2±0.5	104.4±1.3	–65.6±0.6
LQT2	5	1.4±0.1	156.0±25.0	210.9±33.3	11.7±1.6	105.0±2.7	–65.4±1.4
Ventricular-like							
Control	13	1.2±0.1	264.7±15.0	314.4±17.6	26.8±6.3	113.2±2.4	–63.4±1.3
LQT2	16	0.9±0.1[a]	455.3±26.7[b]	538.0±28.5[b]	15.8±0.7	117.3±1.4	–62.4±0.9

AP properties of spontaneously beating human iPSC-derived cardiomyocytes. dV/dt_{max}, maximum rise of the AP upstroke; APA, AP amplitude; MDP, maximum diastolic potential. Mean values ± s.e.m. are shown. Comparison of control iPSC-CMs and LQT2 iPSC-CMs groups was performed with unpaired *t*-test with $P<0.05$ considered statistically significant.
[a]$P=0.05$; [b]$P<0.000005$. CMs, cardiomyocytes.

like LQT2-iPSC-derived cardiomyocytes; therefore, further analysis was restricted to a subset of cardiomyocytes to reduce the effect of any rate-dependent APD adaptation.

Both the APD_{50} and APD_{90} of LQT2-iPSC-derived ventricular-like cardiomyocytes were significantly prolonged compared with control-iPSC- and hESC-derived cardiomyocytes ($P<0.001$; Fig. 4A,B), at an AP frequency of about 1 Hz ($P=0.13$ between groups). The APD_{90} was 516.5±26.1 ms in LQT2-specific cardiomyocytes compared with 310.5±19.6 ms in control-iPSC-derived cardiomyocytes or 338.6±19.9 ms in hESC-derived cardiomyocytes. The APD_{90} did not differ significantly between cardiomyocytes from the two LQT2 iPSC lines (UTA.00514.LQT2 and UTA.00525.LQT2) or between hESC-derived cardiomyocytes and those of control iPSC origin. Collectively, these data indicate that the LQT2-iPSC-derived cardiomyocytes express the disease phenotype, characterized by a prolonged cardiac repolarization phase. Spontaneous arrhythmogenic activity was rare, early after depolarizations (EADs) were observed in only one of 20 LQT2-iPSC-derived cardiomyocytes studied (Fig. 4C) and in no recordings from control iPSC cardiomyocytes ($n=20$).

Ventricular-like cardiomyocytes were subjected to further investigations using voltage clamp (Fig. 5). Using the specific inhibitor E-4031, I_{Kr} was isolated (Fig. 5A) and its magnitude shown to be markedly reduced in LQT2 iPSC cardiomyocytes compared with that in control iPSC cardiomyocytes (Fig. 5B). Tail I_{Kr} density was significantly decreased, by 40-46%, after a depolarizing step to voltages from 0 to +40 mV ($P<0.01$; Fig. 5C). A similar reduction in tail I_{Kr} density (~40%) was seen in experiments when an alternative method, isotonic cesium conditions (Zhang, 2006), was used to isolate I_{Kr} from a different control and LQT2 iPSC line (supplementary

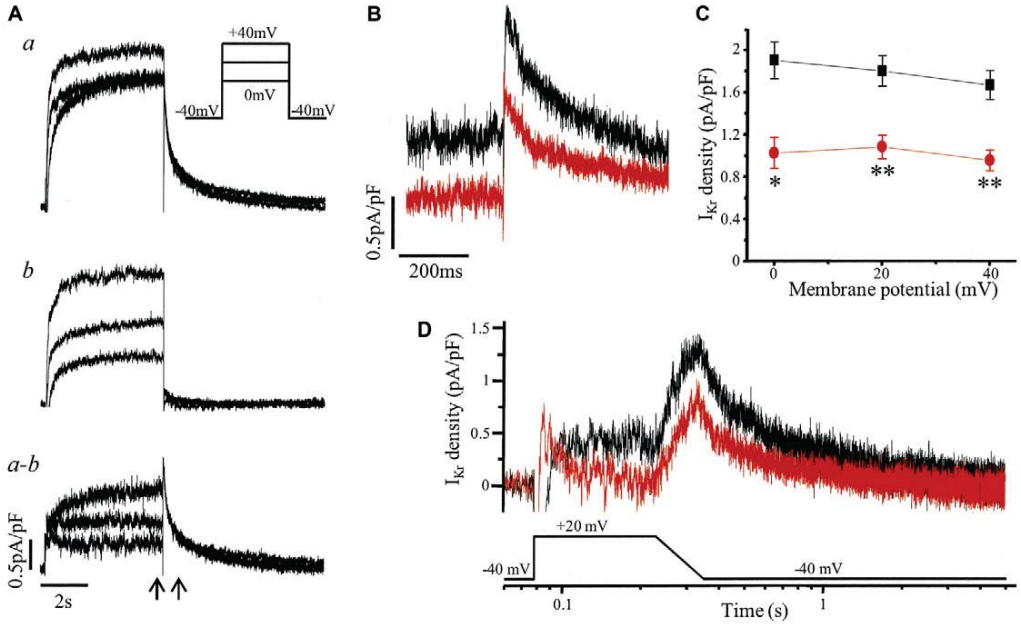

Fig. 5. I_{Kr} recorded from iPSC cardiomyocytes with a ventricular-like AP. (A) Example of the isolation of I_{Kr}. Whole-cell current, here from a control iPS cardiomyocyte, was recorded in the absence (*a*) and then presence of 1 µmol/l E-4031 (*b*), with I_{Kr} defined as the subtracted current (*a*-*b*), i.e. the E-4031-sensitive current. Current was evoked by a 5-second depolarization from a holding potential of –40 mV as shown in the inset. (B) I_{Kr} of a control iPS (black) and LQT2 iPS (red) cardiomyocyte evoked as in A with the time segment between the arrows expanded to show the peak tail currents on return to –40 mV following a step to +20 mV. (C) The peak tail I_{Kr} densities of control iPSC (black; $n=4$) and LQT2 iPSC (red; $n=5$) cardiomyocytes at membrane potentials from 0 to +40 mV were significantly different (*$P<0.01$, **$P<0.005$). (D) I_{Kr} currents of control iPSC (black) and LQT2 iPSC (red) cardiomyocytes evoked by a voltage protocol of step to +20 mV for 150 ms and ramp of 120 ms back to the –40 mV holding potential.

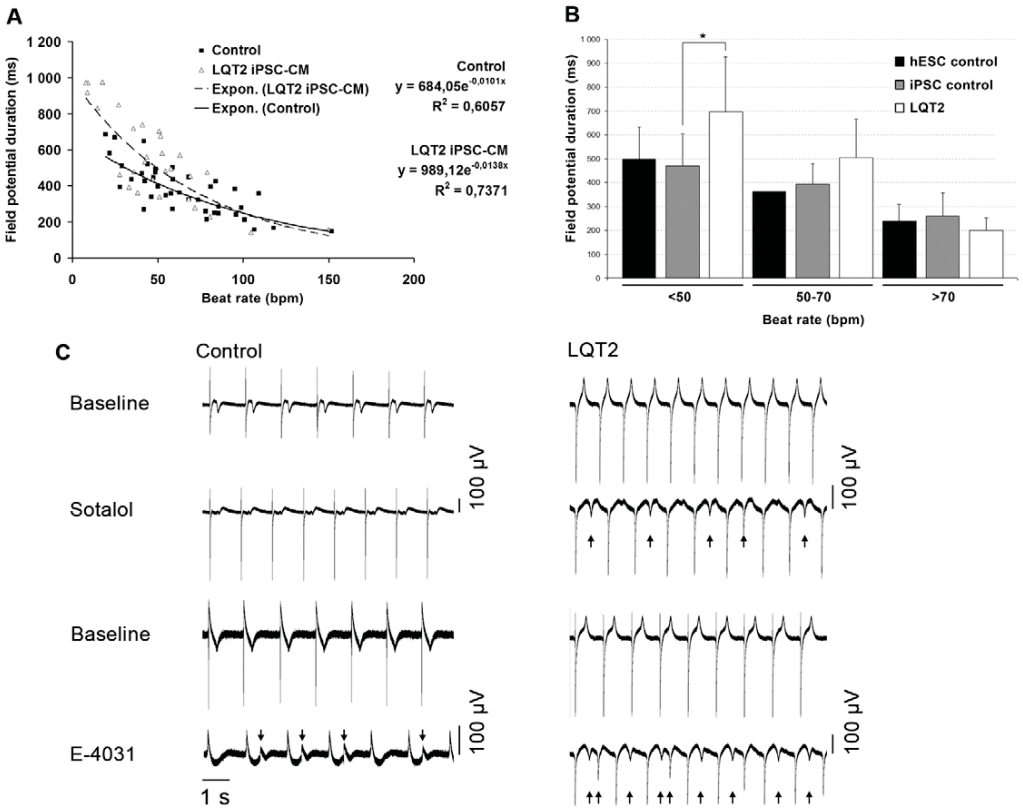

Fig. 6. FPD measured on MEA. (A) The effect of the beating rate on FPD in control and LQT2 cardiomyocytes (CMs). Control and LQT2 cardiomyocytes had a negative correlation with moderately high coefficients of determination (R^2). The exponential function gave the best fit as determined by R^2 between different fitting functions. The LQT2 cardiomyocytes had significantly more prolonged FPD compared with controls, especially at low beating frequencies, as determined by nonlinear regression analysis (P=0.0136). (B) At beating rates below 50 beats per minute (bpm), the FPD of LQT2 cardiomyocytes differed significantly from control cardiomyocytes (*P<0.05) as determined by t-test. (C) Drug responses of control and LQT2 cardiomyocytes. Sotalol (19 µmol/l) and E-4031 (500 nmol/l for LQT2-specific cells and 700 nmol/l for control cells) was administered to the cardiomyocyte aggregates derived from control iPSCs and LQT2 iPSCs. For both cell lines, baseline and drug conditions for sotalol and E-4031 are shown. Arrows mark the site of pharmacologically induced EADs. With 500 nmol/l E-4031 there were no EADs observed in control cells.

material Fig. S1). The reduction in resurgent I_{Kr} during repolarization was also demonstrated with the use of a step-ramp voltage protocol as a simplified version of a cardiac AP (Fig. 5D).

The in vitro cardiac FPD on MEA has been shown to correlate with QT interval properties in the ECG, and FPD recordings of beating cell aggregates give insight into the electrical function of myocardial tissue in vitro (Caspi et al., 2008). We observed a negative correlation between FPD and beating rate both in control cardiomyocytes and LQT2-specific cardiomyocytes (Fig. 6A,B). However, the LQT2 cardiomyocytes had a significantly prolonged FPD compared with controls, especially at low beating frequencies (P=0.014; Fig. 6A,B), as determined by nonlinear regression analysis. The two LQT2 iPSC lines behaved the same way and, thus, their data were combined, as were data from the three different control iPSC lines and hESC-derived cardiomyocytes, because they behaved similarly.

The inotropic response of the iPSC-derived cardiac cells was studied using isoprenaline. A panel of drugs with known QT-prolongation effects, including erythromycin, sotalol and cisapride, and a non-drug compound, E-4031, were investigated. The selective hERG blocker E-4031 increased arrhythmogenicity in control cardiac cells and even more frequently in LQT2 cardiomyocytes (Fig. 6C). Application of sotalol (0.8-19.4 µmol/l), an anti-arrhythmic drug with both β-blocker and class III activity, elicited arrhythmogenicity at the highest tested concentrations only in LQT2 cardiac cells (Fig. 6C). No increased arrhythmogenicity was observed with erythromycin (1.5-16 µmol/l) or cisapride (40-330 nmol/l) in control or LQT2 cardiac cells (data not shown). At baseline, no arrhythmogenicity was observed with control or LQT2 cardiac cells on MEA.

DISCUSSION

In this study we demonstrate that patient-specific iPSCs can be used to model a potentially lethal cardiac arrhythmic disease in vitro. The cells were differentiated into functional cardiomyocytes, which reproduced the phenotypic characteristics of LQT2, including a prolonged repolarization time and increased arrhythmogenicity. Furthermore, at slow beating rates, FPD (QT) was significantly more prolonged in LQT2 cardiomyocytes compared with control cells.

The R176W hERG mutation was reported to have the frequency of 0.5% in apparently healthy individuals (Ackerman et al., 2003) and, according to an epidemiological Finnish study, the mutation is present in about one of 400 Finns (Marjamaa et al., 2009). The majority of these individuals are completely asymptomatic and unaware of their carrier status. This mutation is one of the four founder mutations for LQTS in Finland and these mutations account for almost two-thirds of all established LQTS cases in the country (Fodstad et al., 2004). The QTc interval of LQT2 patients with the R176W mutation is reported to range from 386 to 569 ms, with a mean of 448 ms, whereas the mean for non-carriers was 416 ms (Fodstad et al., 2006). Furthermore, the mutation has also been identified in cases of sudden death (Tester and Ackerman, 2007; Tu et al., 2011). Although our patient had latent LQTS, his family did not. His younger sister died suddenly at the age of 32 when awakened by a telephone and his father died suddenly at the age of 40. The sister was documented to have abnormal QT intervals of up to 582 ms. The symptoms in this family, including palpitations, syncope, and sudden death due to abrupt auditory stimuli during sleep, were typical of LQT2 (Schwartz, 2001; Roden, 2008). In our study, the repolarization time was significantly prolonged in cultured LQT2-specific cardiac cells, compared with control cells, at low beating rates, and this is consistent with the clinical observation that, at slow beating rate, the QT interval is prolonged more in LQT2 patients compared with healthy individuals (Swan et al., 1999).

Although the underlying mechanism of R176W is presently unknown, when heterologously expressed, R176W reduces hERG tail current density by ~75%, although upon coexpression with wild type the difference in current densities was nullified (Fodstad et al., 2006). The decrease of ~43% in I_{Kr} density observed here in iPS cardiomyocytes from a heterozygous R176W individual might reflect the difference in cellular environment, e.g. the composition of the endogenous I_{Kr} channel, which includes both the ubiquitously in vitro expressed hERG1a subunit and hERG1b subunit with its alternatively spliced N-terminus, presence of accessory subunits and/or native interactions. However, it is also possible that this observed discrepancy results from a differential expression of the wild-type and mutant alleles in vitro versus in vivo. In both model systems, R176W does not display a dominant-negative effect, unlike the A614V hERG mutation (Nakajima et al., 1998). iPS cell lines with that particular mutation derived from a severely symptomatic LQT2 patient with recorded TdP have been generated (Itzhaki et al., 2011). This mutation resulted in a decrease in the activating I_{Kr} density of 72% with a depolarization step to 0 mV and of 64% in the tail current density following depolarization to +20 mV. Smaller reductions in these values (43% and 40%, respectively) were obtained for the R176W hERG mutation here. This difference in I_{Kr} reduction translates to the APD: at 1 Hz the ventricular-like LQT2 iPSC cardiomyocyte APD_{90} was 166% and ~200% of control for R176W and A614V, respectively, and in arrhythmogenicity, with EADs rarely observed here (~5%) but frequently (66%) in the report by Itzhaki and coworkers. Thus, the in vitro results obtained with iPSC cardiomyocytes seems to correspond to differences in expression of the disease, i.e. latent versus overt LQTS. Similarly, Matsa et al. demonstrated that the APD of both atrial-like and ventricular-like iPSC cardiomyocytes was significantly prolonged when derived from an LQT2 patient with episodes of syncope, seizures and TdP (Matsa et al., 2011). Although, in the study by Matsa et al., no spontaneous arrhythmicity was observed, such an effect could be induced pharmaceutically by isoprenalin.

One explanation for the genotype-phenotype discordance in LQTS is the repolarization reserve. This concept proposes that redundant mechanisms are available to bring about normal repolarization; therefore, to elicit the full-blown LQTS phenotype multiple hits might be required to sufficiently reduce the reserve (Roden, 2006). Such 'hits' might be the presence of compound mutations, polymorphisms, drug exposure, female gender, hypokalemia or other risk factors (Roden, 2006; Lehtonen et al., 2007). Evidence for the repolarization reserve and its genetic modulation comes from studies of individuals or first-degree relatives of individuals with drug-induced LQTS showing a prolongation of repolarization indices with pharmacological challenge (Kannankeril et al., 2005; Couderc et al., 2009). The unmasking of latent LQTS can occur accidentally (e.g. associated drug-induced TdP) (Lehtonen et al., 2007). In line with the repolarization reserve hypothesis and the clinical data, R176W LQT2 cardiac cells were more sensitive to drug effects that controls. The hERG-channel-specific blocker E-4031 induced arrhythmogenicity in both control and LQT2 cardiac cells, but sotalol induced arrhythmogenic behavior only in LQT2 cardiac cells. Sotalol has been used as a pharmacological challenge and is documented as inducing TdP in a patient carrying a hERG channel mutation (Lehtonen et al., 2007; Couderc et al., 2009). The concentrations of sotalol used in this study are similar to the effective free therapeutic plasma concentration range (1.8-14.7 µmol/l) (Redfern et al., 2003). Sotalol probably exacerbates the underlying defect, because the potency of sotalol towards hERG is similar between wild type and variant in transfected cells (Männikkö et al., 2010).

Comparison of single-cell recordings and MEA analysis and ECG findings of the patients revealed an interesting observation. Although single-cell recordings indicated major differences in repolarization time between control- and LQT2-derived cardiac cells (66% increase in AP_{90} in LQT2 cardiomyocytes), the corresponding differences measured using cell aggregates with the MEA technique were much more moderate (10-20%) and resembled differences in ECG in healthy individuals and LQTS patients (Fodstad et al., 2006). Similar observations can be found in the previously reported iPSC studies on LQTS. AP_{90} duration was reported to be increased by 50% in LQT1 cardiac cells compared with control cells, whereas the difference in ECG was only in the range of 10-15% (Moretti et al., 2010). In the studies with LQT2 cells, the repolarization times were greatly prolonged already at ECG level (50% or more) and similar differences were observed in their MEA recordings (50% difference between control and LQT2 cardiac cells) (Itzhaki et al., 2011; Matsa et al., 2011). However, in both of these studies, the AP_{90} duration was increased by 2- to 2.5-fold compared with control repolarization time. It is possible that cell-to-cell contacts in the syncytium result in compensatory mechanisms with a tendency to protect the repolarization system from major deviation from the normal conditions.

Our results on the abnormal electrophysiological properties and increased drug sensitivity of cardiac cells derived from an asymptomatic *KCNH2* R176W mutation carrier raise an important

issue about LQT2 and also a new challenge, as well as a possibility, for the pharmaceutical industry. LQT2 cell models for severely symptomatic patients (Itzhaki et al., 2011; Matsa et al., 2011) are most useful for studying the pathology of LQT2 and demonstrate in a convincing way that the phenotype of this syndrome can be reproduced in a cell culture model. Our results complement the previous research on LQT2-specific iPSC-derived cardiomyocytes by introducing a cell model for an asymptomatic mutation carrier. According to our findings, even these clinically asymptomatic individuals can possess the inherent electrophysiological abnormality in their cardiac cells. Taking advantage of this large resource of Finnish individuals with the same mutation, it might be possible to evaluate the electrophysiological properties and drug responses of cardiomyocytes from mutation carriers with and without symptoms, and thereby try to identify putative genetic or non-genetic modifiers of LQTS. These types of studies might also assist in the tailoring of individualized drug treatment of these patients. In the future, iPSC technology is likely to be increasingly exploited for drug development and safety studies.

In conclusion, iPSC-derived cardiomyocytes from an individual with LQT2 displayed the disease cardiac phenotype in cell culture conditions even though the individual was relatively asymptomatic. This model provides an additional platform to study the basic pathology of LQTS and to individualize drug treatment in a patient-specific manner. It also provides the means to explore the differences between clinical patients and mutation carriers and to scan the cardiac effects of different drugs on both.

METHODS

The study was approved by the ethical committee of Pirkanmaa Hospital District (R07080).

Cell culture

The LQT2 cells were derived from a 61-year-old man with an R176W mutation of *KCNH2* (hERG-FinB) (Fodstad et al., 2004). Primary fibroblasts from a skin biopsy were cultured under fibroblast culturing conditions: Dulbecco's Modified Eagle's Medium (DMEM) (Lonza, Basel, Switzerland) containing 10% fetal bovine serum (FBS) (Lonza), 2 mmol/l L-glutamine, 50 U/ml penicillin/streptomycin. 293FT cells (Invitrogen, Carlsbad, CA) were maintained similarly with 1% non-essential amino acids (NEAA) (Cambrex, East Rutherford, NJ). Plat-E (Cell Biolabs, San Diego, CA), irradiated SNL-76/7 (HPA Culture Collections, Salisbury, UK) and mouse embryonic fibroblast (MEF; Millipore, Billerica, MA) cells were cultured without antibiotics. iPSCs and hESCs were maintained in KSR medium: knockout (KO)-DMEM (Invitrogen) containing 20% KO serum replacement (KO-SR, Invitrogen), NEAA, L-glutamine, penicillin/streptomycin, 0.1 mmol/l 2-mercaptoethanol and 4 ng/ml basic fibroblast growth factor (bFGF; R&D Systems, Minneapolis, MN). H7 hESCs (WiCell Research Institute, Madison, WI) and iPSC lines FiPS 6-14 and UTA.00112.hFF (derived from foreskin fibroblasts), UTA.01006.WT and UTA.04602.WT (from adult skin fibroblasts) were used as controls.

Generation of iPSC lines

Patient-specific iPSC lines were established using lentivirus infection followed by retrovirus infection into the primary fibroblasts. The following cells, plasmids and reagents were used: 293FT cells, Plat-E cells, pLenti6/UbC/mSlc7a1 vector (Addgene, Cambridge, MA), ViraPower Packaging Mix (Invitrogen), Lipofectamine 2000 (Invitrogen), pMX retroviral vector (hOCT3/4, hSOX2, hKLF4 or hc-MYC; Addgene) and Fugene 6 (Roche Diagnostics, Mannheim, Germany). The protocol used has been described previously (Takahashi et al., 2007). Two LQT2-specific lines were established (UTA.00514.LQT2 and UTA.00525.LQT2) carrying the R176W mutation, which was confirmed by PCR as described previously (Fodstad et al., 2006). The FiPS 6-14 line was derived at the University of Helsinki (provided by Timo Otonkoski) (Rajala et al., 2010). Control iPSC lines from healthy individuals (UTA.01006.WT from a 36-year-old male and UTA.04602.WT from a 55-year-old female) and the UTA.00112.hFF line from human foreskin fibroblasts were established in the same way as the LQT2 lines.

RT-PCR

Total RNA was collected from the iPSC lines at passages 3, 6 and 11 and after cardiac differentiation. For positive pluripotency control, the H7 line was used. RNA from EBs was used as a negative control of pluripotency. RNA was purified with NucleoSpin RNA II kit (Macherey-Nagel, Düren, Germany) and cDNA conversion was performed with a high-capacity cDNA RT kit (Applied Biosystems, Carlsbad, CA). PCR was done with Dynazyme II (Finnzymes Oy, Espoo, Finland) using 1 µl of cDNA as a template and 2 µM primers. As positive controls for exogenous primers, PCR was also done using the transfected plasmids (hOCT3/4, hSOX2, hKLF4 and hc-MYC) as templates. PCR primers for iPSC characterization and detailed reaction conditions have been described previously (Takahashi et al., 2007). Primers for different germ layers and cardiac markers are presented in Table 2. β-actin and *GAPDH* were used as housekeeping controls.

Immunocytochemistry for pluripotency

iPSCs at passage 8 were fixed with 4% paraformaldehyde (Sigma-Aldrich) and stained with anti-OCT3/4 (1:400; R&D Systems), anti-tumor-related antigen (TRA)1-60 (1:200; Millipore), anti-SOX2, anti-NANOG, anti-stage-specific embryonic antigen (SSEA)4 and anti-TRA1-81 (all 1:200; from Santa Cruz Biotechnology, Santa Cruz, CA). The secondary antibodies (Invitrogen) were Alexa-Fluor-568-donkey-anti-goat-IgG, Alexa-Fluor-568-goat-anti-mouse-IgM or Alexa-Fluor-568-donkey-anti-mouse-IgG.

EB formation

EBs were cultured without feeder cells in EB medium (KO-DMEM with 20% FBS, NEAA, L-glutamine and penicillin/streptomycin) without bFGF for 5 weeks. RNA isolation and reverse transcription from EBs was performed as described above. The expression of markers characteristic of ectoderm, endoderm and mesoderm development in EBs was determined using RT-PCR (primers described in Table 2).

Mutation analysis

The hERG-FinB mutation was assayed with restriction enzyme analysis (Fodstad et al., 2006) by amplifying the genomic DNA with primers for *hERG* (forward: 5′-ACCACGTGCCTCTCCTCTC-3′, reverse: 5′-GTCGGGGTTGAGGCTGTG-3′) (reagents from Applied Biosystems) and digesting the amplified PCR product with

Table 2. Primers for RT-PCR of different germ layer markers and cardiac markers.

Gene	Primer F (5′-3′)	Primer R (5′-3′)	Size (bp)
Endodermal markers			
AFP	AGAACCTGTCACAAGCTGTG	GACAGCAAGCTGAGGATGTC	672
SOX17	CGCACGGAATTTGAACAGTA	CACACGTCAGGATAGTTGCAG	166
Mesodermal markers			
α-cardiactin	GGAGTTATGGTGGGTATGGGTC	AGTGGTGACAAAGGAGTAGCCA	486
KDR	GTGACCAACATGGAGTCGTG	TGCTTCACAGAAGACCATGC	218
Ectodermal markers			
SOX1	AAAGTCAAAACGAGGCGAGA	AAGTGCTTGGACCTGCCTTA	158
PAX6	AACAGACACAGCCCTCACAAACA	CGGGAACTTGAACTGGAACTGAC	274
Nestin	CAGCTGGCGCACCTCAAGATG	AGGGAAGTTGGGCTCAGGACTGG	208
Musashi 1	AGCTTCCCTCTCCCTCATTC	GAGACACCGGAGGATGGTAA	161
Cardiac markers			
TNTT2	ATCCCCGATGGAGAGAGAGT	TCTTCTTCTTTTCCCGCTCA	385
MLC2V	GGTGCTGAAGGCTGATTACGTT	TATTGGAACATGGCCTCTGGAT	382
MLC2A	GTCTTCCTCACGCTCTTTGG	GCCCCTCATTCCTCTTTCTC	269
Cx-43	TACCATGCGACCAGTGGTGCGCT	GAATTCTGGTTATCATCGGGGAA	293
MYH7	AGCTGGCCCAGCGGCTGCAGG	CTCCATCTTCTCGGCCTCCAGCT	443
GATA4	GACGGGTCACTATCTGTGCAAC	AGACATCGCACTGACTGAGAAC	474
HERG	GAACGCGGTGCTGAAGGGCT	AACTTGCGCTTGCGTTGCCG	527
Housekeeping control genes			
β-actin	GTCTTCCCCTCCATCGTG	GGGGTGTTGAAGGTCTCAAA	302
GAPDH	AGCCACATCGCTCAGACACC	GTACTCAGCGGCCAGCATCG	302

*Sma*I digestion enzyme (Fermentas GmbH, St Leon-Rot, Germany). The hERG-FinB mutation resulted in deletion of a *Sma*I-cleavage site. *Sma*I-cleaved PCR products were detected with gel electrophoresis: products for wild type were 182, 79, 46 and 23 bp and for R176W heterozygote 182, 125, 79, 46 and 23 bp long.

Karyotype analysis

Karyotypes of the cell lines were defined using standard G-banding chromosome analysis by a commercial company (Medix Laboratories, Espoo, Finland) according to standard procedure.

Teratoma formation

iPSCs were injected into nude mice under the testis capsule. Tumor samples were collected 8 weeks after injection and fixed with 4% paraformaldehyde. The sections were stained with hematoxylin and eosin.

Cardiac differentiation and characterization

Cardiomyocyte differentiation was carried out by co-culturing iPSCs and H7 hESCs with END-2 cells (a kind gift from Christine Mummery, Hubrecht Institute, Utrecht, The Netherlands). END-2 cells were cultured as described earlier (Mummery et al., 2003). The beating areas of the cell colonies were mechanically excised and treated with collagenase A (Roche Diagnostics) as described previously (Mummery et al., 2003). Seven days after dissociation, cells were fixed with 4% paraformaldehyde for immunostaining with anti-cardiac-troponin-T (1:2000; Abcam, Cambridge, MA), anti-α-actinin (1:1500; Sigma-Aldrich, St Louis, MO) and anti-connexin-43 (1:1000; Sigma-Aldrich).

Patch-clamp technique

APs were recorded from spontaneously beating dissociated cells using the perforated patch (by amphotericin) configuration of the patch-clamp technique with an Axopatch 200B amplifier (Molecular Devices, Sunnyvale, CA). A coverslip with the adhered cells was placed in the recording chamber and perfused with extracellular solution consisting of (in mmol/l) 143 NaCl, 4 KCl, 1.8 $CaCl_2$, 1.2 $MgCl_2$, 5 glucose, 10 HEPES (pH 7.4 with NaOH; osmolarity adjusted to 301±3 mOsm). Patch pipettes were pulled from borosilicate glass capillaries (Harvard Apparatus, Kent, UK) and had resistances of 1.5-3.5 MΩ when filled with a solution consisting of (in mmol/l): 122 K-gluconate, 30 KCl, 1 $MgCl_2$, 5 HEPES (pH 7.2 with KOH; osmolarity adjusted to 290±3 mOsm). The final concentration of amphotericin B (solubilized in dimethylsulfoxide) in the pipette was 0.24 mg/ml.

The data was filtered at 2 kHz, and digitized (Digidata 1322A; Molecular Devices) at 10 kHz; data acquisition and analysis was performed with pClamp 9.2 software (Molecular Devices). For some cardiomyocytes, voltage-clamp experiments were also performed to record I_{Kr}. Experiments were conducted at 36±1°C.

Field potential recordings

Field potentials of spontaneously beating cardiomyocyte aggregates were recorded with the MEA platform (Multi Channel Systems, Reutlingen, Germany) at 37°C. MEAs were hydrophilized with FBS for 30 minutes, washed with sterile water and coated with 0.1% gelatin for 1 hour. Cardiomyocyte aggregates were plated onto MEAs in EB medium. FPD and beating frequency were determined manually with AxoScope software (Molecular Devices).

TRANSLATIONAL IMPACT

Clinical issue

Long QT syndrome (LQTS) is a life-threatening cardiac disorder that predisposes individuals to ventricular arrhythmias and sudden death. The syndrome is characterized by a prolonged QT interval (detected by electrocardiography) and can be caused either by genetic defects or as a side effect of certain drugs. LQTS type 2 (LQT2) occurs owing to defective functioning of the hERG potassium channel, and is caused by mutations in the *KCNH2* gene (also known as *HERG*). The drug-induced form of LQTS also occurs owing to altered function of the hERG channel. Because prolongation of QT interval is one of the most common severe side effects of both cardiac and non-cardiac drugs, new drug candidates must be carefully tested for their effects on the hERG channel. However, physiological human cell models to test for this effect were not previously available. The clinical prevalence of LQTS is only ~1:5000, but its genetic prevalence has been estimated to be much higher (1:250 to 1:2000). Therefore, it is possible that asymptomatic carriers of LQTS-associated mutations are more susceptible to the side effect of certain medications, and are at risk of developing severe symptoms in certain settings.

Results

This study investigates whether an LQTS-related phenotype can be detected in an in vitro model based on cells from an asymptomatic carrier of an LQT2-associated *KCNH2* mutation. The authors generate patient-specific induced pluripotent stem cells (iPSCs) from an asymptomatic individual and differentiate them into functional cardiac cells. These cells recapitulate the phenotypic characteristics of LQT2 in vitro, including prolonged repolarization time and increased arrhythmogenicity. Additionally, at slow beating rates, cardiomyocyte aggregates derived from these iPSCs present prolonged field potential duration (QT) compared with control cells. These results are in line with clinical findings that individuals with LQT2 usually display symptoms when heart rate is slow. These results indicate that electrophysiological abnormalities can be detected in iPSC-derived cardiac cells, even when derived from asymptomatic carriers of *KCNH2* mutations.

Implications and future directions

This in vitro model of LQT2 offers a new system with which to evaluate electrophysiological properties and drug responses of cardiomyocytes from *KCNH2* mutation carriers with and without LQTS symptoms. In addition, the model provides a platform from which to study the basic pathology of LQTS and to identify genetic and non-genetic modifiers that can be considered in designing and developing medications to treat distinct patient groups. In addition, the model provides the means to analyze the cardiac side effects of different drugs in carriers of LQTS-associated mutations.

Isoprenaline (Isuprel; Hospira, Lake Forest, IL), D,L-sotalol (Sigma), erythromycin (Abbott, IL), cisapride (Sigma) and E-4031 (Alomone Labs, Jerusalem, Israel) were diluted in 5% FBS containing EB medium for drug tests. Baseline conditions as well as drug effects were recorded for 2 minutes after a 2-minute stabilization period. Baseline FPDs were measured from 43 control cardiomyocyte aggregates and 30 LQT2 cardiomyocyte aggregates.

Statistical methods

Data are given as mean ± s.e.m. or s.d. Comparison of patch-clamp data between LQT2-iPSC and control-iPSC cardiomyocytes was performed using Student's *t*-test for independent data. One-way analysis of variance followed by Tukey test was used for comparison of multiple groups. The I_{Kr} data was assessed using Student's *t*-test for independent data. The difference in FPDs between different populations of spontaneously beating cardiomyocyte aggregates was determined by nonlinear regression analysis using R software. The difference in FPDs between populations when categorized according to beating frequencies was determined by *t*-test with SPSS software (IBM).

ACKNOWLEDGEMENTS

We thank Merja Lehtinen and Henna Venäläinen for technical support, Christine Mummery for providing END-2 cells, Timo Otonkoski for sharing his knowledge, Annukka Lahtinen for help in the LQTS genotyping of the iPSC lines, Heini Huhtala for help on statistical analysis, and Kenta Nakamura, Chris Schlieve and the Gladstone Stem Cell Core for advice and reagents. We also thank Takayuki Tanaka for help in setting up our iPSC system.

COMPETING INTERESTS

The authors declare that they do not have any competing or financial interests.

AUTHOR CONTRIBUTIONS

A.L.L. was involved in iPS cell generation and analysis, cardiomyocyte differentiation and characterization, figure preparation, and writing the manuscript. V.J.K. performed MEA experiments and analysis, wrote parts of the manuscript, was involved in editing the manuscript, and was involved in figure preparation. H.C. designed and performed all patch-clamp experiments and analysis. A.-P.K. provided expertise in electrophysiology. M.P.-M. was involved in cardiac differentiation and cardiomyocyte analysis. E.K. planned and performed cardiac cell differentiation experiments. J.H. designed the MEA experiments. K.K. provided genetic expertise and provided genotyped patients. H.S. provided genetic and cardiological expertise on LQTS. B.R.C. helped design the study. S.Y. provided expertise in iPSC technology. O.S. helped design the study and analyze the results. K.A.-S. was leader of the group, and was involved in the planning and evaluation of the results, and finalizing the manuscript.

FUNDING

This work was supported by the Academy of Finland [grant number 126888]; the Finnish Foundation for Cardiovascular Research; Pirkanmaa Hospital District (EVO); the Finnish Cultural Foundation; Biocenter Finland; and the Sigrid Juselius Foundation.

SUPPLEMENTARY MATERIAL

Supplementary material for this article is available at http://dmm.biologists.org/lookup/suppl/doi:10.1242/dmm.008409/-/DC1

REFERENCES

Ackerman, M. J., Tester, D. J., Jones, G. S., Will, M. L., Burrow, C. R. and Curran, M. E. (2003). Ethnic differences in cardiac potassium channel variants: implications for genetic susceptibility to sudden cardiac death and genetic testing for congenital long QT syndrome. *Mayo Clin. Proc.* **78**, 1479-1487.

Carvajal-Vergara, X., Sevilla, A., D'Souza, S. L., Ang, Y.-S., Schaniel, C., Lee, D.-F., Yang, L., Kaplan, A. D., Adler, E. D., Rozov, R. et al. (2010). Patient-specific induced pluripotent stem-cell-derived models of LEOPARD syndrome. *Nature* **465**, 808-812.

Caspi, O., Itzhaki, I., Arbel, G., Kehat, I., Gepstien, A., Huber, I., Satin, J. and Gepstein, L. (2008). In vitro electrophysiological drug testing using human embryonic stem cell derived cardiomyocytes. *Stem Cells Dev.* **18**, 161-172.

Chiang, C.-E. and Roden, D. M. (2000). The long QT syndromes: genetic basis and clinical implications. *J. Am. Coll. Cardiol.* **36**, 1-12.

Couderc, J.-P., Kaab, S., Hinterseer, M., McNitt, S., Xia, X., Fossa, A., Beckmann, B. M., Polonsky, S. and Zareba, W. (2009). Baseline values and sotalol-induced changes of ventricular repolarization duration, heterogeneity, and instability in patients with a history of drug-induced torsades de pointes. *J. Clin. Pharmacol.* **49**, 6-16.

Curran, M. E., Splawski, I., Timothy, K. W., Vincen, G. M., Green, E. D. and Keating, M. T. (1995). A molecular basis for cardiac arrhythmia: HERG mutations cause long QT syndrome. *Cell* **80**, 795-803.

Fodstad, H., Swan, H., Laitinen, P., Piippo, K., Paavonen, K., Viitasalo, M., Toivonen, L. and Kontula, K. (2004). Four potassium channel mutations account for 73% of the genetic spectrum underlying long-QT syndrome (LQTS) and provide evidence for a strong founder effect in Finland. *Ann. Med.* **36 Suppl. 1**, 53-63.

Fodstad, H., Bendahhou, S., Rougier, J. S., Laitinen-Forsblom, P. J., Barhanin, J., Abriel, H., Schild, L., Kontula, K. and Swan, H. (2006). Molecular characterization of two founder mutations causing long QT syndrome and identification of compound heterozygous patients. *Ann. Med.* **38**, 294-304.

Gai, H., Leung, E. L.-H., Costantino, P. D., Aguila, J. R., Nguyen, D. M., Fink, L. M., Ward, D. C. and Ma, Y. (2009). Generation and characterization of functional cardiomyocytes using induced pluripotent stem cells derived from human fibroblasts. *Cell Biol. Int.* **33**, 1184-1193.

Hancox, J. C., McPate, M. J., El Harchi, A. and Zhang, Y. H. (2008). The hERG potassium channel and hERG screening for drug-induced torsades de pointes. *Pharmacol. Ther.* **119**, 118-132.

Hedley, P. L., Jørgensen, P., Schlamowitz, S., Wangari, R., Moolman-Smook, J., Brink, P. A., Kanters, J. K., Corfield, V. A. and Christiansen, M. (2009). The genetic basis of long QT and short QT syndromes: a mutation update. *Hum. Mutat.* **30**, 1486-1511.

Itzhaki, I., Maizels, L., Huber, I., Zwi-Dantsis, L., Caspi, O., Winterstern, A., Feldman, O., Gepstein, A., Arbel, G., Hammerman, H. et al. (2011). Modelling the long QT syndrome with induced pluripotent stem cells. *Nature* **471**, 225-229.

Kannankeril, P. J., Roden, D. M., Norris, K. J., Whalen, S. P., George, J. A. L. and Murray, K. T. (2005). Genetic susceptibility to acquired long QT syndrome: Pharmacologic challenge in first-degree relatives. *Heart Rhythm* **2**, 134-140.

Lee, G. and Studer, L. (2010). Induced pluripotent stem cell technology for the study of human disease. *Nat. Meth.* **7**, 25-27.

Lehtonen, A., Fodstad, H., Laitinen-Forsblom, P., Toivonen, L., Kontula, K. and Swan, H. (2007). Further evidence of inherited long QT syndrome gene mutations in antiarrhythmic drug-associated torsades de pointes. *Heart Rhythm* **4**, 603-607.

Männikkö, R., Overend, G., Perrey, C., Gavaghan, C. L., Valentin, J. P., Morten, J., Armstrong, M. and Pollard, C. E. (2010). Pharmacological and electrophysiological characterization of nine, single nucleotide polymorphisms of the hERG-encoded potassium channel. *Br. J. Pharmacol.* **159**, 102-114.

Marjamaa, A., Salomaa, V., Newton-Cheh, C., Porthan, K., Reunanen, A., Karanko, H., Jula, A., Lahermo, P. i., Väänänen, H., Toivonen, L. et al. (2009). High prevalence of four long QT syndrome founder mutations in the Finnish population. *Ann. Med.* **41**, 234-240.

Matsa, E., Rajamohan, D., Dick, E., Young, L., Mellor, I., Staniforth, A. and Denning, C. (2011). Drug evaluation in cardiomyocytes derived from human induced pluripotent stem cells carrying a long QT syndrome type 2 mutation. *Eur. Heart J.* **32**, 952-962.

Moretti, A., Bellin, M., Welling, A., Jung, C. B., Lam, J. T., Bott-Flügel, L., Dorn, T., Goedel, A., Höhnke, C., Hofmann, F. et al. (2010). Patient-specific induced pluripotent stem-cell models for long-QT syndrome. *N. Engl. J. Med.* **363**, 1397-1409.

Mummery, C., Ward-van Oostwaard, D., Doevendans, P., Spijker, R., van den Brink, S., Hassink, R., van der Heyden, M., Opthof, T., Pera, M., de la Riviere, A. B. et al. (2003). Differentiation of human embryonic stem cells to cardiomyocytes: role of coculture with visceral endoderm-like cells. *Circulation* **107**, 2733-2740.

Nakajima, T., Furukawa, T., Tanaka, T., Katayama, Y., Nagai, R., Nakamura, Y. and Hiraoka, M. (1998). Novel mechanism of HERG current suppression in LQT2: shift in voltage dependence of HERG inactivation. *Circ. Res.* **83**, 415-422.

Pollard, C. E., Valentin, J. P. and Hammond, T. G. (2008). Strategies to reduce the risk of drug-induced QT interval prolongation: a pharmaceutical company perspective. *Br. J. Pharmacol.* **154**, 1538-1543.

Priori, S., Napolitano, C. and Schwartz, P. (1999). Low penetrance in the long-QT syndrome. *Circulation* **99**, 529-533.

Rajala, K., Lindroos, B., Hussein, S. M., Lappalainen, R. S., Pekkanen-Mattila, M., Inzunza, J., Rozell, B., Miettinen, S., Narkilahti, S., Kerkelä, E. et al. (2010). A defined and xeno-free culture method enabling the establishment of clinical-grade human embryonic, induced pluripotent and adipose stem cells. *PLoS ONE* **5**, e10246.

Redfern, W. S., Carlsson, L., Davis, A. S., Lynch, W. G., MacKenzie, I., Palethorpe, S., Siegl, P. K. S., Strang, I., Sullivan, A. T., Wallis, R. et al. (2003). Relationships between preclinical cardiac electrophysiology, clinical QT interval prolongation and torsade de pointes for a broad range of drugs: evidence for a provisional safety margin in drug development. *Cardiovasc. Res.* **58**, 32-45.

Roden, D. M. (2004). Drug-Induced Prolongation of the QT Interval. *N. Engl. J. Med.* **350**, 1013-1022.

Roden, D. M. (2006). Long QT syndrome: reduced repolarization reserve and the genetic link. *J. Int. Med.* **259**, 59-69.

Roden, D. M. (2008). Long-QT Syndrome. *N. Engl. J. Med.* **358**, 169-176.

Schwartz, P. J. (2001). Genotype-phenotype correlation in the long-QT syndrome: gene-specific triggers for life-threatening arrhythmias. *Circulation* **103**, 89-95.

Swan, H., Viitasalo, M., Piippo, K., Laitinen, P., Kontula, K. and Toivonen, L. (1999). Sinus node function and ventricular repolarization during exercise stress test in long QT syndrome patients with KvLQT1 and HERG potassium channel defects. *J. Am. Coll. Cardiol.* **34**, 823-829.

Takahashi, K., Tanabe, K., Ohnuki, M., Narita, M., Ichisaka, T., Tomoda, K. and Yamanaka, S. (2007). Induction of pluripotent stem cells from adult human fibroblasts by defined factors. *Cell* **131**, 861-872.

Tester, D. J. and Ackerman, M. J. (2007). Postmortem long QT syndrome genetic testing for sudden unexplained death in the young. *J. Am. Coll. Cardiol.* **49**, 240-246.

Tu, E., Bagnall, R. D., Duflou, J. and Semsarian, C. (2011). Post-mortem review and genetic analysis of sudden unexpected death in epilepsy (SUDEP) cases. *Brain Pathol.* **21**, 201-208.

Yazawa, M., Hsueh, B., Jia, X., Pasca, A. M., Bernstein, J. A., Hallmayer, J. and Dolmetsch, R. E. (2011). Using induced pluripotent stem cells to investigate cardiac phenotypes in Timothy syndrome. *Nature* **471**, 230-234.

Yokoo, N., Baba, S., Kaichi, S., Niwa, A., Mima, T., Doi, H., Yamanaka, S., Nakahata, T. and Heike, T. (2009). The effects of cardioactive drugs on cardiomyocytes derived from human induced pluripotent stem cells. *Biochem. Biophys. Res. Commun.* **387**, 482-488.

Yu, J., Vodyanik, M. A., Smuga-Otto, K., Antosiewicz-Bourget, J., Frane, J. L., Tian, S., Nie, J., Jonsdottir, G. A., Ruotti, V., Stewart, R. et al. (2007). Induced pluripotent stem cell lines derived from human somatic cells. *Science* **318**, 1917-1920.

Zhang, S. (2006). Isolation and characterization of IKr in cardiac myocytes by Cs+ permeation. *Am. J. Physiol. Heart Circ. Physiol.* **290**, H1038-H1049.

Zwi, L., Caspi, O., Arbel, G., Huber, I., Gepstein, A., Park, I.-H. and Gepstein, L. (2009). Cardiomyocyte differentiation of human induced pluripotent stem cells. *Circulation* **120**, 1513-1523.

Ahola et al. BioMedical Engineering OnLine 2014, 13:39
http://www.biomedical-engineering-online.com/content/13/1/39

BioMedical Engineering OnLine

RESEARCH Open Access

Video image-based analysis of single human induced pluripotent stem cell derived cardiomyocyte beating dynamics using digital image correlation

Antti Ahola[1*†], Anna L Kiviaho[2†], Kim Larsson[2], Markus Honkanen[3], Katriina Aalto-Setälä[2,4,5] and Jari Hyttinen[1]

* Correspondence: antti.l.ahola@tut.fi
†Equal contributors
[1]Computional Biophysics and Imaging Group, Department of Electronics and Communications Engineering, and BioMediTech, Tampere University of Technology, Tampere, Finland
Full list of author information is available at the end of the article

Abstract

Background: The functionality of a cardiomyocyte is primarily measured by analyzing the electrophysiological properties of the cell. The analysis of the beating behavior of single cardiomyocytes, especially ones derived from stem cells, is challenging but well warranted. In this study, a video-based method that is non-invasive and label-free is introduced and applied for the study of single human cardiomyocytes derived from induced pluripotent stem cells.

Methods: The beating of dissociated stem cell-derived cardiomyocytes was visualized with a microscope and the motion was video-recorded. Minimum quadratic difference, a digital image correlation method, was used for beating analysis with geometrical sectorial cell division and radial/tangential directions. The time series of the temporal displacement vector fields of a single cardiomyocyte was computed from video data. The vector field data was processed to obtain cell-specific, contraction-relaxation dynamics signals. Simulated cardiomyocyte beating was used as a reference and the current clamp of real cardiomyocytes was used to analyze the electrical functionality of the beating cardiomyocytes.

Results: Our results demonstrate that our sectorized image correlation method is capable of extracting single cell beating characteristics from the video data of induced pluripotent stem cell-derived cardiomyocytes that have no clear movement axis, and that the method can accurately identify beating phases and time parameters.

Conclusion: Our video analysis of the beating motion of single human cardiomyocytes provides a robust, non-invasive and label-free method to analyze the mechanobiological functionality of cardiomyocytes derived from induced pluripotent stem cells. Thus, our method has potential for the high-throughput analysis of cardiomyocyte functions.

Keywords: Cardiomyocyte mechanic functionality, Velocity vector analysis, Minimum quadratic difference method

Introduction

The withdrawal of drugs already on the market is most commonly due to cardiac side effects. Cardiac safety analyses are currently done using animals as model organisms and/or ectopic expression of single ion channels in non-cardiac human cells [1]. These applications do not provide an optimal platform to explore the conditions in human cardiac cells. Unfortunately, human cardiomyocytes (CMs) have been very challenging to study, since the myocardial biopsy is a high-risk procedure and primary CMs dedifferentiate quickly and stop beating in cell culture conditions. Also, the available methods to measure the functionality of a cardiomyocyte (CM) are challenging and do not provide high throughput.

Moreover, recent developments in stem cell technology, namely the invention of induced pluripotent stem (iPS) cells, have increased the need for new methods to characterize cells derived from iPS cells. iPS cells can be obtained from any individual by reprogramming already differentiated mature cells such as skin fibroblasts into a pluripotent state [2]. Therefore, by using iPS cells it is possible to obtain genetically defined human pluripotent cells that can be differentiated into the cell type of interest, for example CMs [3]. Recently, it has been shown that human iPS cell-derived CMs have proper electrophysiological properties and assays using these cells can provide a reliable alternative to preclinical in vitro testing [4].

The functional measurement of single CMs has traditionally been laborious and time consuming. There are a few tools available for the study of the electrical properties of individual cells. Patch clamp is a commonly used method for analyzing the functionality of single CMs, but this technique requires special, relatively expensive instrumentation, and laborious manual work that requires highly skilled personnel [5]. Microelectrode arrays (MEA) provide a platform for the analysis of larger aggregates of cells with less manual work. Due to the dimensions of the electrodes and the distances between the electrodes, however, they are not suited for single cell functionality studies [6]. Voltage sensitive dyes such as di-8-ANEPPS provide one solution for the analysis of single CMs. This method, however, is based on fluorescence imaging and the dyes interact with some ion channels, e.g. the product of the human Ether-à-go-go-Related Gene (hERG), and thus potentially alter the electrophysiological properties of the cells [7].

The electrical functionality of single CMs does not directly reveal the mechanical properties of the cells. Atomic force microscopy (AFM) can be used to quantify the mechanical properties of CMs, e.g. force. However, AFM is not well suited for long-term measurements because it interferes with the cell [8]. Cellular electric impedance measured with well plate integrated electrodes is also used to measure the beating characteristics of cardiomyocytes [9]. The spatial resolution of the method is, however, not high enough to study the movements within the cell in detail. High-speed video microscopy can be used to obtain information from the beating cycle. Such methods quantify the movement of single CMs with no intervention. By analyzing the movements of the cells, it is possible to receive data from the mechanobiological functionality of the cell and to combine the data with electrical measurements to understand electro-mechanical coupling. Traditional video-based CM analysis methods [10,11] may not, however, be optimal for the study of single iPS cell-derived CMs. The sarcomere structure of iPS cell-derived CMs is not fully organized [12] and, therefore, their

beating is less uniform with no main contraction direction. Thus, better methods are required that are robust in the detection of movement signals from these types of cells.

Here, we propose a robust, non-invasive method for the analysis of the beating dynamic of single CMs with no clear axis of contraction by using recorded microscope videos. The method is based on digital image correlation (DIC), more specifically its subtype the minimum quadratic difference (MQD) method that has been developed mainly for particle image velocimetry (PIV). Further, we use sectorial derivation of movement directions. The aim is to provide detailed physical information on the dynamics and timing of the contraction and relaxation of stem cell-derived CMs. The previous methods used to analyze video data [10,11] are not well suited for the analysis of heterogeneous beating. Our method is specifically aimed towards the use of CMs derived from iPS cells. We present validation tests of the method using artificial displacement images and current clamp recordings from human iPS cell-derived CMs. Since the CMs derived from the cell line used here have not previously been fully characterized, we also briefly provide the biological characterization data.

Materials and methods

Ethics statement

The study was approved by the Ethical Committee of the Pirkanmaa Hospital District (R08070). A written informed consent from participants has been obtained.

Cell culture

Primary fibroblasts were obtained from skin biopsy and cultured under fibroblast culturing conditions: Dulbecco's modified eagle medium (DMEM, Lonza, Switzerland) containing 10% FBS, 2 mmol/l L-glutamine and 50 U/ml penicillin/streptomycin. 293FT-cells (Invitrogen, CA, USA) were maintained similarly with 1% non-essential amino acids (NEAA, Cambrex, NJ, USA). Plat-E-cells (Cell Biolabs, CA, USA) and irradiated or mitomysin C (Sigma-Aldrich, MO, USA) treated mouse embryonic fibroblast (MEF, Millipore, MA, USA) cells were cultured in the same conditions but without antibiotics. iPS cells were cultured with MEF cells as feeders in KSR-medium: knockout (KO)-DMEM (Invitrogen) containing 20% KO-serum replacement (KO-SR, Invitrogen), NEAA, L-glutamine, penicillin/streptomycin, 0.1 mmol/L 2-mercaptoethanol, and 4 ng/ml basic fibroblast growth factor (bFGF, R & D Systems Inc., MN, USA).

iPS cells

iPS cell lines were established from the dermal fibroblasts of a 55 year old female using lentivirus infection followed by retrovirus infection into the fibroblasts. The following cells, plasmids and reagents were used: 293FT-cells, Plat-E-cells, pLenti6/UbC/mSlc7a1-vector (Addgene, MA, USA), ViraPower™ Packaging Mix (Invitrogen), Lipofectamine™ 2000 (Invitrogen), pMX retroviral vector (hOCT3/4, hSOX2, hKLF4 or hc-MYC, Addgene), and Fugene 6 (Roche Diagnostics, Germany). The full and detailed protocol has been described earlier [2,13]. Two iPS cell lines from the same individual were used for the studies: UTA.04602.WT and UTA.04607.WT.

Characterization of iPS cells

Reverse transcription polymerase chain reaction (RT-PCR). Total RNA was collected from the iPS cells at passage 6 and purified with a NucleoSpin RNA II -kit

(Macherey-Nagel, Germany). cDNA conversion was carried out with a high-capacity cDNA RT -kit (Applied Biosystems, CA, USA) using 200 ng of RNA. RT-PCRs were carried out with Dynazyme II (Finnzymes Oy, Finland) using 1 μl of cDNA as a template and 5 μM primers. As positive controls for exogenous primers, PCR was also carried out using the transfected plasmids (hOCT3/4, hSOX2, hKLF4, and hc-MYC) as templates. Primers and reaction conditions for iPS cell characterization [2] and PCR-primers for different germ layer markers [13] have been described earlier. β-actin and glyceraldehyde 3-phosphate dehydrogenase (GAPDH) were used as housekeeping control genes. **Immunocytochemistry for pluripotency.** iPS cells at passage 8 were fixed with 4% paraformaldehyde (PFA, Sigma-Aldrich) and stained with anti-Oct3/4 (1:400, R & D Systems), anti-TRA1-60 (1:200, Millipore), anti-Sox2, anti-Nanog, anti-SSEA4, and anti-TRA1-81 (all 1:200, Santa Cruz Biotechnology, CA, USA). The secondary antibodies (1:800, Invitrogen) were Alexa-Fluor-568-donkey-anti-goat-IgG, Alexa-Fluor-568-goat-anti-mouse-IgM, or Alexa-Fluor-568-donkey-anti-mouse-IgG. Vectashield mounting medium with DAPI (4′,6-diamidino-2-phenylindole, Vector Laboratories Inc., CA, USA) was used to stain nuclei. **Karyotype analysis.** A commercial company (Medix laboratories, Finland) defined the karyotypes of the iPS cell lines by using G-banding chromosome analysis according to standard protocol. **Formation of embryoid bodies (EBs).** EBs were cultured without feeder cells in EB-medium (KO-DMEM with 20% fetal bovine serum (FBS), NEAA, L-glutamine and penicillin/streptomycin) without bFGF for 5 weeks. RNA isolation and reverse transcription from the EBs was performed as described above. The expression of markers characteristic of ectoderm, endoderm, and mesoderm development in EBs was determined using RT-PCR (see above).

Cardiac differentiation and characterization

CM differentiation was performed by co-culturing iPS cells together with END-2-cells. END-2-cells were cultured as described earlier [14]. To initiate CM differentiation, undifferentiated iPS cell colonies were dissected mechanically into aggregates containing a few hundred cells and placed on the top of Mitomycin C -treated END-2 cells in KSR-culture medium without fetal bovine serum, serum replacement, or basic fibroblastic growth factor. Ascorbic acid (Sigma-Aldrich) was also added into the medium with a final concentration of 2.92 mg/ml [15]. The differentiating cell colonies were monitored by microscopy daily and the medium was changed after 5, 8, and 12 days of culturing. After 14 days, the 10% SR was added to the medium and ascorbic acid was no longer used. **RT-PCR for cardiac markers.** RNA was collected from beating cardiac cells and transcribed into cDNA as described for the pluripotent cells above. The reverse transcription polymerase chain reaction (RT-PCRs) were also carried out in a way similar to that of the pluripotency markers and primers of cardiac markers that have been described earlier [13]. **Immunocytochemical staining.** The spontaneously beating areas of the colonies were mechanically excised and treated with collagenase A (Roche Diagnostics) as described by Mummery et al. [14]. Seven days after dissociation, the cells were fixed with 4% paraformaldehyde for immunostaining with anti-cardiac-troponin-T (1:1500, Abcam, MA, USA), anti-α-actinin (1:1500, Sigma-Aldrich), anti-myosin-heavy-chain (MHC, 1:100, Millipore), anti-atrial-myosin-light-chain (MLC2a, 1:300, Abcam), and anti-ventricular-myosin-light-chain (MLC2v, 1:150, Abcam). The secondary antibodies (1:800, Invitrogen) were Alexa-Fluor-568-donkey-anti-goat-IgG,

Alexa-Fluor-568-coat-anti-mouse-IgG, Alexa-Fluor-488-donkey-anti-rabbit, and Alexa-Fluor-488-donkey-anti-mouse. Vectashield mounting medium with DAPI was used to stain the nuclei. Dissociated CMs were prepared for video recording in the same way as for immunocytochemical staining.

Video microscopy

Videos of the dissociated spontaneously beating single CMs were recorded using video microscopy. Both iPS cell lines were used in the recordings and they gave identical results. Thirteen CMs were video-recorded for 30 s at 30 frames per second under sterile conditions. The CMs were visualized using a Nikon Eclipse TS100 (Nikon Corporation, Japan) microscope and monochrome 8 bit videos were acquired with an Optika DIGI-12 (Optika Microscopes, Italy) camera mounted on the microscope. Additionally, two CMs were videoed and their concurrent action potentials were acquired with current clamp measurement for combined functionality verification. In this series, a high resolution 14 bit Andor XION 885 (Andor Technology, UK) camera mounted on an Olympus IX51 (Olympus Corporation, Japan) microscope was used. Transmission images were acquired for 60 s at 50 frames per second using TILLvisION (TILL photonics GmbH, Germany).

Digital image correlation analysis

The term DIC refers to methods that acquire images and perform analysis for full-field shape, deformation and/or motion measurements [16]. The images are divided into small sub-regions where the grayscale values are cross-correlated between the consecutive image frames to provide a displacement map that indicates the movements of the scene [16]. Standard cross-correlation analysis emphasizes bright pixels due to the multiplication of intensity values [16]. In CM images, however, all image pixels regardless of their grayscale value can contribute to the motion analysis. Therefore, the weighting of bright pixels in the standard cross-correlation analysis is a clear disadvantage. In this study, we removed this disadvantage by using the MQD method [17] that puts equal weight to all image pixels. Additionally, MQD has been shown to be more accurate than other PIV evaluation methods based on correlation [18]. The MQD method was originally developed to evaluate PIV recordings. It uses a least-square principle to obtain the velocity vector field across the image based on two consecutive video frames [16]. Image sub-regions (i, j) are compared between the consecutive image frames (I_1 and I_2) using the function (1):

$$S_{i,j}(dx, dy) = \sum_{x=-N/2}^{N/2} \sum_{y=-N/2}^{N/2} [I_1(i+x, j+y) - I_2(i+x+dx, j+y+dy)]^2, \quad (1)$$

where x and y are the indices to the pixels inside the sub-region of size [N, N]. The sub-region in the second frame I_2 is shifted in x- and y-directions by dx, dy to obtain a value at point (dx, dy) in the quadratic difference map $S_{i,j}$ of sub-region (i, j). The computational ranges of dx and dy can be freely selected to match the application. The location of the minimum value in $S_{i,j}$ reveals the medial displacement of the scene inside the sub-region (i, j). Due to small displacements between CM frames, the necessary sub-pixel accuracy in displacement estimation is obtained by sub-pixel fitting on the

minimum value (dx, dy) in $S_{i,j}$ with a 1-dimensional 3-point Gaussian interpolation fitting function (2) to determine the correlation peak [19].

$$\Delta x = \frac{\ln(S(dx-1,dy)) - \ln(S(dx+1,dy))}{2[\ln(S(dx+1,dy)) - 2\ln(S(dx,dy)) + \ln(S(dx-1,dy))]},$$

$$\Delta y = \frac{\ln(S(dx,dy-1)) - \ln(S(dx,dy+1))}{2[\ln(S(dx,dy+1)) - 2\ln(S(dx,dy)) + \ln(S(dx,dy-1))]} \quad (2)$$

Cardiomyocyte analysis with MQD

Single CMs recorded on video were manually segmented for MQD analysis. The non-moving parts of the cell were cropped outside of the region of interest to decrease processing time and noise. To obtain a cell-specific coordinate system for the beating analysis, the beating focus point of the cell is selected by visual approximation from the video and the region of interest is divided into 8 sectors, each comprising a 45-degree sector from the beating focus (Figure 1A). This enables the analysis of the inconsistent beating patterns of iPS-derived CMs. For each velocity vector in a sector, two dot products are calculated. First with regard to the center line of the sector, to calculate the approximate radial component, and second with regard to the normal of the center line, to calculate the approximate tangential component (Figure 1B). The centerline normals pointing towards sectors 1–4 were selected for sectors 1–4, and the normals pointing towards 5–8 for sectors 5–8. For each sector, the sum of these vector components was calculated. In total, 16 different signals, 8 radial and 8 tangential signals, were obtained from a video.

The analysis was conducted using open source Matlab algorithm mpiv [20]. A 16×16 px subwindow size with a 0.5 overlap ratio was used. The resulting vectors were smoothed using a median filter. Possible stray vectors were determined and removed if the vector was outside the range of 2.5 times the standard deviation from the mean value. Kriging interpolation was used to assign values for vectors that did not have applicable values. Finally, weighting was used to smooth the vector field using a 3×3 kernel $\begin{matrix} 1 & 2 & 1 \\ 2 & 4 & 2 \\ 1 & 2 & 1 \end{matrix}$ as a low-pass filter.

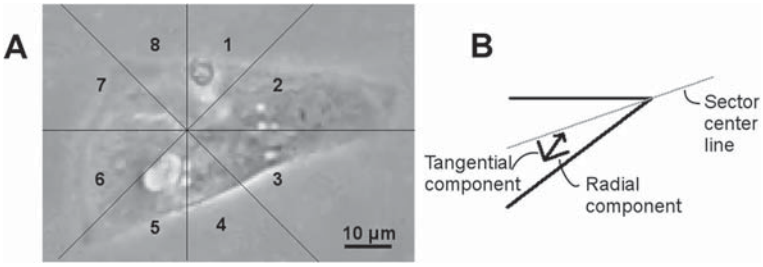

Figure 1 Beating analysis framework. A: The cell is divided into 8 sectors, each being of 45°, with the center point being at the observed beating focus point of the cell. The sectors are numbered in a clockwise manner. **B**: The radial and tangential components of the velocity vectors in each sector are calculated with regard to the sector centerline going through the beating focus point.

Data verification

The proposed beating analysis was verified using artificial displacement images. We modified still CM images so that they modeled the displacement of the pixels during CM beating with known displacement. An image distortion filter [21] was modified and used on a CM image to create artificial distortions that resembled the various stages of a beating iPS cell-derived CM with no main contraction axis. The resulting images were analyzed using the MQD method. Figure 2 illustrates the effect of the artificial distortion on an even grid image and on a CM image.

The artificial images for the video were constructed by stretching the cell with the distortion γ. Each point (x, y) in the original image within a set radius from the determined beating focus was mapped onto a virtual half-sphere of radius R, and a new distance X to the beating focus point was set-based on the desired distortion factor γ, as done in the original image distortion filter.

With this method, an image of a cell was modified with varying values of γ and combined to a video to get artificial cell data resembling that of a beating cell. Artificial images were created using 5 different γ values: −1, −2, −4, −7, and −10. The video was created from a total of 51 frames representing two beats that comprised 10 still frames, 5 frames with decreasing γ values, 5 frames with increasing γ values, 11 still frames, 5 frames with decreasing γ values, 5 frames with increasing γ values, and finally 10 still frames. Figure 2A shows an unmodified, original image of the cell and Figure 2B an image distorted using the explained method with γ = −10. The values of X define the displacement that can be compared with the results of the MQD analysis due to symmetry.

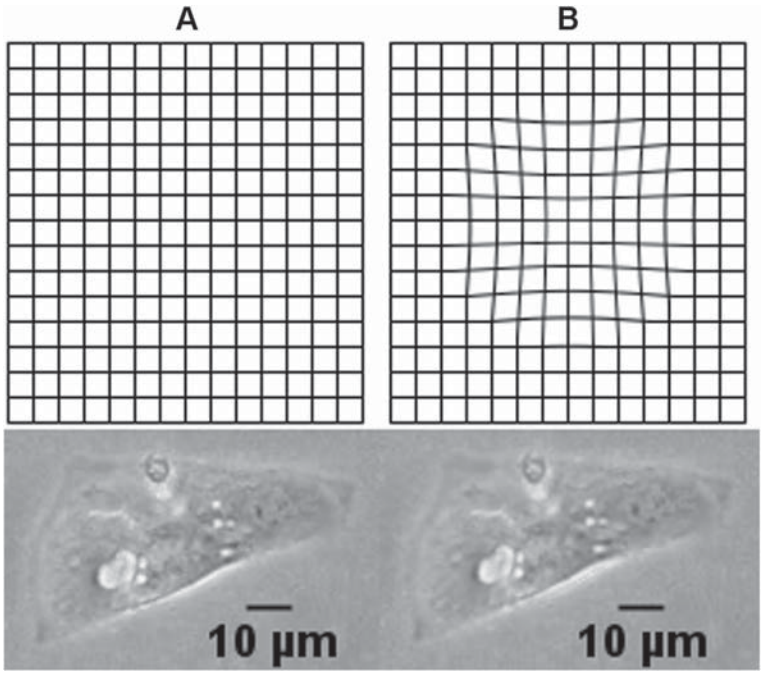

Figure 2 Artificial data set created from a cardiomyocyte image. An even grid and a cardiomyocyte image are shown to illustrate the effect of the artificial deformation that was used to create the data set. **A**: An even grid and a cardiomyocyte image without the artificial deformation. **B**: An even grid and a cardiomyocyte image with the described deformation applied, γ = 10.

Noise resistance testing

The noise resistance of the proposed method was tested by adding multiplicative speckle noise to each frame of the generated artificial video data that was obtained from modifying a CM image, as explained above. The cell size was 6796 pixels. Speckle noise was added to each image using the equation $J = I + \sqrt{12 * V} * I * I_r$, where I is the original image, J is the resulting image, V is variance and I_r is uniformly distributed random noise between values −0.5 and 0.5, with mean of 0. 8. The following noise variances were used: 0, 0.03, 0.05, 0.07, 0.09, 0.011, 0.013, and 0.015.

Beating analysis of cardiomyocytes

The analysis was carried out for the 13 CMs recorded on video. The time required for each phase of beating was measured: the contraction, the time it stayed contracted, the relaxation time, and the time it stayed relaxed. The beating frequency was also measured.

Current clamp measurement

To further verify the findings, the proposed video analysis was conducted from video data recorded from iPS cell-derived CMs with concurrent current clamp measurement. Action potentials were recorded using the Axopatch 200B patch clamp amplifier connected to an acquisition computer via AD/DA Digidata 1440 (Molecular devices, USA). The measurement was carried out at room temperature in gap free mode using the standard current clamp configuration in perforated patch mode. The HEPES (4-(2-hydroxyethyl)-1-piperazineethanesulfonic acid)-based extracellular perfusate for current clamp recordings comprised (in mmol/l): 143 NaCl, 5 KCl, 1.8 $CaCl_2$, 1.2 $MgCl_2$, 5 glucose, and 10 HEPES. The pH was adjusted to 7.4 with NaOH and the osmolarity set to 300 ± 2 mOsm (Gonotec, Osmomat 030, Labo Line Oy, Finland). The intracellular solution comprised (in mmol/l): 122 $KMeSO_4$, 30 KCl, 1 $MgCl_2$, and 10 HEPES. KOH was used to set pH to 7.15 and the osmolarity was set to 295 ± 2 mOsm. Amphotericin B (Sigma-Aldrich) was used as a membrane perforation agent and was dissolved in dimethyl sulfoxide to a final concentration in the patch pipette of 0.24 mg/ml. Current-clamp recordings were digitally sampled at 20 kHz and filtered at 5 kHz using the lowpass Bessel filter on the recording amplifier.

Combining current clamp and video analysis

TTL synchronization pulses (1 pulse per frame) were delivered by the digital signal processor-driven imaging control unit (programmed in TILLvisION) to synchronize the transmission frames and current clamp data sampling. The pulses and current clamp data were concurrently sampled using 2 channels in current clamp. The video data obtained simultaneously with the current clamp measurement was processed using the proposed method.

Results

Characterization of induced pluripotent stem cells

The generated iPS cells were first characterized by the morphology of the cell colonies and the individual cells that exhibited similar characteristics to those of human embryonic stem cells: compact and round in shape (Figure 3A), defined edges and distinct cell borders (Figure 3B). The iPS cells also expressed endogenous pluripotent marker genes at the

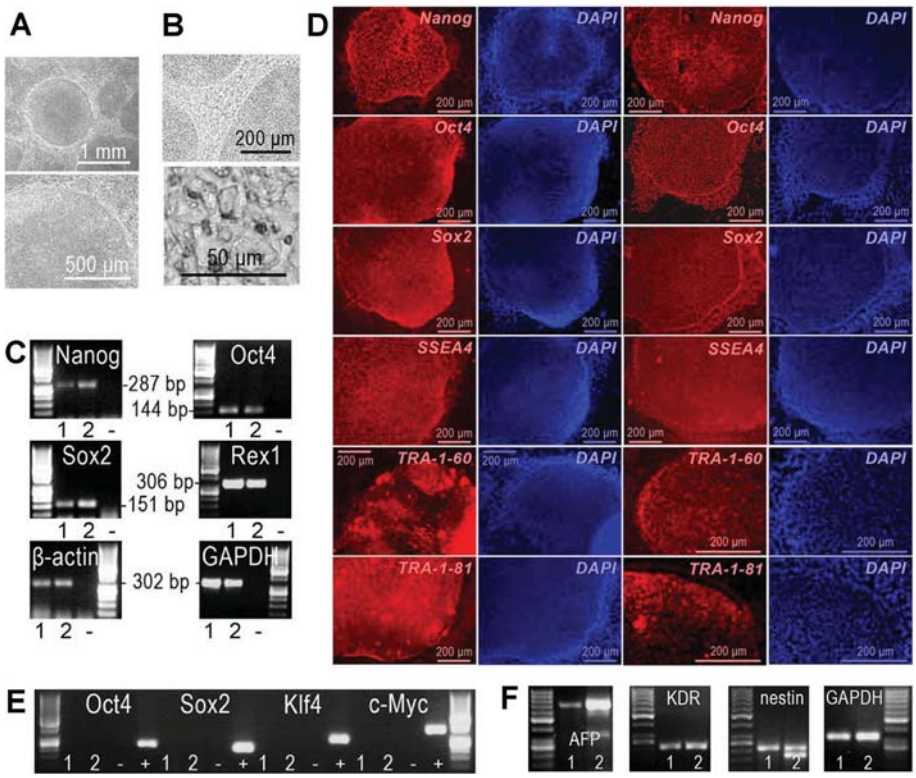

Figure 3 Characterization of iPS cells for their pluripotency. Number 1 represents the cell line UTA.04602.WT and 2 the line UTA.04607.WT. **A**: iPS cells formed typical colonies for pluripotent stem cells that are rather compact and round in shape. **B**: The iPS cell colonies typically had well defined edges and distinct cell borders, and the iPS cells had a high nucleus to cytoplasm -ratio and a large nucleoli characteristic for stem cells. **C**: Endogenous pluripotency gene expression was studied using RT-PCR. Nanog, Oct4, Sox2 and Rex1 were all expressed at mRNA level in the iPS cells. β-actin and GAPDH were used as housekeeping control genes for both endogenous and exogenous markers. **D**: The expression of pluripotency genes was also studied at the protein level by immunocytochemical staining. The iPS cell expressed several markers for the pluripotent state: Nanog, Oct4, Sox2, SSEA4, TRA-1-60, and TRA-1-81 (all in red). Pictures in the left panel are from the line UTA.04602.WT and the ones on the right side are from UTA.04607.WT. Blue in all pictures indicates the DAPI staining of nuclei. **E**: Using RT-PCR, it was shown that all the transgenes were silenced in the iPS cells. Negative control is marked with "-" and positive control with "+". **F**: Embryoid body (EB) -assay was used to define the pluripotency of the iPS cells *in vitro*. Markers for all three germ layers were detected from the EBs formed from both cell lines. Alpha-fetoprotein (AFP) was used as a marker for endoderm, kinase insert domain receptor (KDR, also known as vascular endothelial growth factor receptor 2 (VEGFR-2) was used as a marker for mesoderm and nestin was used as an ectoderm marker. GAPDH was used as an endogenous control gene.

mRNA level that was shown by RT-PCR (Figure 3C). The expression of pluripotency genes also at the protein level was demonstrated by the immunocytochemical staining of different markers for pluripotent stem cells (Figure 3D). On the other hand, transgene expression was turned off in the iPS cells (Figure 3E). To confirm the pluripotent state of the iPS cells, an EB formation assay was carried out. The cells from the EBs were shown to express marker genes from all three germ layers: endoderm, ectoderm, and mesoderm (Figure 3F). The generated cell lines were also analyzed for their karyotypes and were both found to be normal (Figure 4A and B).

Characterization of the cardiomyocytes differentiated from iPS cells

Generated iPS cells were differentiated into spontaneously beating CMs that expressed different cardiac markers. Using RT-PCR, it was shown that troponin T (TNTT2),

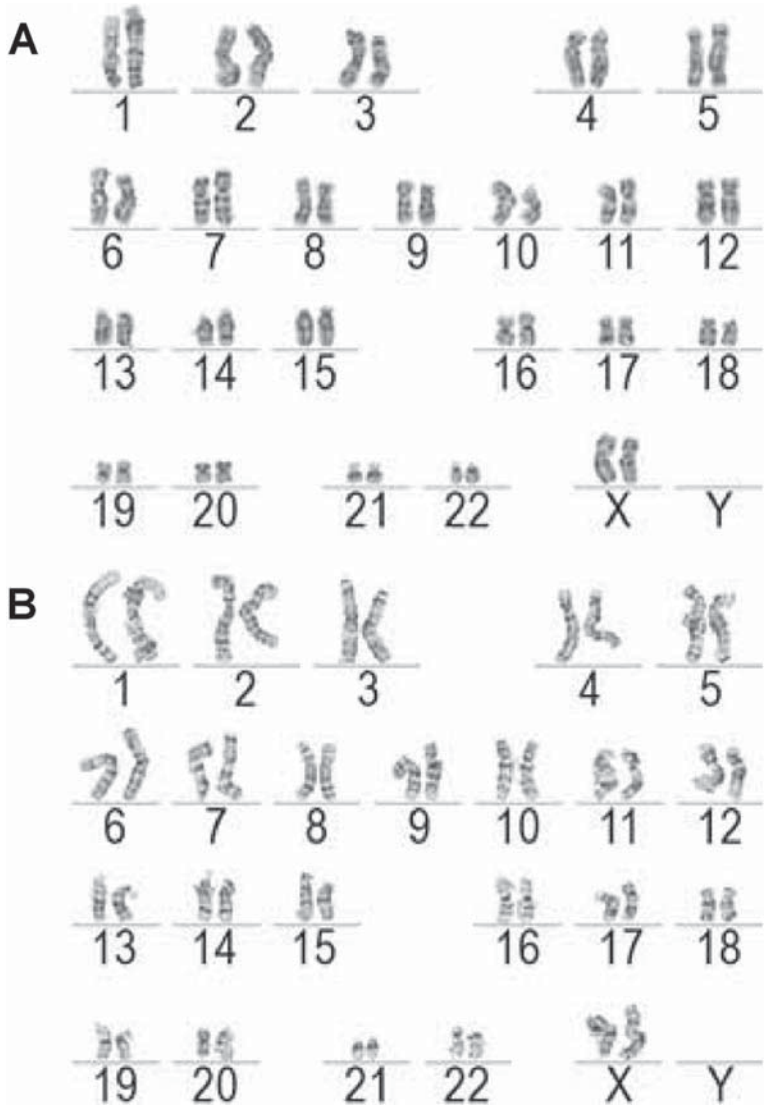

Figure 4 Karyotype analysis from iPS cells. A & **B**: The lines were verified for normal karyotypes (G: UTA.04602.WT and H: UTA.04607.WT).

MLC2v, MLC2a, connexin-43 (Cx-43), myosin heavy chain (MYH7), hERG, and GATA4 were expressed in the cells (data not shown for hERG and GATA4) (Figure 5A). The expression of cardiac marker genes at the protein level was also confirmed (Figure 5B). With immunocytochemical staining, it was also shown that both atrial and ventricular cells were present among the iPS cell-derived CMs (data not shown). The electrical properties of the iPS cell-derived CMs were also characterized using a microelectrode array that revealed that the cell aggregates exhibited appropriate beating rates and field potentials (Figure 5C and D).

Beating signals of iPS cell-derived CMs

The method was applied on iPS-derived CMs to obtain beating signals. One such signal that shows two beats is shown in Figure 6A. For radial components, contraction was

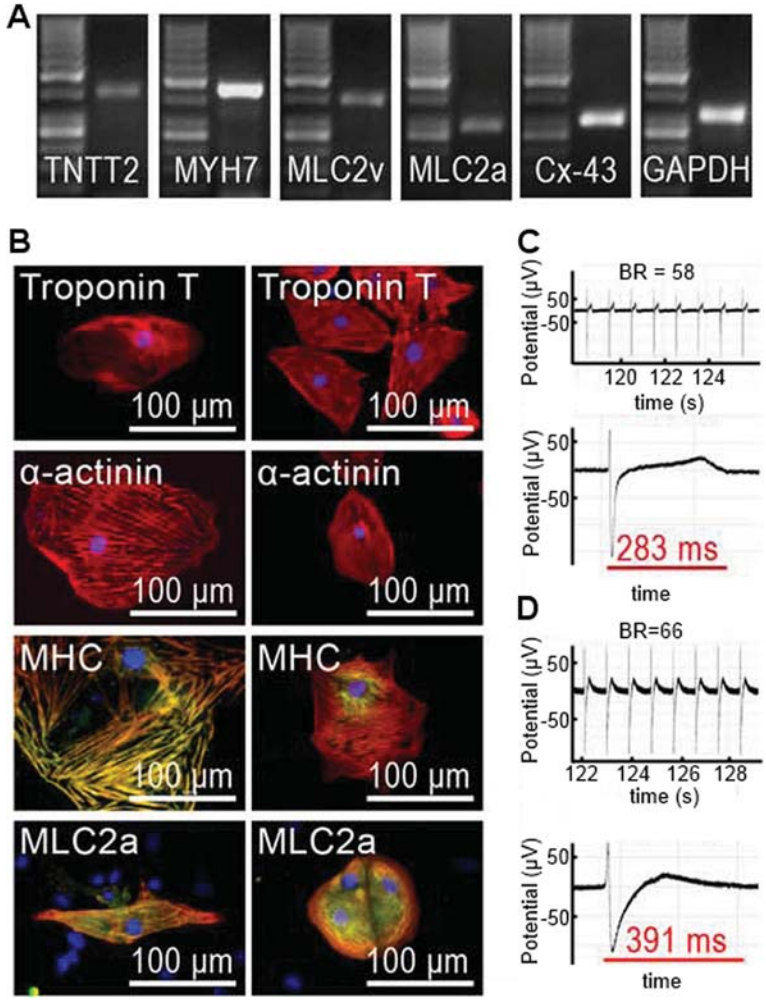

Figure 5 Cardiomyocytes differentiated from the iPS cells. A: Several cardiac markers were discovered using RT-PCR indicating their expression at mRNA level. Data from UTA.04602.WT is shown here. **B**: By immunocytochemical staining it was shown that the iPS cell-derived cardiac cells express proteins specific for cardiomyocytes. Cardiac troponin T, α-actinin, myosin heavy chain (MHC) and atrial myosin light chain 2 (MLC2a) were detected from the cells. The pictures on the left side are from the line UTA.04602.WT and the pictures on the right side are from UTA.04607.WT. In the pictures showing MHC and MLC2a with green fluorescent, red indicates troponin T and in all pictures DAPI staining of nuclei is seen in blue. **C** & **D**: A micro electrode array (MEA) was used to define the electrical properties of the iPS cell-derived cardiomyocytes. The beating rates (BR) and field potential durations (FPD) of cell aggregates were evaluated (B: UTA.04602.WT, BR = 58, FPD = 283 ms and C: UTA.04607.WT, BR = 66, FPD = 391 ms).

defined negative (Figure 6A II) and relaxation positive (Figure 6A III). Figure 6B illustrates a typical signal.

From the 13 measured cells, the time parameters of the different phases of the beating were calculated from the sum displacement signal using the proposed method. The phases were the following: contraction, time the cell was contracted, relaxation, and the time the cell was relaxed. The average values of three analysis signals for each cell were calculated. The results for each cell measurement are presented in Table 1.

Figure 6C shows all 16 velocity signals obtained from one of the measured cells.

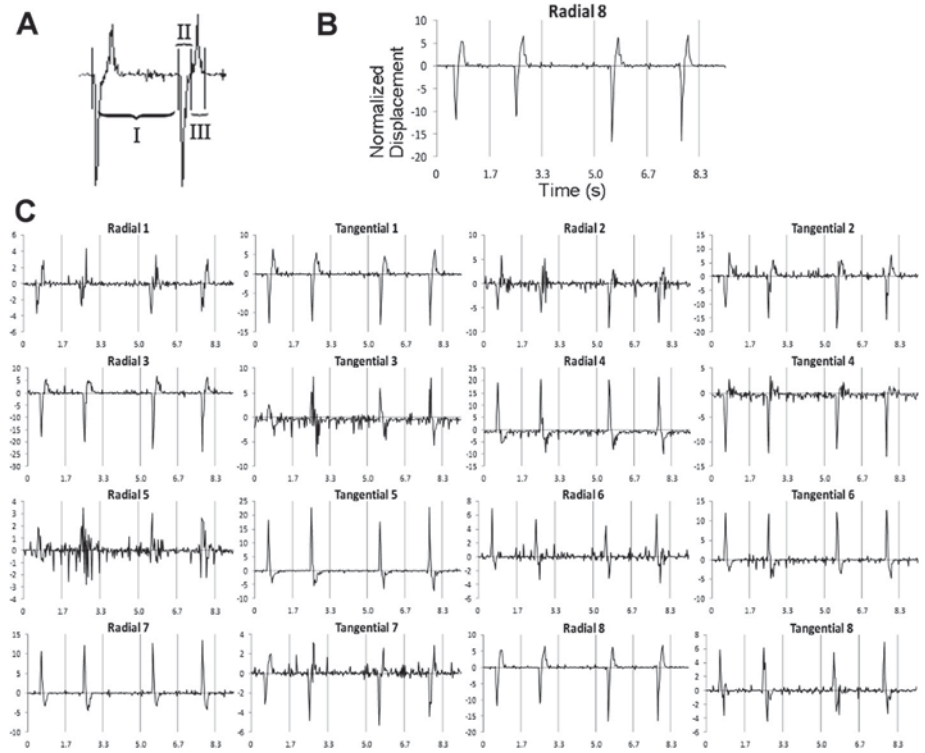

Figure 6 The beating signals obtained from an iPS cell-derived CM. A: The classification of beating phases. The time between each individual beat is marked with I. Contraction movement is defined as negative movement (marked with II) and relaxation movement as positive (marked with III). **B**: An enlarged image of the sector 8 radial component. **C**: The beating signals of each sector obtained from one of the measured CMs. For various sectors, the contraction seems to push certain areas away from the perceived beating focus point. This results in an upward peak in lieu of a downward peak due to the fusiform nature of the beating. While most sectors produce a signal of high quality, sectors such as radial 5 have too little movement to generate a well-formed displacement signal.

Method verification using artificial displacement images

The DIC analysis results created using artificial displacement images are illustrated in Figure 7. The figure shows (A) the division of the cell into analysis sectors, (B) the displacement vector field during the contraction phase, (C) the known displacement velocity, and (D) the results of the DIC analysis (red) shown with the known displacement velocity (blue). The average correlation coefficient between the known displacement field and the analysis results for all 16 signals was 0.9525.

For noise resistance testing, 8 videos with speckle noise were created using different noise variances. The proposed analysis was applied to these videos. For each video, 3 segments were chosen. The average correlation between the resulting signals and the known displacement was calculated as a function of noise variance. The results for three different sectors are shown in Table 2. Example images of different noise levels are shown in Figure 8A-D.

Comparison with current clamp recording

Spontaneously beating iPS cell-derived CMs had the characteristics of ventricular- type cells. The cells were beating individually and not part of a larger beating cell cluster.

Table 1 Multiple cell analysis

Cell	Frequency (bpm)	Contraction (ms)	Contracted (ms)	Relaxation (ms)	Relaxed (ms)
1	12.03	451	18	571	3949
2	18.20	419	0	612	2265
3	22.78	321	0	444	1868
4	23.64	360	1	447	1730
5	24.12	164	0	202	2122
6	24.56	427	8	535	1472
7	25.98	179	0	346	1784
8	26.34	225	13	594	1446
9	29.13	225	0	318	1517
10	36.45	267	1	324	1053
11	41.82	216	3	295	921
12	43.13	274	30	361	727
13	66.34	209	7	315	373

Results obtained from multiple cell analysis. The times of the different beating phases in milliseconds and the corresponding beats per minute (bpm) were measured from 13 cells.

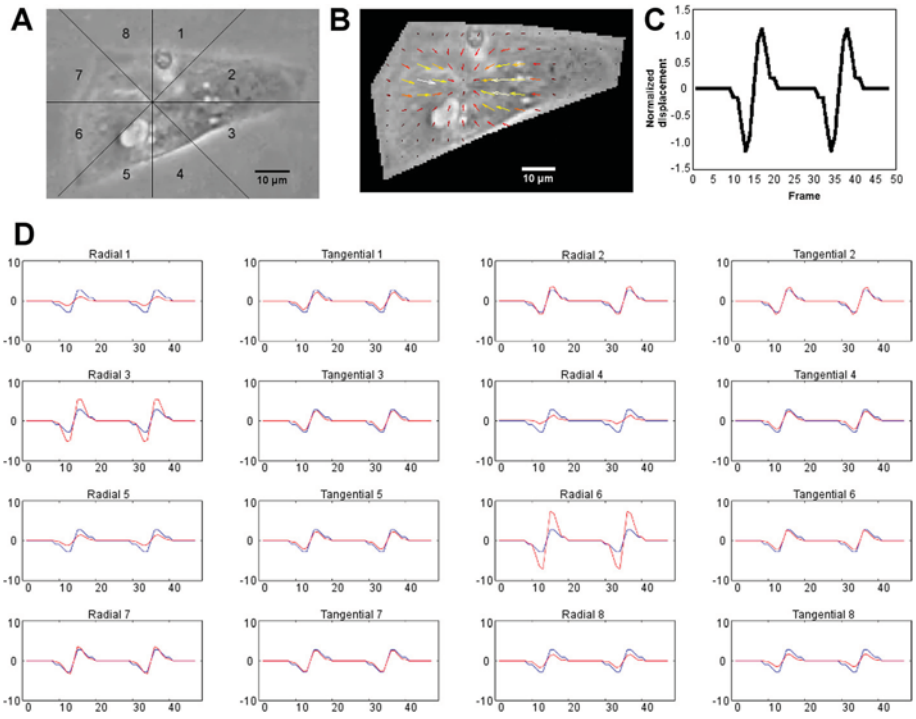

Figure 7 Comparison of measured and known motion signals in different sectors. A CM image was modified using image-processing methods with varying parameters to create a video resembling the contraction and relaxation of the cell. In the upper row are illustrated **A**: the sector division, **B**: the velocity vector field during the contraction, and **C**: the known displacement velocity. Since the artificial displacement has circular symmetry, a horizontal cross-sectional displacement is shown. **D**: The proposed method was applied to the video data and the signal marked with red was obtained. A blue signal illustrates the known displacement field.

Table 2 Analysis result correlation with known displacement

	Radial component 1		Radial component 3		Radial component 5	
Noise variance	AVG	SD	AVG	SD	AVG	SD
0	0.964	0.000	0.952	0.000	0.939	0.000
0.003	0.922	0.034	0.956	0.005	0.781	0.150
0.005	0.761	0.111	0.950	0.013	0.532	0.152
0.007	0.480	0.364	0.926	0.076	0.359	0.389
0.009	0.490	0.177	0.894	0.050	0.456	0.209
0.011	0.423	0.342	0.671	0.310	0.334	0.228
0.013	0.183	0.385	0.441	0.250	0.325	0.324
0.015	0.259	0.335	0.435	0.440	−0.041	0.410

The average correlations (AVG) of the analysis results with the known displacement field and their standard deviations (SD). Noise with variances ranging from 0 to 0.015, with example images shown in Figure 6A-D, was added to video frames that comprised the artificial displacement images of a cardiomyocyte. The average correlation of 8 videos between the analysis results and the known displacement was determined, along with the standard deviation.

The velocity vector data was integrated with respect to time in order to obtain position data, and compared with the current clamp data to see the relationship between the mechanical and electrical activity. The time between the peaks of electrical activity and mechanical activity was calculated from the synchronized data.

The DIC signal onset occurred after the action potential onset and the action potential declined earlier. Figure 9 shows both signals from one of the recorded cells in the same graph. The basic action potential parameters for the recorded cell are listed in Table 3. The time difference between the peaks of action potentials and the maximum displacement was 306 ms with a 40 ms standard deviation. The result is in line with previously reported values [22].

Discussion

We developed a microscope video analysis method to provide accurate and detailed information on the beating motion dynamics of single CMs, especially those derived from stem cells. We observed that our DIC-based methods are promising for the study of

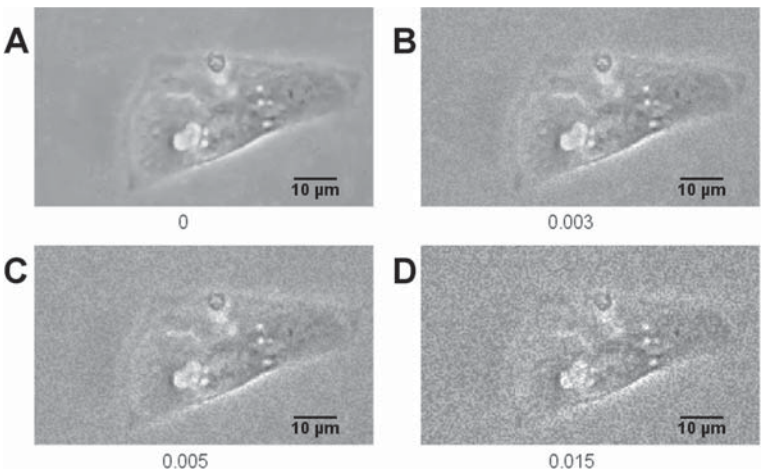

Figure 8 Assessment of the effect of noise on video beating analysis. Varying degrees of speckle noise variance were added to a video for testing noise resistance. **A-D**: Example images for four noise variance levels are shown: 0, 0.003, 0.005, and 0.015.

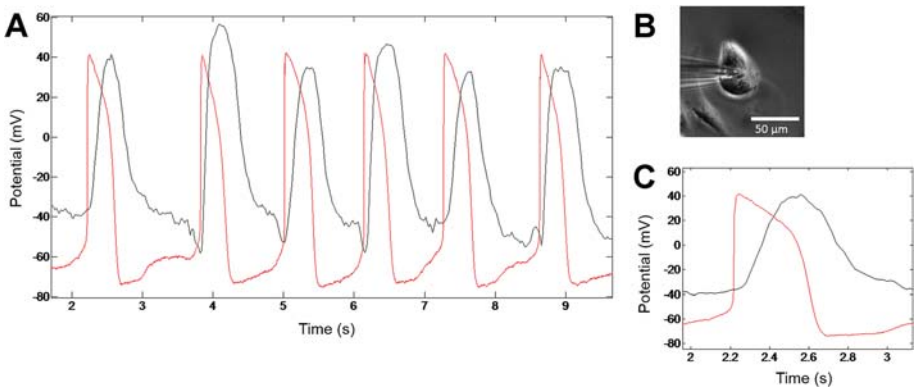

Figure 9 Combined current clamp and displacement data for a cell. A: Concurrent action potential and displacement signal, integrated with respect to time from the movement data obtained from the video data, are plotted in the same figure. The action potential data is shown in red and the movement data in black. For current clamp data, the potential in mV is shown, whereas for movement data, the y-axis is arbitrary. **B**: Image from the video data used for the analysis of a CM being recorded with current clamp. **C**: An enlarged part of the signal showing the time difference between the action potential and the displacement signal.

the mechanical functions of CMs because they enable the cell geometry-based beating parameters of cells to be calculated. Previously, DIC had been used for the analysis of cell cultures [11] and the morphogenesis of the heart and changes in blood flow during embryogenesis [23]. The displacement vector analysis approach has also been used for the analysis of the motion of living embryos [24]. In these *in vivo* studies, fluorescent particles were injected into the embryos and the motion of the particles inside the heart was analyzed. Our method does not require the invasion of the cell or the use of an artificial tracer and can be used for detailed single cell analysis.

DIC was found to be a viable complement to electrical studies in CM research. In this study, we demonstrated that MQD can be successfully used to analyze single beating CMs. Further, dividing the cell into sectors and calculating the radial and tangential signals for different parts of the cell provides a way to derive basic cell motion directions and thus motion signals related to cell geometry. This enabled the robust detection of all movements. This is especially important for iPS cell-derived CMs that do not beat as uniformly as fully matured native CMs. As also shown here, the beating does not have a main contraction axis and the beating shows fusiform characteristics.

In comparison to other similar methods that analyse contraction [10,11], our analysis that uses a sector approach is advantageous for iPS cell-derived CMs that lack the well-organized structure of mature native cells. Our results show that the eight sectors and directional components provide signals that can be used to analyze the mechanical behavior of an IPS cell-derived CM. Because it does not depend on mathematical estimators such as the principal components of motion vectors, the method is simple and

Table 3 Action potential parameters

Unpatched (bpm)	Patched (bpm)	Vmax (dV/dT)	APD10 (ms)	APD50 (ms)	APD90 (ms)	APA (mV)
39	42.52	43.08	97.67	279.53	371.00	116.30

CM action potential parameters in current clamp experiment. Beats per minute (bpm) for unpatched and patched cells are listed. Maximal rise velocity (Vmax), action potential durations at 10%, 50% and 90% of repolarization (APD10, APD50, and APD90, respectively), and action potential amplitude (APA) are listed.

robust. In our method dividing the cell into sectors depends on the visual selection of the beating focus point. While this approach allows flexibility in analysis, it could result in a source of user based error. As the optimal selection of the beating focus point is not inherently clear, automated methods for beating focus point detection well warranted.

Our results indicate that our method provides a reliable signal, and the results of the simulated data show that the method performs well in challenging noise conditions. The sector analysis withstood noise very well and provided high correlation figures compared to simulated movements. In addition, the speckle noise applied in the noise resistance provides a good approximation of video noise. The simulation results indicate that our method is also applicable with relatively low quality video data and that the standard cameras used in microscopes are capable of producing video data that can be used for reliable motion analysis.

We used current clamp, considered as a gold standard for the analysis of single CMs [25] as a reference method to verify the timing of beating. The region of interest for the analysis was partly hampered by the patch pipette that blocked a large part of the view to the cell. Still, the mechanical behavior of the beating cells, which corresponded to electrical activity measured with current clamp, could be detected with the MQD method with good accuracy. Furthermore, we observed that the beating of the cell during the patching was noticeably weaker indicating that patching can alter the function. Thus, non-invasive and non-label methods such as those presented here are well warranted for the detailed functional analysis of CMs.

Some issues should be taken into account when making the video recordings and the motion analysis. For example, the cells in our test were of varying sizes and, despite our best efforts, the video focus was not uniform for all cells. In some videos, noise in the recording and video packing artifacts caused noise in the motion analysis signal. This was especially observed for the cells that had weak beating, videos that were slightly out of focus, and cells that had a uniform surface pattern. The calculated contraction and relaxation times for different cells were, however, similarly proportioned despite the noise. Based on these findings, it can be stated that high quality recordings are not required. Since the method creates the signal based on the moving patterns inside the cell, it can also provide a good signal when the cell is attached to the surface and the outline does not move.

In many cases, the dissociated CMs are attached to the bottom of the culture plate in such a way that the outline of the cell does not move and the movement can only be seen by observing the moving patterns inside the cell. Some cells, however, also had a moving outline. As a result, the cells have varying and fusiform movement patterns. However, our method was able to derive the movement dynamics of all these cells by using the cell geometry-based sectorial and directional summation of the PIV vectors. The sectorial approach has specific benefits for the analysis of cells such as stem cell-derived CMs with varying and inhomogeneous movement patterns inside the cells or with a lack of a main axis of contractility. Due to these reasons, quantifying the extent of the contraction or contractility of the dissociated CMs derived from iPS cells, e.g. in pixels per time unit or movement in micrometers, is not meaningful.

Conclusions

MQD analysis using a sector approach provides a novel way for the non-invasive and non-labeled function analysis of the biomechanics of CMs, especially those derived

from stem cells. Motion analysis in general has clear advantages over other existing methods: it requires very little training for personnel, it does not require external hardware apart from a microscope and a video camera, it can be used for high throughput screening, and it is non-invasive and label-free**.** Motion analysis can also reveal information that is beyond the electrical properties and ion movements of the cardiac cells such as actual biomechanical timing and possible intracellular motion defects. Motion analysis is, therefore, an important addition to any electrical study. Moreover, the motion analysis method may provide an important addition to the traditional way of studying cell functionality, especially the actual mechanical movement, namely the timing of contraction and relaxation of CMs. Our method is especially designed to provide robust motion information from fusiform inhomogeneously beating dissociated CMs derived from stem cells.

In conclusion, these capabilities in conjunction with improved stem cell technologies that produce patient specific cell lines make the proposed system a good candidate for high throughput drug screening, safety analysis, and the basic studies of cardiac diseases using stem cell-derived CMs.

Abbreviations

AFP: Alpha-fetoprotein; AFM: Atomic force microscopy; APA: Action potential amplitude; APD: Action potential duration; AVG: Average correlation; bFGF: Basic fibroblast growth factor; BR: Beating rate; CM: Cardiomyocyte; Cx-43: Connexin-43; DAPI: 4′,6-diamidino-2-phenylindole; DIC: Digital image correlation; DMEM: Dulbecco's modified eagle medium; EB: Embryoid body; FBS: Fetal bovine serum; FPD: Field potential duration; GAPDH: β-actin and glyceraldehyde 3-phosphate dehydrogenase; HEPES: 4-(2-hydroxyethyl)-1-piperazineethanesulfonic acid; hERG: Human ether-à-go-go-related gene; iPS: Induced pluripotent stem; KDR: Kinase insert domain receptor; KO: Knockout; KO-SR: Knockout serum replacement; KSR: Knockout serum replacement -medium; MEA: Micro electrode array; MEF: Mouse embryonic fibroblast; MHC: Myosin-heavy-chain; MLC2a: Atrial myosin light chain; MLC2v: Ventricular myosin light chain; MQD: Minimum quadratic difference; MYH7: Myosin heavy chain; NEAA: Non-essential amino acids; PFA: Paraformaldehyde; PIV: Particle image velocimetry; RT-PCR: Reverse transcription polymerase chain reaction; SD: Standard deviation; TNTT2: Troponin T; VEGFR-2: Vascular endothelial growth factor receptor 2.

Competing interests

A patent application concerning the method has been filed. There are no other conflicts of interests.

Authors' contributions

AA developed and tested the method, analyzed the videos, modeled the artificial beating and drafted the manuscript. AK conducted the iPS cell production, CM differentiation and characterization, recorded the videos, and drafted the applicable parts of the manuscript. She also observed the need for the method. KL conducted the patch clamp experiment and drafted the applicable parts of the manuscript. MH participated in conception of the method and assisted with manuscript drafting. KA-S and JH participated in the development of the method, the design and coordination of the study, and helped to draft the manuscript. KA-S also participated in formulating the original necessity for the method. All authors read and approved the final manuscript.

Acknowledgements

We would like to thank Prof. Mummery (Hubrecht Institute, Utrecht, The Netherlands) for providing the END-2 cells for co-culturing.

This study was funded partly by personal research grants from Finnish Cultural Foundation, Pirkanmaa Regional Fund; Tampere Graduate Program in Biomedicine and Biotechnology, Institute of Biomedical Technology, University of Tampere, Finland; Stemfunc project funded by the Academy of Finland (decision number 122947); Human spare parts project funded by Finnish Funding Agency for Technology and Innovation (TEKES); Finnish Foundation for Cardiovascular Research; Pirkanmaa hospital district (EVO).

Author details

[1]Computional Biophysics and Imaging Group, Department of Electronics and Communications Engineering, and BioMediTech, Tampere University of Technology, Tampere, Finland. [2]Heart Group, BioMediTech, University of Tampere, Tampere, Finland. [3]Pixact Oy, Postitorvenkatu 16, FI-33840 Tampere, Finland. [4]Heart Hospital, Tampere University Hospital, Tampere, Finland. [5]Medical School, University of Tampere, Tampere, Finland.

Received: 23 September 2013 Accepted: 1 April 2014
Published: 7 April 2014

References

1. Pollard C, Valentin JP, Hammond T: **Strategies to reduce the risk of drug-induced QT interval prolongation: a pharmaceutical company perspective.** *Br J Pharmacol* 2008, **154:**1538–1543.

2. Takahashi K, Tanabe K, Ohnuki M, Narita M, Ichisaka T, Tomoda K, Yamanaka S: **Induction of pluripotent stem cells from adult human fibroblasts by defined factors.** *Cell* 2007, **131:**861–872.
3. Zhang J, Wilson GF, Soerens AG, Koonce CH, Yu J, Palacek SP, Thomson JA, Kamp TJ: **Functional cardiomyocytes derived from human induced pluripotent stem cells.** *Circ Res* 2009, **104:**e30–e41.
4. Harris K, Aylott M, Cui Y, Louttit JB, McMahon NC, Sridhar A: **Comparison of electrophysiological data from human-induced pluripotent stem cell-derived cardiomyocytes to functional preclinical safety assays.** *Toxicol Sci* 2013, **134:**412–426.
5. Brüggemann A, Stoelzle S, George M, Behrends JC, Fertig N: **Microchip technology for automated and parallel patch-clamp recording.** *Small* 2006, **2:**840–846.
6. Braeken D, Huys R, Jans D, Loo J, Severi S, Vleugels F, Borghs G, Callewaert G, Bartic C: **Local electrical stimulation of single adherent cells using three-dimensional electrode arrays with small interelectrode distances.** *Conf Proc IEEE Eng Med Biol Soc* 2009, **2009:**2756–2759.
7. Novakova M, Bardonova J, Provaznik I, Taborska E, Bochorakova H, Paulova H, Horky D: **Effects of voltage sensitive dye di-4-ANEPPS on guinea pig and rabbit myocardium.** *Gen Physiol Biophys* 2008, **27:**45–54.
8. Liu J, Sun N, Bruce MA, Wu JC, Butte MJ: **Atomic force mechanobiology of pluripotent stem cell-derived cardiomyocytes.** *PLOS ONE* 2012, **7:**e37559.
9. Peters MF, Scott CM, Ochalski R, Dragan YP: **Evaluation of cellular impedance measures of cardiomyocyte cultures for drug screening applications.** *Assay Drug Dev Technol* 2012, **10:**525–532.
10. Hayakawa T, Kunihiro T, Dowaki S, Uno H, Matsui E, Uchida M, Kobayashi S, Yasuda A, Shimizu T, Okano T: **Noninvasive evaluation of contractile behaviour of cardiomyocyte monolayers based on motion vector analysis.** *Tissue Eng Part C* 2012, **18:**21–32.
11. Kamgoué A, Ohayon J, Usson Y, Riou L, Tracqui P: **Quantification of cardiomyocyte contraction based on image correlation analysis.** *Cytometry A* 2009, **75:**298–308.
12. Xi J, Khalil M, Shishechian N, Hannes T, Pfannkuche K, Liang H, Fatima A, Haustein M, Suhr F, Bloch W, Reppel M, Saric T, Wernig M, Jänisch R, Brockmeier K, Hescheler J, Pillekamp F: **Comparison of contractile behavior of native murine ventricular tissue and cardiomyocytes derived from embryonic or induced pluripotent stem cells.** *FASEB J* 2010, **24:**2739–2751.
13. Lahti AL, Kujala VJ, Chapman H, Koivisto AP, Pekkanen-Mattila M, Kerkelä E, Hyttinen J, Kontula K, Swan H, Conklin BR, Yamanaka S, Silvennoinen O, Aalto-Setälä K: **Model for long QT syndrome type 2 using human iPS cells demonstrates arrhythmogenic characteristics in cell culture.** *Dis Model Mech* 2012, **5:**220–230.
14. Mummery C, Oostwaard DW, Doevendans P, Spijker R, van den Brink S, Hassink R: **Differentiation of human embryonic stem cells to cardiomyocytes: role of coculture with visceral endoderm-like cells.** *Circulation* 2003, **107:**2733–2740.
15. Takahashi T, Lord B, Schulze PC, Fryer RM, Sarang SS, Gullans SR, Lee RT: **Ascorbic acid enhances differentiation of embryonic stem cells into cardiac myocytes.** *Circulation* 2003, **107:**1912–1916.
16. Sutton MA, Orteu JJ, Schreier HW: *Image Correlation for Shape, Motion and Deformation Measurements.* New York: Springer-Verlag; 2009.
17. Gui L, Merzkirch W: **A method of tracking ensembles of particle images.** *Exp Fluids* 1996, **21:**465–468.
18. Gui L, Merzkirch W: **Comparative study of the MQD method and several correlation-based PIV evaluation methods.** *Exp Fluids* 2000, **28:**36–44.
19. Willert C, Gharib M: **Digital particle image velocimetry.** *Exp Fluids* 1991, **10:**181–193.
20. Mori N, Chang KA: **Introduction to MPIV.** http://www.oceanwave.jp/softwares/mpiv/.
21. Kroon DJ: **Pinch and Spherize Filter.** http://www.mathworks.com/matlabcentral/fileexchange/22573.
22. Bers DM: *Excitation-contraction Coupling and Cardiac Contractile Force – Second Edition.* Dordrecht, The Netherlands: Kluwer Academic Publishers; 2001.
23. Ohn J, Tsai HJ, Liebling M: **Joint dynamic imaging of morphogenesis and function in the developing heart.** *Organogenesis* 2009, **5:**248–255.
24. Lu J, Pereira F, Fraser S, Gharib M: **Three-dimensional real-time imaging of cardiac cell motions in living embryos.** *J Biomed Opt* 2008, **13:**014006.
25. Kornreich B: **The patch clamp technique: principles and technical considerations.** *J Vet Cardiol* 2007, **9:**25–37.

doi:10.1186/1475-925X-13-39
Cite this article as: Ahola *et al.*: Video image-based analysis of single human induced pluripotent stem cell derived cardiomyocyte beating dynamics using digital image correlation. *BioMedical Engineering OnLine* 2014 **13**:39.